

NTIS # PB2009-

SSC-458

**RELIABILITY-BASED
PERFORMANCE ASSESSMENT OF
DAMAGED SHIPS**



This document has been approved
For public release and sale; its
Distribution is unlimited

SHIP STRUCTURE COMMITTEE
2009

Ship Structure Committee

RADM Brian M. Salerno
U. S. Coast Guard Assistant Commandant,
Assistant Commandant for Marine Safety, Security and Stewardship
Chairman, Ship Structure Committee

{Name}
{Title}
Naval Sea Systems Command

Mr. Christopher McMahon
Director, Office of Ship Construction
Maritime Administration

Mr. Kevin Baetsen
Director of Engineering
Military Sealift Command

UNITED STATES COAST GUARD
Mr. Jeffrey Lantz,
Commercial Regulations and Standards for the
Assistant Commandant for Marine Safety, Security
and Stewardship
Mr. Jeffery Orner
Deputy Assistant Commandant for Engineering and
Logistics

Dr. Roger Basu
Senior Vice President
American Bureau of Shipping

Mr. Donald Roussel
Director General, Marine Safety,
Safety & Security
Transport Canada

Dr. Neil Pegg
Group Leader - Structural Mechanics
Defence Research & Development Canada - Atlantic

EXECUTIVE DIRECTOR
Lieutenant Commander, Jason Smith
U. S. Coast Guard

ADMINISTRATIVE ASSISTANT
Ms. Jeannette Y. Grant
U. S. Coast Guard

SHIP STRUCTURE SUB-COMMITTEE

AMERICAN BUREAU OF SHIPPING (ABS)

Mr. Glenn Ashe
Mr. Derek Novak
Mr. Phil Rynn
Mr. Balji Menon

DEFENCE RESEARCH & DEVELOPMENT CANADA ATLANTIC

Dr. David Stredulinsky
Mr. John Porter

MARITIME ADMINISTRATION (MARAD)

Mr. Chao Lin
Mr. Carl Setterstrom
Mr. Richard Sonnenschein

MILITARY SEALIFT COMMAND (MSC)

Mr. Michael W. Touma
Mr. Paul Handler

NAVY/ONR / NAVSEA/ NSWCCD

{Name}
{Name}
{Name}
{Name}

TRANSPORT CANADA

Paul Denis Vallee

UNITED STATES COAST GUARD

CDR Charles Rawson
Mr. James Person
CAPT Paul Roden
Mr. Rubin Sheinberg

SOCIETY OF NAVAL ARCHITECTS AND MARINE ENGINEERS (SNAME)

Mr. Jaideep Sirkar
Mr. Al Rowen
Mr. Norman Hammer

Member Agencies:

*American Bureau of Shipping
Defence Research and Development Canada
Maritime Administration
Military Sealift Command
Naval Sea Systems Command
Society of Naval Architects & Marine Engineers
Transport Canada
United States Coast Guard*



**Ship
Structure
Committee**

Address Correspondence to:

COMMANDANT (CG-5212/SSC)
ATTN (EXECUTIVE DIRECTOR/SHIP
STRUCTURE COMMITTEE)
US COAST GUARD
2100 2ND ST SW STOP 7126
WASHINGTON DC 20593-7126
Website: <http://www.shipstructure.org>

**SSC – 458
SR – 1456**

SEPTEMBER 12, 2009

**EXACT MAPPING OF RESIDUAL STRESS IN SHIP HULL STRUCTURES BY USE OF
NEUTRON DIFFRACTION**

A contributing factor to the failure of ship hulls can be the residual stresses introduced during the welding process of connecting the stiffeners to the steel plates of a ship hull. This report presents a detailed study on these residual stress distributions found at a typical weld-stiffener connection. Most previous studies focus on the surface stress values and only one or two of the three stress components. The weaknesses in these studies were a result of the limits of the testing methods used. In order to produce the most accurate image of the stress field, the non-destructive, highly accurate testing method of neutron diffraction was used. The specimens were designed to examine both one and two stiffener residual stress distributions. The one stiffener specimens investigated the basic connection and the effect of a shortened stiffener and the residual stress field found around the termination of the stiffener in the parent plate. The two stiffener specimens were designed to examine the result of changing the spacing of the stiffener and the heat input used during the welding process. The test results from this study were compared to existing residual stress models. The residual stress distributions found in this study provide a better understanding of the stress patterns present when constructing a ship hull.

A handwritten signature in black ink, appearing to read 'B. Salerno', is written over a faint, circular watermark or seal. The signature is fluid and cursive.

BRIAN M. SALERNO
Rear Admiral, U.S. Coast Guard
Chairman, Ship Structure Committee

1. Report No. SSC - 458	2. Government Accession No.	3. Recipient's Catalog No.	
4. Title and Subtitle EXACT MAPPING OF RESIDUAL STRESS IN SHIP HULL STRUCTURES BY USE OF NEUTRON DIFFRACTION		5. Report Date May, 2009	
		6. Performing Organization Code	
7. Author(s) Sreekanta Das and Sara Y. Kenno		8. Performing Organization Report No. SR-1456	
9. Performing Organization Name and Address University of Windsor 401 Sunset Ave Windsor, ON N9B 3P4		10. Work Unit No. (TRAIS)	
		11. Contract or Grant No. W7707-078019/001/HAL	
12. Sponsoring Agency Name and Address COMMANDANT (CG-5212/SSC) ATTN (ADMIN ASST/SHIP STRUCTURE COMMITTEE) US COAST GUARD 2100 2ND ST SW STOP 7126 WASHINGTON DC 20593-7126		13. Type of Report Final Report	
		14. Sponsoring Agency Code CG- 5	
15. Supplementary Notes Sponsored by the Ship Structure Committee and its member agencies			
16. Abstract <p>Failure of ship hulls may be a result of a combination of various factors. Residual stress caused by welding of the stiffeners on to the steel plates is one of the contributing factors to the failure. This study was completed for a more in-depth look at the residual stress distribution found at a typical weld-stiffener connection of ship hulls. Six small specimens were built and the sizing of the specimens was designed so that they could be accommodated in the test facility available at the Canadian Neutron Beam Centre in the Chalk River Laboratories. The specimens were made out of 9.53 mm thick plate of 350 WT grade structural steel stiffened by L127x76.2x9.53 angle stiffeners. The non-destructive neutron diffraction method was used to collect strain data at locations within the volume of the specimens. The method of neutron diffraction uses the crystal lattice of the sample material as an internal strain gauge. The test results were analyzed to determine the distribution of all the three components of the residual stress in the parent steel plate and in the stiffened plate specimens. The spacing between two stiffeners and the welding heat input were varied to examine the effect these variables on the residual stress levels. A shortened stiffener specimen was also built to investigate the residual stresses in and around the termination of the stiffener in the parent plate.</p>			
17. Key Words		18. Distribution Statement Distribution Available From: National Technical Information Service U.S. Department of Commerce Springfield, VA 22151 Ph. (703) 487-4650	
19. Security Classif. (of this report) Unclassified	20. Security Classif. (of this page) Unclassified	21. No. of Pages	22. Price

CONVERSION FACTORS

(Approximate conversions to metric measures)

To convert from	to	Function	Value
LENGTH			
inches	meters	divide	39.3701
inches	millimeters	multiply by	25.4000
feet	meters	divide by	3.2808
VOLUME			
cubic feet	cubic meters	divide by	35.3149
cubic inches	cubic meters	divide by	61,024
SECTION MODULUS			
inches ² feet ²	centimeters ² meters ²	multiply by	1.9665
inches ² feet ²	centimeters ³	multiply by	196.6448
inches ⁴	centimeters ³	multiply by	16.3871
MOMENT OF INERTIA			
inches ² feet ²	centimeters ² meters	divide by	1.6684
inches ² feet ²	centimeters ⁴	multiply by	5993.73
inches ⁴	centimeters ⁴	multiply by	41.623
FORCE OR MASS			
long tons	tonne	multiply by	1.0160
long tons	kilograms	multiply by	1016.047
pounds	tonnes	divide by	2204.62
pounds	kilograms	divide by	2.2046
pounds	Newtons	multiply by	4.4482
PRESSURE OR STRESS			
pounds/inch ²	Newtons/meter ² (Pascals)	multiply by	6894.757
kilo pounds/inch ²	mega Newtons/meter ² (mega Pascals)	multiply by	6.8947
BENDING OR TORQUE			
foot tons	meter tons	divide by	3.2291
foot pounds	kilogram meters	divide by	7.23285
foot pounds	Newton meters	multiply by	1.35582
ENERGY			
foot pounds	Joules	multiply by	1.355826
STRESS INTENSITY			
kilo pound/inch ² inch ^{1/2} (ksi√in)	mega Newton MNm ^{3/2}	multiply by	1.0998
J-INTEGRAL			
kilo pound/inch	Joules/mm ²	multiply by	0.1753
kilo pound/inch	kilo Joules/m ²	multiply by	175.3

TABLE OF CONTENTS

Technical Report Documentation Page	iii
CONVERSION FACTORS.....	iv
LIST OF FIGURES	vii
LIST OF TABLES.....	xii
LIST OF ABBREVIATIONS AND SYMBOLS	xiii
1 INTRODUCTION	1
1.1 General	1
1.2 Objective	1
2 LITERATURE REVIEW	2
2.1 Background	2
2.2 Numerical Modelling	3
2.3 Destructive Test Methods.....	4
2.3.1 Sectioning Method.....	4
2.3.2 Contour Method.....	4
2.4 Semi-destructive Test Methods.....	8
2.4.1 Hole-drilling Method	8
2.4.2 Blind Hole-drilling Method	11
2.5 Non-Destructive Test Methods	13
2.5.1 X-ray Diffraction Method.....	13
2.5.2 Magnetic Barkhausen Noise Method.....	14
2.5.3 X-ray Diffraction Method vs. Hole-drilling Method	16
2.5.4 Neutron Diffraction Method	18
3 TEST FACILITY	32
3.1 Stress Scanner	33
3.2 Powder Diffractometer.....	33
3.3 Weld Station.....	33
4 TEST MATRIX	35
5 MATERIAL PROPERTIES AND WELDING SPECIFICATIONS	37
5.1 Mechanical Properties.....	37

5.2	Welding Specifications	38
6	TEST SETUP AND REFERENCE SAMPLES	42
6.1	Test Setup.....	42
6.2	Stress Free Samples and Calibration.....	45
7	TEST RESULTS FOR PHASE I.....	47
7.1	Specimen Details.....	47
7.1.1	Specimen 1.....	47
7.1.2	Specimen 2.....	48
7.1.3	Specimen 3.....	49
7.2	Test Results	50
7.2.1	Specimen 1.....	50
7.2.1.1	Normal Stress for Specimen 1	50
7.2.1.2	Transverse Stress for Specimen 1.....	55
7.2.1.3	Longitudinal Stress for Specimen 1	60
7.2.2	Specimen 2.....	65
7.2.2.1	Normal Stress for Specimen 2.....	66
7.2.2.2	Transverse Stress for Specimen 2.....	69
7.2.2.3	Longitudinal Stress for Specimen 2	71
7.2.3	Specimen 3.....	76
7.2.3.1	Normal Stress for Specimen 3	78
7.2.3.2	Transverse Stress for Specimen 3.....	80
7.2.3.3	Longitudinal Stress for Specimen 3	82
8	TEST RESULTS FOR PHASE II.....	87
8.1	Specimen Details.....	87
8.1.1	Specimen 4.....	87
8.1.2	Specimen 5.....	87
8.1.3	Specimen 6.....	88
8.2	Test Results	90
8.2.1	Specimen 4.....	90
8.2.1.1	Transverse Strain for Specimen 4.....	91
8.2.1.2	Longitudinal Strain for Specimen 4.....	103

8.2.2	Specimen 5.....	106
8.2.2.1	Normal Stress for Specimen 5.....	109
8.2.2.2	Longitudinal Stress for Specimen 5.....	112
8.2.2.3	All Stresses at Weld Centerline for Specimen 5.....	114
8.2.3	Specimen 6.....	116
8.2.3.1	Normal Stress for Specimen 6.....	119
8.2.3.2	Transverse Stress for Specimen 6.....	121
8.2.3.3	Longitudinal Stress for Specimen 6.....	124
8.2.3.4	All Stresses at Weld Centerline for Specimen 6.....	127
9	COMPARISON OF RESULTS.....	129
10	PORTABLE DEVICES.....	135
11	SUMMARY, CONCLUSIONS, AND RECOMMENDATIONS.....	135
12	ACKNOWLEDGEMENTS.....	138
13	REFERENCES.....	139

LIST OF FIGURES

Figure 2.1:	FE representation of the specimens (Hu & Jiang, 1998).....	5
Figure 2.2:	(a) Distance from edge of plate (mm) vs. Stress at plate (MPa); (b) Distance from edge of flange (mm) vs. Stress at flange (MPa); (c) Distance from junction of plate and web (mm) vs. Stress at web (MPa). (Hu & Jiang, 1998).....	6
Figure 2.3:	The stress maps measured with the contour method and neutron diffraction (Prime, et al., 2004).....	7
Figure 2.4:	Comparison of experimental and simulation residual stresses (Cho, et al., 2004).....	10
Figure 2.5:	Residual stresses in welded specimens (Weng & Lo, 1992).....	12
Figure 2.6:	Surface residual stress distributions of (a) RS1 - 14kJ/cm, no restraint, (b) RS2 - 14kJ/cm, with restraint, (c) RS3 - 17kJ/cm, no restraint (Gao, et al., 1997).....	15
Figure 2.7:	Test specimen with a typical crack and residual stress distribution (Rörup, 2005).....	17
Figure 2.8:	Analysis of the weld-induced residual stresses in the longitudinal direction (Rörup, 2005).....	17
Figure 2.9:	Lattice spacing with incident (ki) and refracted (kf) beam.....	18
Figure 2.10:	Lattice planes (Hutchings, et al., 2005).....	19

Figure 2.11:	Cross-sectional details of the multipass weld runs used to make the butt joints in the 8mm and 12mm thick plates of RQT701 steel - (a) 8 mm plate thickness with low heat input (1 kJ/mm), (b) 8 mm plate thickness with high heat input (3 kJ/mm), (c) 12 mm plate thickness with low heat input, & (d) 12 mm plate thickness with high heat input (James, et al., 2006)	21
Figure 2.12:	Specimen - 12 mm thick, overmatched weld metal at low heat input 1kJ/mm (a) Longitudinal (x) stress profile at four depths (b) Transverse (y) stress profile at four depths (c) Through-thickness (z) stress profile at four depths (James, et al., 2006)	22
Figure 2.13:	Pseudo-strain measured by ND and SD across the weld, (PM = parent material, HAZ = heat affected zone, WM, weld material) (Paradowska, Finlayson, et al., 2006)	23
Figure 2.14:	Pseudo-strain measured by ND and SD through the thickness (Paradowska, Finlayson, et al., 2006).....	23
Figure 2.15:	Location of deep-hole drilling measurements on the 100 mm thick plate specimen (Wimpory, et al., 2003).....	24
Figure 2.16:	Transverse stresses in the 100 mm T-plate - ND measurement on a 12.5 mm slice and DHD measurement (Wimpory, et al., 2003).....	25
Figure 2.17:	Longitudinal stresses in the 100 mm T-plate obtained by ND on a 12.5 mm slice and by DHD (Wimpory, et al., 2003)	26
Figure 2.18:	Three-dimensional stresses 10mm from surface of side B—flat butt weld (Pearce & Linton, 2006)	26
Figure 2.19:	The direction of the measurements (transverse x, normal y, longitudinal would be z) using neutron diffraction on the single bead-on-plate (Price, et al., 2006).....	28
Figure 2.20:	Change in stress in fully restrained sample in comparison to unrestrained sample (Price, et al., 2006).....	28
Figure 2.21:	Longitudinal stress derived from measurements of {110}, {002} and {112} reflections in the high strength steel SNC631 as a function of position through the weld (Holden, Suzuki, et al., 2006)	30
Figure 2.22:	Centerline longitudinal strain measured in the two as-welded 12-mm-thick plates using neutrons and synchrotron X-rays (Ganguly, Fitzpatrick, & Edwards, 2006)	31
Figure 3.1:	Layout of the Chalk River Laboratories (NRC, 2008)	33
Figure 3.2:	L3 Spectrometer at Chalk River Laboratories (NRC, 2008)	34
Figure 5.1:	Nominal Stress-Strain Behaviour of Plate and Angle.....	38
Figure 5.2:	Clamp locations during welding	40

Figure 6.1:	Tilted telescope pointed at the y-centre of rotation of the specimen	43
Figure 6.2:	Level telescope pointed at the x-centre of rotation of the specimen.....	43
Figure 6.3:	Wire mount used to sight centre of rotation with telescopes	44
Figure 6.4:	Stress-free reference samples.....	46
Figure 6.5:	Nickel-reference sample in cadmium container	46
Figure 7.1:	Specimen 1 (a) is a photo and (b) is the sketch.....	47
Figure 7.2:	Specimen 2 (a) is a photo and (b) is the sketch.....	48
Figure 7.3:	Specimen 2 (a) is a photo and (b) is the sketch.....	49
Figure 7.4:	Detail for Measurement Points for Specimen 1	50
Figure 7.5:	Normal stresses through the depth in transverse (T) direction (line 1-2)	52
Figure 7.6:	Normal stresses through the depth in longitudinal (L) direction (line 1-3)	53
Figure 7.7:	3-D view of normal stress distribution in transverse (T) direction.....	54
Figure 7.8:	3-D view of normal stress distribution in longitudinal (L) direction.....	55
Figure 7.9:	Transverse stress through the depth in transverse (T) direction (line 1-2)	57
Figure 7.10:	Transverse stress through the depth in longitudinal (L) direction (line 1-3)	58
Figure 7.11:	3-D view of transverse stress distribution in transverse (T) direction (line 1-2) ..	59
Figure 7.12:	3-D view of transverse stress distribution in longitudinal (L) direction (line 1-3)60	
Figure 7.13:	Longitudinal stress through the depth in transverse (T) direction (line 1-2)	62
Figure 7.14:	Longitudinal stress through depth in longitudinal (L) direction (line 1-3).....	63
Figure 7.15:	3-D view of transverse stress distribution in transverse (T) direction (line 1-2) ..	64
Figure 7.16:	3-D view of transverse stress distribution in longitudinal (L) direction (line 1-3)65	
Figure 7.17:	Detail for Measurement Points for Specimen 2.....	66
Figure 7.18:	Measurement Spacing in mm.....	67
Figure 7.19:	Normal stresses through the depth in transverse (T) direction (at L = 0 mm, line 3-1-4).....	68
Figure 7.20:	Normal stresses through the depth in transverse (T) direction (at L = 133 mm, line 5-2-6).....	69
Figure 7.21:	Transverse stresses through the depth in transverse (T) direction (at L = 0 mm, line 3-1-4).....	70
Figure 7.22:	Transverse stresses through the depth in transverse (T) direction (at L = 133 mm, line 5-2-6).....	71

Figure 7.23:	Longitudinal stress through the depth in transverse (T) direction (at L = 0 mm, line 3-1-4).....	72
Figure 7.24:	Longitudinal stress through the depth in transverse (T) direction (at L = 133 mm, line 5-2-6).....	73
Figure 7.25:	3-D view of longitudinal stress distribution in transverse (T) direction (at L = 0 mm, line 3-1-4)	74
Figure 7.26:	3-D view of longitudinal stress distribution in transverse (T) direction (at L = 133 mm, line 5-2-6)	75
Figure 7.27:	All stresses at Transverse = -10 mm, Normal = 8.9 mm (line 1-2)	76
Figure 7.28:	Detail for Measurement Points in Specimen 3	77
Figure 7.29:	Measurement Spacing in mm.....	77
Figure 7.30:	Normal stresses through the depth in transverse (T) direction (line 2-1-3).....	80
Figure 7.31:	Transverse stresses though the depth in transverse (T) direction (line 2-1-3).....	81
Figure 7.32:	Longitudinal stresses through the depth in transverse (T) direction (line 2-1-3) .	84
Figure 7.33:	3-D view of longitudinal stress distribution in transverse (T) direction (line 2-1-3)	85
Figure 8.1:	Specimen 4 (a) is a photo and (b) is the sketch.....	88
Figure 8.2:	Specimens 5 and 6 (a) is a photo and (b) is the sketch	89
Figure 8.3:	Detail for Measurement Points for Specimen 4.....	91
Figure 8.4:	Spacing of measurements (in mm) in transverse direction on Specimen 4 (lines 1, 3, 4, 5, and 6)	92
Figure 8.5:	Transverse strain at various depths in the transverse (T) direction on line 1 (at L = 200 mm)	93
Figure 8.6:	Transverse strain at various depths in the transverse (T) direction on line 1 (at L = 200 mm)	94
Figure 8.7:	Transverse strain at various depths in the transverse (T) direction on line 3 (at L = 20 mm)	95
Figure 8.8:	Transverse strain at various depths in the transverse (T) direction on line 4 (at L = 0 mm)	96
Figure 8.9:	Transverse strain at various depths in the transverse (T) direction on line 5 (at L = -20 mm).....	97
Figure 8.10:	Transverse strain at various depths in the transverse (T) direction on line 6 (at L = -60 mm).....	98

Figure 8.11:	Transverse strain at a depth of 8.4 mm in the transverse (T) direction on lines 1, 3, 4, 5, and 6.....	99
Figure 8.12:	Transverse strain at various depths in the longitudinal (L) direction on line 7 (at T = 10 mm).....	100
Figure 8.13:	Transverse strain at various depths in the longitudinal (L) direction on line 8 (at T = 30 mm).....	101
Figure 8.14:	Transverse strain at various depths in the longitudinal (L) direction on line 9 (at T = 50 mm).....	102
Figure 8.15:	Transverse strain at a depth of 8.4 mm in the longitudinal (L) direction on lines 7, 8, and 9.....	103
Figure 8.16:	Longitudinal strain at a depth of 8.4 mm in the transverse (T) direction on lines 1, 3, 4, 5, and 6.....	105
Figure 8.17:	Longitudinal strain at a depth of 8.4 mm in the longitudinal (L) direction on lines 7, 8, and 9.....	106
Figure 8.18:	Detail for Measurement Points for Specimen 5.....	107
Figure 8.19:	Spacing of the transverse direction measurements (in mm) on Specimen 5 (line 1-2-3-4).....	1
Figure 8.20:	Normal stress through the depth in the transverse (T) direction on line 1-2-3-4 (at L = 0 mm).....	110
Figure 8.21:	Transverse stress through the depth in the transverse (T) direction on line 1-2-3-4 (at L = 0 mm).....	111
Figure 8.22:	Longitudinal stress through the depth in the transverse (T) direction on line 1-2-3-4 (at L = 0 mm).....	113
Figure 8.23:	All stresses at first welded stiffener, at T = -390 mm, at N = 8.4 mm (on line 3-6).	115
Figure 8.24:	All stresses at second welded stiffener, at T = +10 mm, at N = 8.4 mm (on line 2-5).....	116
Figure 8.25:	Details for Measurement Points for Specimen 6.....	117
Figure 8.26:	Spacing of measurements (in mm) in transverse direction for Specimen 6 (on line 1-2-3).....	118
Figure 8.27:	Normal stress at various depths in the transverse (T) direction on line 1-2-3 (at L = 0 mm).....	120
Figure 8.28:	Average normal stress distributions along the transverse lines (line 1-2-3-4 for Specimen 5 and line 1-2-3 for Specimen 6).....	121

Figure 8.29:	Transverse stress at various depths in the transverse (T) direction on line 1-2-3 (at L = 0 mm)	123
Figure 8.30:	Average transverse stress distributions along the transverse lines (line 1-2-3-4 for Specimen 5 and line 1-2-3 for Specimen 6).....	124
Figure 8.31:	Longitudinal stress at various depths in the transverse (T) direction on line 1-2-3 (at L = 0 mm)	126
Figure 8.32:	Average longitudinal stress distributions along the transverse lines (line 1-2-3-4 for Specimen 5 and line 1-2-3 for Specimen 6).....	127
Figure 8.33:	All stresses at second welded stiffener, Transverse = 10 mm, Normal = 8.4 mm (on line 2-4).....	128
Figure 9.1:	Specimen Details (Dexter & Pilarski, 2000).....	130
Figure 9.2:	Sectioning coupons used for measuring residual stress distributions (Dexter & Pilarski, 2000).....	131
Figure 9.3:	Faulkner residual stress model compared to measured values of two specimens (Dexter & Pilarski, 2000).....	131
Figure 9.4:	Faulkner model for residual stresses (Dexter & Pilarski, 2000).....	132
Figure 9.5:	Specimen 3, two stiffeners spaced at 250 mm, high heat input.....	132
Figure 9.6:	Specimen 5, two stiffeners spaced at 400 mm, high heat input.....	133
Figure 9.7:	Specimen 6, two stiffeners spaced at 400 mm, moderate heat input	134

LIST OF TABLES

Table 4-1:	Test Matrix for Phase I	36
Table 4-2:	Test Matrix for Phase II	36
Table 5-1:	Mechanical Properties of Material.....	37
Table 5-2:	Welding Specifications Phase I	41
Table 5-3:	Welding Specifications for Phase II	41
Table 6-1:	Set-up Specifications for Phase I	45
Table 6-2:	Set-up Specifications for Phase II.....	45

LIST OF ABBREVIATIONS AND SYMBOLS

$2\theta_M$: reflection angle of the monochromating crystal

$2\theta_{hkl}^B$: Bragg diffraction angle

3-D: three-dimensional

ϵ_{hkl} : strain in the direction of the scattering vector

ϵ_{Normal} : normal strain component

$\epsilon_{Transverse}$: transverse strain component

$\epsilon_{Longitudinal}$: longitudinal strain component

φ : angle between the incident beam and the refracted beam

φ_0 : angle corresponding to the reference sample between the incident beam and the refracted beam

λ : de Broglie wavelength of a neutron

ν : Poisson's ratio

ψ : rotation angle between the neutron beam and the detector

σ_{xx} , σ_{Normal} : normal stress component

σ_{yy} , $\sigma_{Transverse}$: transverse stress component

σ_y : yield stress

σ_z , $\sigma_{Longitudinal}$: longitudinal stress component

$\mu strain$: micro strain

ALARA: as low as reasonably achievable

bcc: body-centred cubic

CANDU: Canada Deuterium Uranium

CMM: Coordinate Measuring Machine

CNBC: Canadian Neutron Beam Centre

CRL: Chalk River Laboratories

d_0 : lattice spacing of stress-free reference sample

d_{hkl} : perpendicular distance between lattice planes hkl

D-T: Deuterium-Tritium

DHD: deep hole drilling

E : energy of the neutron

E : modulus of elasticity

EDM: electro-discharge machining

FCAW: flux-cored arc welding

fcc : face-centred cubic

FE: finite element

G_{hkl} : reciprocal lattice vector, perpendicular to the lattice planes

GTAW: gas tungsten arc welding

h : Planck's constant

HAZ: heat affected zone

hkl : lattice planes

IGV: instrumental gauge volume, volume over which the average strain is measured in the sample

k : wave vector of the neutron with a magnitude of $2\pi/\lambda$

k_f : refracted beam

k_i : incident beam

L: longitudinal

m_n : mass of the neutron

MAG: metal active gas

MBN: magnetic Barkhausen noise

MIG: metal inert gas

N: normal

ND: neutron diffraction

NGV: nominal gauge volume, sample volume defined by apertures

NRU: National Research Universal

p : momentum of the particle

PM: parent material

SAW: submerged arc welding

SD: synchrotron X-ray diffraction

SGV: sample gauge volume, volume over which the strain measurement is averaged, from the diffraction peak in the IGV

T: transverse

TIG: tungsten inert gas

\mathbf{v} : velocity

ν : frequency of radiation

WM: weld material

1 INTRODUCTION

1.1 General

Failure of ship hulls is often a result of a combination of factors. Ship hull structures are made of steel plates stiffened by beams and girders. The residual stresses that develop due to the welding of the stiffeners on to the steel plates is one of the contributing factors to the failure. This study was completed for a more in-depth look at the residual stress distribution found at a typical weld-stiffener connection of ship hulls. The state-of-the-art Neutron Diffraction (ND) method was used in this study to determine three-dimensional (3-D) stress distributions of typical welded stiffened plates used in ship hulls. This report discusses the results obtained from this study. This report also presents a detailed literature review on the methods available for measuring residual stresses in welded steel members.

1.2 Objective

This is a scoping study aimed at investigating the true 3-D state of stress distribution using the ND method. The following are the tasks designed to fulfil the objective:

- (a) Undertake an extensive literature review on various numerical and experimental techniques available for determining residual stress distributions;
- (b) Undertake a feasibility study to determine application of the ND method for accurately mapping three-dimensional residual stress distributions at typical ship hull connections;
- (c) Conduct tests to measure residual stress distributions using ND method on stiffened plate samples, and;
- (d) Identify the possibilities for technology and product development activities for measuring residual stresses in actual ship structures.

2 LITERATURE REVIEW

2.1 Background

Residual stresses are caused by thermomechanical processing of steel. These processes alter the shape of the metal and/or induce a temperature gradient which generates residual stress. Processes that alter the physical shape include machining, forging, rolling, drawing, etc. The welding, casting, and quenching processes introduce a temperature gradient to the metal.

Residual stresses develop in welded structures primarily as the result of differences in the amount the weld metal shrinks as it hardens and cools to the surrounding temperature. Residual stresses are highly unpredictable and often non-uniform. In order to produce acceptable results, several locations on the specimen must be measured for strain, since a steep gradient in strain may be produced by residual stresses.

Residual stresses are usually calculated from the elastic strain values and using the elastic constitutive relationship. The elastic strain measured is either the existing strain or the change in strain when residual stresses are released. The elastic strain values are converted to stress values using the elastic strain constants. Residual stresses developed during the welding process are macrostresses (Type I) that are continuous from grain to grain and from phase to phase. (Hutchings, et al., 2005)

The method for measuring residual stress and the locations and number of measurements depend on the expected stress field. Preliminary tests may be required for a better estimate of the residual stress field. The chosen method also may depend on the nature of the specimen, for example, if the sample is too large to move and measure in a laboratory, the measurements need to be carried out using portable measurement devices in the field.

A scaled version of the actual specimen may be used for determining the residual stress distribution. However, it must be large enough to avoid improper readings, when a laboratory test method is chosen. Generally, the rule that is followed is that the length and width of the plate should be at least three times the plate thickness. (Hutchings, et al., 2005)

There are various test methods available for measuring the residual stresses. These methods are divided into three major categories: (i) destructive, (ii) semi-destructive, and (iii) non-destructive. Large and small differences among the results obtained from these methods exist depending on gradients of stresses, levels of maximum stress values, and types and shapes of specimens used.

It is suggested that the required test area or volume must be less than 1 mm^2 or 1 mm^3 , respectively, to produce an accurate image of the stress field. (Hutchings, et al., 2005) The peak stress values may be missed if the test areas or volumes are too large for the very sharp stress gradients. Thus, the test area or volume size must be optimized for the best data collection with the minimal number of measurements taken, to detect the peak stresses and their values. The magnitude of the stress gradient is inversely proportional to the size of the finite element measured along that gradient. The type of test chosen may produce different types of errors. These errors are due to material characteristics of the steel such as, crystallographic texture, phase composition, grain size, and plastic strain. Residual stresses can also be determined using numerical methods which are discussed next.

2.2 Numerical Modelling

The residual stress distribution can also be determined using numerical methods such as finite element (FE) method. ABAQUS (Simulia, 2008), which is a commercially available general purpose FE code, often used to determine the residual stress distribution in solids and structures (Prime, et al., 2004). ABAQUS can be used to model the behaviour of solids under externally applied loads and body forces. ABAQUS is capable of three-dimensional models subject to static and dynamic loading patterns. Other commercially available FE codes such as ADINA (Hu & Jiang, 1998), ANSYS (Cho, et al., 2004), and Sysweld+ (Price, et al., 2006) are also available and used for determining residual stresses. FE modelling is often used to validate data collected using physical testing methods. Once all of the base residual stress information is collected, parametric studies can be performed. FE modelling can then determine the residual stresses in more complex structures that could otherwise not be tested due to limitations in the physical testing methods.

2.3 Destructive Test Methods

Destructive testing is the most commonly used technique for determining residual stress distributions. This is because the method is convenient and simple. Destructive methods are basically stress relaxation techniques, where the residual stress within a finite element (very small volume) is released and the change in strain is measured. As a result of destructive testing, the sample becomes inoperative and therefore, there must be enough material to test and destroy. Destructive tests produce good results when the nature of the stress field and the magnitude of stress gradient are known. The stress field determined can be triaxial, biaxial, or uniaxial producing a stress gradient that is three, two, or one-dimensional, respectively.

2.3.1 Sectioning Method

The most widely used form of destructive testing is the sectioning method. The sectioning method uses strain gauges to read the initial strain values. The material is then removed around the gauges and the final strain readings are taken. The strain due to residual stress in the metal is the difference between the initial and final strain values. The methods of removal include milling, sawing, grinding, drilling, and lathe turning. The method of metal removal can introduce high stress levels at the surface of the material and must be accounted for. The surface stresses introduced in this method can be minimized or even be removed by using electrochemical methods. Some metal removal methods reduce the residual stress by introducing heat and the process of annealing to the specimen. Chemical or electrolytic polishing is one type of material removal sectioning processes that does not change the actual residual stress pattern in the metal.

2.3.2 Contour Method

Recent interest has been in another form of destructive testing called the contour method. In this method, the specimen is cut by an electro-discharge machine with a flat cut. The specimen deforms as the residual stresses relax. The deviations of the contours are measured using laser scanning. The laser scanning determines the out-of-plane stresses. This method provides a two-dimensional stress field normal to the cut and is best used for measuring the longitudinal stress in

a weld. The method is generally used when the stress levels are low and the specimens are smaller in size.

Hu and Jiang (1998) conducted laboratory tests to determine the ultimate strength of stiffened panels with varying amounts and types of damage. Then they compared the test results with the results obtained from nonlinear finite element analysis. The metal used in the specimens was hot-rolled 350 WT steel (CSA, 2004). The length of all the specimens was 2000 mm (Figure 2.1). The stiffeners were tee sections with flange dimensions of 103.9 mm x 8.1 mm and web dimensions of 136.8 mm x 6.2 mm. The plate was 500 mm wide and 9.7 mm thick. Coupon test data indicted a yield strength of 425 MPa for the plate, 411 MPa for the web, and 395 MPa for the flange. The residual stresses were found in the longitudinal direction (Figure 2.1) using the sectioning method. Figure 2.2 shows the residual stress distributions obtained in the longitudinal direction. The nonlinear finite element models were developed using ADINA (ADINA R & D, 2008). A four-node quadrilateral shell element was used to simulate the plate and stiffeners. The residual stress due to welding was simulated using a thermal stress application. The FE models and the laboratory tests provided similar stress patterns. However, the magnitude varied since the actual welding processes were not as closely monitored. The longitudinal stress values were tensile near the weld with a steep conversion to compressive stress away from the weld (Figure 2.2(a)). The maximum value of stress was almost equal to the tensile yield stress of the metal. The results from the FE method and the physical tests are compared in Figure 2.2. The FE analyses indicated that the behaviour of a stiffened panel is greatly affected by the degree and location of the residual stresses from welding.

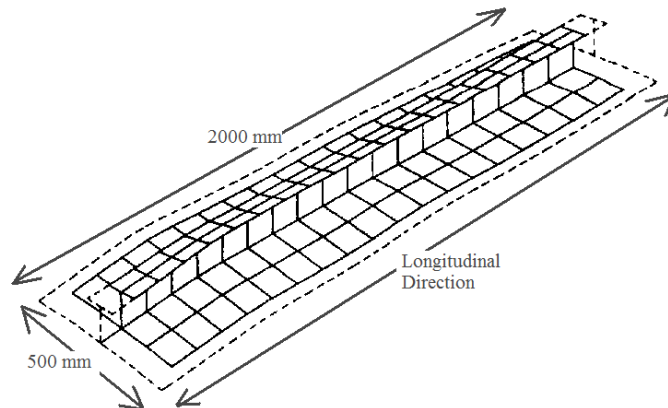


Figure 2.1: FE representation of the specimens (Hu & Jiang, 1998)

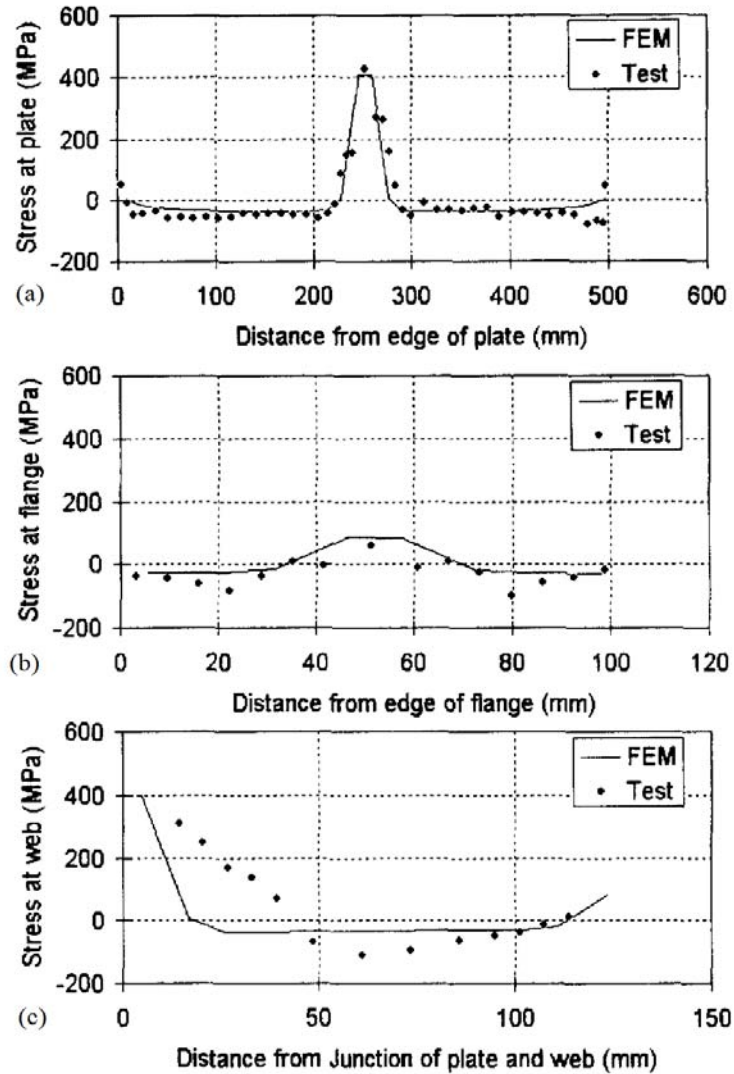


Figure 2.2: (a) Distance from edge of plate (mm) vs. Stress at plate (MPa); (b) Distance from edge of flange (mm) vs. Stress at flange (MPa); (c) Distance from junction of plate and web (mm) vs. Stress at web (MPa). (Hu & Jiang, 1998)

Prime et al. (2004) used the contour method with laser scanning to measure residual stresses normal to the cross-section. The specimens were ferritic steel BS 4360 grade 50D (ASTM, 2007) with minimum yield strength of 355 MPa. The plate was flame-cut to a size of 1000 mm x 150 mm x 12.5 mm with an 8 mm U-groove at the centre. A 12-pass weld was made in the groove using tungsten inert gas (TIG) and metal active gas (MAG) wire for the welding process. The plate was clamped for all passes except the last two, resulting in a 7° bend in the plate from the weld line. The plate was then cut into 200 mm wide strips from the centre of the plate for

testing. The 200 mm samples were measured using the contour method and neutron diffraction. A comparison between two contour methods using the higher resolution non-contact laser surface contouring method and using the conventional touch probe machine, (typically using a Coordinate Measuring Machine (CMM)) were undertaken. The stress distribution from the contour methods were finally determined using FE code, ABAQUS. The results between the two contours methods showed a good agreement. However, higher resolution was possible with the laser scanning, which is the best choice for more moderate variations in stress profiles. The comparison between the neutron diffraction results and the contour methods showed a good agreement as well. The results obtained from the neutron diffraction method and the laser surface contouring method are shown in Figure 2.3.

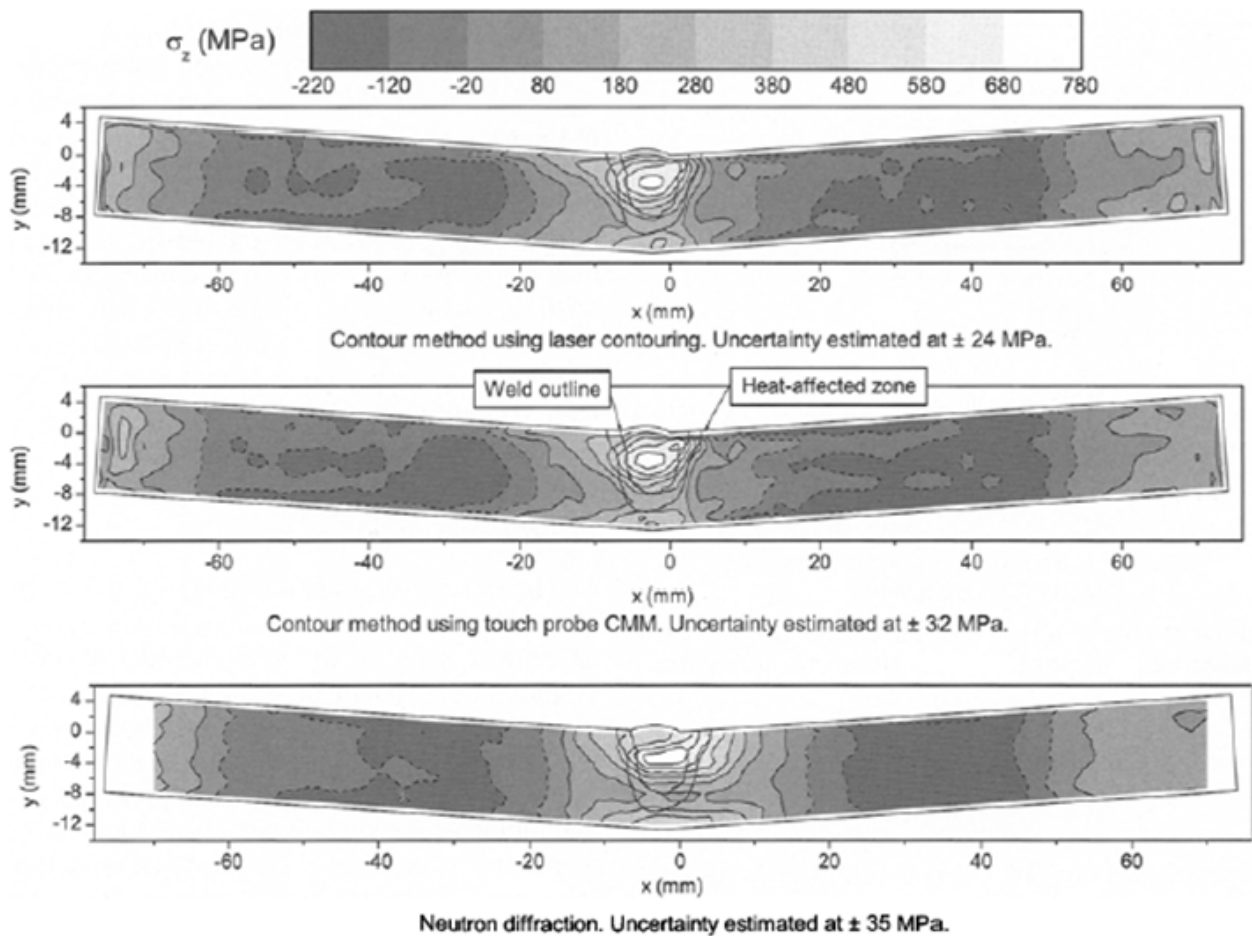


Figure 2.3: The stress maps measured with the contour method and neutron diffraction (Prime, et al., 2004)

2.4 Semi-destructive Test Methods

Semi-destructive test methods are commonly used when the integrity of the sample need to be kept intact. The majority of semi-destructive methods are stress relaxation techniques, similar to the destructive methods. These methods do not completely destroy the component but still inflict minimal damage to the surface of the sample. Examples of semi-destructive test methods are: hole-drilling, ring coring, trepanning, indentation, and spot annealing methods.

2.4.1 Hole-drilling Method

The most commonly used semi-destructive method is the hole-drilling method which uses shallow holes, deep holes, or through thickness holes. The method uses rosette strain gauges to measure the change in the surface strain caused by residual stresses which are released when a hole is drilled in the surface. The remaining material then readjusts to reach equilibrium. Another method called the ring coring method is similar to the hole-drilling method, except a ring is drilled around the strain gauge and a cylinder of metal is isolated around the gauge of strain-free material. The depth of the measurement in both methods is roughly equal to the diameter of the hole. The most accurate results are obtained at a depth of half the diameter. (Hutchings, et al., 2005)

Since the stress is assumed constant over the entire area, these methods should not be used where the stress gradient is high. Local plastic yielding occurs during the drilling process; therefore areas where the stresses are greater than one-third the yield strength must be avoided. The drilling also causes strain hardening in the area around the hole and can cause an error of up to 70 MPa (10 ksi). The thickness of the measured sample must be at least four times the hole diameter and the holes must be spaced at least eight times their diameter to obtain accurate results.

Wilken (1976) examined the use of the hole-drilling method in comparison with the splitting-up (sectioning) method. The hole-drilling method is a semi-destructive method and thus, useful for in-service structures. In comparison with the splitting-up method, the hole-drilling method was found to be much easier to apply and yielded similar results. However, the hole-drilling method

requires the use of complicated mathematical computations and makes several assumptions which may be incorrect. The assumptions are:

1. The stress is uniform across the whole thickness of the sheet.
2. The plate is unlimited in all directions.
3. The validity of Hooke's law.
4. The constant nature of residual stresses in the region of the measuring point.
5. The avoidance of plastic deformation at the edge of the drilled hole, affected by placing the measuring sensor at a certain distance from it.

The accuracy of the hole-drilling method was first compared to the splitting up (sectioning) method on plated I-girders welded in various sequences. The results obtained from the two methods were considered accurate within reasonable error limits and proved the validity of the hole-drilling method. Then hole-drilling experiments were carried out on the welds of the longitudinal frame of a ship. Compressive residual stresses were found in the webs and high tensile residual stresses were found in the flange near the weld. The ship was in service for 18 months and no cracks had developed at the time when the hole-drilling procedure was conducted.

Several ships experienced catastrophic failures in the 1940s. Therefore, Meriam et al. (1946) conducted several tests on actual ship subassemblies to determine a method of measurement of residual stresses from welding. Strain gauges were used and holes were drilled around the gauge to remove the plug of metal containing the gauge. Two measurements were taken: (i) after the welding process and (ii) after the drilling. All strains measured were assumed to be elastic and elastic constitutive equations were used to convert the measured strain values to stresses. Due to the nature of the equipment available at the time, the shortest gauge length for strain measurements was 6 mm ($\frac{1}{4}$ in); consequently the steep nature of the stress near the weld was averaged over the area and precise values could not be obtained. This method only allowed measurement of surface stresses and no measurements through the thickness of the plate were undertaken. All stresses were assumed as to average over the plate thickness, and therefore remain constant through the thickness. The final results found using this method were satisfactory with an error of ± 13.8 MPa (± 2000 psi).

Cho et al. (2004) compared the residual stresses due to welding process and due to post-weld heat treatment using commercially available FE code, ANSYS (ANSYS, 2008), and the hole-drilling method. The type of metal used was SM400B (A131 Gr. 50) with a yield stress of 294.2 MPa, a Young's Modulus of 210.8 GPa, and a Poisson's ratio of 0.3, all measured at 20°C. A ten pass regular butt weld, a twelve pass K-type butt weld, and a nine pass V-type weld were analyzed using the FE method. The ten pass butt weld produced a minimum residual stress of -267 MPa (compression) and a maximum value of 333 MPa (tension). Following the post-weld heat treatment the maximum residual stress found was 38 MPa. The K-type weld produced a range of residual stresses from -300 MPa to 316 MPa which were reduced to a 39 MPa maximum following the heat treatment. The V-type weld produced a minimum residual stress of -239 MPa and a maximum value of 265 MPa, which were reduced to -34.2 and 30.7 MPa, respectively following the heat treatment. The welding process was simulated in ANSYS with the time for the heat transfer analysis for each weld pass as the total weld length (varies) divided by the welding velocity (20 cm/min). The hole-drilling method of measuring surface residual stresses was used on the butt weld and the results were consistent. A post-weld heat treatment was programmed for the K- and V-type welds and produced a significant drop (85%) in residual stress values. The results for the ten pass regular butt weld are compared in Figure 2.4.

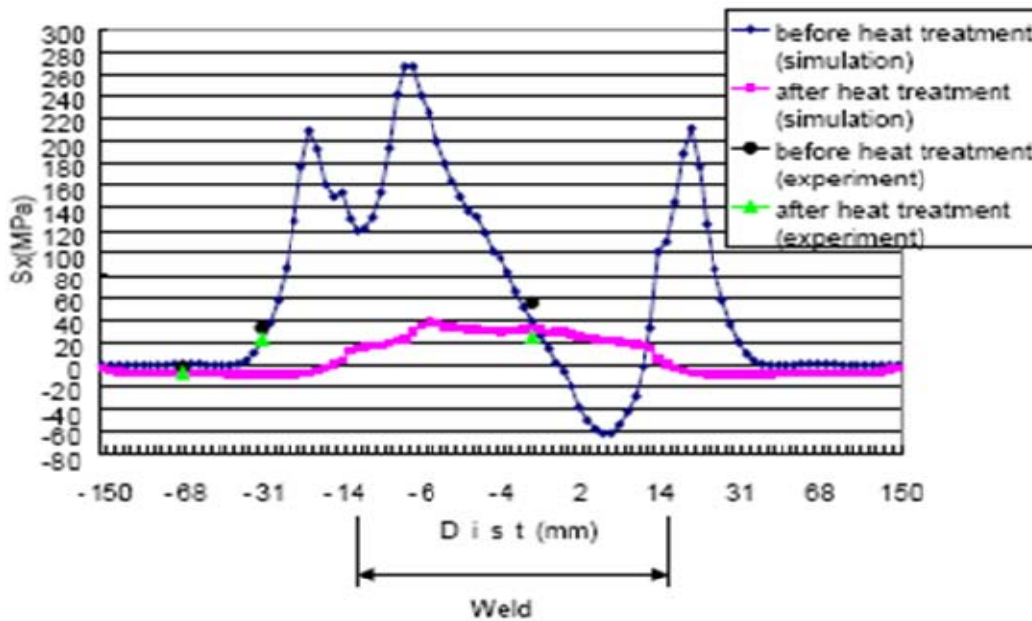


Figure 2.4: Comparison of experimental and simulation residual stresses (Cho, et al., 2004)

Somerville et al. (1977) measured distortions and residual stresses in stiffened panels. The panels were constructed of various sizes and welded with varying sizes and spacing of stiffeners. Two types of steel were used: (a) mild steel (yield stress = 262 MN/m² or 262 MPa) and (b) 'B' quality steel (yield stress = 355 MN/m²). They studied the contraction of the stiffener weld as it cools and the compressive stresses that develop in the plate. They measured surface strains using dial gauges. The stiffeners caused limited or no access to some areas. Thus, modifications in measurement techniques were made using indents instead of drilled holes. The results of these tests provided a very rough estimate of the residual stress field and the distortion effects. The lack of equipment available at the time of testing provides little correlation with the results achieved from more recent experiments.

2.4.2 Blind Hole-drilling Method

Weng and Lo (1992) used the blind hole-drilling method as specified in ASTM E837 (ASTM, 2008b) to measure the residual stresses in welded structures and compared the results to those found using the sectioning method. Since hole-drilling creates local plasticity due to stress concentration in the metal, calibration tests were performed to determine calibration coefficients. The ASTM E837 method provides calibration coefficients but only when stress values are less than 50% of the yield stress. Twelve samples were produced using A36 and A572 grade 50 structural steel plates of thicknesses 15 mm and 32 mm. Residual stresses were measured in three different types of joints: butt, tee, and corner. The welding was done using the submerged arc welding (SAW) method. The diameter of the drill used was 1.57 mm, and the maximum depth of the hole is 1.2 times the diameter (that is 1.88 mm), as specified in ASTM E837 (ASTM, 2008b). The hole-drilling method, therefore, could only measure surface stresses and not the internal stresses. Also, due to the nature of the strain gauges and hole-drilling technique, the residual stresses were measured only to the edge of the weld and the stresses within in the weld and welded part could not be measured. The residual stress near the weld was found to be in the range of 84% to 100% of the yield stress (that is in the range of 312 MPa to 377 MPa) and therefore, required the recalculated calibration coefficients for the local plasticity from drilling the holes. For surface stress measurements, the hole-drilling method was found to have similar results to those found using the sectioning method. The results are shown in Figure 2.5. The

results are plotted by distance from welded edge (mm) versus the residual stress (MN/m^2). Figure 2.5(a) shows the residual stress values found in both the x- and y-directions of the butt welded joint. Figure 2.5(b) shows the residual stress values (MN/m^2) for the tee joint plotted against the distance from the welded edge (mm). Figure 2.5(c) shows the residual stress in the x- and y-directions on the corner welded plate.

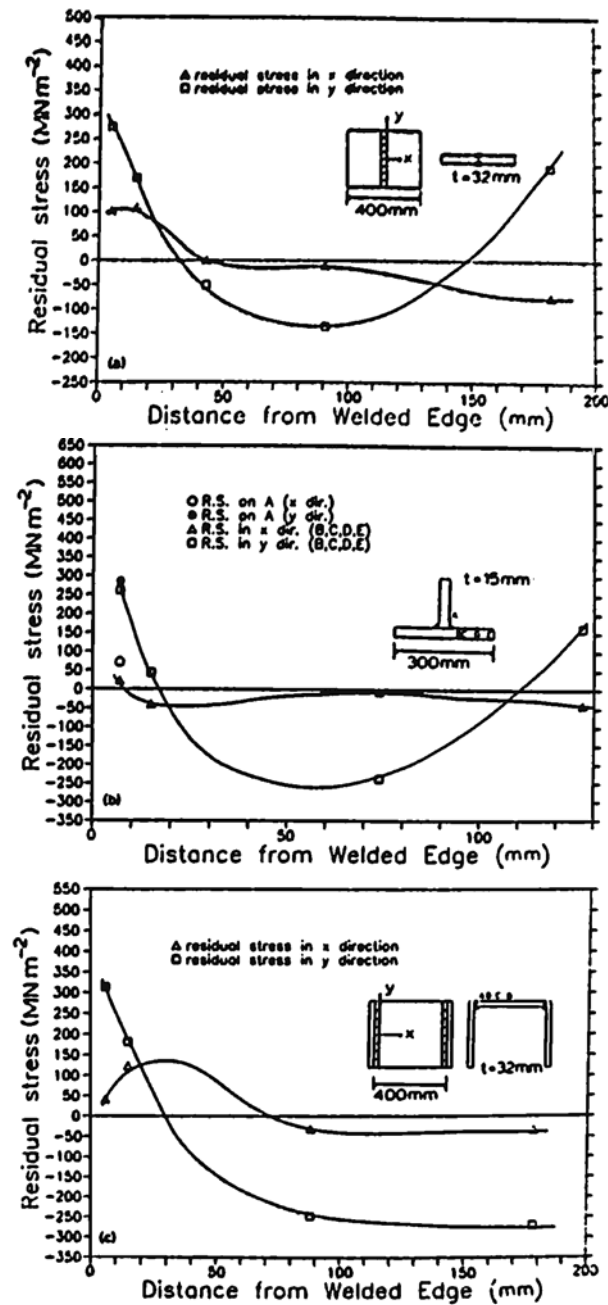


Figure 2.5: Residual stresses in welded specimens (Weng & Lo, 1992)

2.5 Non-Destructive Test Methods

Non-destructive test methods produce no permanent physical damage to the specimen and structure. The most common methods are X-ray diffraction, the magnetic Barkhausen noise technique, and Neutron Diffraction (ND). Since the ND method was used in the current study, a detailed discussion is made on this method.

2.5.1 X-ray Diffraction Method

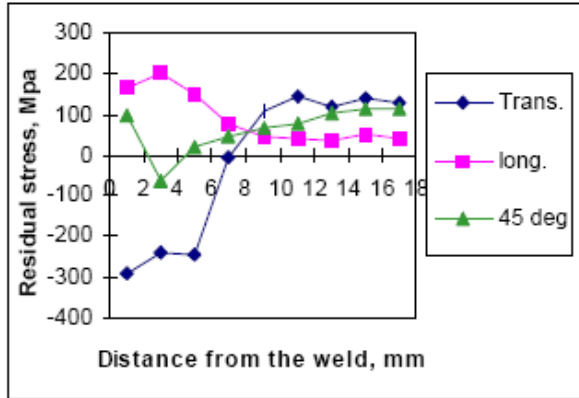
X-ray radiation was discovered in 1896, and used for residual strain determination 20 years later when Bragg's equations were formulated. X-ray diffraction has minimal capability of penetrating the crystalline structures of typical engineering materials. The penetration path length is adjustable by appropriate selection of specific x-ray energies and wavelengths, but is still limited to a few tens of microns. X-rays are diffracted by the cloud of electrons surrounding the nucleus of the sample material. Recently, with the introduction of third-generation synchrotron sources, which provide higher x-ray energies, there are no absorption edges and the attenuation length increases noticeably with increasing energy. It is claimed that the use of synchrotron sources provides relatively high x-ray intensities that they produce leads to path length of centimetres in steel (Krawitz, 2001).

Gao et al. (1998) tested three welded HSLA-100 (ASTM, 2007) steel plate specimens with WIC joint configuration using standard X-ray diffraction to determine the residual stress fields. The plates were 19 mm thick and were heat treated, quenched, hardened to produce yield strengths between 690 MPa and 830 MPa. All specimens were preheated to 50°C then gas metal arc welding was used. The first specimen was welded with no restraints on its edges and with a heat input of 14 kJ/cm. The second specimen was restrained and was subjected to the same heat input as the first specimen (14 kJ/cm). The third specimen was not restrained and welded with a higher heat input of 17 kJ/cm. The X-ray diffraction measurements were acquired using with a portable apparatus. Subsurface measurements were achieved using electropolishing, removing 50 µm layers between each reading. Conventional X-ray diffraction can only measure approximately several microns deep into most engineering materials. The residual stress measurements were taken in the longitudinal, transverse, and 45° directions from the weld bead.

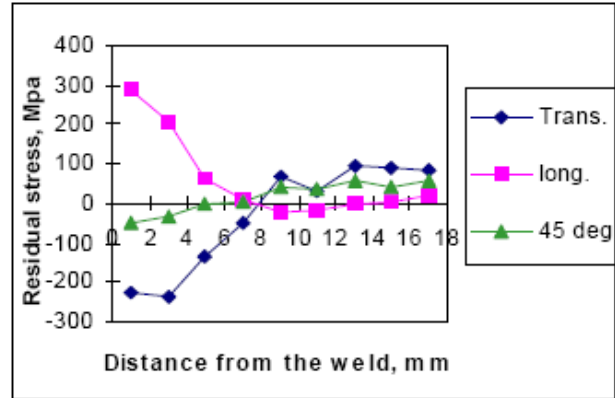
The longitudinal stress component is in the direction of the weld, the transverse stress component is perpendicular to the weld direction, and the 45° direction bisects these two stress components. The results from these experiments show that welding heat input has a significant effect on the residual stress values. A higher heat input produces less residual stress. The decrease is a result of a slowed cooling rate which causes a restriction in shrinkage and phase transformations. They also found that the restraining of the sample also has a considerable effect on the residual stress field. It was found that additional tensile residual stresses may be introduced due to the restraint. However, phase transformations may occur during restraint and produce compressive stresses. The measurements obtained using the X-ray diffraction technique show similar stress fields as previously established ((Weng & Lo, 1992) and (Hu & Jiang, 1998)). The longitudinal surface stresses were tensile near the weld and compressive away from the weld. At the surface of the plate, the transverse stresses were compressive near the weld and increased to tensile stresses as the distance from the weld increases. The stresses measured at 45° from the weld were found to be values within the envelope of the longitudinal and transverse stresses. The results are shown in Figure 2.6 for all three samples for the three different directions of surface residual stresses. Figure 2.6(a) shows the first sample that was welded with the low heat input (14 kJ/cm) and no end restraints. Figure 2.6(b) shows the residual stress in the second sample, with the low heat input (14 kJ/cm) and end restraints, plotted against the distance from the weld. Figure 2.6(c) shows the residual stress values of the third sample, with high heat input (17 kJ/cm) with end restraints, plotted against the distance from the weld.

2.5.2 Magnetic Barkhausen Noise Method

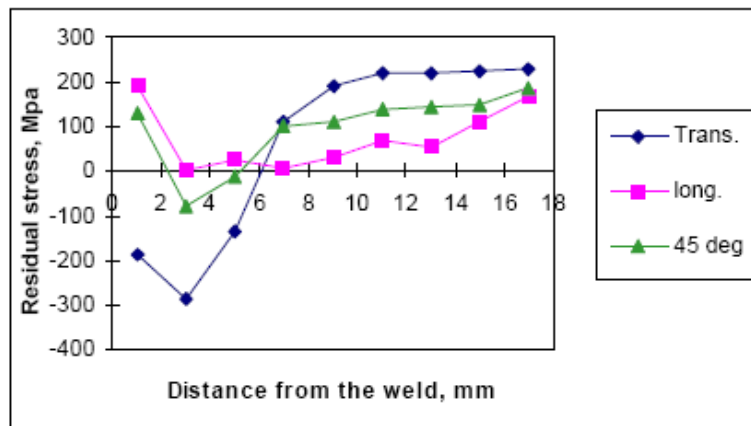
The magnetic Barkhausen noise (MBN) technique is used in ferromagnetic metals to measure the number and magnitude of sudden magnetic reorientations made by expansion and contraction of the magnetic fields. The stresses are measured by the inductive measurement of a noise-like signal, generated when a magnetic field is applied to the metal. However, the depth of measurement only varies between 0.01 and 1.5 mm. The maximum penetration depth depends on frequency range of Barkhausen noise signal analyzed and the conductivity and permeability of the sample material.



(a) Sample RS1



(b) Sample RS3



(c) Sample RS2

Figure 2.6: Surface residual stress distributions of (a) RS1 - 14kJ/cm, no restraint, (b) RS2 - 14kJ/cm, with restraint, (c) RS3 - 17kJ/cm, no restraint (Gao, et al., 1997)

Gauthier et al. (1998) studied the use and validity of the MBN method. The MBN method uses the theory that a ferromagnetic material, such as structural steel, when undergoing a change in magnetization will produce noise in the form of voltage pulses which are induced in a coil set near the sample. The MBN signal increases with the presence of tensile stresses and decrease in the presence of compressive stresses therefore, provides an accurate picture of the residual stress field. The sample used was an L-shaped cold-formed steel beam with a yield stress of 466 MPa and an elastic modulus of 203 GPa. The results were compared with the cutting and sectioning method, the hole drilling method, and X-ray diffraction method. All these methods provided comparable results. The MBN method requires very close ($\sim 0.1 \mu\text{m}$) proximity to the sample and the stress measurements in the corner of the sample are not accurate. Therefore, the use of

this method in measuring welds of stiffeners does not produce acceptable results of the sharp gradients present in the welding stress field.

2.5.3 X-ray Diffraction Method vs. Hole-drilling Method

Rörup (2005) tested a 550 mm x 120 mm x 12.5 mm 355 MPa steel plate with 150 mm x 30 mm x 12.5 mm longitudinal stiffeners were welded on both surfaces of the plate using a two pass fillet weld, as shown in Figure 2.7. The plates were all saw cut from one larger plate. The specimen was loaded with two constant compressive cyclic load ranges; 140 N/mm² or 180 N/mm². The test showed that after an initial fatigue crack, perpendicular to the stiffener, the growth rate increases under the compressive loading cycle until a sudden deceleration or stop in expansion. The initial residual stresses were measured using both the X-ray diffraction method and the hole drilling method. The stresses were found to be lesser on the surface of the plate where the stiffener was welded later, the bottom of the plate. The redistributed stress field at the crack tip due to the cyclic loading was measured using the neutron diffraction and X-ray diffraction methods for comparison. These results were then compared with the FE model and analysis as shown in Figure 2.8. The residual stress was modeled in the FE analysis using heat flux input. The FE analysis predicted similar stress values as was found in the physical experiments. The residual stresses due to the welds controlled the fatigue life of the plate under a compressive cyclic load. The fatigue life of the stiffened panel increased due to the crack propagation phase of the loading. At the weld toe and the crack tip, the residual stresses are in tension. With the introduction of the cyclic compressive loading, the crack propagates in the compressive residual stress region. The crack as it expands, moves the tensile stress region forward as it loses strength, which in turn causes the crack growth to slow or stop completely.

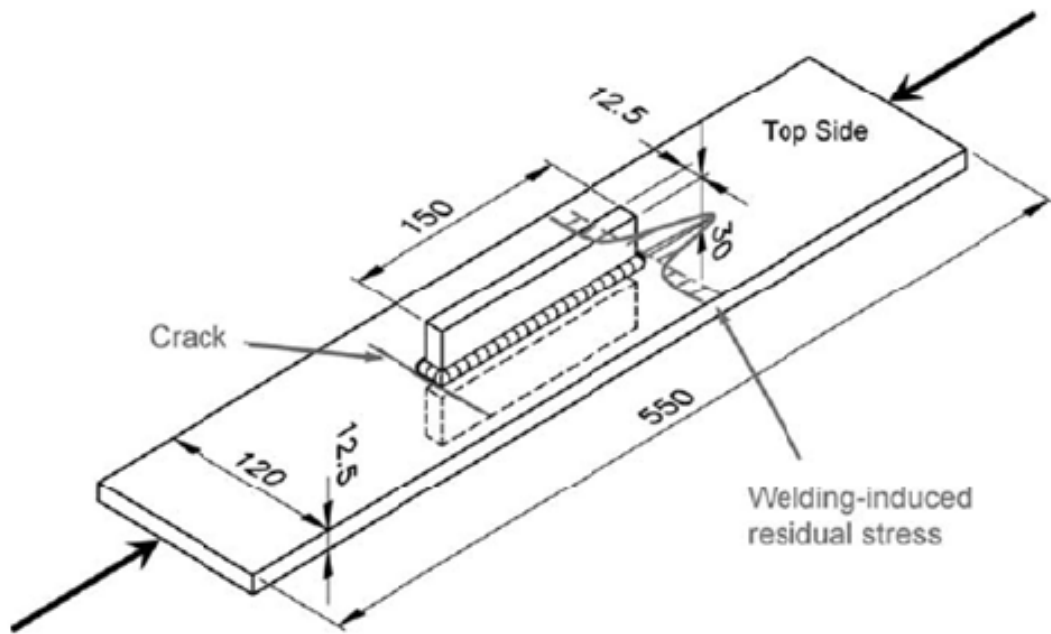


Figure 2.7: Test specimen with a typical crack and residual stress distribution (Rörup, 2005)

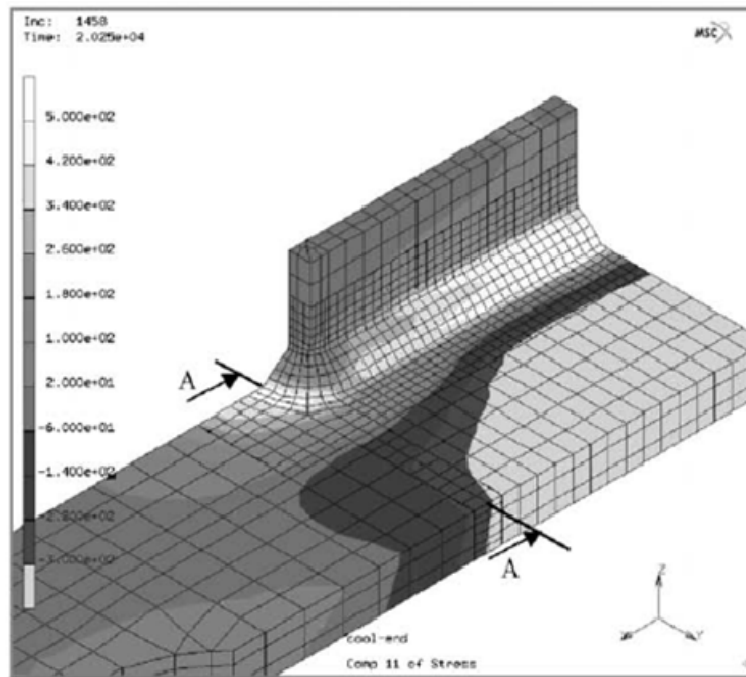


Figure 2.8: Analysis of the weld-induced residual stresses in the longitudinal direction (Rörup, 2005)

2.5.4 Neutron Diffraction Method

Neutron diffraction method is a non-destructive test method. This method uses either a steady state reactor or a pulsed neutron source. A steady state reactor is designed for research and produces a high neutron flux with a minimal amount of heat, in contrast to a reactor used for nuclear power. The reactor generates a Maxwellian distribution of neutron energies that are dependent on temperature. A monochromator is used to remove a single usable wavelength from the neutron beam, which is used to provide the scattering data from the material. A steady state reactor produces a constant wavelength for testing procedures. A pulsed neutron source generates neutrons using a process called spallation. A burst of high-energy particles (protons or electrons) strike a metal sheet which produces a broad range of neutron energies with a broad range of velocities. Therefore, these neutrons will take varying amounts of time to reach the detector or time-of-flight instrument, producing the scattering information of the material.

The ND method utilizes the crystal lattice of the sample material as an atomic strain gauge. The average elastic lattice strain in the gauge volume is calculated as the difference in the lattice plane spacing compared to the lattice plane spacing of the stress-free sample. A beam of neutrons, with wavelength λ , from a continuous source diffractometer is passed through the sample and diffracts in accordance with Bragg's law, as in Equation 2.1.

$$\lambda = 2d_{hkl} \sin \theta_B \quad (2.1)$$

where, d_{hkl} is the lattice spacing of the planes hkl in the crystalline solid, as shown in Figure 2.9.

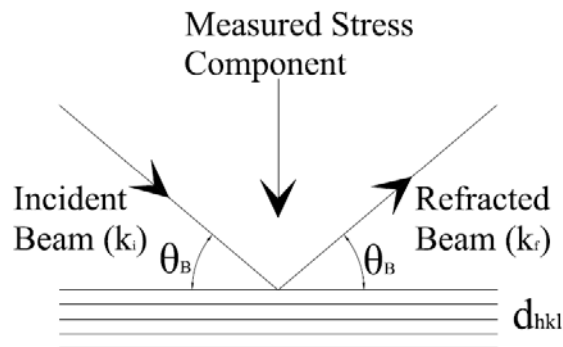


Figure 2.9: Lattice spacing with incident (k_i) and refracted (k_f) beam

$2\theta_{hkl}$ is the angle at which the neutrons are scattered coherently and elastically by the properly oriented lattice planes hkl and is called Bragg's angle. In this figure, the incident beam is labelled as k_i and the refracted beam as k_f . G_{hkl} is the reciprocal lattice vector, perpendicular to the lattice planes.

Crystal space lattices are categorized according to their symmetry, translation, reflection, and rotational characteristics. There are 14 crystal space lattices called *Bravais lattices*, the most common for engineering materials are the *face-centred cubic (fcc)*, *body-centred cubic (bcc)*, and *hexagonal*.

All lattice points are on a plane in the crystal, known as *Miller indices*, and denoted hkl . The hkl plane intersects the axes of the unit cell at a/h , b/k and c/l , where hkl are the lowest integers with the proper ratio of intercepts, as shown in Figure 2.10. As stated before, the perpendicular distance between planes is d_{hkl} .

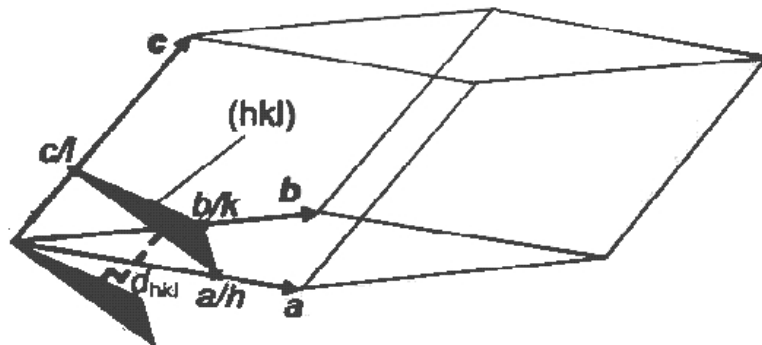


Figure 2.10: Lattice planes (Hutchings, et al., 2005)

The de Broglie wavelength of the neutron, λ , is related to the momentum, p , of the particle as shown in Equation 2.2.

$$p = m_n v = \frac{h\kappa}{2\pi} = h\kappa \quad (2.2)$$

where, m_n is the mass of the neutron, v is the velocity, h is Planck's constant, κ is the wave vector of the neutron with a magnitude of $2\pi/\lambda$. The energy of the neutron is shown in Equation 2.3.

$$E = \frac{1}{2} m_n v^2 = h\nu \quad (2.3)$$

where, ν is the frequency of radiation. For wavelengths useful for diffraction, thermalized neutron energies are significantly less than the equivalent energies of X-rays or electrons.

The lattice spacing (d_{hkl}) expands with tensile stresses and contracts with compressive stresses. The difference in lattice spacing is measured by the shift in Bragg diffraction angle, $2\theta_{hkl}$. Strain in the direction of the scattering vector is given by Equation 2.4.

$$\epsilon_{hkl} = \frac{\Delta d}{d} = -\Delta\theta_{hkl} \cot\theta_{hkl} \quad (2.4)$$

As a neutron approaches the nucleus of an atom, four outcomes are possible: (i) coherent scattering, (ii) incoherent scattering, (iii) absorption by the nucleus, and (iv) the most likely event is no scattering. Coherent scattering relates the space and time between atoms, whereas incoherent scattering is the individual atom relations with space and time. When the neutron is absorbed, the compound formed with the nucleus creates an emission of γ -rays, which may radioactively decay. The coherently scattered neutrons diffract at well-defined angles allowing for ease of measurement, whereas, incoherent scattering is isotropic and creates a background beneath the diffraction peaks, much smaller than the diffraction peaks from the coherently scattered neutrons.

Neutron diffraction can penetrate tens of centimetres into common engineering materials and is a non-destructive testing method that can monitor the stress changes due to an environmental factor, external loading, and body forces. Neutron diffraction measures the strain averaged over a sample volume defined by apertures, called Nominal Gauge Volume (NGV). The Instrumental Gauge Volume (IGV) is the volume over which the average strain is measured in a sample and is therefore, larger than the NGV. The Sampled Gauge Volume (SGV) is the volume over which the strain measurement is averaged, taken from the diffraction peak in the IGV. If the sampled gauge volume is greater than the characteristic volume, then the corresponding strain is not measured since it averages to zero.

James et al. (2006) used neutron diffraction technique for measurement of residual stress in high strength steel (tensile strength > 600 MPa) butt welds and for determination of how residual stress depends on various factors such as, weld heat input, plate thickness, and filler material. The welding method used was metal inert gas (MIG) with a shielding gas composed of 80%

argon and 20% carbon dioxide. The transverse stress measurements were made at mid-depth and 1 mm below the surface. The normal and longitudinal stress values were also collected. All the measurements were completed using the neutron diffraction method. However, the study primarily focused on fatigue cracking, which initiates at the toe of the weld and develops parallel to the weld as a result of transverse stresses. The normal stresses were in compression in the upper portion of the plate and in tension in the lower portion of the plate. However, these values were small and all nearing zero therefore, producing a plane stress problem. The study also evaluated the use of undermatched, matched, and overmatched filler material. The specimen with undermatched filler material exhibited lower tensile maximum stresses than the matched and overmatched specimens. The compressive maximum stresses in the undermatched specimen are associated with the heat affected zone, while in the overmatched specimen; the compressive maximum stresses were outside of the heat affected zone. Specimens with two plate thicknesses were tested: 8 and 12 mm, and the thinner plate showed higher residual stress values than the thicker plate due to the fast rate of cooling, which were worsened by the lesser weld heat input. The details of the specimens are shown in Figure 2.11. The stress values obtained from the 12 mm thick specimen with overmatched weld metal with a low heat input (see Figure 2.11(c)) are shown in Figure 2.12.

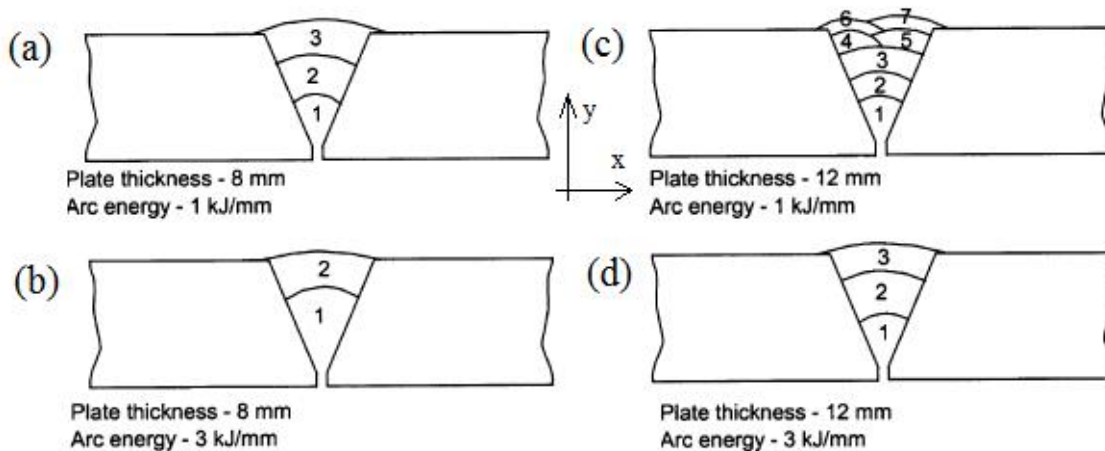


Figure 2.11: Cross-sectional details of the multipass weld runs used to make the butt joints in the 8mm and 12mm thick plates of RQT701 steel - (a) 8 mm plate thickness with low heat input (1 kJ/mm), (b) 8 mm plate thickness with high heat input (3 kJ/mm), (c) 12 mm plate thickness with low heat input, & (d) 12 mm plate thickness with high heat input (James, et al., 2006)

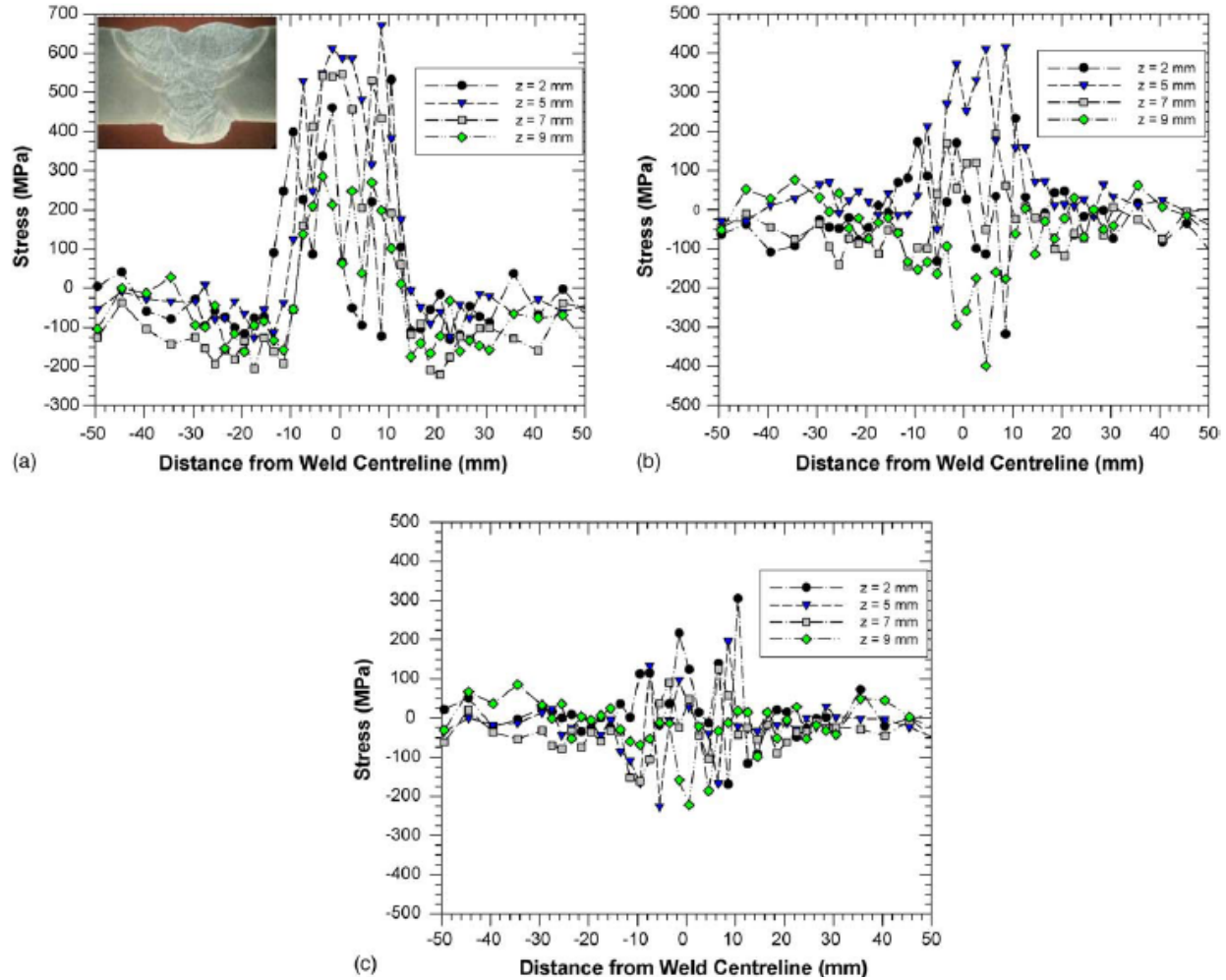


Figure 2.12: Specimen - 12 mm thick, overmatched weld metal at low heat input 1kJ/mm (a) Longitudinal (x) stress profile at four depths (b) Transverse (y) stress profile at four depths (c) Through-thickness (z) stress profile at four depths (James, et al., 2006)

Paradowska et al. (2006) examined the reference samples used in the ND and synchrotron X-ray diffraction (SD) testing. The pseudo-strain values were the object of the testing and relate to the difference between the lattice spacing at a point and the average spacing across the sample. The specimens were low carbon steel welded using the flux-cored arc welding (FCAW) process. The samples were then created using electro-discharge machining (EDM) to generate a cube and a comb for testing. The measurements were taken in the transverse and normal directions of the weld using both methods as shown in Figure 2.13 and Figure 2.14, respectively. The final values showed that both neutron diffraction method and synchrotron X-ray diffraction method, the reference sample may be taken from the parent material. The microstructure and texture in the

weld and the heat affected zone does not warrant the expensive procedure of manufacturing a comb for the specific reference values of each area.

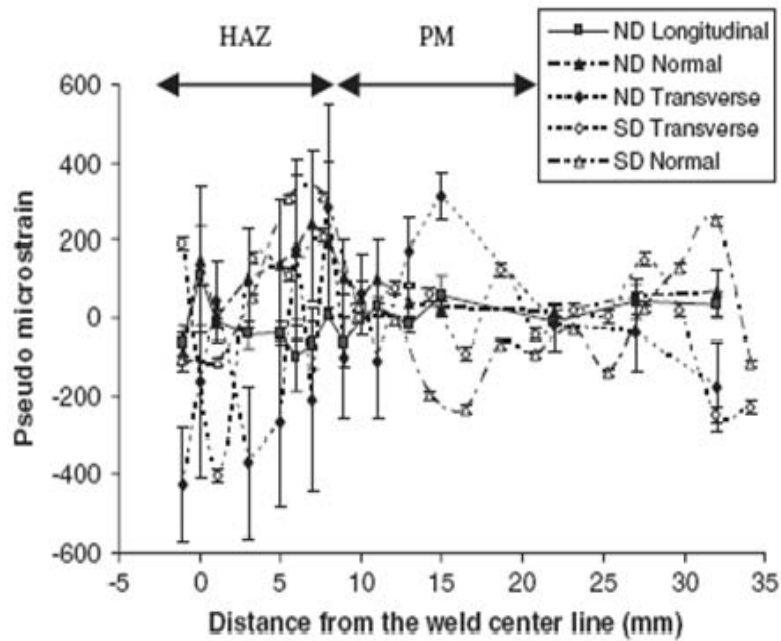


Figure 2.13: Pseudo-strain measured by ND and SD across the weld, (PM = parent material, HAZ = heat affected zone, WM, weld material) (Paradowska, Finlayson, et al., 2006)

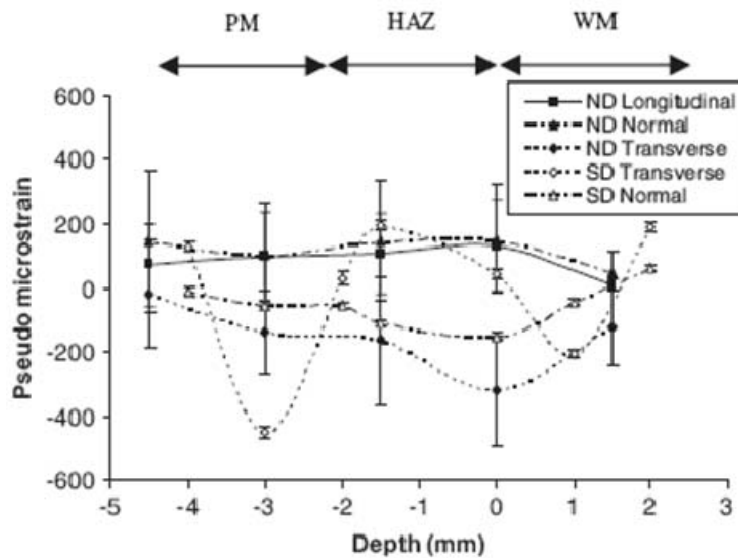


Figure 2.14: Pseudo-strain measured by ND and SD through the thickness (Paradowska, Finlayson, et al., 2006)

Wimpory et al. (2003) measured residual stress in T-plate ferritic steel weldments of 25 mm, 50 mm, and 100 mm thick base plates for residual stress using the neutron diffraction method and the deep hole drilling (DHD) method. The 25 mm thick base plate was welded using a T-fillet weld and the 50 mm and 100 mm thick base plates were welded using partial penetration welds. The 25 mm and 50 mm plates were restrained to prevent distortion, however the 100 mm thick plate (Figure 2.15) was rigid enough and thus, no clamps were used. The finished welded specimens were sliced into 12.5 mm thick samples for measuring residual stresses using neutron diffraction method.

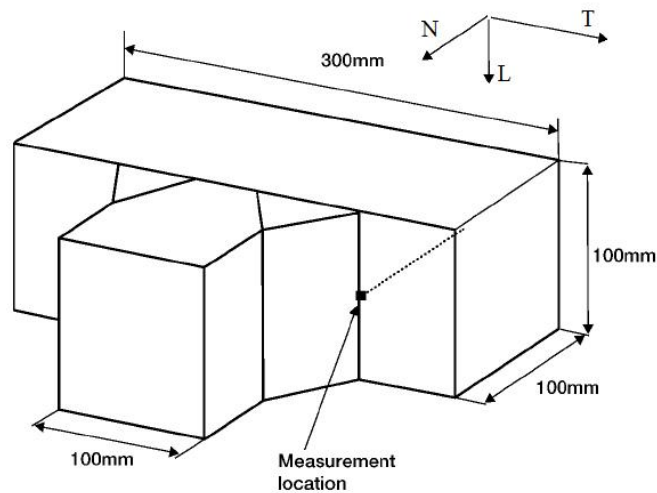


Figure 2.15: Location of deep-hole drilling measurements on the 100 mm thick plate specimen (Wimpory, et al., 2003)

A 100 mm thick section of the 100 mm thick T-plate weld was used for the deep-hole drilling method. The neutron diffraction tests were conducted at three different nuclear reactors; two monochromatic sources and one polychromatic source. The reference samples were taken from the base plate material in an area of no stress. A reference sample should also have been taken in the weld material for comparison. The steps in the deep-hole drilling method were as follows: a smooth reference hole was drilled and measured at various depths and angles then a cylinder surrounding the reference hole was extracted and the reference hole was again measured at the same locations. This method provided the longitudinal and transverse residual stresses. The normal stresses could be obtained if the axial distortions were also measured, but were not recorded in this study. The deep-hole measurements were taken at the point of intersection

between the plate and the weld and continued towards the edge of the plate, as shown in Figure 2.15. Measurements were not taken into the weld and the stiffener. Figure 2.16 and Figure 2.17 show the results obtained from deep-hole method and the neutron diffraction method, respectively. A good agreement was obtained between the two methods. Neutron diffraction measurements were also taken on a post-weld heat treated sample of a 25 mm T-plate weld. The results showed that overall the residual stress in the sample were close to zero, however a post-weld heat treatment is not feasible in the construction of a ship. The results of all of these experiments were also compared with previous experiments that were conducted and again showed a good agreement. The results were also compared with the British Energy R6 and BS 7910 which show representations of residual stress fields for varying weld configurations. This comparison showed that these standards are very conservative and do not provide a very accurate picture of the stress distribution.

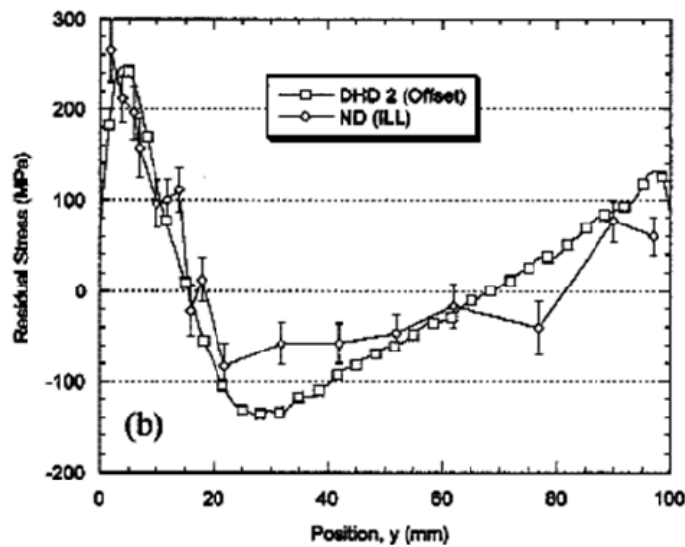


Figure 2.16: Transverse stresses in the 100 mm T-plate - ND measurement on a 12.5 mm slice and DHD measurement (Wimpory, et al., 2003)

Pearce and Linton (2006) used neutron diffraction method to determine the residual stresses within a curved plate and a butt weld specimen. Both samples were constructed from BIS 812 Ema Steel. The measurements were conducted using the 211 peak and neutrons with a wavelength of 1.4 Å. The stresses were measured in the longitudinal, transverse, and normal directions. The results shown in Figure 2.18 have similar profiles as previously measured samples using different methods of measurement.

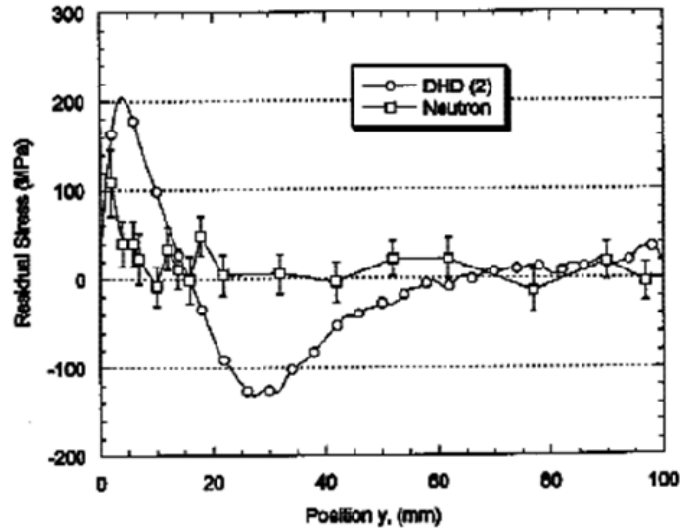


Figure 2.17: Longitudinal stresses in the 100 mm T-plate obtained by ND on a 12.5 mm slice and by DHD (Wimpory, et al., 2003)

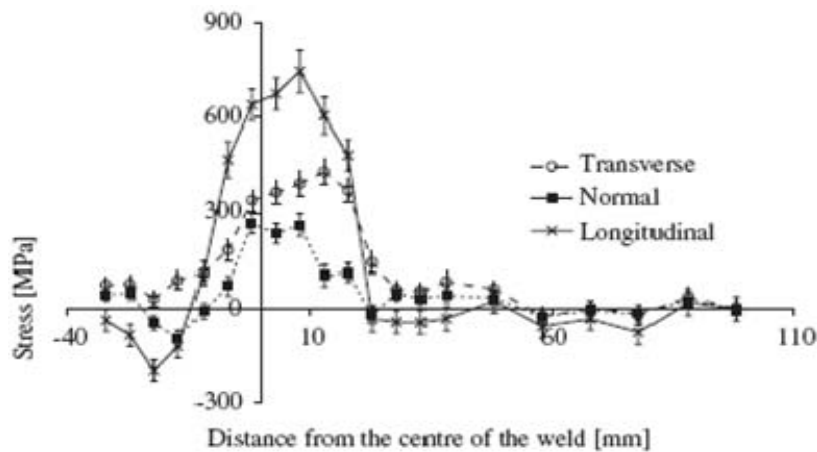


Figure 2.18: Three-dimensional stresses 10mm from surface of side B—flat butt weld (Pearce & Linton, 2006)

Lorentzen and Ibsø (1995) evaluated the residual stresses in welds used in offshore structures using the neutron diffraction method for better understanding of the fatigue life of the structure when imposed to cyclic and stochastic loading. The specimens were constructed of St.52-3 (Fe510C) steel of 8 mm and 16 mm thicknesses, and were butt welded on either side of the plate with 5 mm and 10 mm plates, respectively. No post-weld heat treatments were used. The strain measurements were taken in the longitudinal direction only and the normal and transverse directions were ignored. The two directions were disregarded because of tests that were

previously completed indicates that the principal directions change as a function of depth into the material. Therefore, to properly measure internal strains, the principal axes must be re-evaluated at all measurement depths. Only the surface stresses were found for this study since fatigue cracks generally occur due to the high tensile stresses at the surface of the material. The values obtained showed a maximum residual stress value of 50% the material yield stress.

Webster and Wimpory (2001) suggested procedures for obtaining consistent results using the neutron diffraction method of measurement. Their study shows that by placing the beam apertures as near the sample as possible minimizes the irregularities in identifying the centroid of the sample. Planes that do not exhibit bulk behaviour and are affected by plastic strain must be ignored. Single crystals within these planes are anisotropic and when subjected to different reflections will result in different strains, forming an erroneous field of stress. A proper value for the stress-free lattice spacing must also be obtained. The stress-free values should be taken from the parent material, as well as from the welding material.

Price et al. (2006) examined the residual stresses caused using MIG (metal inert gas) welding of a single bead-on-plate of low-carbon steel and the influence of restraint. The study was conducted using a 200 x 100 x 12 mm plate, where the first specimen was unrestrained and the second specimen was fully restrained by tack welding to a very thick steel plate. A 14 mm weld was made through the centre of the plate as shown in Figure 2.19. The neutron diffraction measurements were undertaken using a wavelength of 1.4 \AA and detector angle of $2\theta_B = 73.5^\circ$. The transverse and normal stresses were found to be low, especially compared to the fully restrained sample, due to the deformation during welding of the unrestrained sample. In the centre of the weld the normal and transverse stresses were compressive for the unrestrained sample and tensile for the fully restrained sample. The peak stress was in the longitudinal direction occurred near the centre of the weld, and was observed to be higher than the specified yield stress of 285 MPa in the parent metal and 445 MPa in the weld metal; this is due to the increased hardness of the steel in the weld region. These peak values were also found to be higher in the fully restrained sample compared to the unrestrained sample, as shown in Figure 2.20. The experimental results of the unrestrained sample were compared with three-dimensional finite element modelling; using a commercial program called Sysweld+. Qualitatively, all of the data for transverse, normal, and longitudinal values were in agreement with the observed values

during the experiments. However, the longitudinal stress values were in disagreement which was a result of the unrefined mesh and the true calibration of the welding heat source in the model.

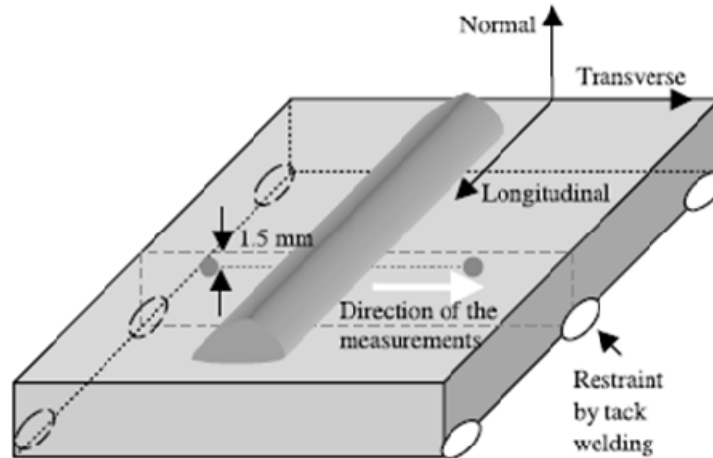


Figure 2.19: The direction of the measurements (transverse x, normal y, longitudinal would be z) using neutron diffraction on the single bead-on-plate (Price, et al., 2006)

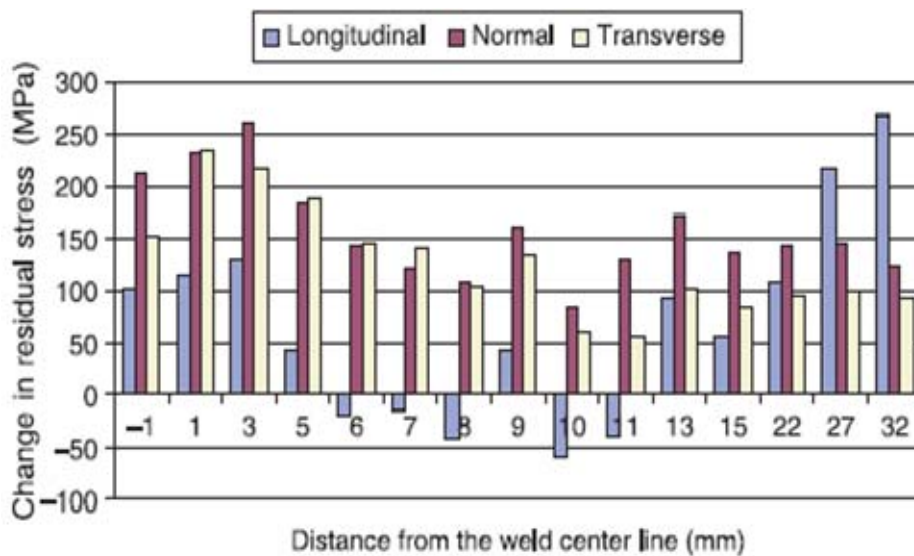


Figure 2.20: Change in stress in fully restrained sample in comparison to unrestrained sample (Price, et al., 2006)

Paradowska et al. (2005) studied the residual stress distribution in single and multi bead-on low carbon steel welds and correlated the data to construction methods and integrity specifications. The effect of restraint, the start and end of the weld and multi-pass welds were closely examined

using the neutron diffraction technique. The hardness and microstructure was determined across the plate, weld, and heat affected zone. The hardness of the weld and the heat affected zone were a result of a critical cooling environment and the lack of a post-weld heat treatment. The results showed that for the unrestrained sample the normal and transverse stresses in the centre of the weld were compressive, whereas in the restrained sample these stresses were in tension. Overall, the transverse and normal stresses were low in the unrestrained sample as it was permitted to deform during the welding process. The longitudinal peak stress in the weld was higher than the yield stress of the plate metal, which corresponds to the increased hardness values in the weld and heat affected zone. The residual stresses in the transverse and normal directions peaked at half the maximum longitudinal stress values, which occurred in the heat affected zone below the middle of the weld bead. The start and end of the weld had high increases in stress levels and surpassed the yield strength of the plate material. For the plates with two, three, and four weld passes, the welds overlapped 50%. When the second weld pass was made, the weld underneath the overlap the residual stress values increased threefold but the uncovered weld portion increased by only 70%. For the third weld pass, the stress remained the same beneath the weld and decreased under the second pass to almost zero. The final weld pass caused the residual stress transfer from all other weld passes into the final weld with a general widening of the peak stress field. The tensile residual stresses in the toe of the weld were reduced, with the fourth weld pass, to more favourable compressive values and lower tensile values. The collected data can be utilized in the design of welds. The longitudinal stresses cause transverse hydrogen cracking, in the toe of the weld the transverse stresses cause the introduction of fatigue cracks, and the sequence of multi-weld passes greatly affects the distribution of the residual stress field.

Holden et al. (2006) investigated several factors relating to measurement of residual stress in welds. These factors include the varying microstructure through the weld and the change in plastic deformation in the weld zone. They emphasized the importance of obtaining the reference samples from a companion weld, in order to understand and determine more accurate stress distributions. Three different samples using neutron diffraction were studied: a butt weld between 8.6 mm thick, highly textured Zr-4 plates, a double-v butt-weld between 10 mm weakly textured high-strength steel plates as shown in Figure 2.21 and a double-v butt-weld between 10 mm hot-rolled 304-type stainless steel plates. The results of their study confirmed that texture

near the weld does not affect the stress field. Also, Type II strains from annealing and cooling can affect the macroscopic strains; therefore, intergranular strains can affect the measurement values.

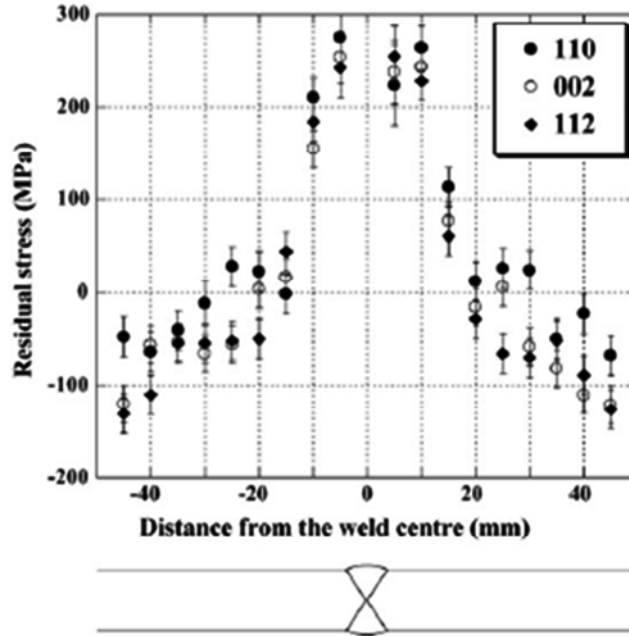


Figure 2.21: Longitudinal stress derived from measurements of $\{110\}$, $\{002\}$ and $\{112\}$ reflections in the high strength steel SNC631 as a function of position through the weld (Holden, Suzuki, et al., 2006)

Ganguly et al. (2006) examined the residual stresses in a 12-mm-thick variable-polarity plasma-arc welded aluminum 2024-T352 alloy plate using neutron diffraction. The residual stresses were measured using a combination of neutron and synchrotron X-ray diffraction after the plate was machined down to 7 mm thickness on either side of the weld (typical machining for the aerospace industry). The comparison of the two methods is shown in Figure 2.22. Synchrotron X-ray diffraction measurements were quick, made high penetration depths and allowed for very small gauge-volumes. However, synchrotron X-rays have very low diffraction angles, so it was impractical to measure strain in the normal direction. Therefore, a combination of synchrotron X-ray measurement for the longitudinal and transverse directions and the use of neutron diffraction for the normal direction provided excellent results. The transverse direction was measured using both methods to compare results obtained from the different machines. A stress-free reference comb, measured using both methods, showed a deviation of d_0 across the weld.

The 12 mm thick specimens were also compared with the contour method and the results were agreeable. It was found that the machining stresses caused by skimming the sample from 12 mm to 7 mm caused little change in the stress distribution. The residual stress results showed high tensile stress in the longitudinal direction near the weld and the stresses in the normal and transverse directions were considerably lesser.

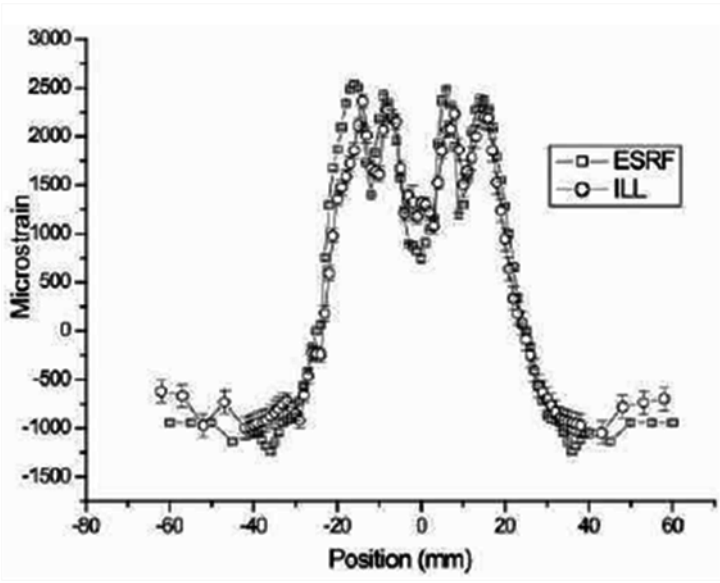


Figure 2.22: Centerline longitudinal strain measured in the two as-welded 12-mm-thick plates using neutrons and synchrotron X-rays (Ganguly, Fitzpatrick, & Edwards, 2006)

3 TEST FACILITY

All the experimental works for the current study were completed at the Canadian Neutron Beam Centre (CNBC) in the Chalk River Laboratories (CRL) located in Chalk River, Ontario, Canada. The CRL is equipped with a CANDU (Canada Deuterium Uranium) reactor, which uses pressurized heavy water (deuterium oxide) and uranium as fuel in the reactor. The source originates in an area of the moderator/reflector specially designed to optimize the thermal neutron flux. The beam tubes transport neutrons from the source to the region beyond the outer shielding of the reactor where neutron scattering instruments are situated. The beam tube usually contains an absorbing shutter to switch off most of the beam, or can be flooded with water to reduce the beam intensity to very low levels. The latter allows work to be carried out safely in the instrument's beam exit region, where monochromating crystals or choppers may be located. The energy of the neutrons in the core of a reactor (2 to 3 MeV) is much too high to be useful for diffraction experiments and therefore the beam is thermalized by a moderator.

Guide tubes are usually of rectangular cross-sections and, as the walls must be optically flat, made of float glass usually coated with a metal such as nickel. The use of a slightly bent guide, of several kilometres radius, allows for the removal of unwanted γ and fast neutron background, being transmitted through the walls into a biological shielding absorber surrounding the guide. The use of guides enables neutron beams to be transported to "guide halls," which are located outside the main reactor shell. The various instruments on the same guide may take different vertical sections of the guided beam or the part of the beam transmitted through the monochromator of an upstream instrument. The layout design of the reactor is shown in Figure 3.1 and it is being used for the current study at the University of Windsor.

The current study used the L3 Spectrometer, an ANDI Diffractometer, that is equipped with a 32-wire position sensitive detector. This equipment is shown in Figure 3.2. The National Research Universal (NRU) Reactor at the CRL produces 120MW, with a 3×10^{18} neutron/m² thermal neutron flux. Key features of the centre include the following equipments.

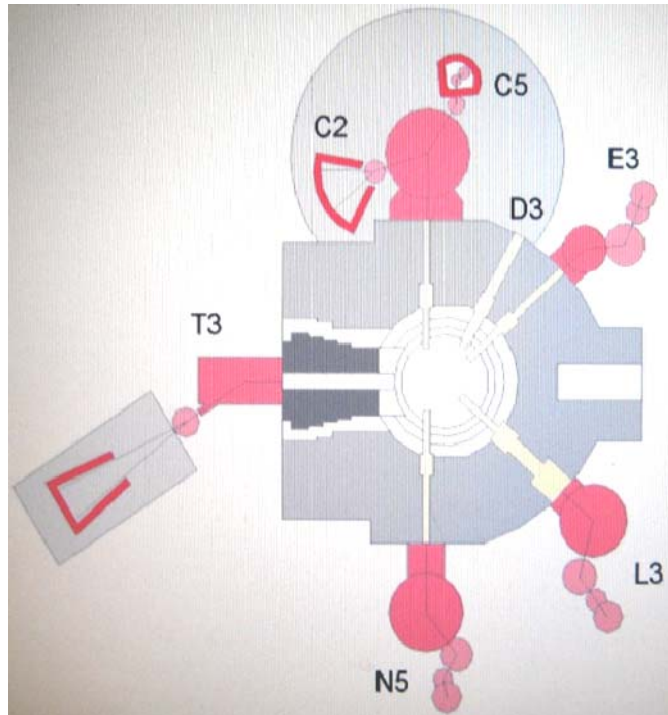


Figure 3.1: Layout of the Chalk River Laboratories (NRC, 2008)

3.1 Stress Scanner

The stress scanner has a typical minimum spatial resolution of 1 mm^3 , locating accuracy better than 0.1 mm , strain precision $0.5\text{E-}4$, 32-element multiwire ^3He detector for high throughput, and a selection of computer-controlled positioning systems, handling loads up to 500 kg .

3.2 Powder Diffractometer

A 800-channel detector spanning 80 degrees of scattering angle simultaneously for high throughput with continuously variable wavelength and adjustable collimation before monochromator 0.2 , 0.4 or 0.6 degrees.

3.3 Weld Station

This is used for in-situ studies of GTAW (gas tungsten arc welding) with a stationary welding torch and moving sample. Typically, the danger of contamination at a neutron laboratory is nominal, with radiation being the chief concern; monitors are usually found on the equipment throughout the laboratory. Access to the measurement equipment is restricted by the use of interlocks when the neutron beam is engaged. All possible radiation is viewed as potentially hazardous, and exposure should be limited. The ALARA (as low as reasonably achievable) principle of exposure to radiation should always be respected.



Figure 3.2: L3 Spectrometer at Chalk River Laboratories (NRC, 2008)

The radiation profile of a sample after testing is assessed by a health physicist; who decides immediate access or request the sample to be placed in a radioactive material storeroom until the radioactive decay can occur. Usually the radiation level of the material to be permitted to leave the facility is $0.1 \mu\text{Sv}$ at its surface. When a subject requires immediate removal from the facility, there are shielding, packaging, and certification requirements that are met to comply with national and international standards.

4 TEST MATRIX

A total of six plate specimens were built and tested at the CRL to determine the true 3-D distributions of residual stresses in typical ship hulls. These six specimens were initially separated in groups and the plan was to test these two groups of specimens in two phases each phase being twelve to fifteen days. However, during the tests on first two specimens, it became obvious that the time required for completion of all the tests for each phase is at least two times than what was originally assumed at the planning stage. As a result, the tests were completed in three phases and each phase required from three to four weeks. However, the test procedures and test results is presented in two phases for the sake of discussions and understanding the results.

The test matrices for two phases are shown in Table 4-1 and Table 4-2, respectively. Specimen 1 was a plane plate (without any stiffener) specimen and it was measured for residual strains that were created from the manufacturing and rolling process of the parent plate. Specimen 2 was stiffened with one stiffener and a high heat input was used in the welding process. This specimen was used to study the effect of welding a stiffener on the plate specimen.

Specimens 3 and 5 were stiffened with two stiffeners and both specimens were built using similar heat input (high heat input). However, the spacing between the two stiffeners was changed. For Specimen 3, the spacing was relatively short (250 mm) whereas, for Specimen 5, the spacing was relatively large (400 mm). Therefore, Specimen 5 was used to study the effect of spacing of stiffeners.

Specimens 5 and 6 were similar specimens and both had two stiffeners spaced at 400 mm on centre. However, the level of heat input was varied in these two specimens. The objective was to study the effect of level of heat input on the distributions of residual stresses and thus, the stress distributions obtained from Specimen 6 were compared with those obtained from Specimen 5.

Specimen 4 was very similar to Specimen 2 that is, both these specimens had one stiffener and level of heat input was also same (high heat input). However, the stiffener in Specimen 4 was shorter than the Specimen 2. PTC members suggested adding this specimen to study the effect of discontinuity of the stiffener which may occur due to constraints in the ship hull geometry and/or other construction constraints.

Table 4-1: Test Matrix for Phase I

Specimen	Plate dimension (L x W x D) (mm)	Stiffener Details	Welding Method	Heat Input
1	400 mm x 400 mm x 9.5 mm	No stiffener	No welding	Not applicable
2	600 mm x 400 mm x 9.5 mm	One 600 mm long stiffener at 150 mm from one edge of the plate	MCAW	High (~2.6 kJ/mm)
3	600 mm x 400 mm x 9.5 mm	Two 600 mm stiffeners spaced 250 mm apart (75 mm from both edges)	MCAW	High (~2.4 kJ/mm)

Table 4-2: Test Matrix for Phase II

Specimen	Plate dimension (L x W x D) (mm)	Stiffener Details	Welding Method	Heat Input
4	600 x 400 x 9.53	One 400 mm long stiffener at 150 mm from edge along 600 mm direction	MCAW	High (~2.5 kJ/mm)
5	400 x 600 x 9.53	Two 400 mm long stiffeners spaced 400 mm apart (100 mm from both edges)	MCAW	High (~2.5 kJ/mm)
6	400 x 600 x 9.53	Two 400 mm long stiffeners spaced 400 mm apart (100 mm from both edges)	MCAW	Moderate (~1.75 kJ/mm)

5 MATERIAL PROPERTIES AND WELDING SPECIFICATIONS

5.1 Mechanical Properties

The material used in this study for the plates and stiffeners was 350 WT steel (CSA, 2004). Mechanical properties of the parent plate metal, the stiffener metal, and the weld wire metal are shown in Table 5-1. Quantity of material required for both phases was ordered at the same time to ensure use of same materials for both phases. All of the specimens were cut from two large plates using water-jet technology in order to minimize the additional residual stresses induced by the cutting process. The stiffeners were L-shaped of dimension 127 mm x 76.2 mm x 9.5 mm. They were cut from one large stiffener using a band saw, which is a cold-cut method.

Table 5-1: Mechanical Properties of Material

Metal	Grade	Average ultimate strength (MPa)	Average yield strength (MPa)	Elongation at rupture (%)
Plate	350WT	527.5	405	41
Stiffener	300W	507.3	350	39
Weld Wire	E70C-6M H4	512.7	390	35

Quasi-static tension (pull) tests were conducted according to ASTM Standard (ASTM, 2008a) in the Structures Laboratory at the University of Windsor. Two samples cut from the plate material were tested and showed to have higher yield strength than recommended for a 350 WT steel (CSA, 2004). The average modulus of elasticity and stress at upper yield point (first yield stress) for the plate material obtained from the pull tests are 208 GPa and 405 MPa, respectively (Figure 5.1). The modulus of elasticity of the angle section was found to be 204 GPa and the first yield stress was found to be 350 MPa. The yield stress was determined from the first non-linear point (first yield point) of the nominal stress-strain plot. Full nominal stress-strain curves for two plate

samples and two angle samples are shown in Figure 5.1. Two coupon specimens from weld pool of weld material were prepared and tested and the nominal stress-strain plots obtained from these one of these specimens are shown in this figure as well. The second weld pool specimen was tested to find the elastic modulus of the material. The upper yield point of the weld metal was found to be 390 MPa and the modulus of elasticity was 209 GPa.

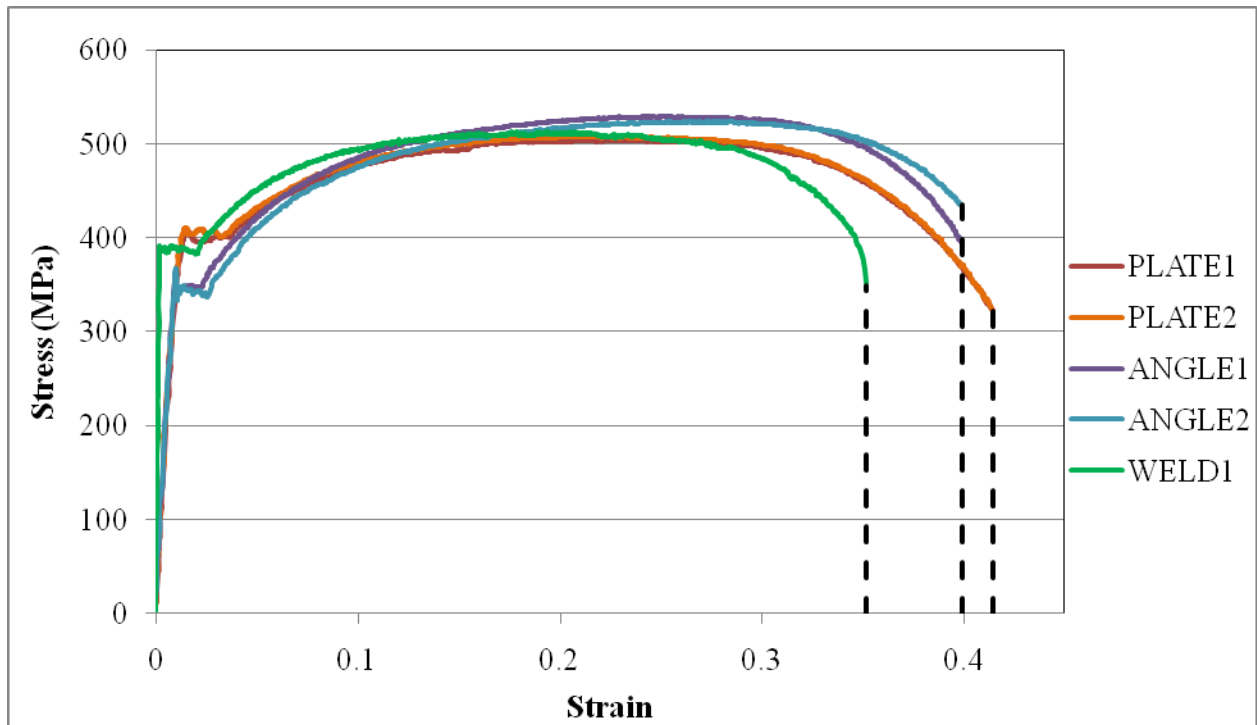


Figure 5.1: Nominal Stress-Strain Behaviour of Plate and Angle

5.2 Welding Specifications

Metal core arc welding (MCAW) process was used for welding the stiffeners for both phases. A licensed welder at the Windsor Welding Institute, Windsor, ON, completed all the welding processes. The specimens were fully restrained during the welding and the cooling process (See Figure 5.2). Large C-clamps were used to restrain the specimen to the welding table. Six clamps were used on the plate as shown in Figure 5.2 and two additional clamps were used to hold each stiffener in place during the welding and cooling process. Specimen 1 was accidentally released from restraints within ten minutes of completion of the welding and this caused a 5° bend

upwards in the plate on one corner of the parent plate. No bending or other deformation or distortion was noticed in other specimens in both phases.

The heat input used was calculated to be higher (and was controlled using a constant current and a constant welding speed as shown in Table 5-2) in both specimens of Phase I. The properties of the wire metal that was used were detailed in the previous section. The diameter of the wire metal for Phase I was 0.89 mm (0.035 in). Welding for Phase I was completed manually by the welder and as a result, an unwanted stop and start occurred in welding of Specimen 1 and welding of second stiffener of Specimen 2. However, later on it was suggested that the start and stop be taken as a parameter to study how residual stress pattern changes if an accidental stop and start occurs in the welding in real ship hull construction.

A welding gun onto an automated trolley system that allowed the welding gun to move at a constant speed was used in Phase II to avoid the problem of stop and start that occurred in Phase I and also to obtain a more consistent weld. As a result, welding was not stopped and a more consistent and uniform weld was achieved in Phase II and the heat input level could be controlled in a desired manner. The heat input for Specimens 4 and 5 were kept at a higher level similar to what was used for the specimens in Phase I. An average value of the heat input used in Phase I was used for Specimens 3 and 4 of Phase II and thus, the level of heat input for these two specimens for Phase II was high (~2.5 kJ/mm). The heat input level for Specimen 6 was lowered to the level of moderate heat input (~1.75 kJ/mm) as shown in Table 5.3 to study the effect of heat input on the residual stress distributions. The diameter of the wire metal for Phase II was 0.89 mm (0.035 in) for Specimens 4 and 5, and was 1.14 mm (0.045 in) for Specimen 6. Table 5-3 shows the welding specifications used for Phase II.

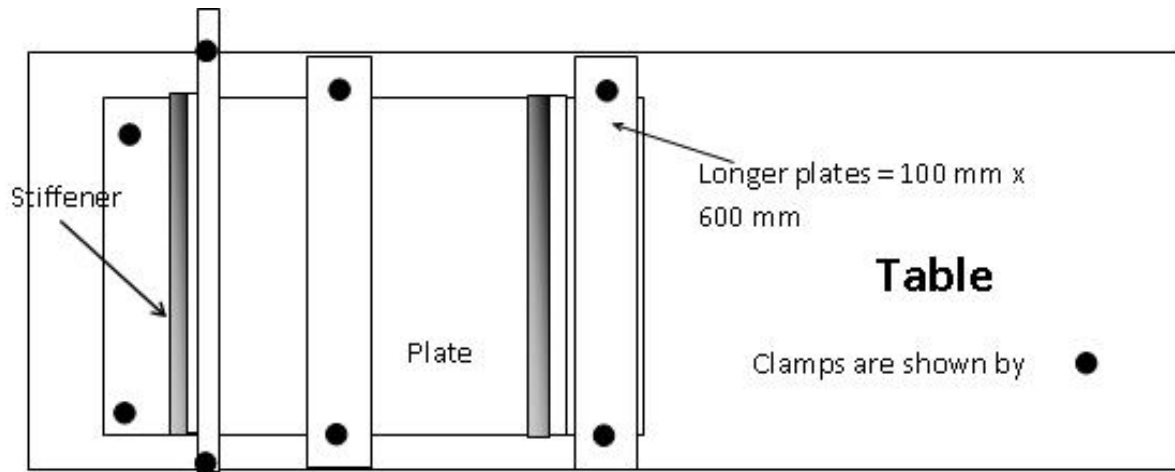


Figure 5.2: Clamp locations during welding

Table 5-2: Welding Specifications Phase I

Specimen	Stiffener	Average Voltage (V)	Average Current (A)	Wire Speed (mm/sec)	Total Time (sec)	Travel Speed (mm/min)	Average Heat Input (kJ/mm)	Number of Stops	Cooling Time (min)
2	1	25.6	185	231.1	338	106.5	2.6	1 for 1 minute	55
3	1	25.4	185	231.1	270	133.3	2.4	None	120
	2	26	188	231.1	320	112.5		1 for 1 minute	120

Table 5-3: Welding Specifications for Phase II

Specimen	Stiffener	Average Voltage (V)	Average Current (A)	Wire Speed (mm/sec)	Total Time (sec)	Travel Speed (mm/min)	Average Heat Input (kJ/mm)	Number of Stops	Cooling Time (min)
4	1	27.2	191	228.6	199	75.2	2.5	None	80
5	1	27.2	190	228.6	210	109.1	2.5	None	1080
	2	27.6	171	228.6	195	123.1		None	1020
6	1	29.2	271	232.8	90	266.7	1.75	None	65
	2	29.2	273	232.8	87	275.9		None	60

6 TEST SETUP AND REFERENCE SAMPLES

6.1 Test Setup

The neutron diffraction (ND) method was used to measure all three strain components and measurements were carried out on the L3 Spectrometer at the Chalk River Laboratories (CRL), Canada. The test set-up was required to be changed and adjusted for each specimen and for measurements of each stress component since the specimen dimensions were very large. As a result, the time required for stress measurements was almost three times of what was originally estimated. The test set-up required specialized skills and careful attention. A special mounting hardware was required to be built to ease some of the set-up difficulties that were encountered during strain measurements.

The centre of rotation of the mounting platform was located by moving the horizontal plane (X and Y components) as well as rotating the ψ angle (angle between the neutron beam and the detector). The centre of rotation was determined in order to align the incident and scattered slits for alignment of the specimen. It is not possible to identify the exact location of the measurements if proper alignment is not ensured.

There are two telescopes that were used to align the centre of rotation. The first telescope called the “tilted telescope” (Figure 6.1) is used to sight the y-centre and the second telescope called the “level telescope” (Figure 6.2) is used to sight the x-centre. In order to align each of these telescopes properly a wire is mounted (Figure 6.3), driven, and rotated until the telescopes are aligned. Once the centre is found the values are preset to zero and a plumb bob is adjusted to coincide with the centre as well. This plumb bob was used as a back-up for centering in case the telescopes were accidentally knocked out of place during measurements. The rotation of ψ (angle between the neutron beam and the detector) is adjusted to the centre of rotation as well as the incident and detector slit positions.

Tilted telescope



Figure 6.1: Tilted telescope pointed at the y-centre of rotation of the specimen



Figure 6.2: Level telescope pointed at the x-centre of rotation of the specimen

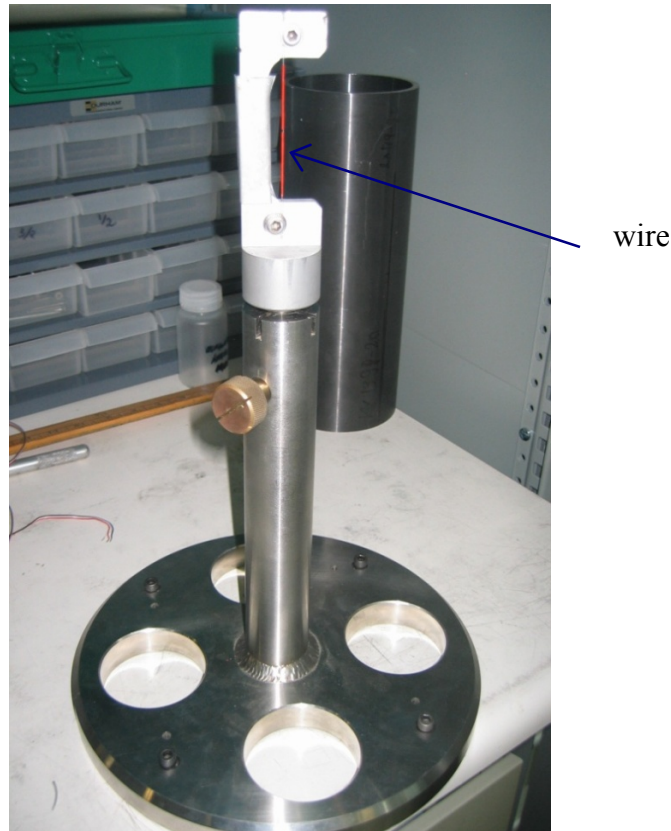


Figure 6.3: Wire mount used to sight centre of rotation with telescopes

A computer software program called “*powder*” was used to determine the initial wavelength (λ) that was used in the experiments. The program was an in-house program developed by the scientists at the CNBC and the full details of the program will not be disclosed here. The program calculates the optimal wavelength for the test material to be measured. The steel specimens tested have a main component *bcc* phase with numerous Miller indices. Once the most favourable wavelength was chosen using the *powder* program, the optimal reflection angle was calculated for the monochromating crystal, which in this study a Germanium (Ge) crystal was used.

For Phase I, two different set-ups and numerous scattering slit sizes were used. The specifications of each set-up are shown in Table 6-1. The second set-up was necessary when the plate specimen was positioned for the 45° longitudinal strain measurement since in this orientation the neutron counts were very low. By changing the wavelength (λ) and subsequently, the reflection of the monochromating crystal ($2\theta_M$) and ψ angle, it was possible to continue the

scans at a relatively faster rate. The scattering slit size also varied throughout the specimens from as small as 1 mm x 1 mm x 2 mm to as large as 1.5 mm x 1.5 mm x 20 mm. The count times for each measurement were optimized to collect the required amount of data in a shorter amount of time, given that there were so many measurement points where the stresses were required to be collected across all of the specimens.

Table 6-1: Set-up Specifications for Phase I

Set-up	Wavelength	Reflection of Ge crystal	2 θ M	Ψ
1	1.665 Å	115	98.93°	-44.9°
2	1.5398 Å	115	90°	-41.4°

For Phase II, only one set-up but numerous scattering slit sizes were used. The specifications of the set-up are shown in Table 6-2. The scattering slit size also varied throughout the specimens from as small as 1 mm x 1 mm x 2 mm to as large as 1 mm x 1 mm x 40 mm. The set-up was the same as the secondary set-up used in Phase I. The count times for each measurement were optimized to be able to collect the many measurement points across all of the specimens.

Table 6-2: Set-up Specifications for Phase II

Set-up	Wavelength	Reflection of Ge crystal	2 θ M	Ψ
1	1.5398 Å	11 <u>5</u>	90°	-41.4°

6.2 Stress Free Samples and Calibration

The stress-free reference samples for the plate were produced on-site at the CRL. Three small “matchstick” prisms were cut, with the longest dimension in the longitudinal direction of the plate specimens, as shown in Figure 6.4. The first reference sample had dimensions of 2 mm x 2.5 mm x 20 mm (Normal x Transverse x Longitudinal). The second reference sample was shorter than the first one. However, the second specimen was also parallel to the longitudinal axis of the plate with dimensions of 2 mm x 2.5 mm x 15 mm (Normal x Transverse x Longitudinal). The third reference sample was cut perpendicular to the longitudinal axis with dimension of 2 mm x 10 mm x 2.5 mm (Normal x Transverse x Longitudinal).

The nickel calibration is a small cadmium container filled with nickel powder, shown in Figure 6.5. The nickel calibration values were used in all of the final stress value calculations. The angle between the incident beam and the refracted beam is φ and the φ_0 is the angle corresponding to the reference sample. The values of λ and φ_0 , as well as their error values, were found using a standard deviation and chi-squared fit. The nickel calibration was completed at the beginning and end of each set-up to ensure consistency in the numbers throughout the entire set of measurements. The values for λ and φ_0 were specific to one test set-up and for a specific value of $2\theta_M$. The nickel calibration had to be repeated several times during measurements for specimens in Phase II due to scheduled shutdowns of the reactor and unexpected power outages to ensure that no instrumentation was affected by these events.

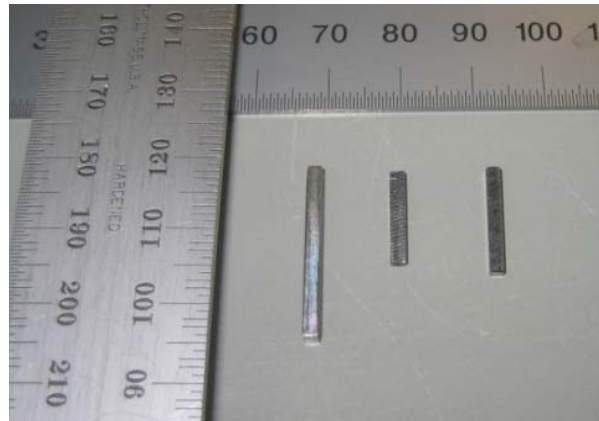


Figure 6.4: Stress-free reference samples



Figure 6.5: Nickel-reference sample in cadmium container

7 TEST RESULTS FOR PHASE I

As mentioned earlier, a total of six specimens were tested to measure the three-dimensional (3-D) stress distributions. Phase I included two stiffened plate specimens and one plane plate specimen (see Table 4-1) and Phase II included three stiffened plate specimens (see Table 4-2). The details of each test specimen and the test results for specimens in Phase I are discussed in the subsequent sections and sub-sections.

7.1 Specimen Details

7.1.1 Specimen 1

The test matrix (Table 4-1), test setup, test method, and welding specifications are discussed in earlier sections. Specimen 1 with its dimensions is shown in Figure 7.1. This specimen was tested to determine the residual stresses that were created due to the manufacturing and rolling process of the base plate. The dimension of this specimen are 400 mm long x 400 mm wide x 9.5 mm thick and the specimen had no stiffener.

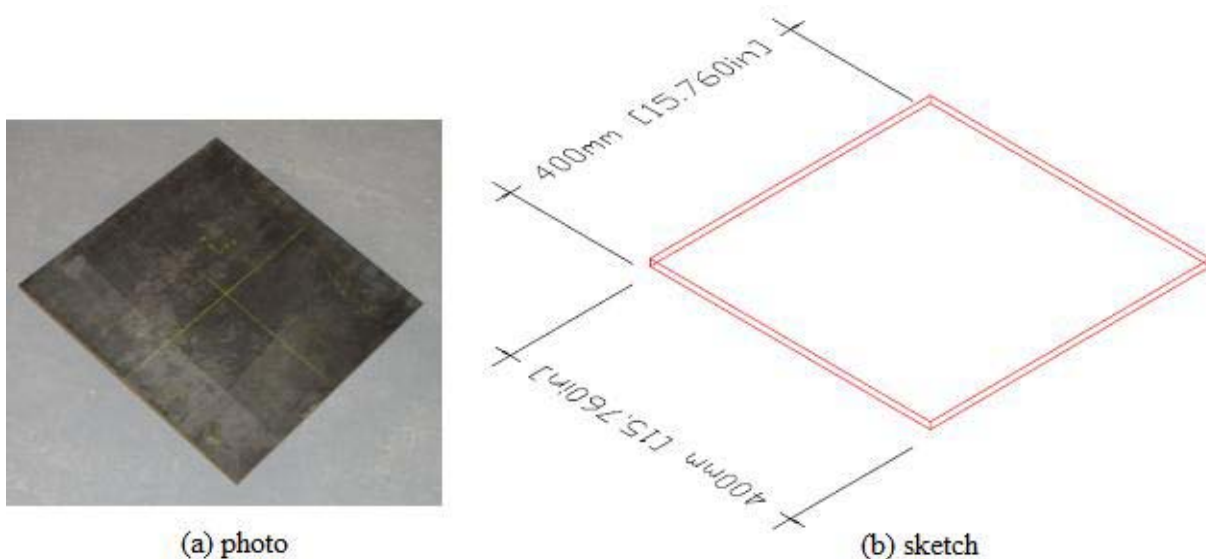


Figure 7.1: Specimen 1 (a) is a photo and (b) is the sketch

7.1.2 Specimen 2

This specimen was a stiffened plate and only one 600 mm long stiffener was welded. The dimension of this specimen are 600 mm long x 400 mm wide x 9.5 mm thick and one L-shaped stiffener of size 127 mm x 76.2 mm x 9.5 mm (Figure 7.2).

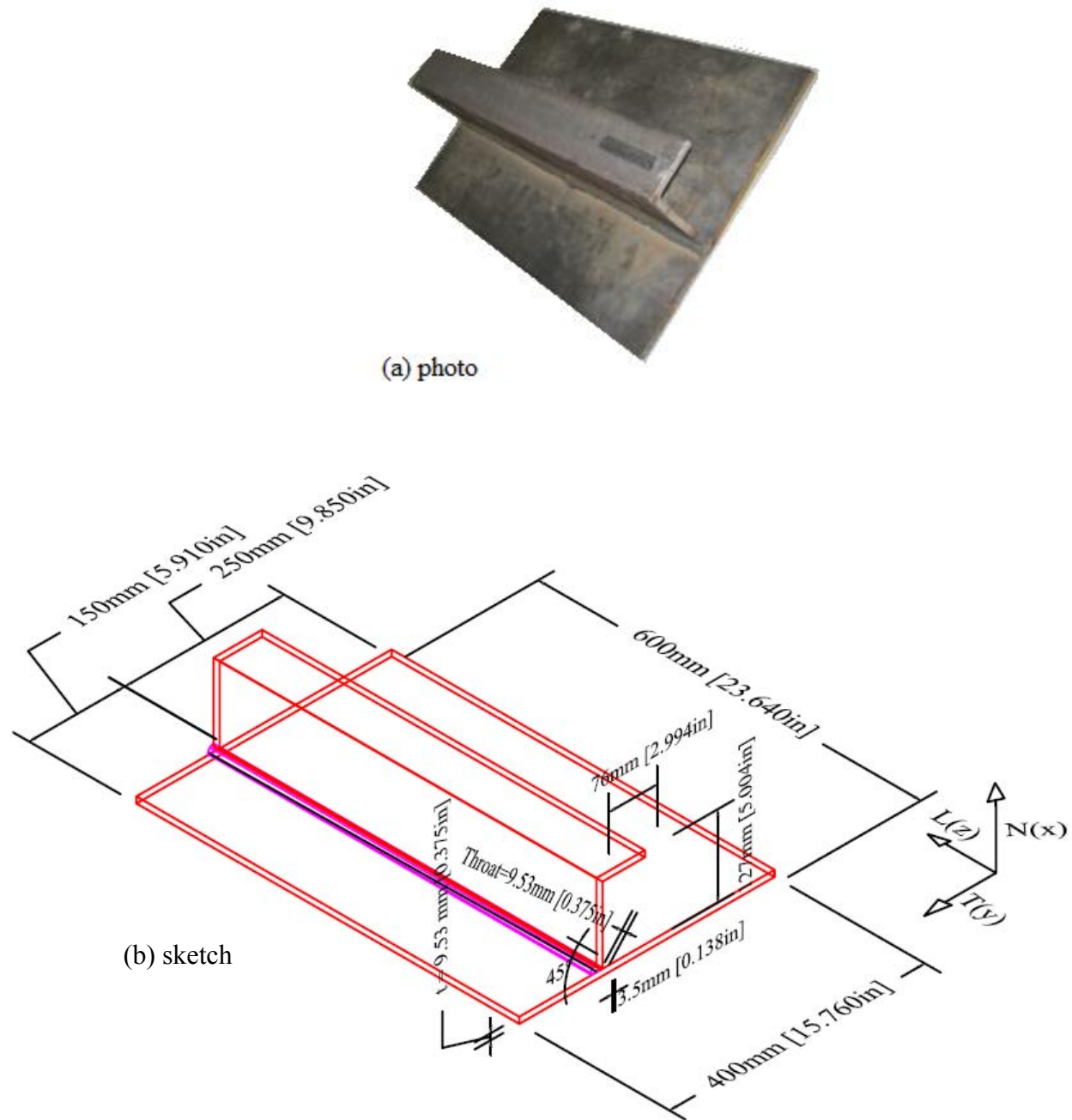


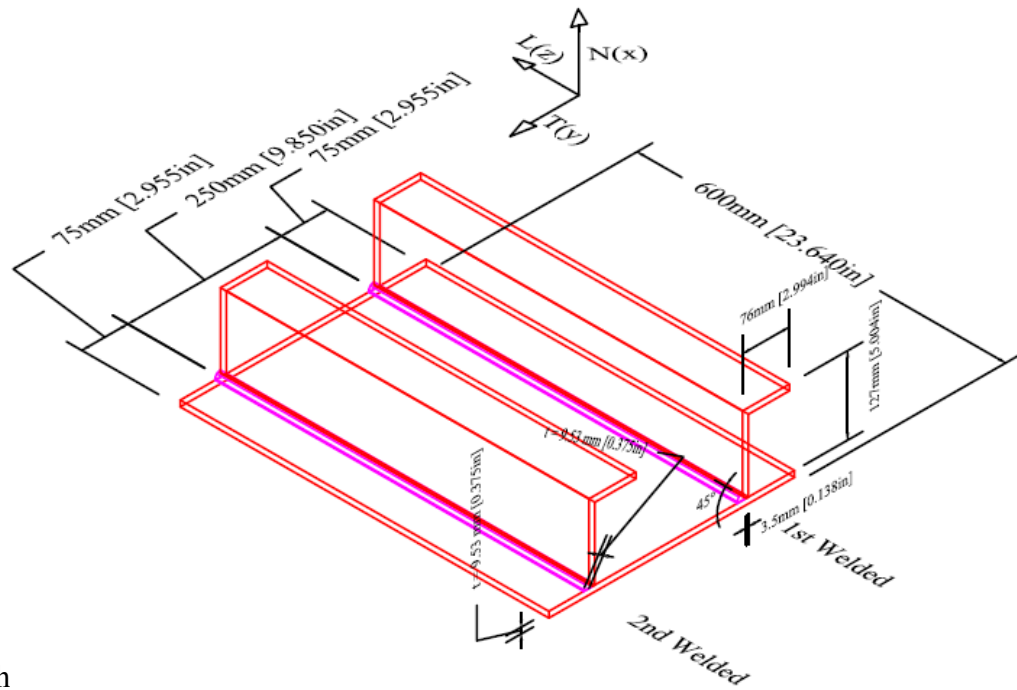
Figure 7.2: Specimen 2 (a) is a photo and (b) is the sketch

7.1.3 Specimen 3

This specimen as shown in Figure 7.3 was a stiffened plate and two 600 mm long stiffener at a spacing of 250 mm on centers were welded. The dimensions of this specimen are 600 mm long x 400 mm wide x 9.5 mm thick and with two L-shaped stiffeners of size 127 mm x 76.2 mm x 9.5 mm.



(a) Photo



(b) sketch

Figure 7.3: Specimen 2 (a) is a photo and (b) is the sketch

7.2 Test Results

7.2.1 Specimen 1

Specimen 1 as shown in Figure 7.1 and Figure 7.4 was a plane plate with dimensions of 400 mm long (L) x 400 mm wide (T) x 9.5 mm thick (N). No stiffener was welded on this specimen. The objective was to determine if there were any stresses in the parent plate due to the hot rolling process and the cutting process. The specimen was measured for residual strain along the longitudinal (L) and transverse (T) directions at seven depths through the normal (N) direction. Figure 7.4 shows the origin (point 1) and the lines (1-2 and 1-3) on which the measurements were taken. All the three normal strain components were measured to calculate all three stress components.

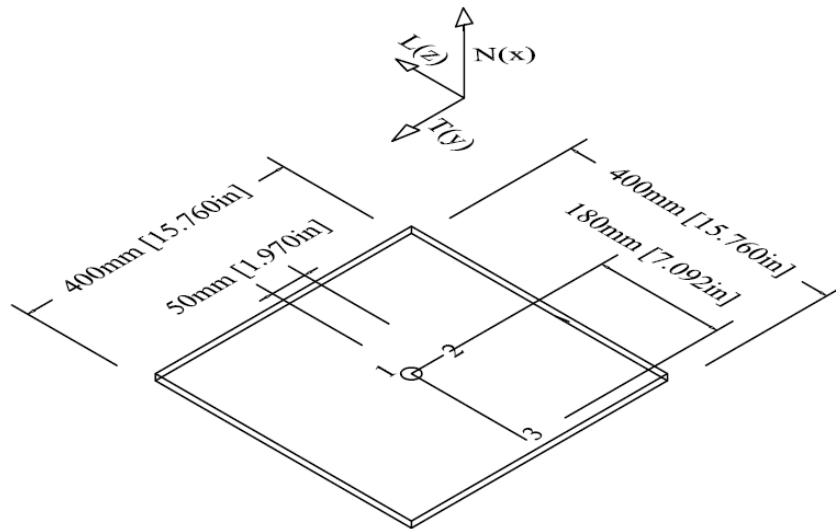


Figure 7.4: Detail for Measurement Points for Specimen 1

7.2.1.1 Normal Stress for Specimen 1

The normal stresses are calculated using Equation 7.1.

$$\sigma_{\text{Normal}} = \frac{E}{1 + \nu} \left(\epsilon_{\text{Normal}} + \frac{\nu}{(1 - 2\nu)} (\epsilon_{\text{Normal}} + \epsilon_{\text{Transverse}} + \epsilon_{\text{Longitudinal}}) \right) \quad (7.1)$$

where,

E = modulus of elasticity

ν = Poisson's ratio

ε = the strain value for a particular component

The normal stress is the stress component in the direction through the plate thickness (in the direction of N in Figure 7.4) and it was measured at 10 mm intervals along the transverse direction (T) for 50 mm length from the centre of the plate (that is, along line 1-2) and at 20 mm, 40 mm, and 60 mm intervals along the longitudinal direction (L) for 180 mm length from the centre of the plate (that is, along line 1-3). The measurements were taken at seven depths through the thickness of the plate (N) at each measurement point. Therefore, a total of 77 (=7 x 11) measurements were acquired for 11 (5 in transverse direction + 5 in longitudinal direction + origin) measurement points.

The normal stresses on lines 1-2 and 1-3 are shown in Figure 7.5 and Figure 7.6, respectively. Each line in these figures shows the stress levels through the depth of plate at a specific distance from the origin (point 1 in Figure 7.4). Each line shows how the normal stress component (stress component in the direction of N in Figure 7.4) at a particular measurement point changes through the depth (thickness) of the plate specimen. For example, the line shown with no marker in Figure 7.5 represents the normal stress value at a point which is 10 mm away from the centre (point 1) of the plate specimen and along line 1-2 (Figure 7.4). Figure 7.7 and Figure 7.8 show three-dimensional (3-D) views of the normal stresses in the transverse and longitudinal directions, respectively. It can be seen that the first measurement point was at 0.6 mm below the top surface of the plate and the last measurement point was at 8.4 mm below the top surface or 1.1 mm above the bottom surface of the plate.

The normal stresses do not show any specific pattern for stress distribution. It may primarily be due to the nature of normal stresses through a plate created during the rolling process. The stress values range from -42 MPa to +78 MPa, though in most cases it was between -20 MPa and +30 MPa and are mostly within the error bars of each other.

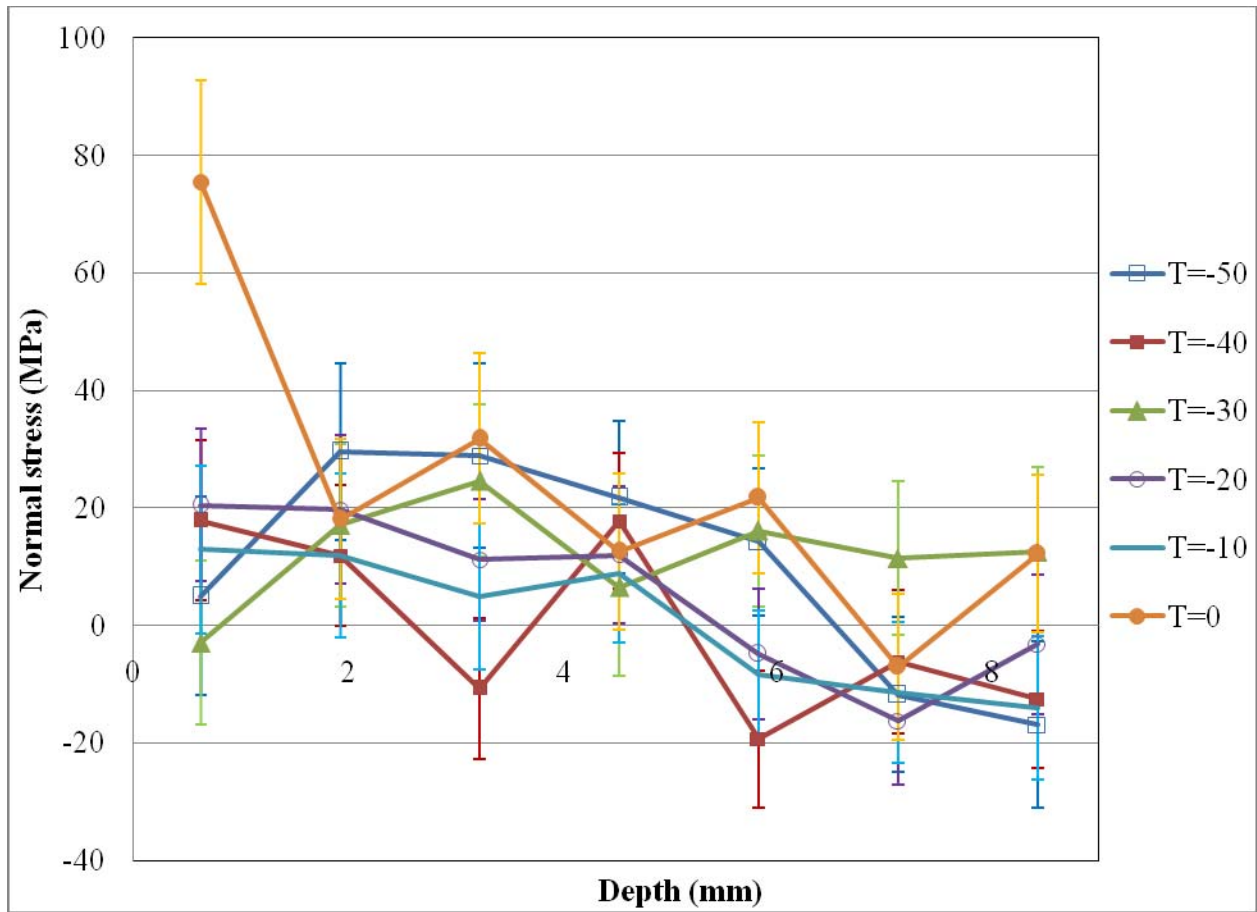


Figure 7.5: Normal stresses through the depth in transverse (T) direction (line 1-2)

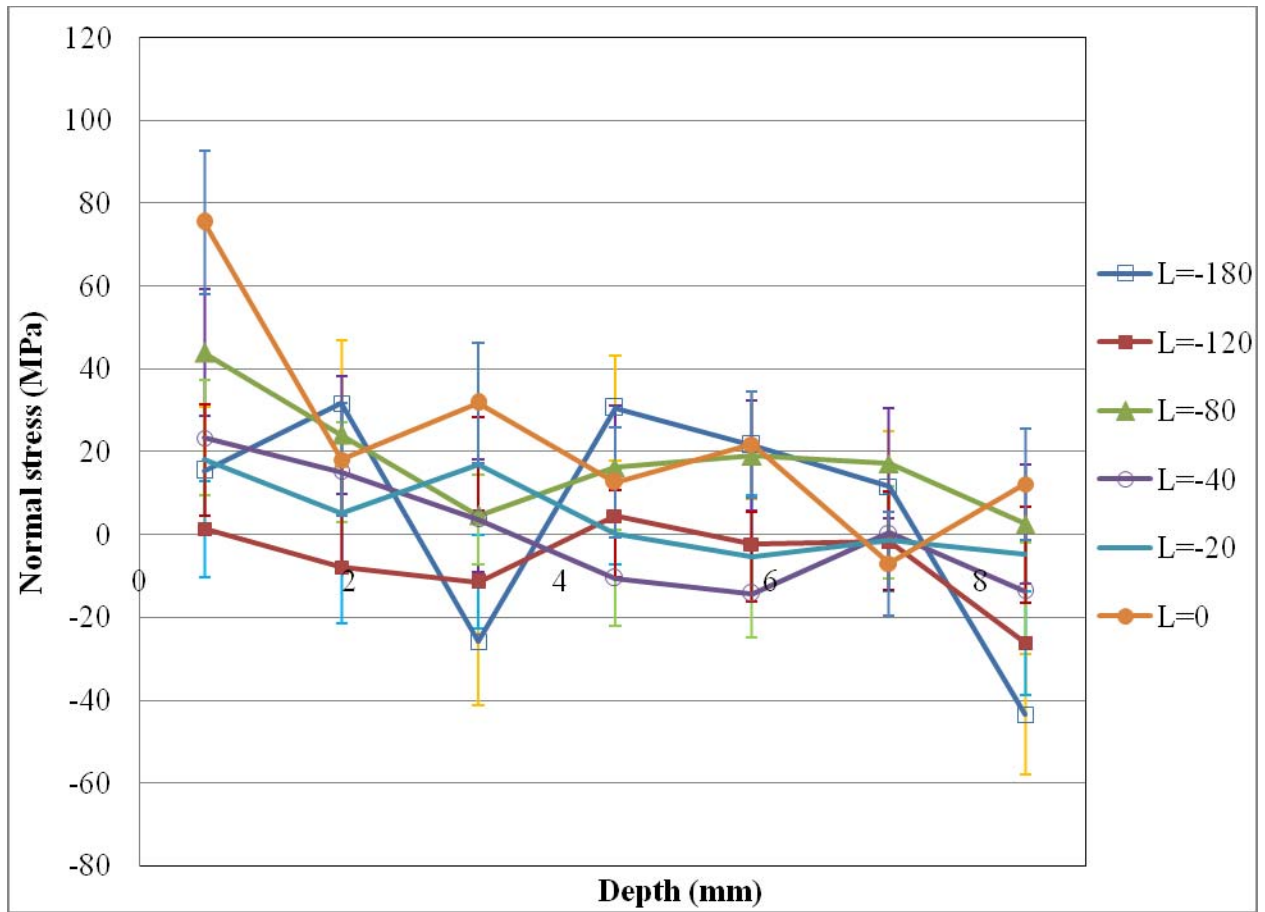


Figure 7.6: Normal stresses through the depth in longitudinal (L) direction (line 1-3)

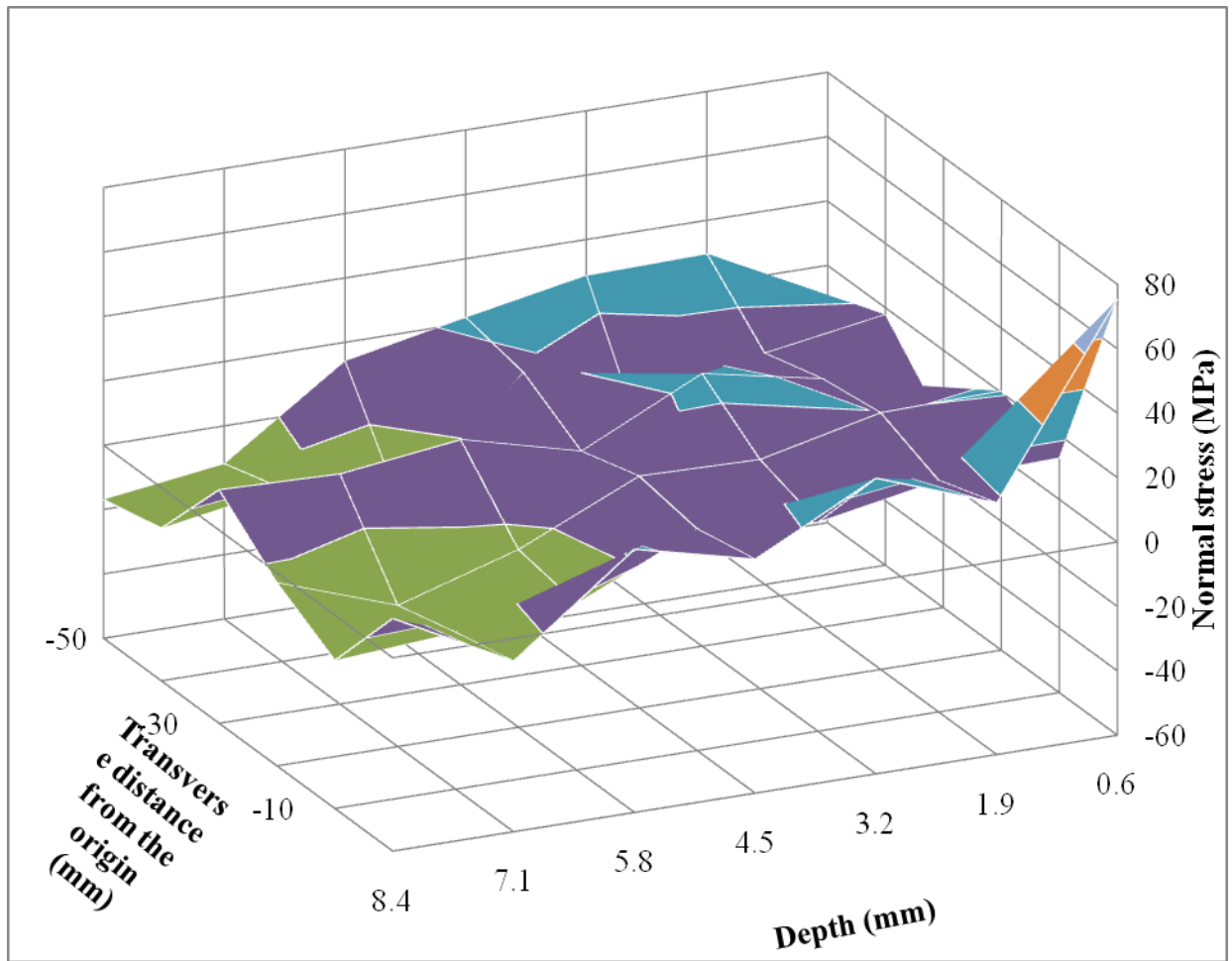


Figure 7.7: 3-D view of normal stress distribution in transverse (T) direction

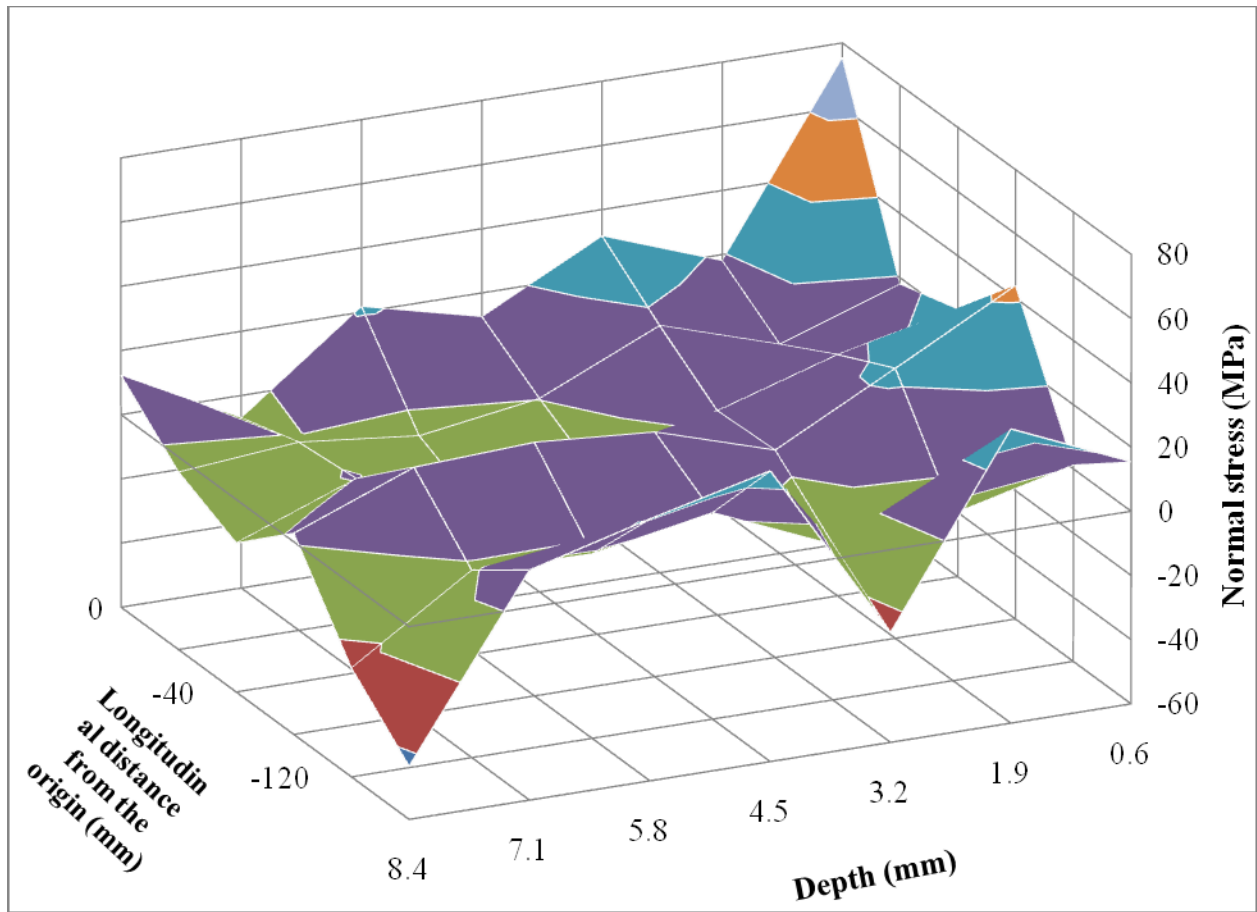


Figure 7.8: 3-D view of normal stress distribution in longitudinal (L) direction

7.2.1.2 Transverse Stress for Specimen 1

The transverse stresses are calculated using all three strain components using Equation 7.2.

$$\sigma_{\text{Transverse}} = \frac{E}{1 + \nu} \left(\epsilon_{\text{Transverse}} + \frac{\nu}{(1 - 2\nu)} (\epsilon_{\text{Normal}} + \epsilon_{\text{Transverse}} + \epsilon_{\text{Longitudinal}}) \right) \quad (7.2)$$

The transverse stress is the stress in the direction of what would be perpendicular to the stiffener if there was a stiffener on this plate (direction T in Figure 7.4). The stress measurements for the transverse component were acquired at the same measurement points as were acquired for the normal component, that is at 10 mm intervals along the transverse direction (line 1-2) and up to a distance of 50 mm from the centre (point 1) of the plate and at 20 mm, 40 mm and 60 mm intervals along the longitudinal direction (line 1-3) and up to a distance of 180 mm from the

centre (point 1) of the plate. The measurements were taken at seven depths through the thickness of the plate at each point thus, a total of 77 ($= 7 \times 11$) measurements were obtained.

One dimensional distribution for the transverse stress component on lines 1-2 and 1-3 are shown in Figure 7.9 and Figure 7.10, respectively. Each line shows the stress levels through the depth of plate at a specific measurement point. Figure 7.11 and Figure 7.12 show three-dimensional distributions of the transverse stress component in the transverse (T) and longitudinal (L) directions, respectively.

The transverse stress distributions show a much clearer pattern through the thickness (along N) of the plate. It can be seen that the transverse stress value changes its sign from positive to negative, then from negative to positive and finally, to negative again as the depth of the plate increases. The maximum negative value of transverse stress is at about 3 mm below the top surface and the maximum positive stress value is at about 6 mm from top surface. The change in transverse stress values through the thickness of the plate indicates that the parent plate had a locked-in bending stress in the transverse direction and it may have happened due to the rolling process of plate production.

A cold cut method called “water-jet cut” was used in this study and it is assumed that this did not introduce any additional stresses. The range of stresses in the transverse component also has a broader range (in the range of roughly 110 MPa in compression to 80 MPa in tension) than the normal stresses from this Specimen, which ranged from -42 MPa to +78 MPa. The error bars are not shown on these figures since the results are reasonably consistent. There are a few points that do seem to vary from most of the others, however, they are still within the error limit.

The three-dimensional distributions (Figure 7.11 and Figure 7.12) show a better representation of the bending stress in the transverse and longitudinal directions through the depth. These figures also show the changes in maximum negative and positive stresses along both the transverse (T) and longitudinal (L) directions. It is observed that the transverse stress value at a specific measurement depth (at a specific depth in the N direction) does not change much with the change in distance from the origin in the transverse or longitudinal direction.

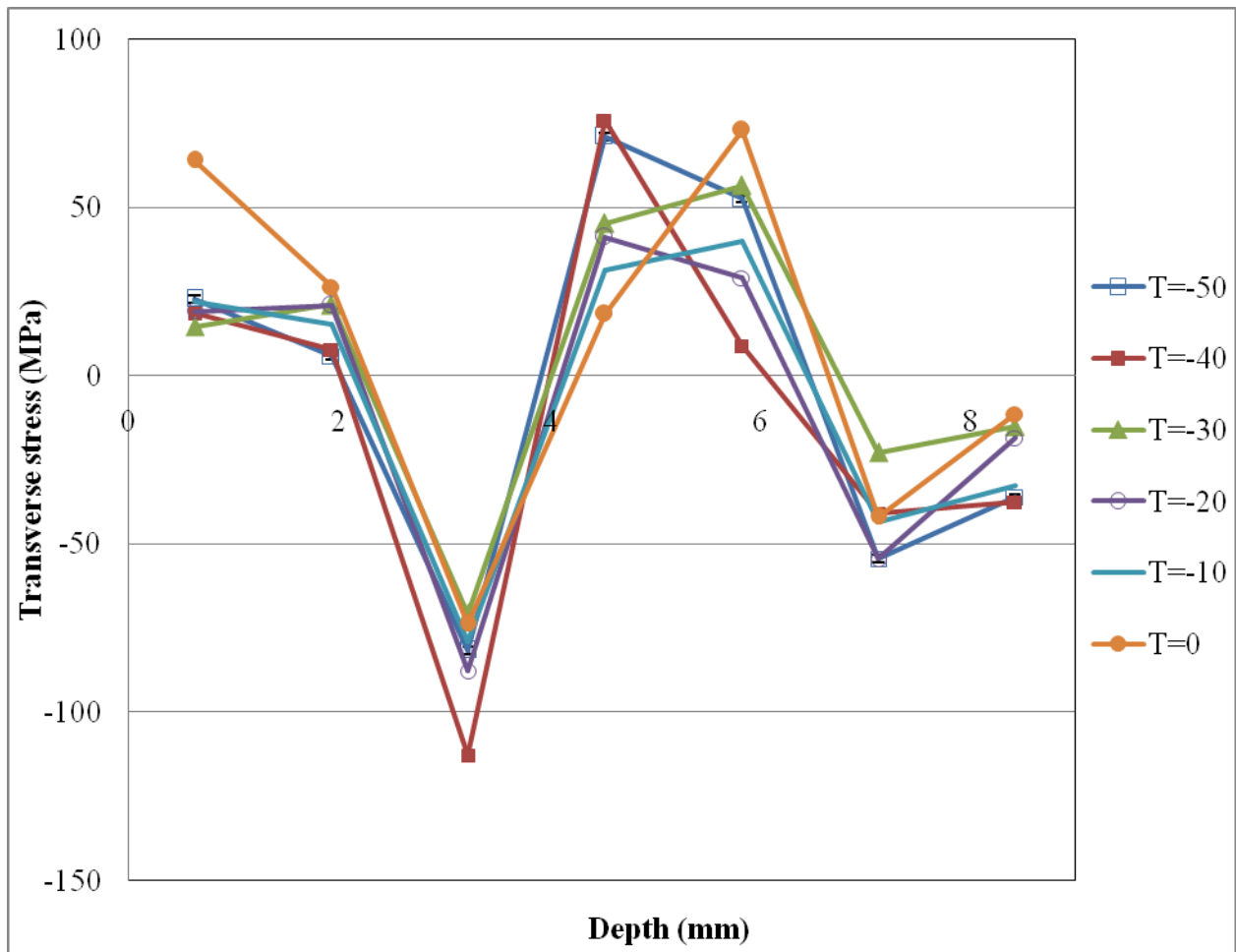


Figure 7.9: Transverse stress through the depth in transverse (T) direction (line 1-2)

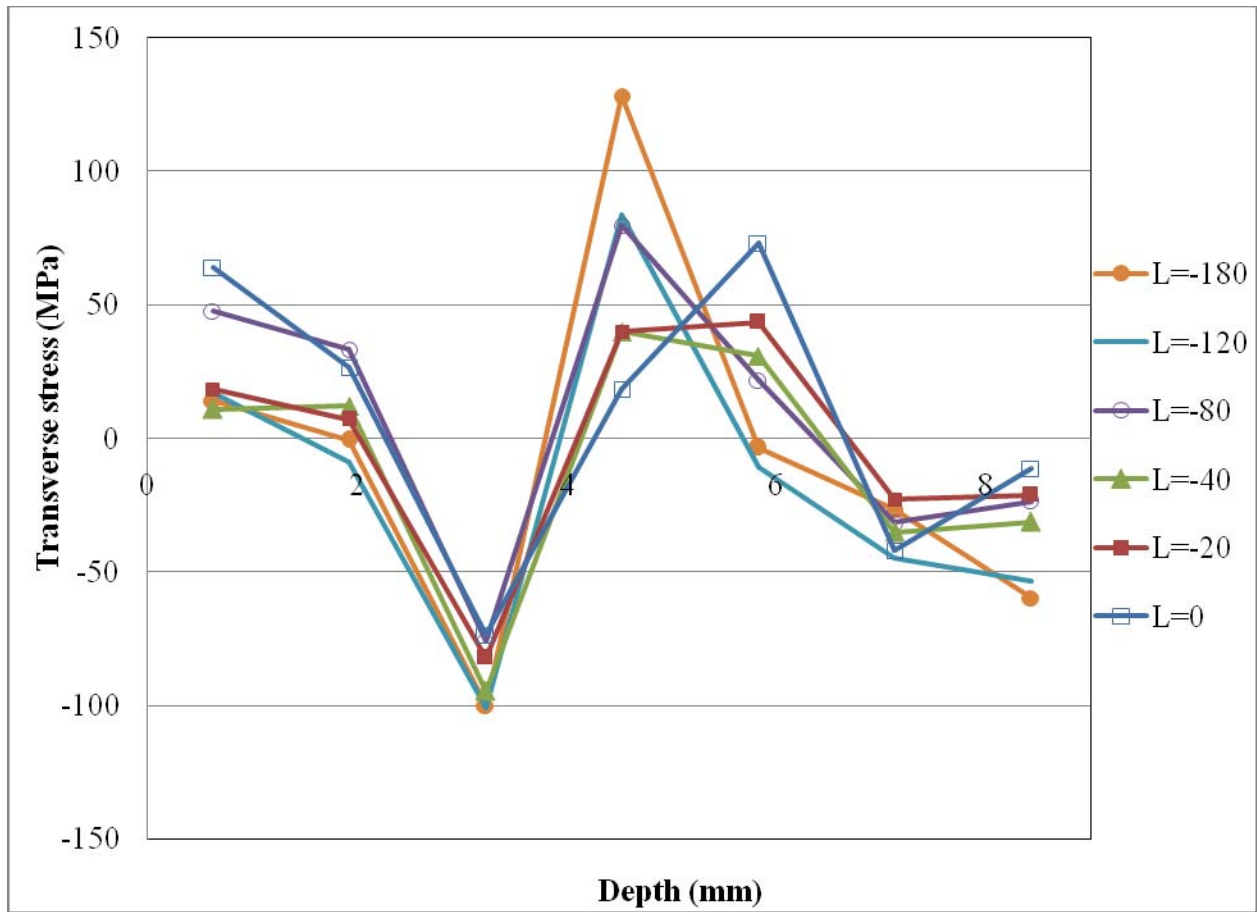


Figure 7.10: Transverse stress through the depth in longitudinal (L) direction (line 1-3)

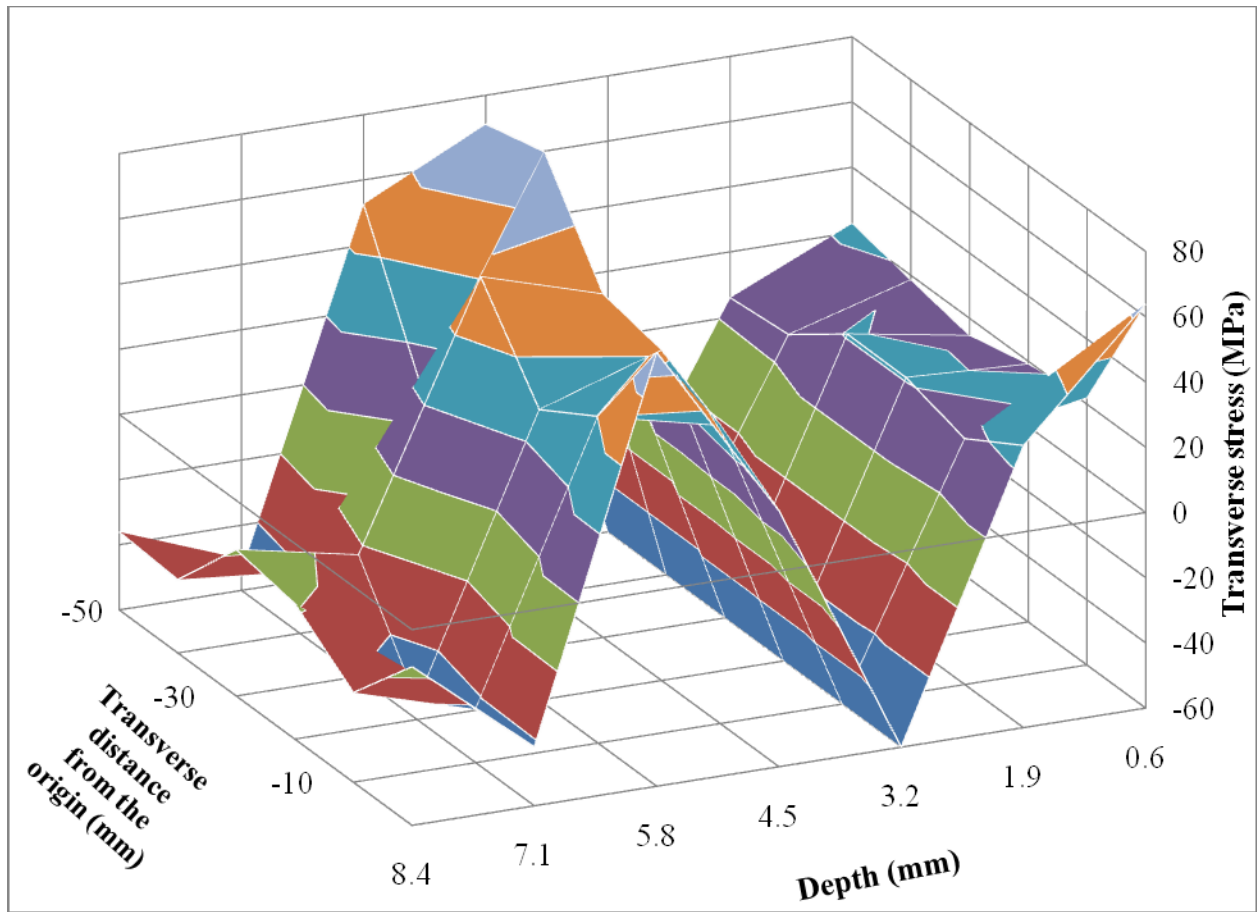


Figure 7.11: 3-D view of transverse stress distribution in transverse (T) direction (line 1-2)

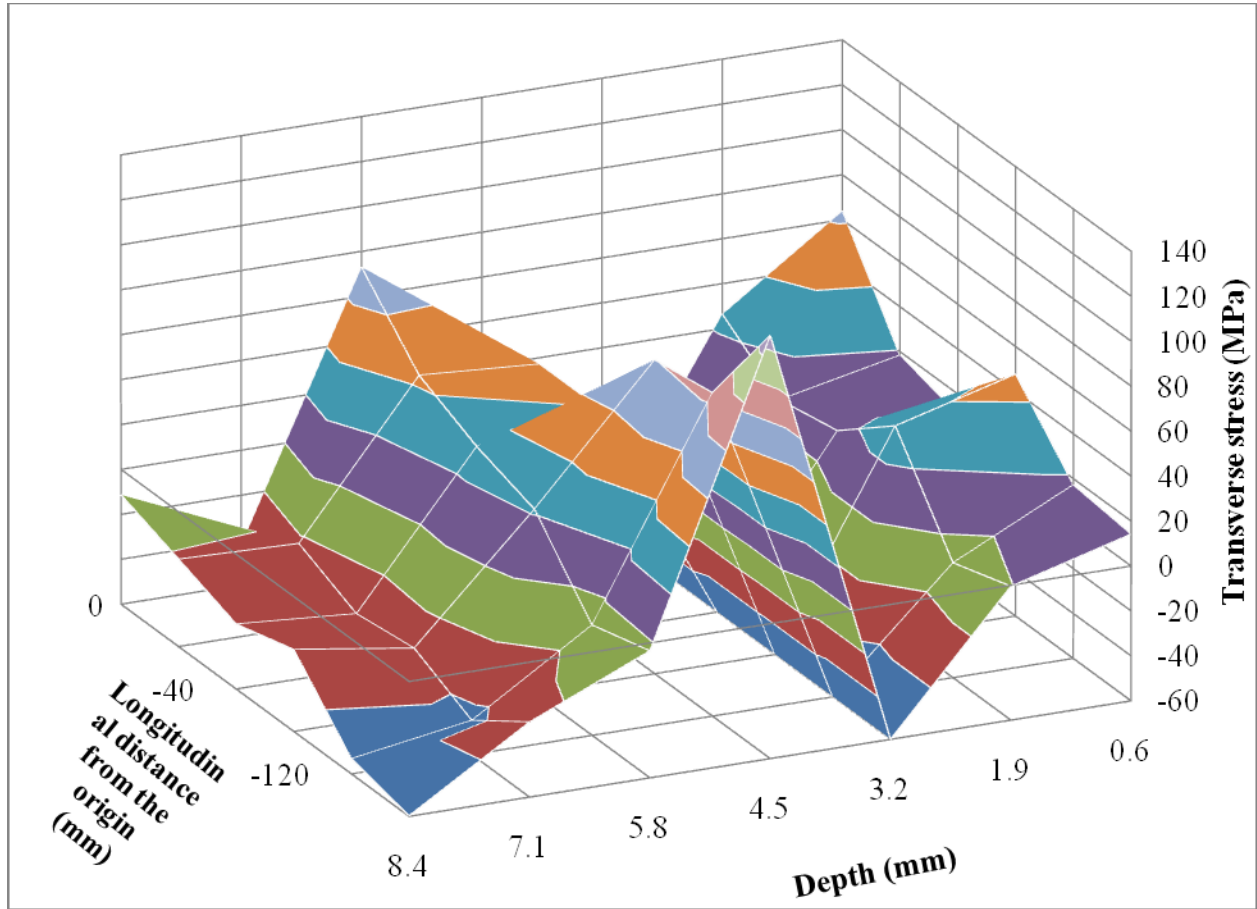


Figure 7.12: 3-D view of transverse stress distribution in longitudinal (L) direction (line 1-3)

7.2.1.3 Longitudinal Stress for Specimen 1

The longitudinal stresses are calculated using Equation 7.3.

$$\sigma_{\text{Longitudinal}} = \frac{E}{1 + \nu} \left(\epsilon_{\text{Longitudinal}} + \frac{\nu}{(1 - 2\nu)} (\epsilon_{\text{Normal}} + \epsilon_{\text{Transverse}} + \epsilon_{\text{Longitudinal}}) \right) \quad (7.3)$$

The longitudinal stress is the stress in the direction of what would be parallel to the stiffener (direction along L in Figure 7.4) if there was a stiffener on this plate. The stress measurements were taken at the same measurement points along lines 1-2 and 1-3 in Figure 7.4 as it was done for the other two stress components, that is, at 10 mm intervals along the transverse direction (line 1-2) and until 50 mm from the centre (point 1) of the plate and at 20 mm, 40 mm, and 60 mm intervals along the longitudinal direction (line 1-3) and until 180 mm from the centre (point 1) of the plate (see Figure 7.4). The measurements were taken at seven depths through the

thickness (in N direction) of the plate at each point, for a total of 77 points (11 locations x 7 depths).

Figure 7.13 and Figure 7.14 illustrate one-dimensional distributions of longitudinal stresses for Specimen 1. Three-dimensional longitudinal stresses are shown in Figure 7.15 and Figure 7.16. The longitudinal stresses show a clear pattern similar to that was found for transverse stress distribution. (Please compare Figure 7.13 with Figure 7.9 and compare Figure 7.14 with Figure 7.10) Therefore, it is obvious that a bending stress in the longitudinal direction as well was created during the rolling process of the plate. The maximum negative (compression) longitudinal stress was found at 3 mm below the top surface of the plate and the maximum positive (tension) longitudinal stress was found at 6 mm below the top surface of the plate. The range of longitudinal stress values were found to be between 40 MPa in compression to 90 MPa in tension. The error bars are not shown on these plots because a consistent pattern in stress distribution is found. The variance of the points is still close to within the error limits.

The three-dimensional distributions (Figure 7.15 and Figure 7.16) also show the bending stress through the depth as well as the shallower maximum and minimums along the plate in both the transverse (T) and longitudinal (L) direction, similar to the transverse stress distribution.

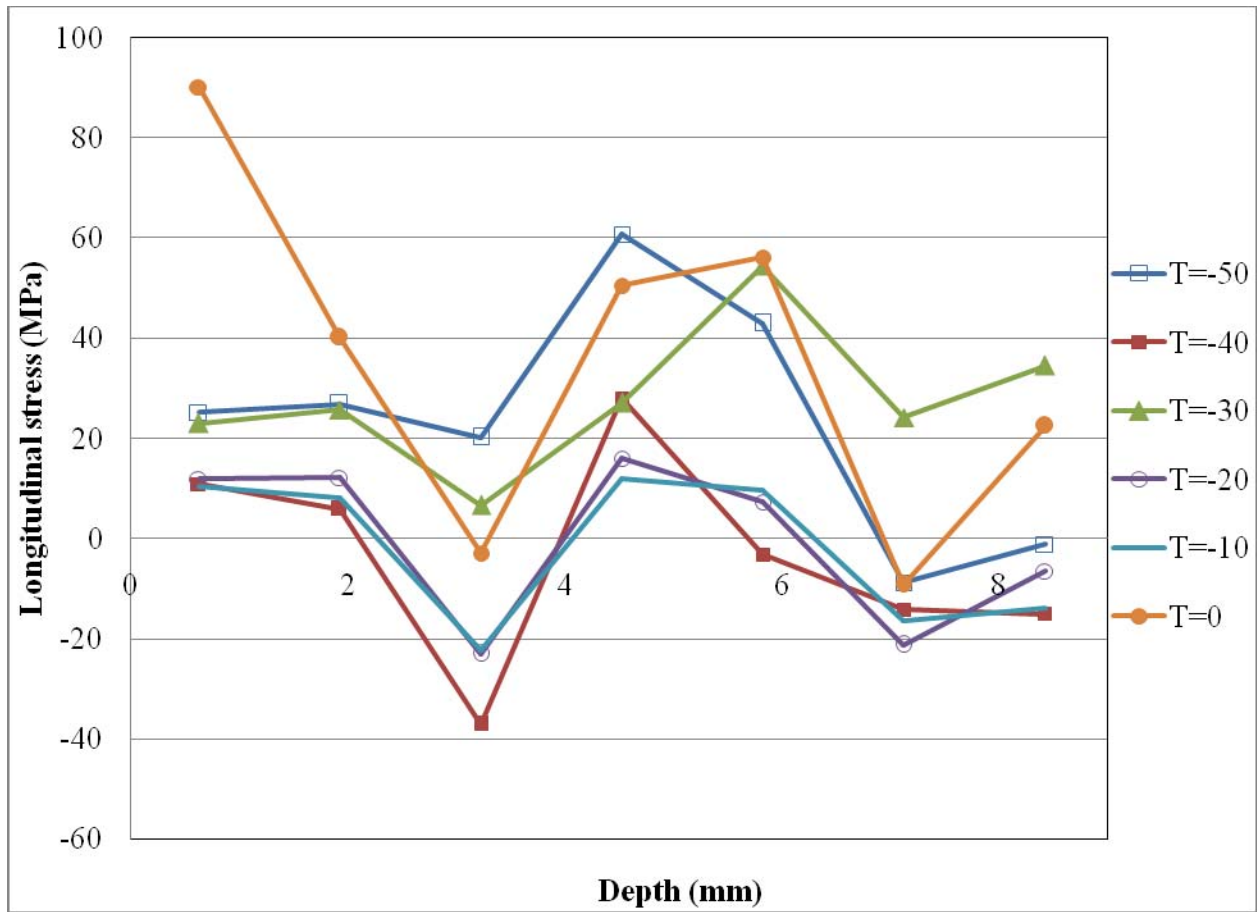


Figure 7.13: Longitudinal stress through the depth in transverse (T) direction (line 1-2)

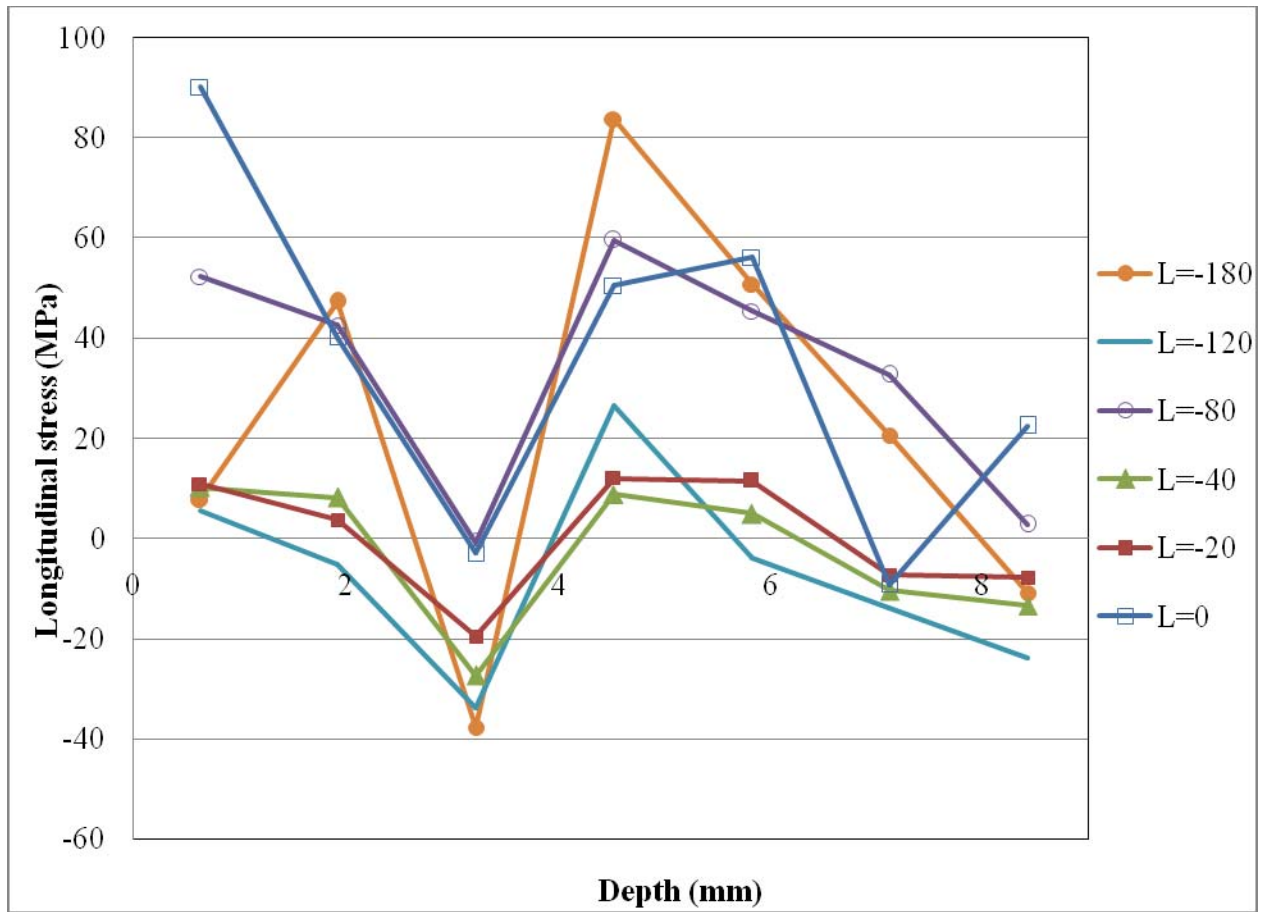


Figure 7.14: Longitudinal stress through depth in longitudinal (L) direction (line 1-3)

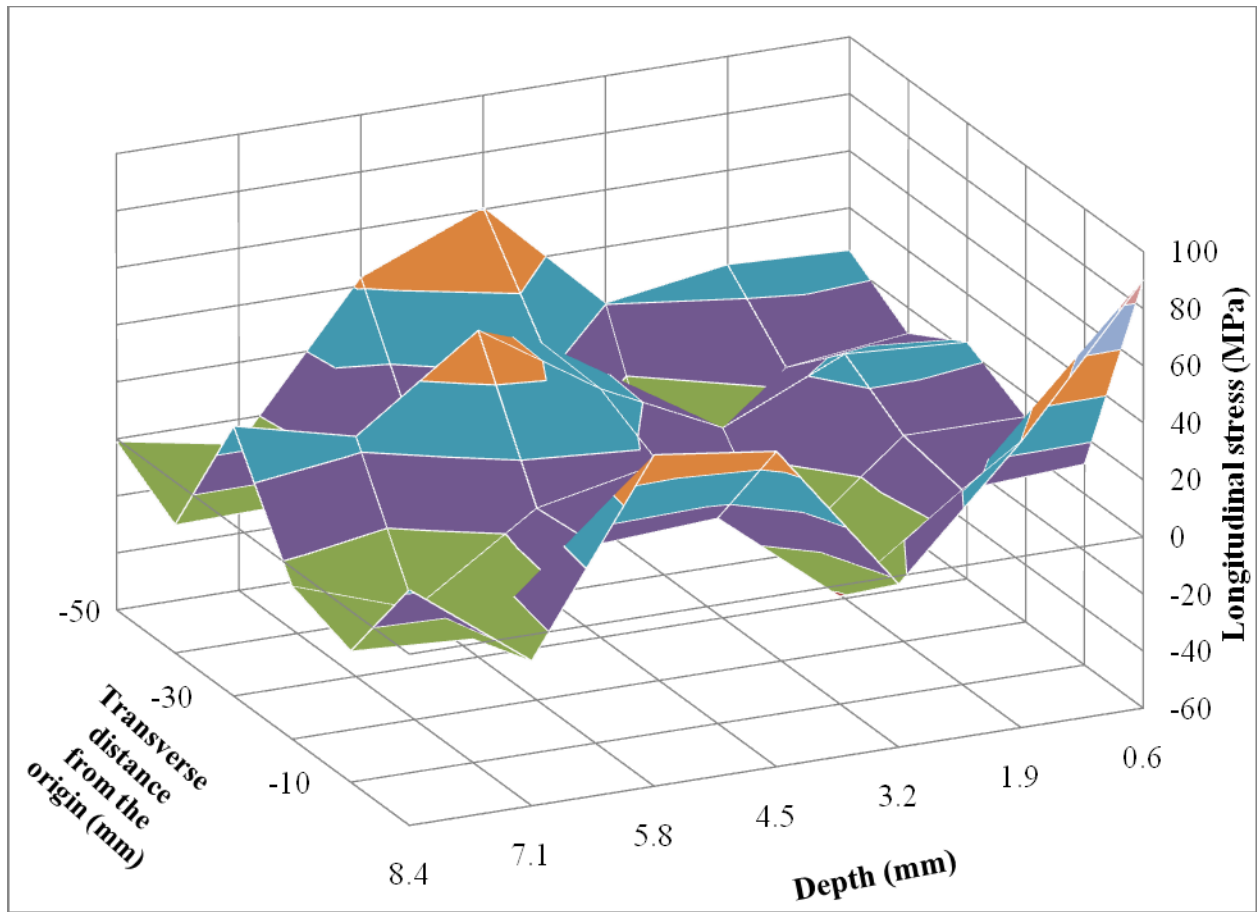


Figure 7.15: 3-D view of transverse stress distribution in transverse (T) direction (line 1-2)

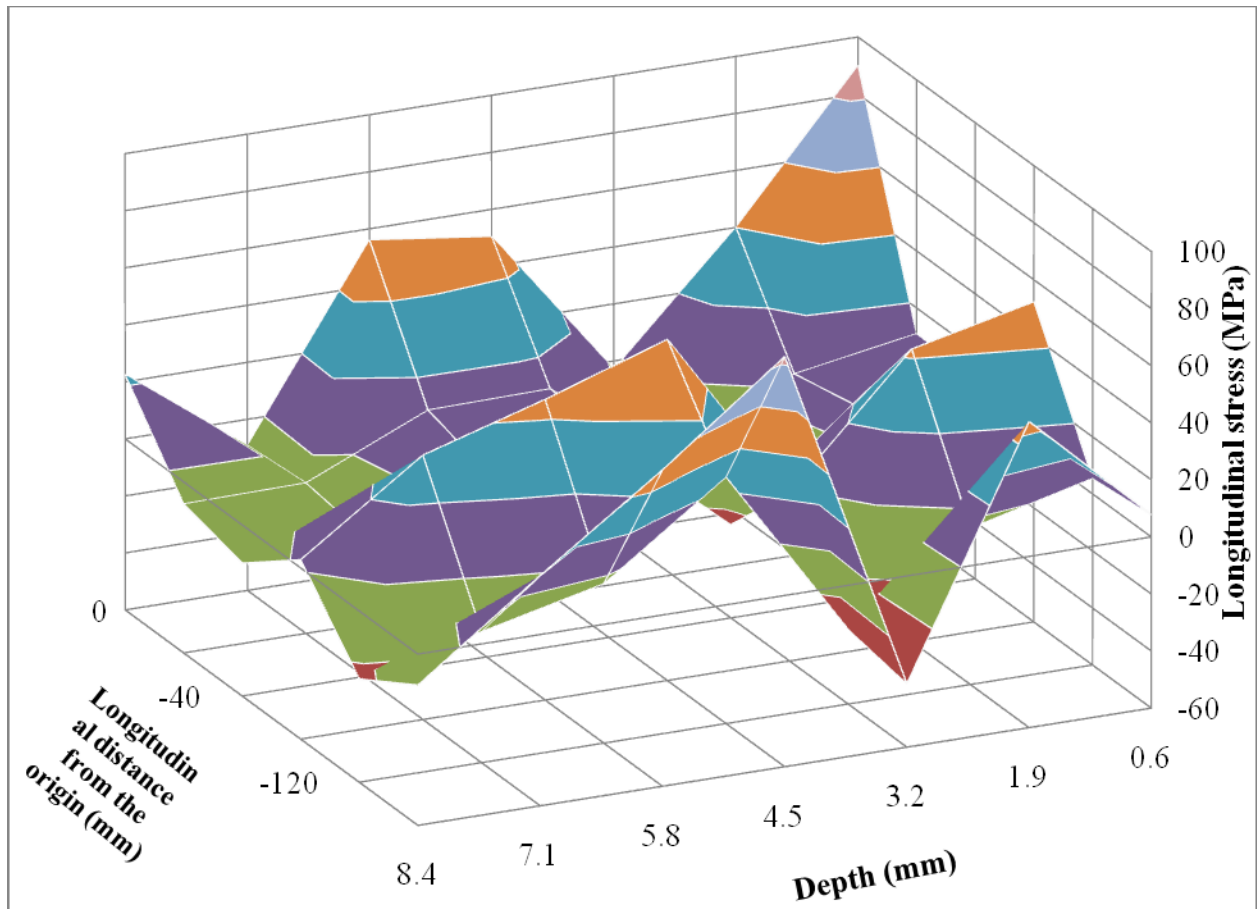


Figure 7.16: 3-D view of transverse stress distribution in longitudinal (L) direction (line 1-3)

7.2.2 Specimen 2

Specimen 2 was a stiffened plate with the dimensions of 400 mm wide (T) x 600 mm long (L) x 9.5 mm thick (N) as shown in Figure 7.2 and Figure 7.17. Only one 600 mm long angle stiffener was welded on this specimen. The objective was to determine the effects of welding a stiffener on the residual stress distributions and to compare with those for the parent plate with no stiffener (Specimen 1). The specimen was measured for three residual strain components: (i) normal (N), (ii) transverse (T), and (iii) longitudinal (L) at seven depths through the normal (N) direction. Figure 7.17 shows the origin (point 1) and the lines (3-1-4, 5-2-6, and 1-2) on which the measurements were undertaken.

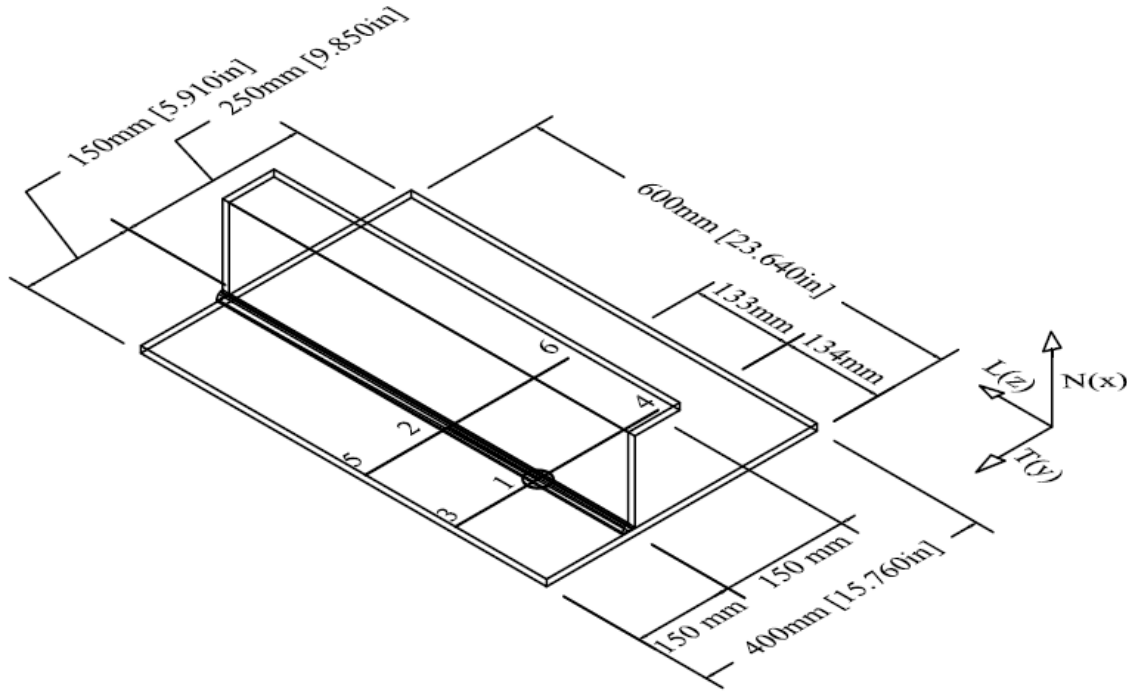


Figure 7.17: Detail for Measurement Points for Specimen 2

7.2.2.1 Normal Stress for Specimen 2

The normal stresses (σ_x or σ_{normal}) are calculated using all three strain components as shown in Equation 7.1. The normal stress was measured along the transverse direction until 150 mm on either side of the stiffener (line 3-4 and line 5-6) and 133 mm along the weld centreline (line 1-2) in the longitudinal direction (Figure 7.17).

As mentioned earlier (Table 5-2), the welding for this specimen could not be completed in a single non-stop run. The welding was stopped once and restarted after one minute at point 2 in Figure 7.17. The stop and start caused the weld overlap at that point. The line 3-1-4 was chosen at a distance of 133 mm ($L = 133$ mm) which was away from the stop and start (point 2 in Figure 7.17) in the welding process. Thus, the location of the origin (point 1 in Figure 7.17) was at the mid-length between point 2 and the nearest edge of the plate such that edge effects and weld inconsistencies (stop and start in welding) are minimized. The spacing of the measurements was as small as 1 mm near the centre of the weld and gradually increased up to 40 mm further away from the weld, as shown in Figure 7.18. For line 3-1-4, the measurements were taken at seven depths of the plate (through N axis) along the transverse (T) direction at 31 locations, for a total

of 217 (=31 x 7) measurement points. Measurements on line 5-2-6 (at L = 133 mm in Figure 7.17) were also acquired at 31 locations as was acquired for line 3-4 but at three depths for a total of 93 (=31 x 3) measurement points. The measurements along the weld centreline (line 1-2) were only taken at one depth (at N = 8.9 mm) since it was found that the normal stress component does not change along the length of the weld (along the L-axis). However, this stress values showed changes at points where weld was not uniform or welding was interrupted such as at point 2, where welding was stopped and started. These measurements were taken at seven points plus at other two points at L = 0 mm and L = 133 mm. The total number of measurements taken on this specimen is 317 points (= 217 + 93 +7).

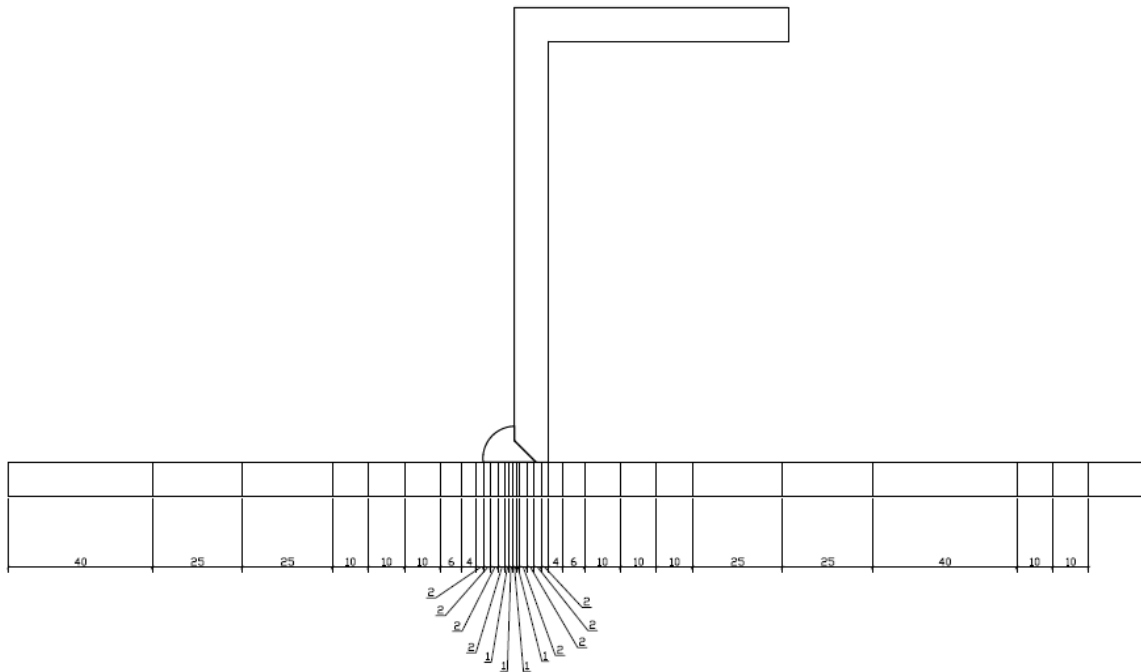


Figure 7.18: Measurement Spacing in mm

One dimensional distributions for normal stresses (σ_x or σ_{normal}) for lines 3-1-4 (at L = 0 mm) and for line 5-2-6 (at L = 133 mm) are shown Figure 7.19 and Figure 7.20, respectively. Each line shows the variation in normal stress through the cross-section or depth (depth, N) of the plate at a specific distance from the origin (point 1 in Figure 7.17). It should be noted that a different graphical representation is shown for this stress component, as compared to the Figures for Specimen 1. For example in Figure 7.19, the line with the open squares shows the stress levels at 1.1 mm from the bottom face (the face of the plate with no stiffener) of the plate and the line

with crosses shows the stress values closest to the surface of the plate with stiffener. Figure 7.20 shows the same distribution for normal stress but for line 5-2-6 (at $L = 133$ mm). Only three measurements along the depth were obtained to reduce the beam time. The three-dimensional stress plots are not shown for this stress component since they do not provide any valuable information.

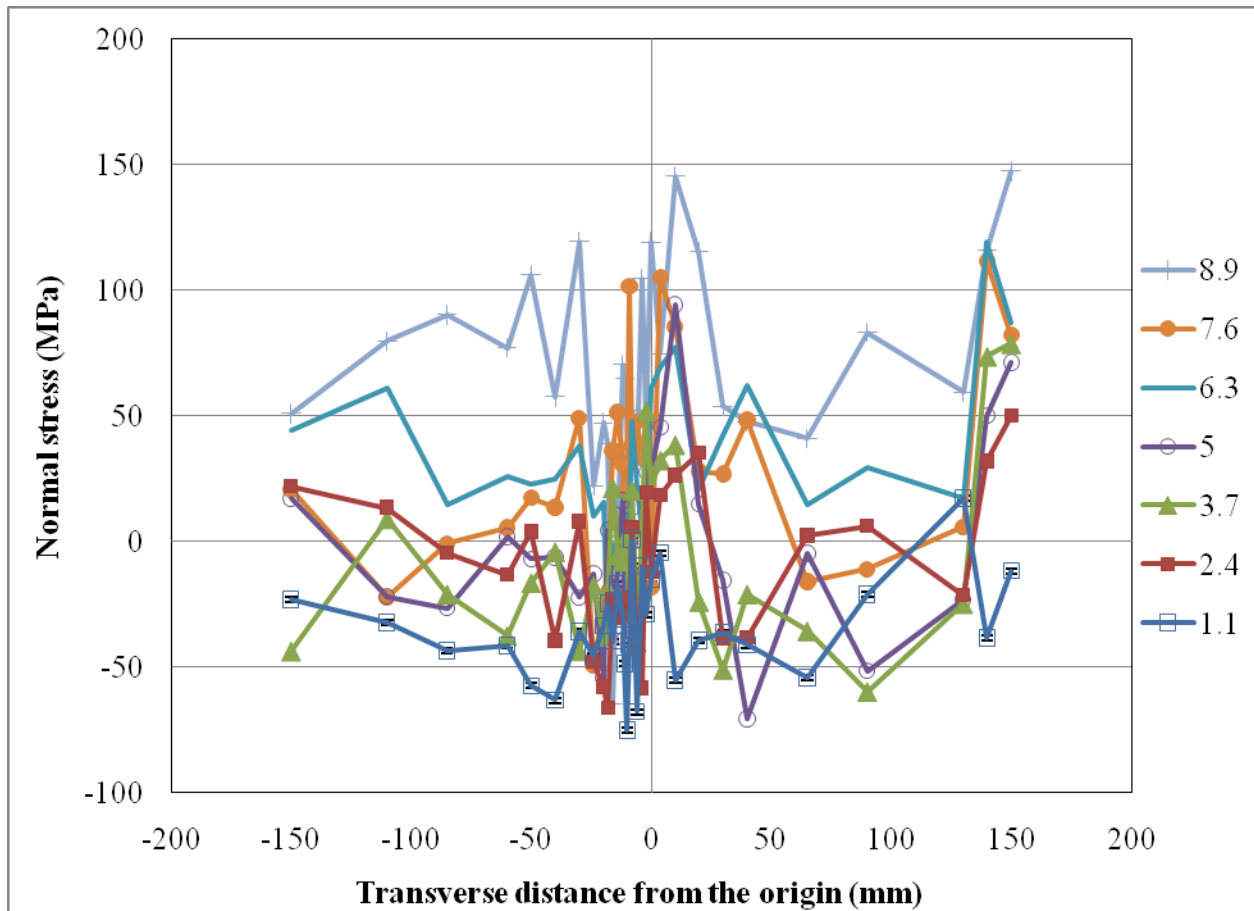


Figure 7.19: Normal stresses through the depth in transverse (T) direction (at $L = 0$ mm, line 3-1-4)

Similar to Specimen 1, the distributions for normal stress do not show any specific pattern and this is primarily due to the nature of pre-existing locked-in normal stresses in the parent plate that may have developed from the rolling process. The stress values range from about 75 MPa in compression to 150 MPa in tension, with the maximum value near the weld centreline. These values are nearly double the values found in the parent plate, that is, Specimen 1 (Specimens 1 had the stress values in the range of 40 MPa in compression to 80 MPa in tension).

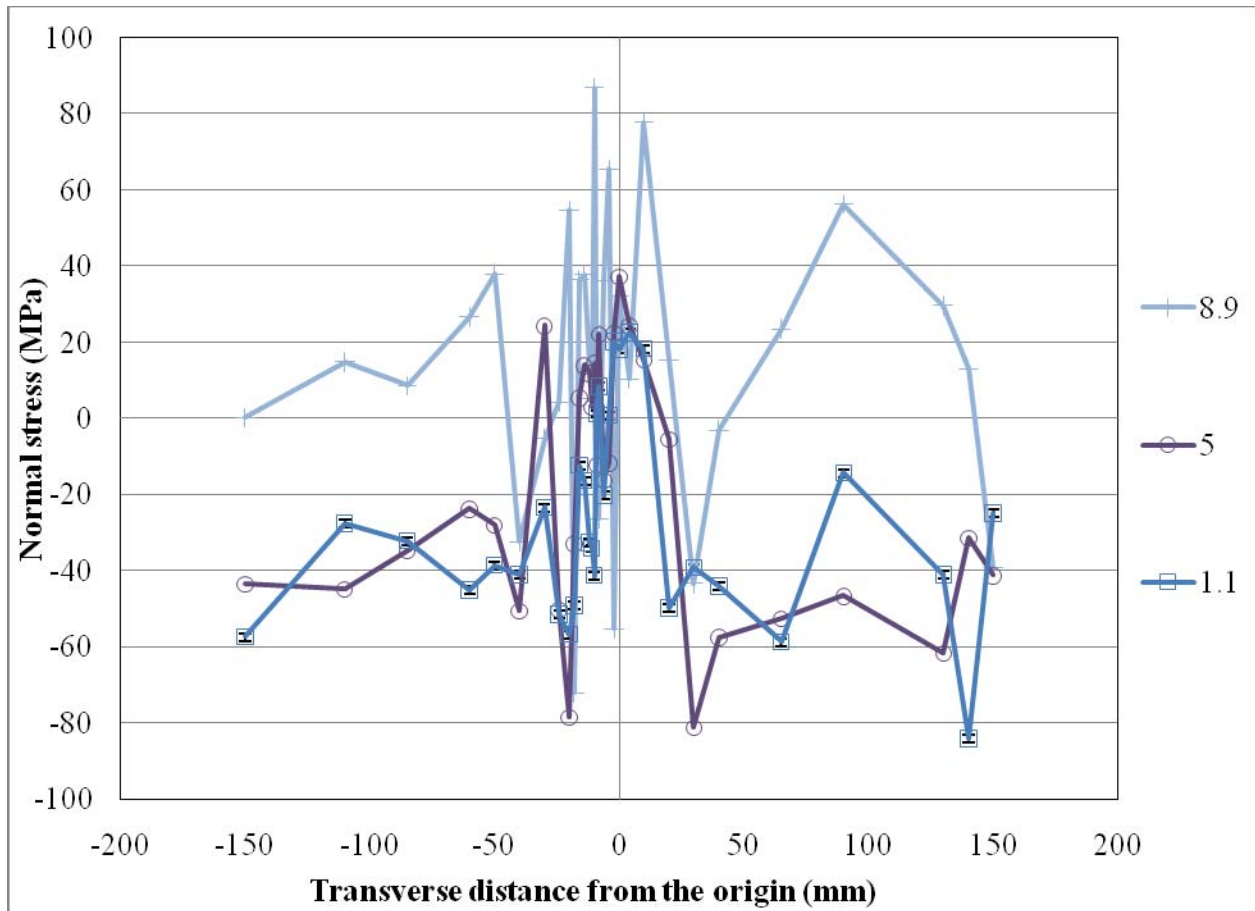


Figure 7.20: Normal stresses through the depth in transverse (T) direction (at L = 133 mm, line 5-2-6)

7.2.2.2 Transverse Stress for Specimen 2

The transverse stresses (σ_y or $\sigma_{\text{transverse}}$) are calculated using Equation 7.2 and measured at the same points where the normal stress component was measured (Figure 7.17). The measurement points are shown in Figure 7.18. Similar to the measurements for the normal stress component, transverse stress component was also measured at seven depths on line 3-1-4 (at L = 0 mm) and at three depths on line 5-2-6 (at L = 133 mm). The measurements along the weld centreline were only taken at one depth (at N = 8.9 mm) because it was found that the transverse stress component does not change if the distance along the length of the stiffener (L-axis) changes. However, the stress value changes at locations where there were inconsistencies in the weld itself (for example, at L = 133 mm, point 2).

One-dimensional distributions for transverse stress are shown Figure 7.21 and Figure 7.22 for line 3-1-4 (at $L = 0$ mm) and line 5-2-6 (at $L = 133$ mm), respectively. The three-dimensional stress plots are not shown for this specimen since they do not follow any clear pattern.

The transverse stresses show a pattern with maximum positive (tensile) stress being at the centre of the weld (line 1-2 in Figure 7.17). The stress value on line 3-1-4 (at $L = 0$ mm) ranges from about 120 MPa in compression to 150 MPa in tension, showing the maximum value around the weld centreline. The stress values on line 5-2-6 (at $L = 133$ mm) range from about 170 MPa in compression to 50 MPa in tension. The difference found on this line as compared to line 3-1-4 seems to be due to the stop and start of the weld (at $L = 133$ mm, point 2). These values are nearly 50% higher as compared to the parent plate (Specimen 1).

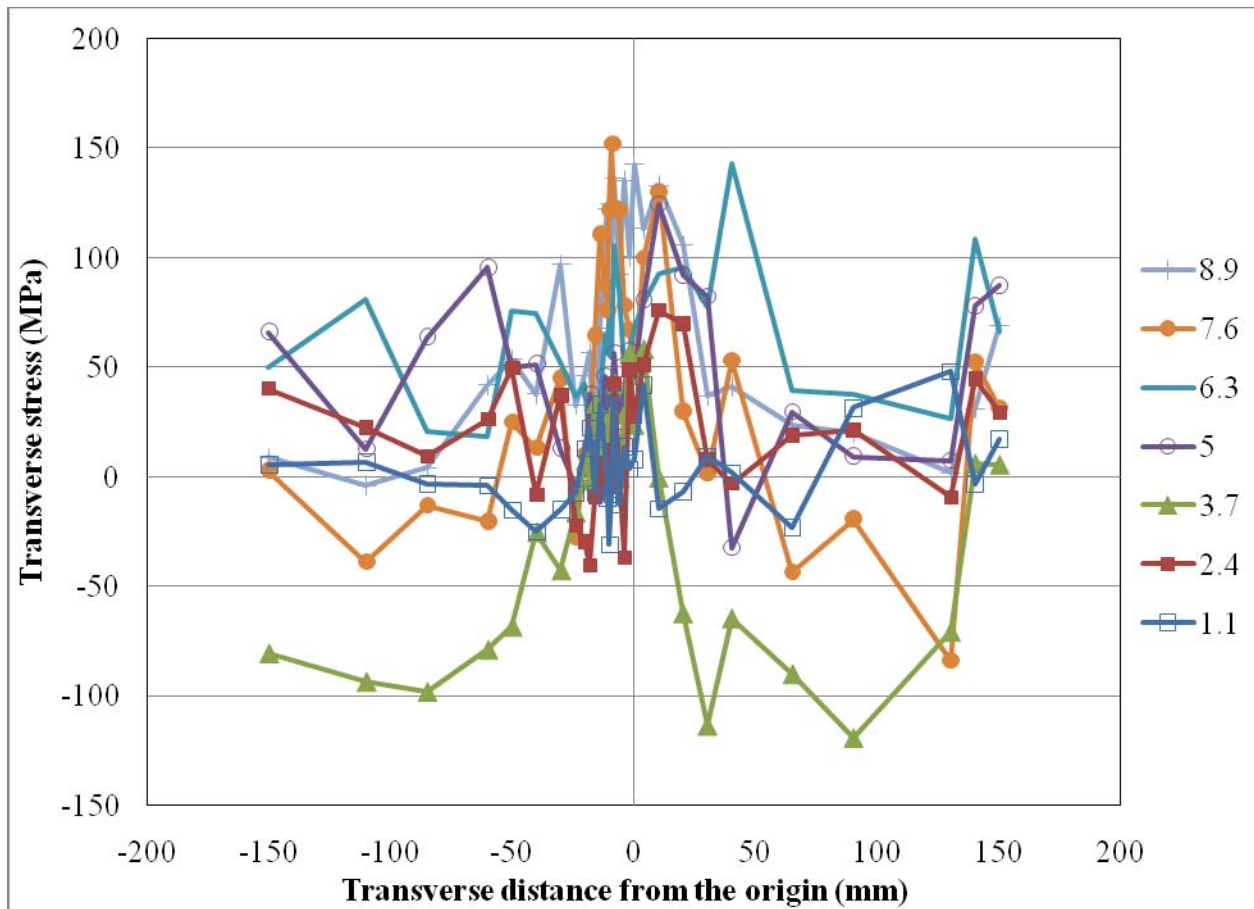


Figure 7.21: Transverse stresses through the depth in transverse (T) direction (at $L = 0$ mm, line 3-1-4)

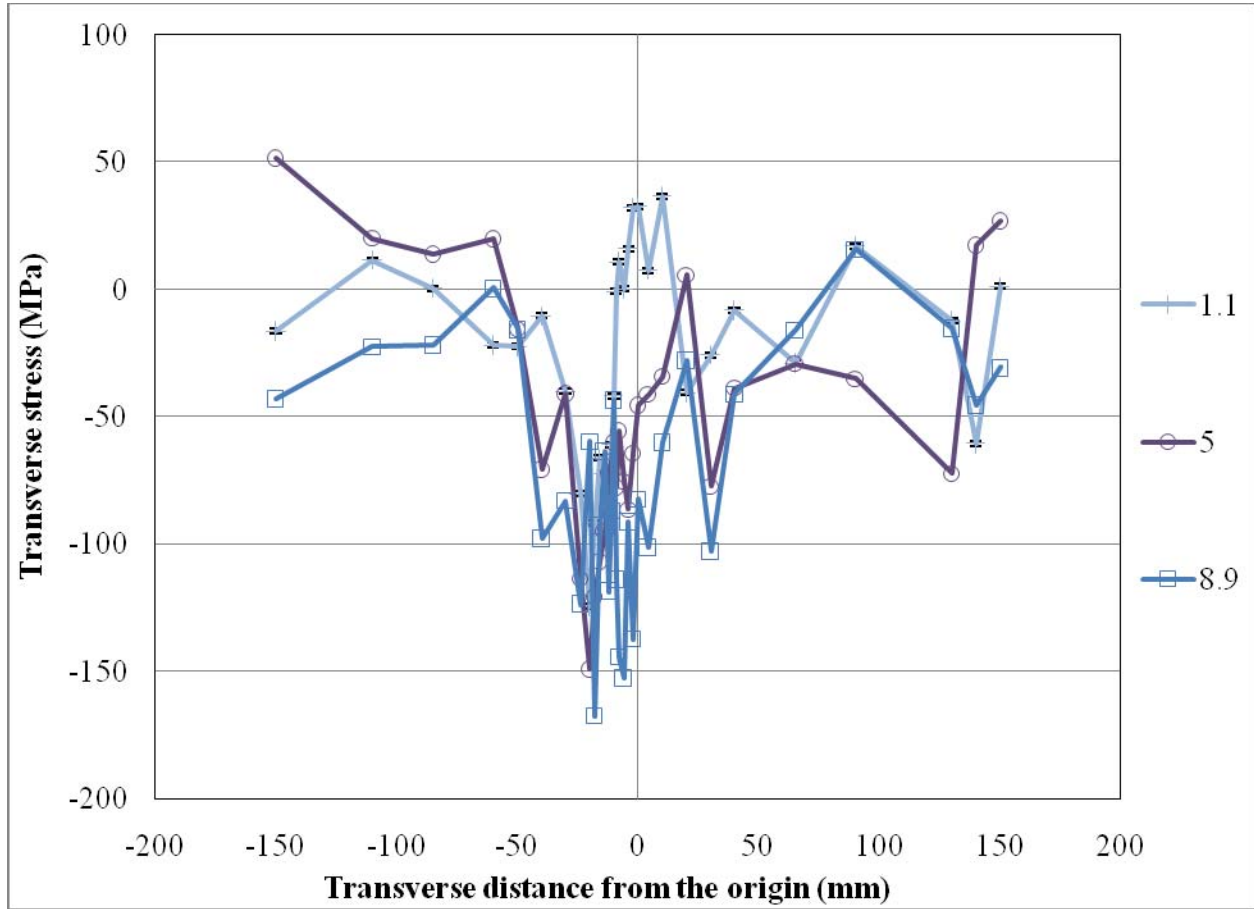


Figure 7.22: Transverse stresses through the depth in transverse (T) direction (at L = 133 mm, line 5-2-6)

7.2.2.3 Longitudinal Stress for Specimen 2

The longitudinal stress (σ_z or $\sigma_{\text{longitudinal}}$) was calculated using Equation 7.3 and were measured at the same points and depths as was done for the other two stress components (Figure 7.17 and Figure 7.18).

Figure 7.23 and Figure 7.24 show one-dimensional distributions for the longitudinal stress for lines 3-1-4 (at L = 0 mm) and 5-2-6 (at L = 133 mm), respectively. Better and much more obvious patterns are found in the distribution of this stress component. These figures show that the stress value remains unchanged even if the depth of the plate is changed. The stress value reduces as the transverse (T) distance from the weld increases and finally, it becomes compressive (negative) at about 50 mm on both sides from the centre of the weld. The three-

dimensional distributions for longitudinal stresses are shown in Figure 7.25 and Figure 7.26. However, these plots are not drawn to scale.

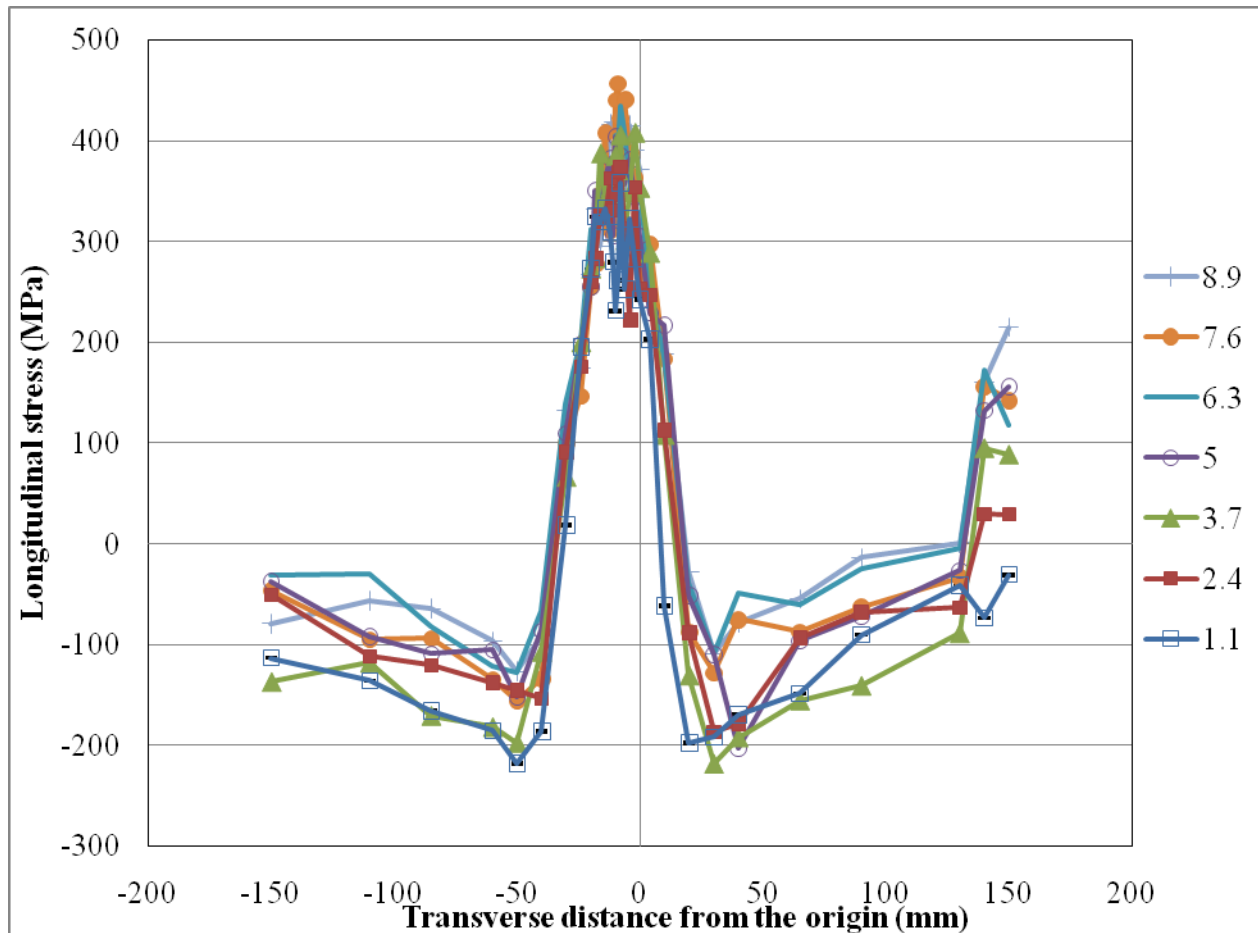


Figure 7.23: Longitudinal stress through the depth in transverse (T) direction (at L = 0 mm, line 3-1-4)

The maximum positive (tension) value is located at the centreline (on line 1-2 in Figure 7.17) of the weld. The stress value on line 3-1-4 (at L = 0 mm) range from about 200 MPa in compression to 450 MPa in tension. It should be noted that the first (upper) yield stress obtained from material tests on the plate is 405 MPa. The stress value on line 5-2-6 (at L = 133 mm) range from about 200 MPa in compression to 375 MPa in tension. The reduction in longitudinal stress value on line 5-2-6 (at L = 133 mm) seems to be due to the stop and start of the weld at this location. These values compared with the parent plate (Specimen 1 which had longitudinal stress value in the range of 40 MPa in compression to 90 MPa in tension) are nearly five times larger.

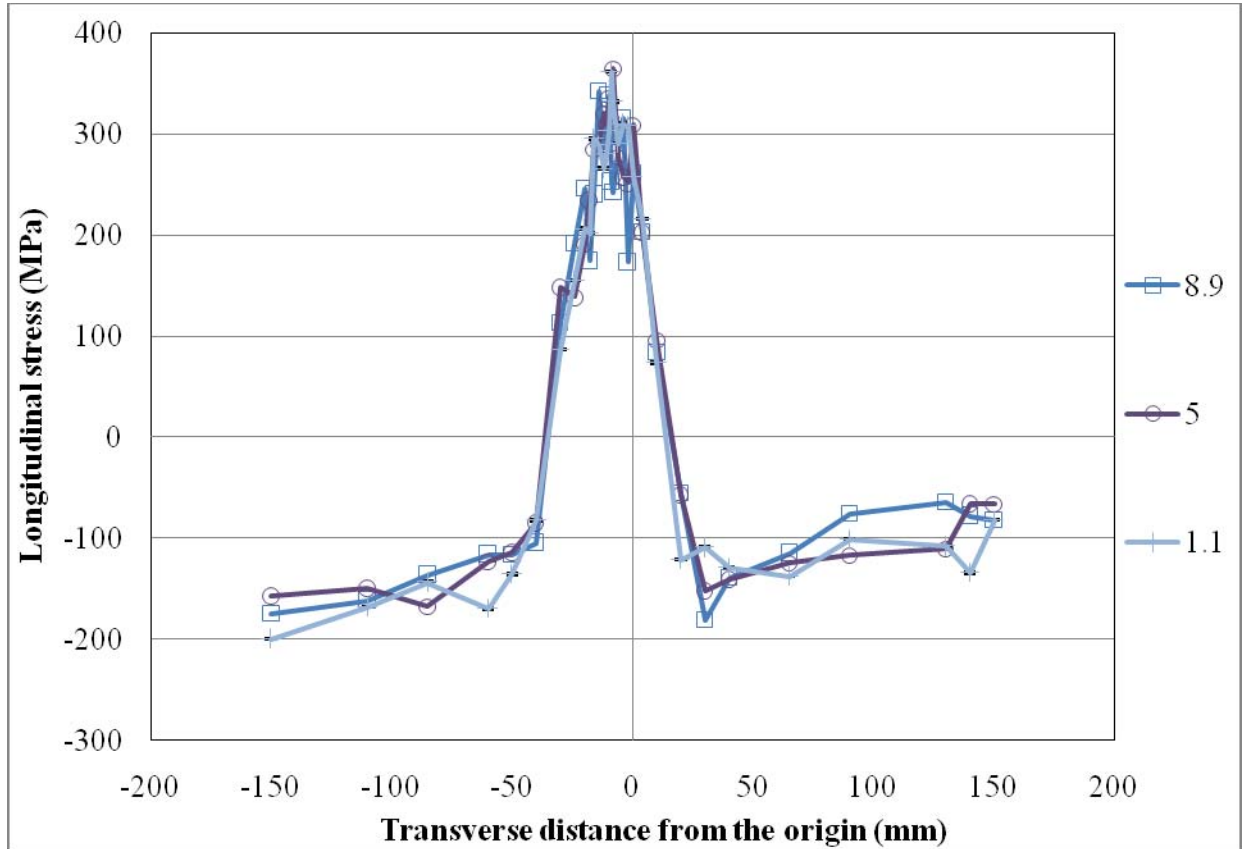


Figure 7.24: Longitudinal stress through the depth in transverse (T) direction (at L = 133 mm, line 5-2-6)

In Figure 7.25 and Figure 7.26, the three-dimensional stress distribution plots (not-to-scale) illustrate the stress level remains almost constant through the depth and transversely across the weld. A pivot table was used to organize this data and magnifies the area directly under the weld. From 10 mm on either side of the centreline of the weld, the stress measurements were taken at 1 mm or 2 mm intervals, and these measurements show in detail the even levels of stress within the weld. The stress levels do not vary more than 50 MPa from one end of the weld bead to the other.

One-dimensional distributions of the three stress components along the longitudinal direction (line 1-2 in Figure 7.17) are shown in Figure 7.27. It can be seen that stress level rises within 10-15 mm from origin (point 1) and then the stress level remains unchanged until about 20 mm away from the stop and start of the weld. The stress level reduces as the stop and start weld zone is approached. Due to the limitation in the set-up and the instrument, stress measurements further away into the weld overlap zone (stop and start zone) could not be taken.

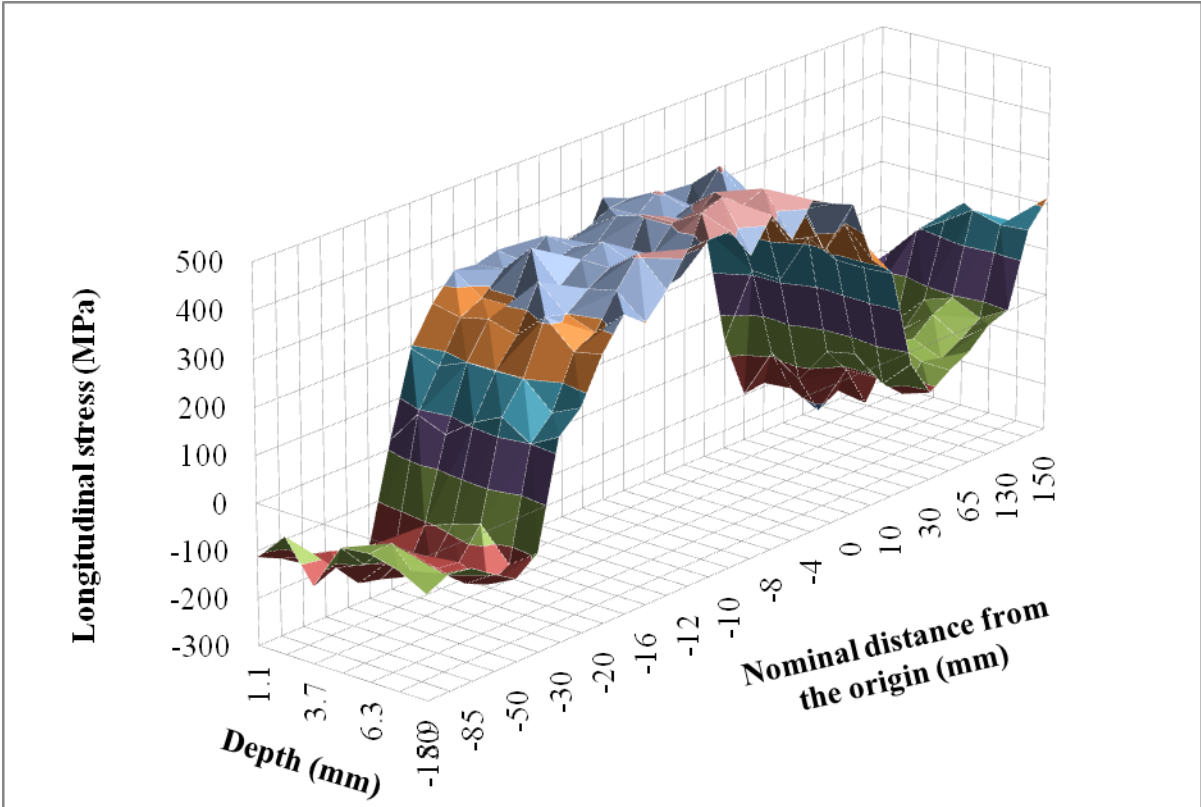


Figure 7.25: 3-D view of longitudinal stress distribution in transverse (T) direction (at L = 0 mm, line 3-1-4)

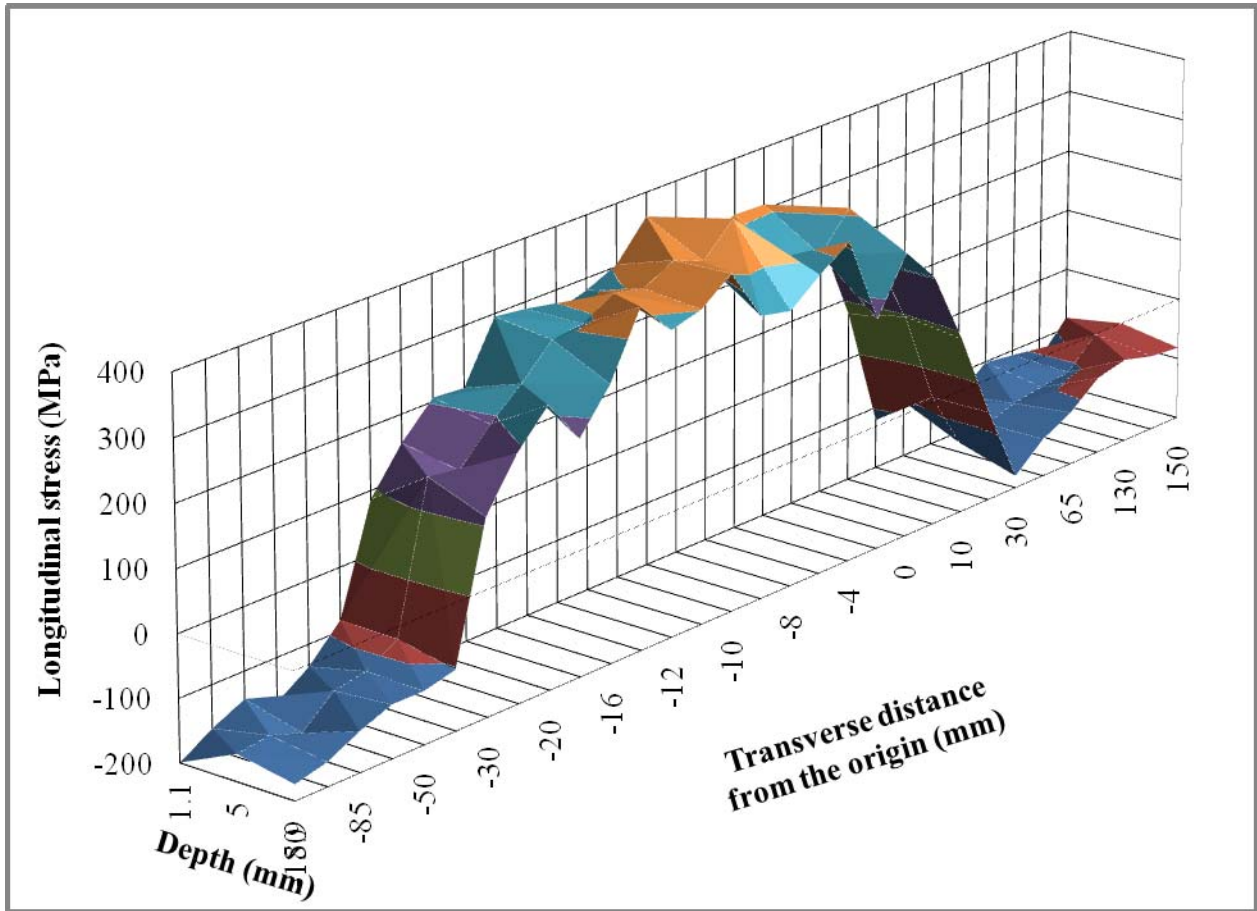


Figure 7.26: 3-D view of longitudinal stress distribution in transverse (T) direction (at L = 133 mm, line 5-2-6)

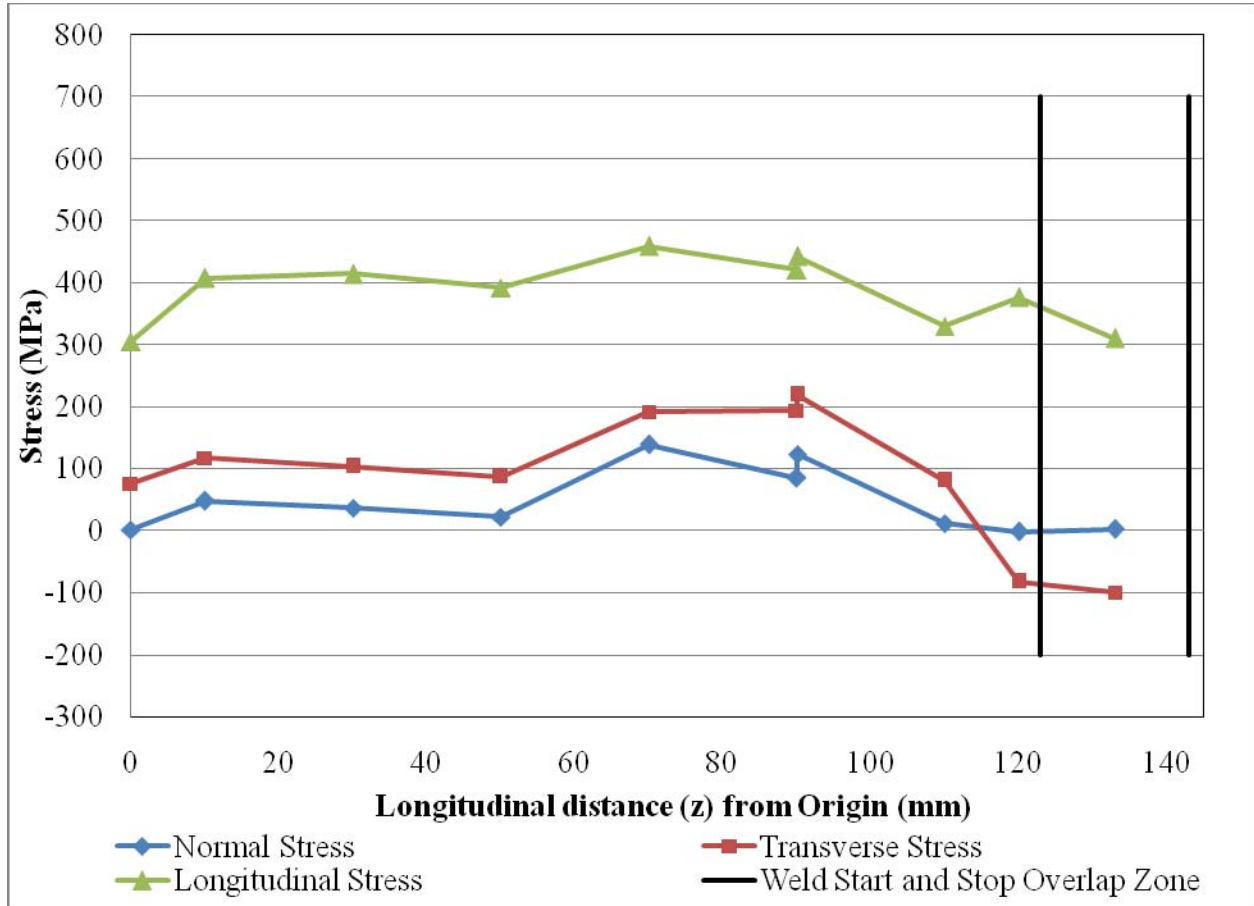


Figure 7.27: All stresses at Transverse = -10 mm, Normal = 8.9 mm (line 1-2)

7.2.3 Specimen 3

Specimen 3 was a stiffened plate which was 400 mm wide (T) x 600 mm long (L) x 9.5 mm thick (N). It had two 600 mm long stiffeners and the primary objective was to study the effects of welding a second stiffener on the stress distribution of the first welded stiffener. The specimen was measured for residual strain along the longitudinal (L) and transverse (T) directions at seven depths through the normal direction. Figure 7.28 shows the origin (point 1) and the lines (2-1-3) on which stress measurements were taken. Figure 7.29 shows the spacing of the measurements across the transverse direction of the plate.

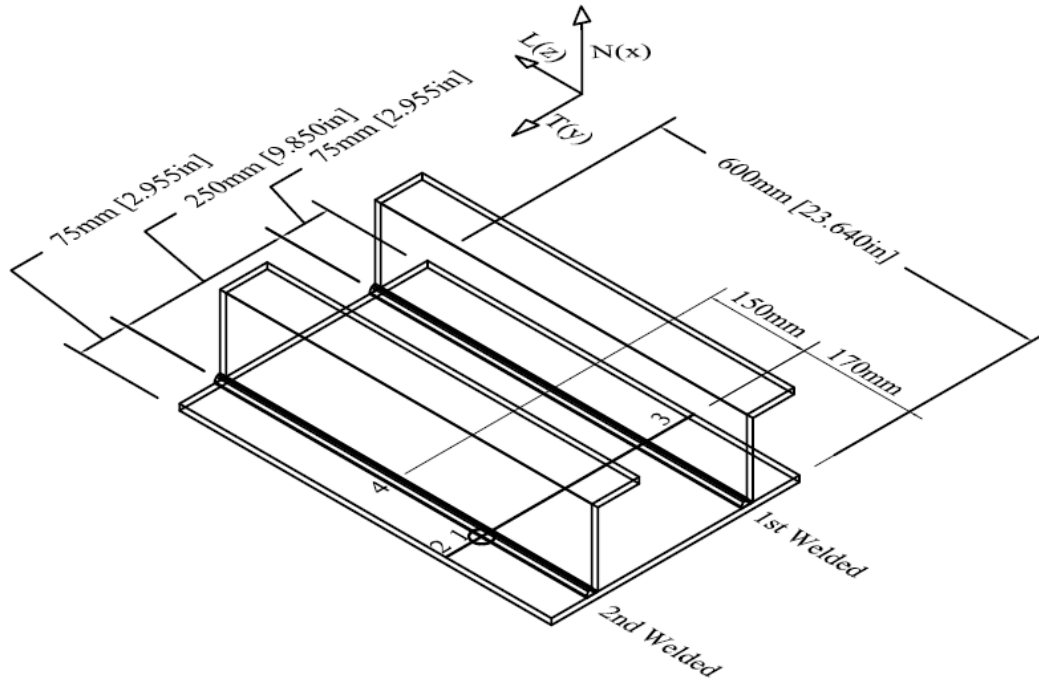


Figure 7.28: Detail for Measurement Points in Specimen 3

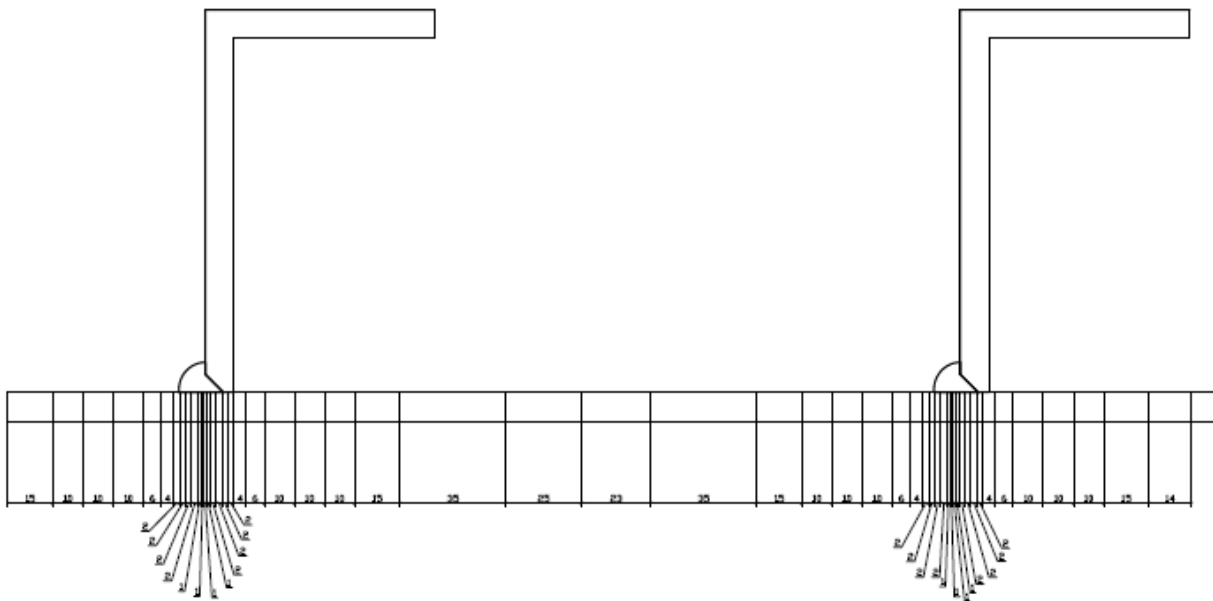


Figure 7.29: Measurement Spacing in mm

7.2.3.1 Normal Stress for Specimen 3

The normal stresses (σ_x or σ_{normal}) are calculated using all three strain components as shown in Equation 7.1. The normal stresses were measured along the entire transverse direction (on line 2-1-3) of 400 mm (Figure 7.28).

As mentioned earlier (Table 5-2) and for Specimen 3, the welding of stiffener 2 of this specimen could not be completed in a single non-stop run. The welding was stopped once and restarted after one minute on the second welded stiffener at 150 mm away (in positive L direction) from line 2-1-3 in Figure 7.28. The stop and start caused the weld overlap at that point (point 4 in Figure 7.28). The position of line 2-1-3 was chosen, as was done for Specimen 2, based on the location of a stop and start (point 4 in Figure 7.28) in the welding process. The location of the origin (point 1 in Figure 7.28) was chosen at the mid-length between the stop and start of the weld and the edge of the plate such that edge effect and the effect of weld inconsistency (stop and start in welding) are minimized. The spacing of the measurements was similar to those of Specimen 2. Near the centre of the weld where the focus of this study is, spacing was as small as 1 mm and gradually increased up to 40 mm further away from the weld, as shown in Figure 7.29. The measurements were taken at three depths in the transverse (T) direction (on line 2-1-3) at 54 locations, for a total of 162 points (= 54 x 3) and at seven depths in 11 locations (on same line 2-1-3) for a total of 44 points (= 11 x 4) to verify whether or not the strain values through the thickness of the plate changes. The total number of measurements taken on this specimen is 206 points (= 162 + 44).

The one-dimensional distribution for normal stresses (σ_x or σ_{normal}) for line 2-1-3 is shown in Figure 7.30. Each line shows the normal stress through the cross-section of the plate at specific distance from the origin (point 1 in Figure 7.28). It should be noted that a different graphical representation is shown for this stress component, as compared to the similar plots for Specimen 1. The lines at 8.9 mm, 5 mm, and 1.1 mm were depths where the three measurements were taken across the entire transverse direction and provide the most comprehensive picture of the normal stresses. The additional measurements collected at the four other depths (at 7.6 mm, 6.3 mm, 3.7 mm, and 2.4 mm) complete the picture of the stresses through the thickness of the plate (depth, N) to confirm the consistency of the stresses in this direction. For example, in Figure 7.30, the line with the crosses shows the stress levels at 8.9 mm from the bottom face of the plate

(measurements closest to the face where stiffeners are welded) with a minimum value of 119 MPa in compression to a maximum value of 32 MPa in tension. These values compared to those found in Specimen 2 for the same normal stress component ranging from 5 MPa in compression to 147 MPa in tension, show the range is roughly equal at 150 MPa of change, though the absolute values are shifted down for Specimen 3. This possibly shows that the stress balance for this specimen is located elsewhere. The three-dimensional stress plots are not shown for this stress component since they do not provide any valuable information.

Similar to both Specimens 1 and 2, the normal stress component does not show any clear pattern and this is again due to the presence of the locked-in normal stresses evident in the parent plate that likely developed during the rolling process. The normal stress values range from 150 MPa in compression to 32 MPa in tension, with the maximum value close to the weld centreline. These values are slightly lower than the range found on Specimen 2 (75 MPa in compression to 150 MPa in tension) and roughly 50% higher than the range found in Specimen 1 (40 MPa in compression to 80 MPa in tension).

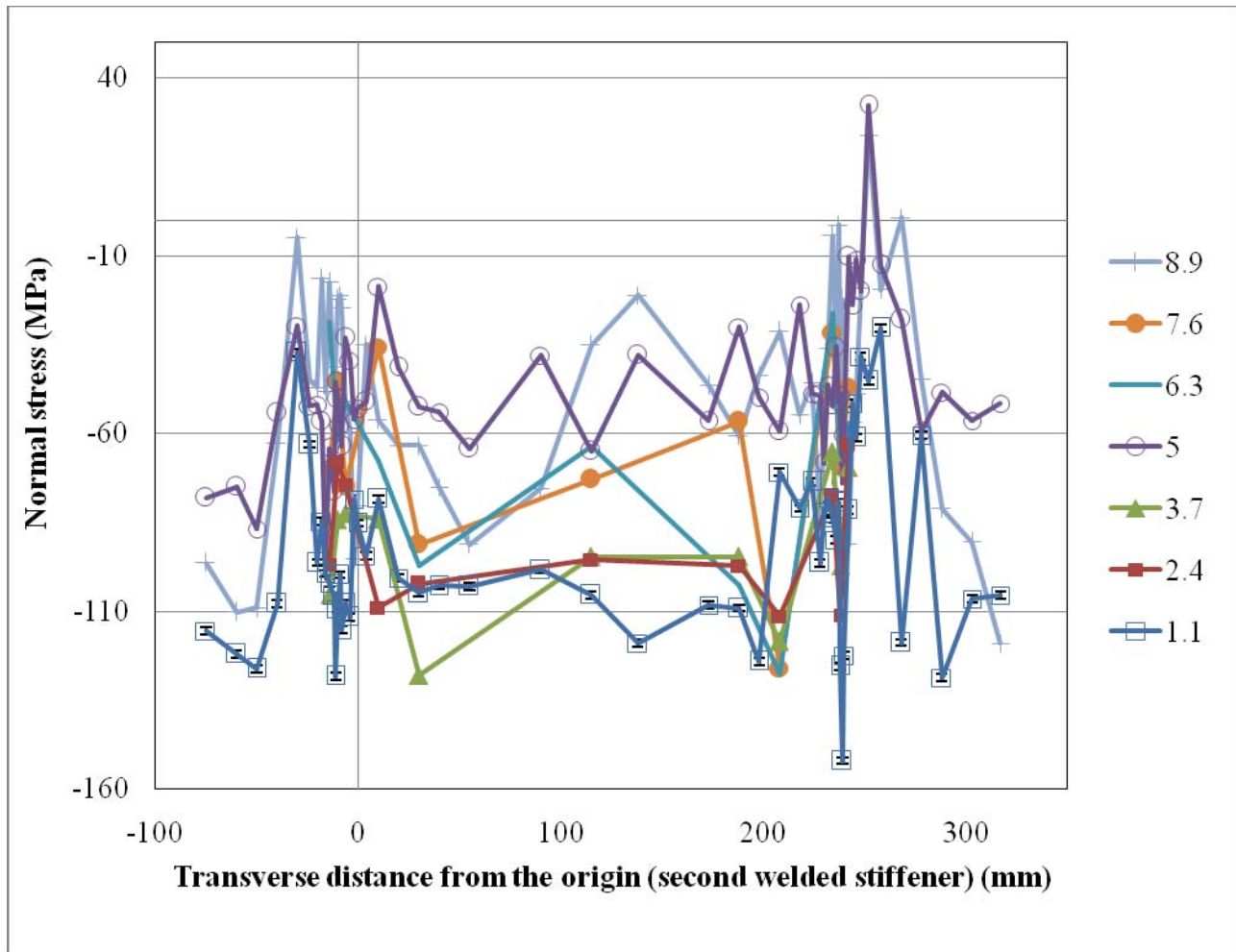


Figure 7.30: Normal stresses through the depth in transverse (T) direction (line 2-1-3)

7.2.3.2 Transverse Stress for Specimen 3

The transverse stresses (σ_y or $\sigma_{\text{transverse}}$) are calculated using Equation 7.2 and measured at the same points where the normal stress component was measured (Figure 7.28). The measurement points are shown in Figure 7.29. Similar to the measurements for the normal stress component, the transverse stress was also measured at three depths in 54 locations for a total of 162 measurement points. However, due to time constraints only nine locations were measured through the thickness to verify stress value, therefore 36 points (= 9 x 4). The total number of measurements that were taken on this plate was 198 points (= 162 + 36).

The one-dimensional distributions for transverse stress are shown Figure 7.31 for line 2-1-3. The three-dimensional stress plots are not shown for this specimen since they do not follow any clear pattern.

The stress values on line 2-1-3 range from about 240 MPa in compression to 50 MPa in tension. The stress values at a depth of 3.7 mm show a difference of approximately 100 MPa (compression) from the other depths through the thickness. This difference is best explained by the inherent locked-in stresses found in the parent plate, where at a depth of 3.7 mm the values were at the minimum. For example, at the distance 115 mm from the origin the change in stress levels between a depth of 2.4 mm and 3.7 mm is about negative 90 MPa. For Specimen 1, the change in transverse stress levels between 2.4 mm and 3.7 mm depths is similar, that is about negative 100 MPa. As was shown in Specimen 1, the maximum tensile stresses are found in between the depths of 5 mm and 6.3 mm, which is also apparent in Specimen 3.

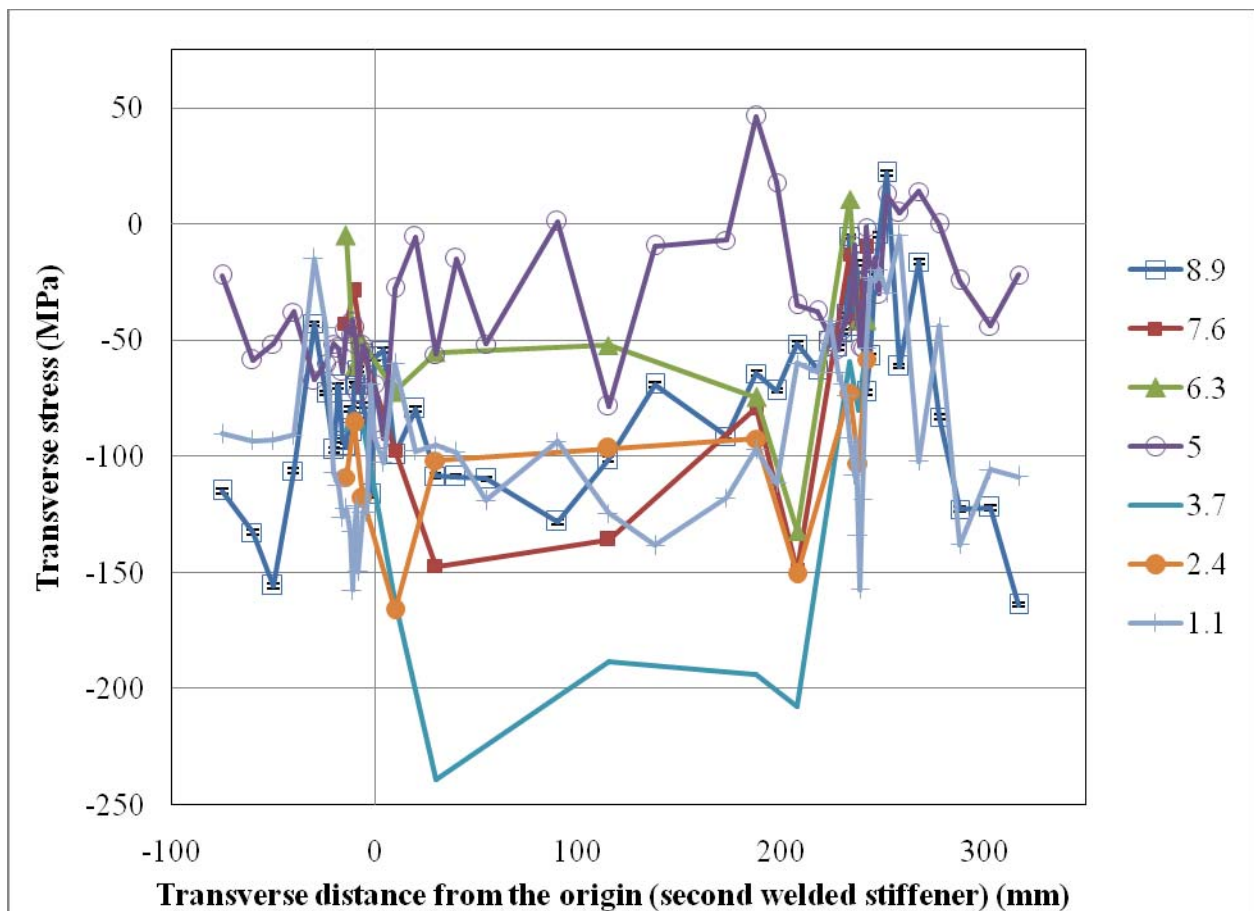


Figure 7.31: Transverse stresses though the depth in transverse (T) direction (line 2-1-3)

7.2.3.3 Longitudinal Stress for Specimen 3

The longitudinal stress (σ_z or $\sigma_{\text{longitudinal}}$) was calculated using Equation 7.3 and were measured at the same points and depths as was done for the normal and transverse stress components (Figure 7.28 and Figure 7.29). The longitudinal strain component was collected using two different set-ups and therefore, two different sets of constants. The second set-up was similar to the longitudinal set-up for Specimens 1 and 2, and was completed in October of 2008 during the third visit to CRL. The first set-up had the plate positioned at 45° and was used to collect the difficult points that were under the stiffeners.

Figure 7.32 shows the one-dimensional distribution for the longitudinal stress for line 2-1-3. The pattern of distribution of the stress values is better for this stress component. This figure shows that the depth does not affect the stress levels as much as it did for the transverse stress component. This figure shows the peak in tensile (positive) stresses occur at the weld and as the transverse (T) distance from the weld increases the stresses reduce to a compressive (negative) stresses and plateau (stress distribution between two stiffeners) is about 150 MPa in compression. The three-dimensional view (not-to-scale) of these stresses is shown in Figure 7.33 for the three depths (at 8.9 mm, 5 mm, and 1.1 mm).

The maximum tension (positive) stresses are at the centreline of the weld at a depth of 8.9 mm, equal to 430 MPa with an error of ± 15 MPa. Therefore, the longitudinal stress level at the weld is found to be higher than the yield stress (405 MPa) obtained from material tests on the plate. The peak stress values are slightly higher on the first welded stiffener (max = 430 MPa in tension) than the second welded stiffener (max = 386 MPa in tension), with stress error levels of approximately ± 10 MPa to ± 30 MPa. The majority of the peak values at the weld centreline are in the range of 400 MPa, just below the yield stress level.

This figure also shows that the stress values on line 2-1-3 range from 360 MPa in compression to 430 MPa in tension. These values if compared with similar values for Specimen 2 (which had one stiffener and welded with same heat level) measured at $L = 0$ mm (200 MPa in compression to 450 MPa in tension) are more compressive. The same values compared with the parent plate (Specimen 1 which had longitudinal stress value in the range of -40 MPa to +90 MPa) the range is roughly six times greater in Specimen 3. Therefore, at the stiffener spacing of 250 mm, the

tensile stress levels are higher at the first welded stiffener. The spacing of 250 mm still allows for interaction between the stress fields from each stiffener, producing an area of compression stress (plateau) between the stiffeners. Therefore, it may be concluded that in this specimen welding of second stiffener reduced the tensile stress levels (occurs under the weld) and creates a definite compressive stress plateau in between the two stiffeners.

The plateau between the two stiffeners shows that once at a certain distance from the centreline of the weld the stress levels stabilize and show little variation. The plateau between roughly 20 mm and 208 mm from the origin, shows a range of longitudinal stress values from -220 MPa to -100 MPa, with stress error levels of approximately ± 10 MPa to ± 30 MPa.

Figure 7.33 illustrates the three-dimensional stress distribution plot (not-to-scale) and it can be seen that the stress level remains almost constant through the depth and transversely across the weld. A pivot table was used to organize this data and magnifies the area directly under the weld. From 10 mm on either side of the centreline of the weld, the stress measurements were taken at 1 mm or 2 mm intervals, and these measurements show in detail the even levels of stress within the weld. The stress levels do not vary more than 50 MPa within each weld bead, from one edge of the weld to the other edge of the same weld bead.

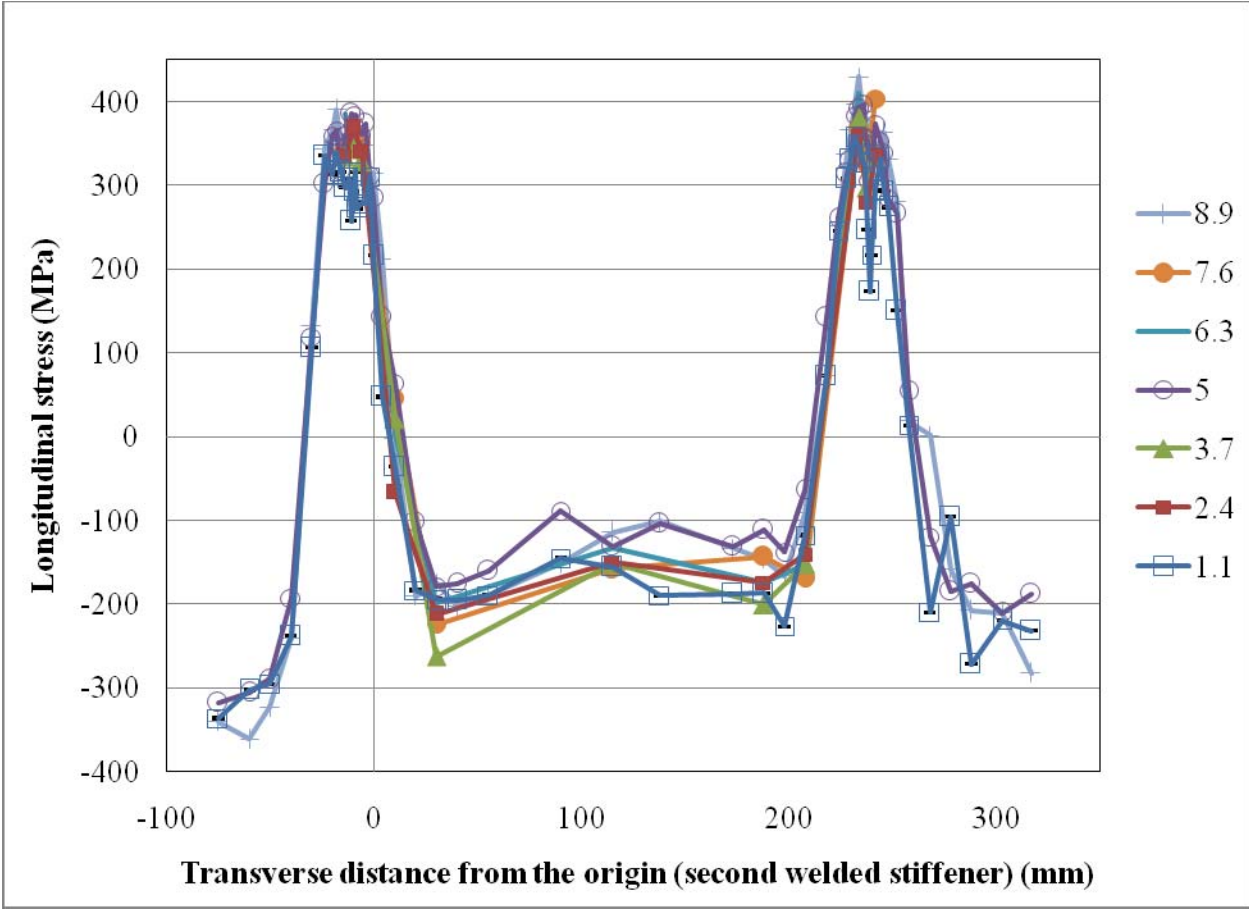


Figure 7.32: Longitudinal stresses through the depth in transverse (T) direction (line 2-1-3)

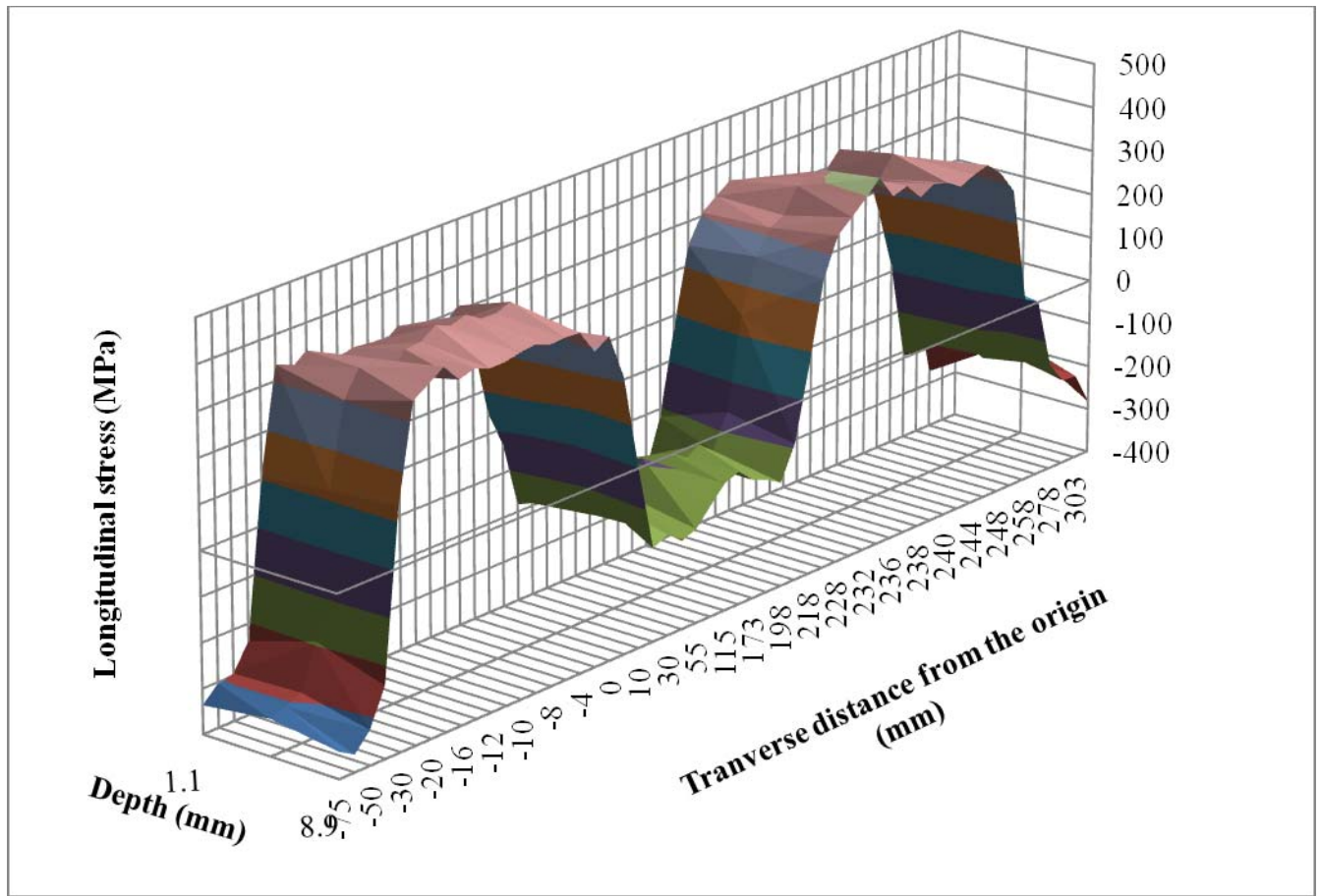


Figure 7.33: 3-D view of longitudinal stress distribution in transverse (T) direction (line 2-1-3)

8 TEST RESULTS FOR PHASE II

As mentioned earlier, a total of three stiffened plate specimens were tested to measure the three-dimensional (3-D) stress distributions (see Table 4-2 and Table 5-3). Specimen 4 was added to study the effect of termination of a stiffener on the residual stress distributions. Specimens 5 and 6 were designed to study the effect of change in spacing of stiffeners and effect of level of heat input on the residual stress distributions. All the measurements for Specimens 5 and 6 were completed. Beam time required for taking measurements of all the three strain components of Specimen 4 was found to be very long. Therefore, it was decided to take measurements on Specimen 4 for the transverse component at three depths and the longitudinal component at one depth only. Following sections and sub-sections discuss the geometry, shape, and other details for the three specimens tested in Phase II.

8.1 Specimen Details

8.1.1 Specimen 4

The test matrix (Table 4-2), test setup, test method, and welding specifications are discussed in earlier sections. Specimen 4 with its dimensions is shown in Figure 8.1. This specimen was tested to determine the effect of sudden discontinuity of the stiffener that is, to study what happens when a stiffener is not continued until the edge of the plate. The dimensions of this specimen are 600 mm long x 400 mm wide x 9.5 mm thick and the stiffener was 400 mm long that is, the stiffener was 200 mm shorter than the length of the parent plate.

8.1.2 Specimen 5

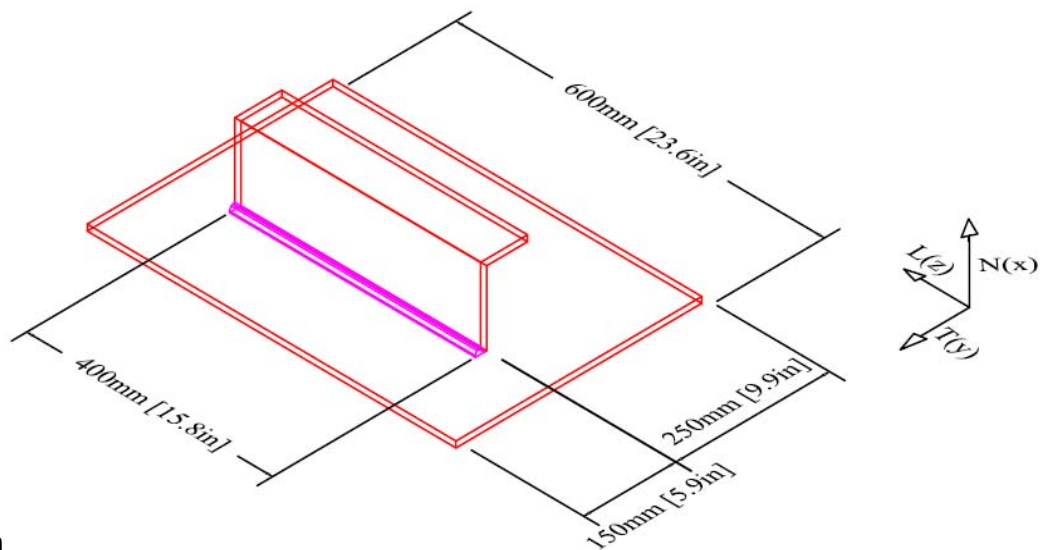
Specimen 5 as shown in Figure 8.2 was a stiffened plate with dimensions of 400 mm long (L) x 600 mm wide (T) x 9.5 mm thick (N). Two 400 mm long stiffeners were welded on this plate spaced at 400 mm on centre using high heat input (~2.5 kJ/mm). The objective was to determine the effect of stiffener spacing on residual stress distributions.

8.1.3 Specimen 6

Specimen 5 and 6 are similar specimens. However, the stiffeners for Specimen 6 were welded with moderate heat input (~ 1.75 kJ/mm) and the objective was to determine the effect of level of heat input on the residual stress distributions.



(a) photo

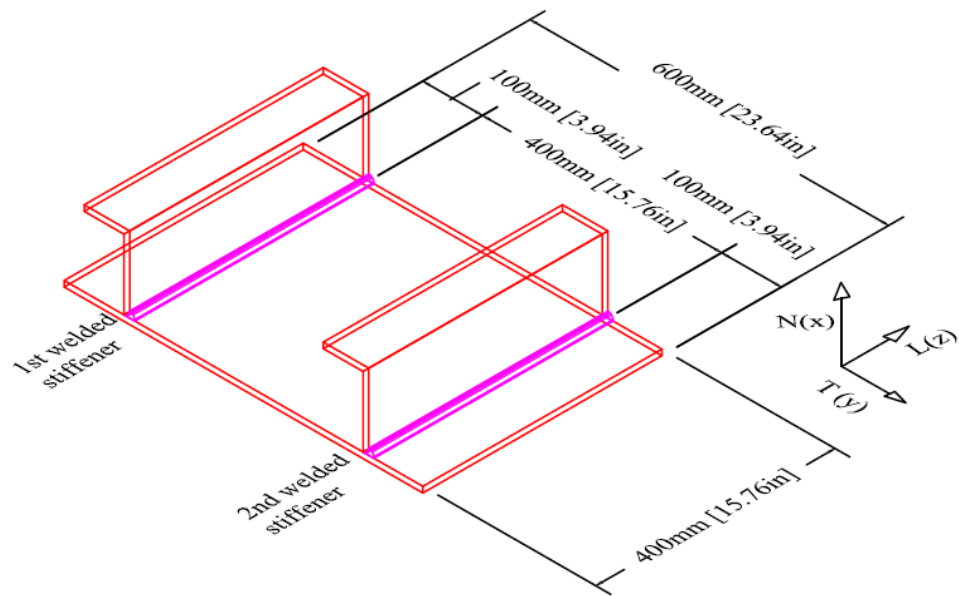


(b) sketch

Figure 8.1: Specimen 4 (a) is a photo and (b) is the sketch



(a) photo



(b) sketch

Figure 8.2: Specimens 5 and 6 (a) is a photo and (b) is the sketch

8.2 Test Results

8.2.1 Specimen 4

Specimen 4 is shown in Figure 8.1 and Figure 8.3. It was a 600 mm long and 400 mm wide stiffened plate and one 400 mm long angle stiffener (127 mm x 76 mm x 9.5 mm) was welded on this plate at 150 mm from one of the two longer edges and centered in the 600 mm direction of the plate. The objective was to determine the stress distribution around the toe of the weld near the termination of the stiffener. The specimen was measured for residual strain along the longitudinal (L) and transverse (T) directions at three depths (through the normal (N) direction). The transverse strain component was measured at three depths and the longitudinal strain was collected at one depth, closest to the weld (at $N = 8.4$ mm). Therefore, the normal strain component has not been collected for this specimen. The normal strain component and the remaining longitudinal component depths could not be collected since the necessary beam time required for these measurements is too high and the beam time used by then had already significantly exceeded the allotted time.

A small open circle along line 4 in Figure 8.3 shows the origin of the coordinate system. This figure also shows all the lines where the measurements were taken for this specimen (lines 1 through 9). As mentioned before, only longitudinal and transverse strain components were measured. Since, all the three strain components are needed to calculate the stress components, stress distributions could not be plotted for this specimen. Therefore, the strain distributions for the longitudinal and transverse components are presented for Specimen 4. On lines 7, 8, and 9 the strain measurements were taken from 0 to -30 mm and from 0 to +40 mm in the longitudinal direction (along L in Figure 8.3).

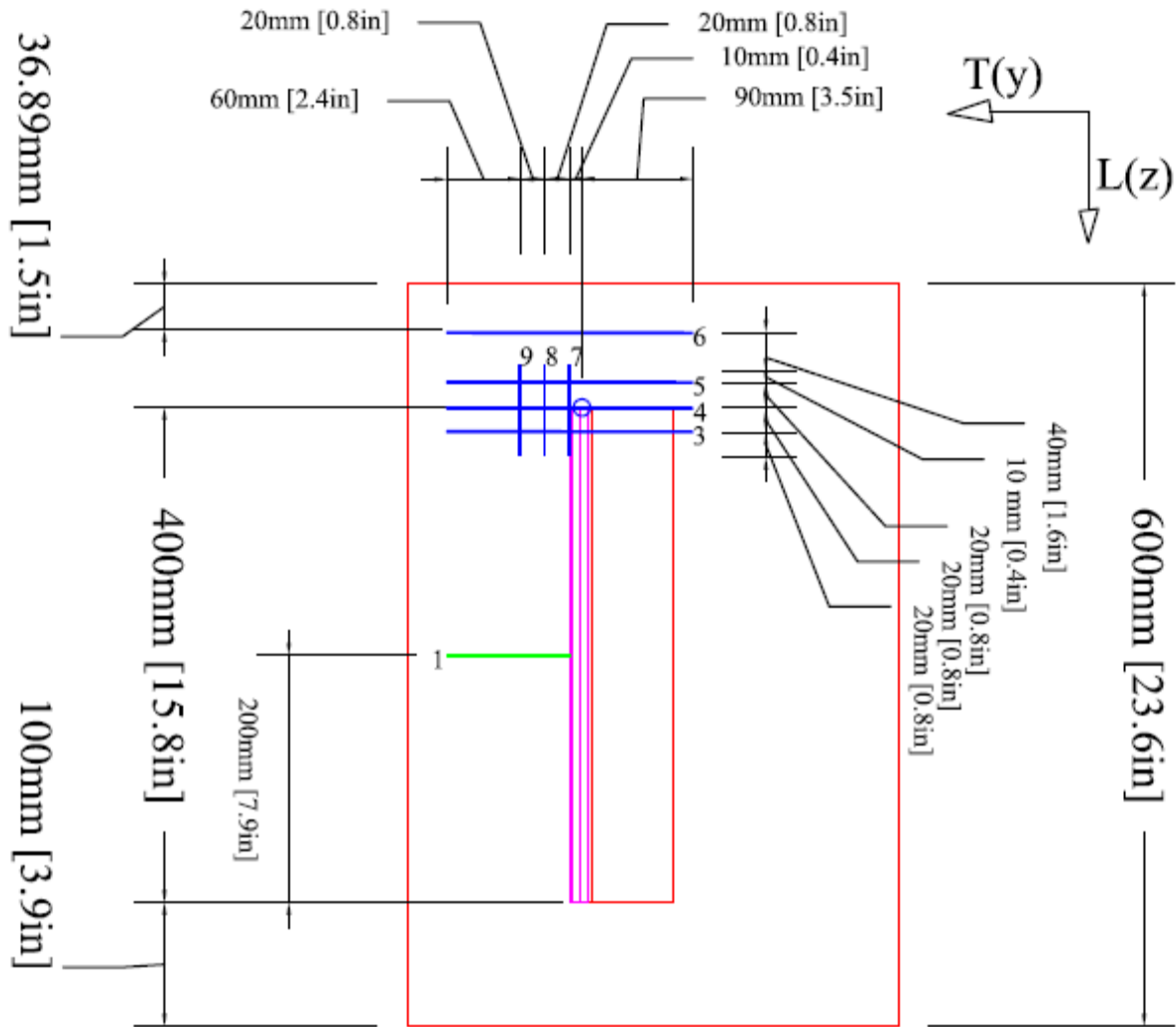


Figure 8.3: Detail for Measurement Points for Specimen 4

8.2.1.1 Transverse Strain for Specimen 4

The transverse strain is the strain in the direction perpendicular to the stiffener (in the direction T in Figure 8.3). The strain measurements for the transverse component were acquired along line 1 and also along lines 3 through 9. The spacing between two consecutive measurements points was smaller near the weld since the strain gradient is expected to be higher there. Figure 8.4 shows the points where transverse strain measurements on lines 1, 3, 4, 5, and 6 were taken. The longitudinal direction strain measurements were taken evenly at 5 mm along lines 7, 8, and 9. Lines 7, 8, and 9 are 40 mm from the origin into the stiffener and 30 mm from the origin away from the stiffener towards line 6. The measurements were taken at three depths through the

thickness of the plate at each point thus, a total of 411 ($= 3 \times 137$) measurements were taken for this specimen.

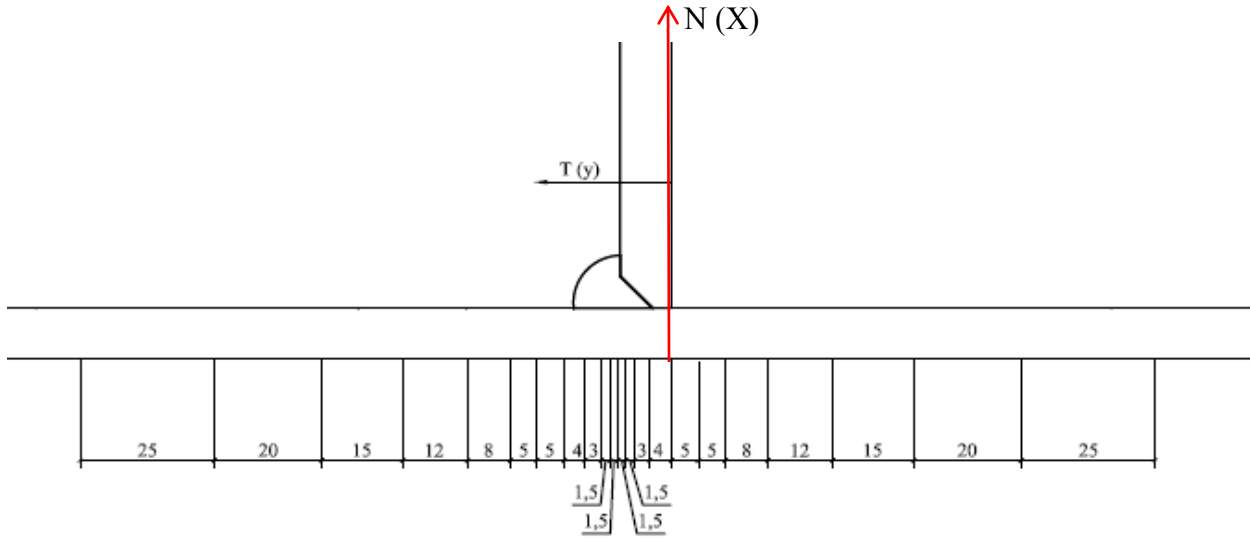


Figure 8.4: Spacing of measurements (in mm) in transverse direction on Specimen 4 (lines 1, 3, 4, 5, and 6)

Strains on line 1 of this specimen were measured to compare the strain values near the termination line of the stiffener. It may be worth mentioning here that the strain measured on line 1 for this specimen agrees well with the strain values found in Phase I for Specimen 2 (specimen with single stiffener that runs through the full length of the plate) along line 4-1-3 (see Figure 7.17). The transverse strain values for line 1 for Specimen 4 are shown in Figure 8.5. The transverse strain values for Specimen 2 are presented in Figure 8.6.

Line 4 is located exactly at the edge (termination line) of the stiffener, line 3 is located 20 mm away from line 4 and in the negative L direction, line 5 is located 20 mm away from line 4 in the positive L direction, and line 6 is 60 mm away from line 4 in the positive L direction. One dimensional transverse strain distributions for line 3, 4, 5, and 6 are shown in Figure 8.7, Figure 8.8, Figure 8.9, and Figure 8.10, respectively. Each line on these figures shows the strain distribution along the transverse direction at a specific depth and on a specific line of the plate. For example, the line with circle markers in Figure 8.8 shows the strain distribution of transverse strain component at 4.8 mm depth on line 4 (that is, at $N = 4.8$ mm in Figure 8.1) of the plate.

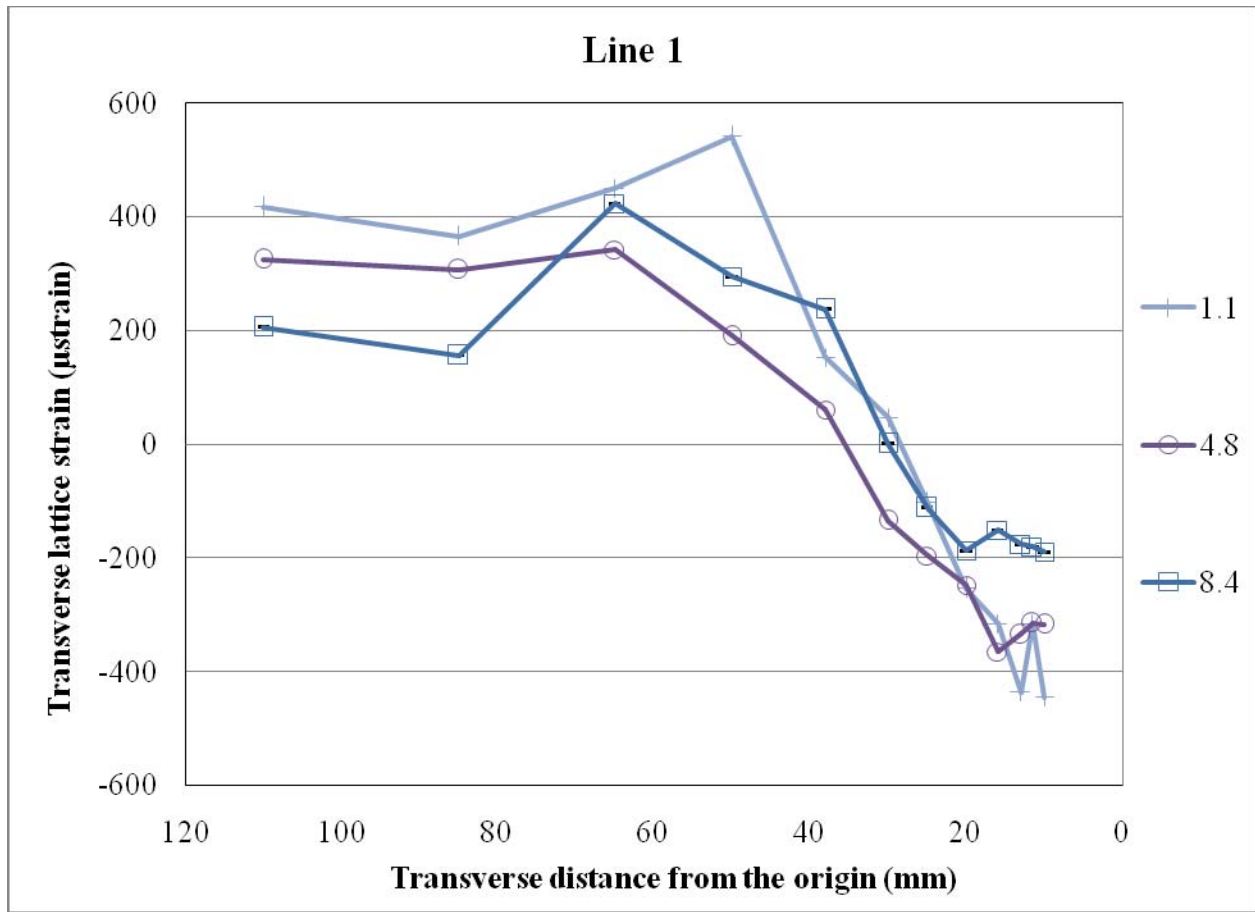


Figure 8.5: Transverse strain at various depths in the transverse (T) direction on line 1 (at L = 200 mm)

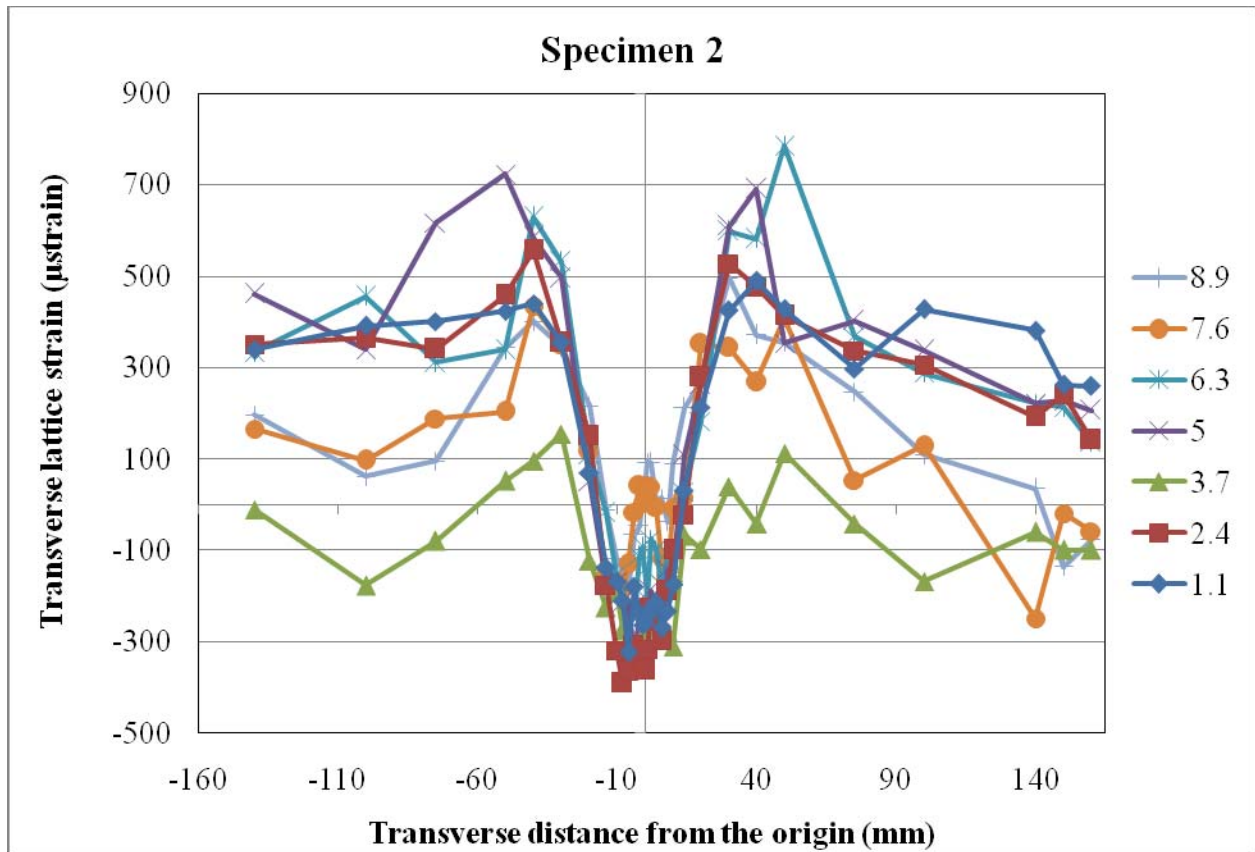


Figure 8.6: Transverse strain at various depths in the transverse (T) direction on line 1 (at L = 200 mm)

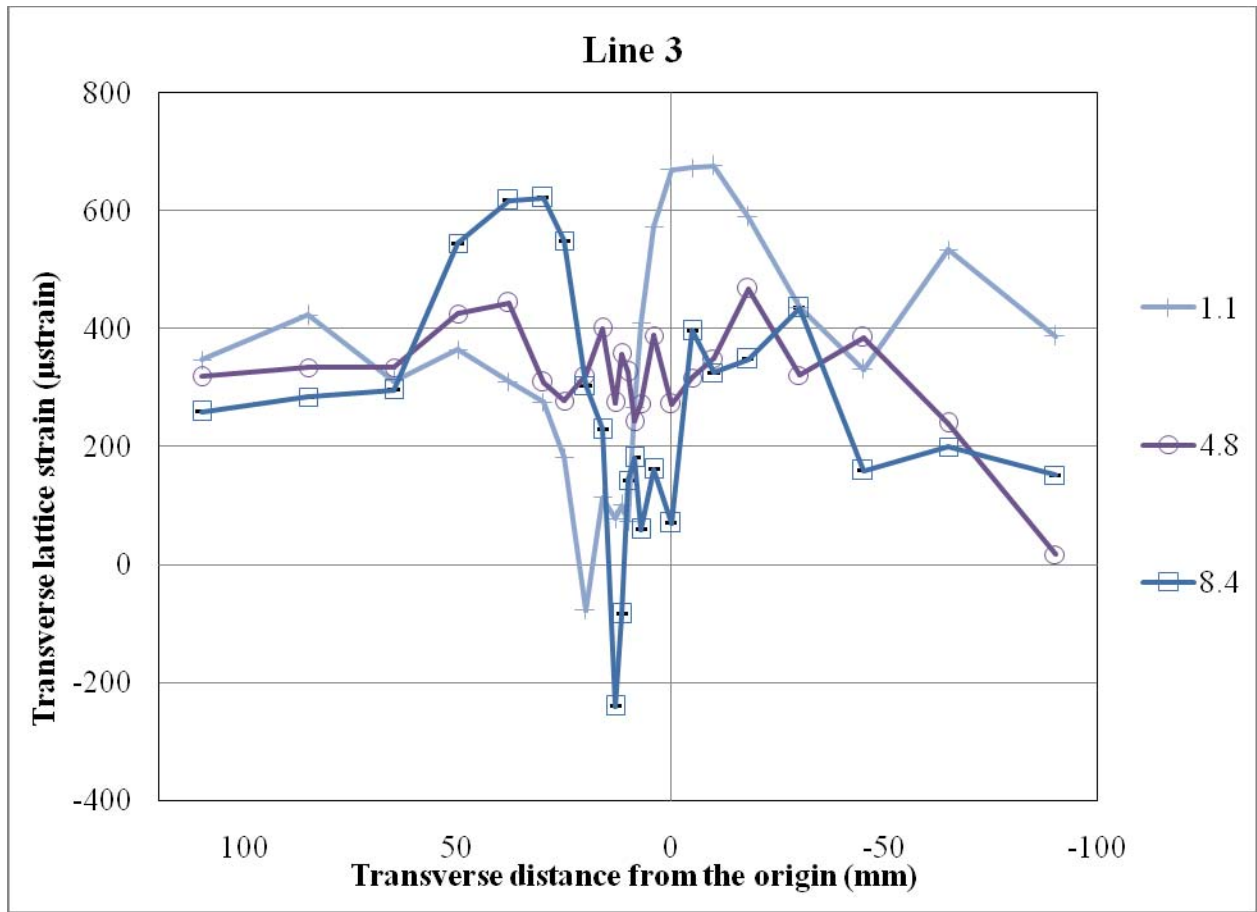


Figure 8.7: Transverse strain at various depths in the transverse (T) direction on line 3 (at L = 20 mm)

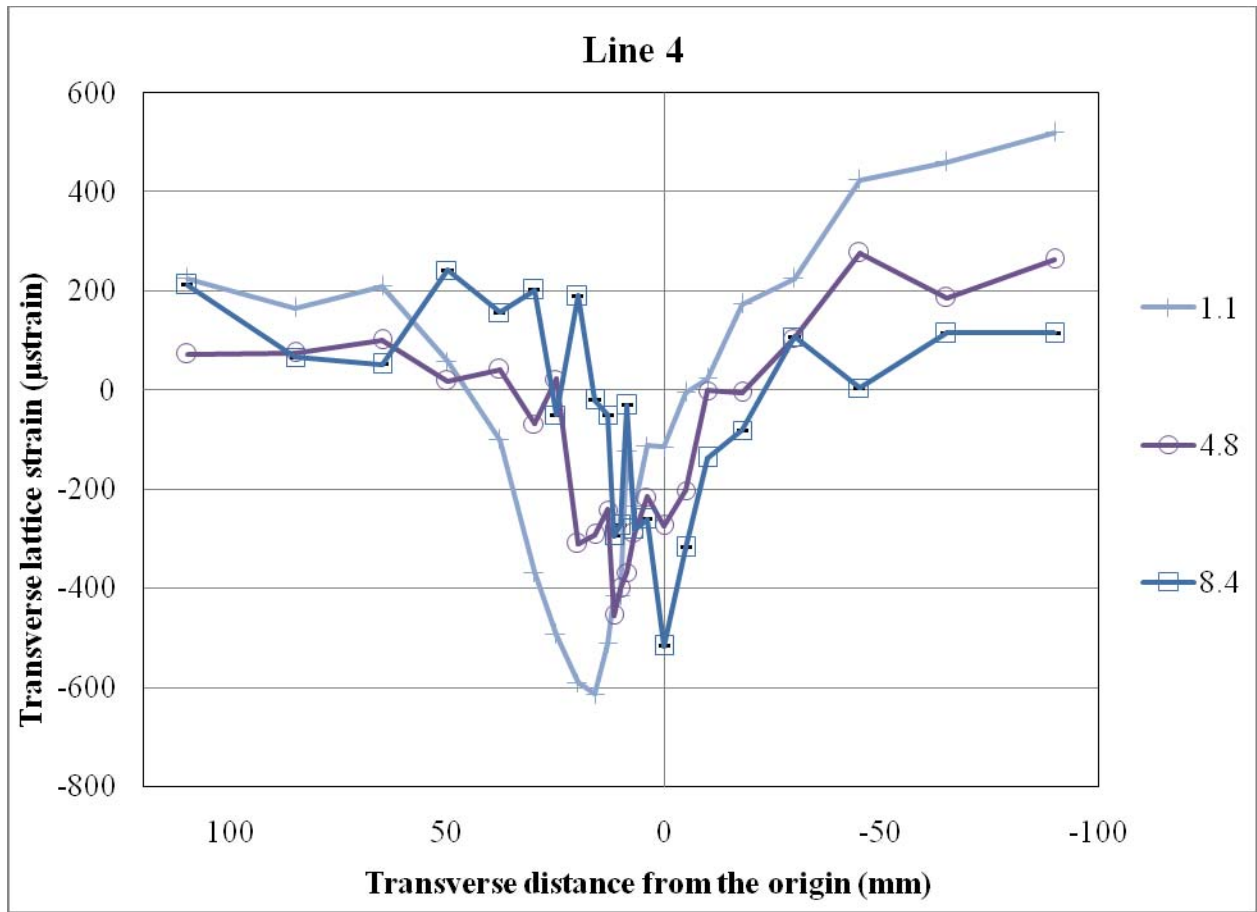


Figure 8.8: Transverse strain at various depths in the transverse (T) direction on line 4 (at L = 0 mm)

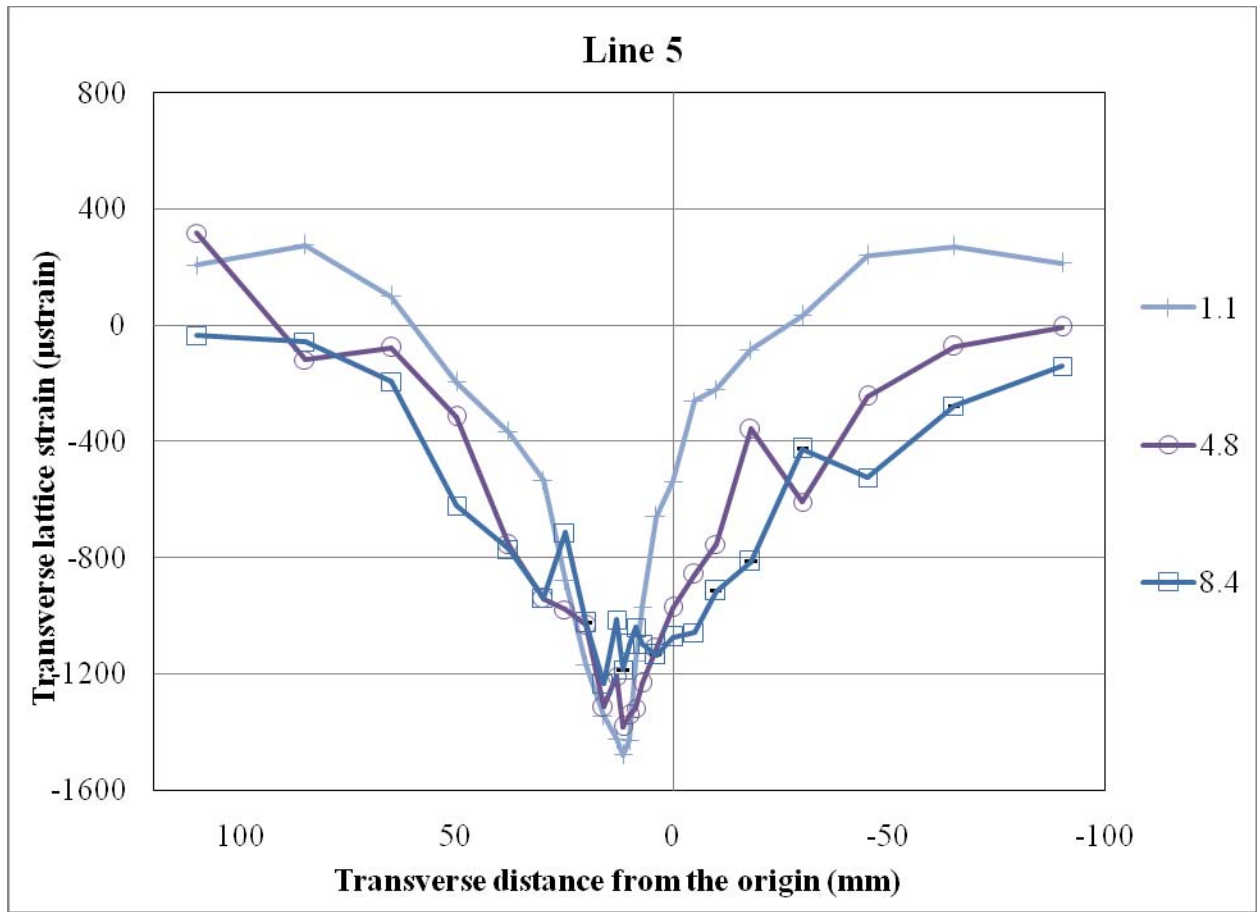


Figure 8.9: Transverse strain at various depths in the transverse (T) direction on line 5 (at L = -20 mm)

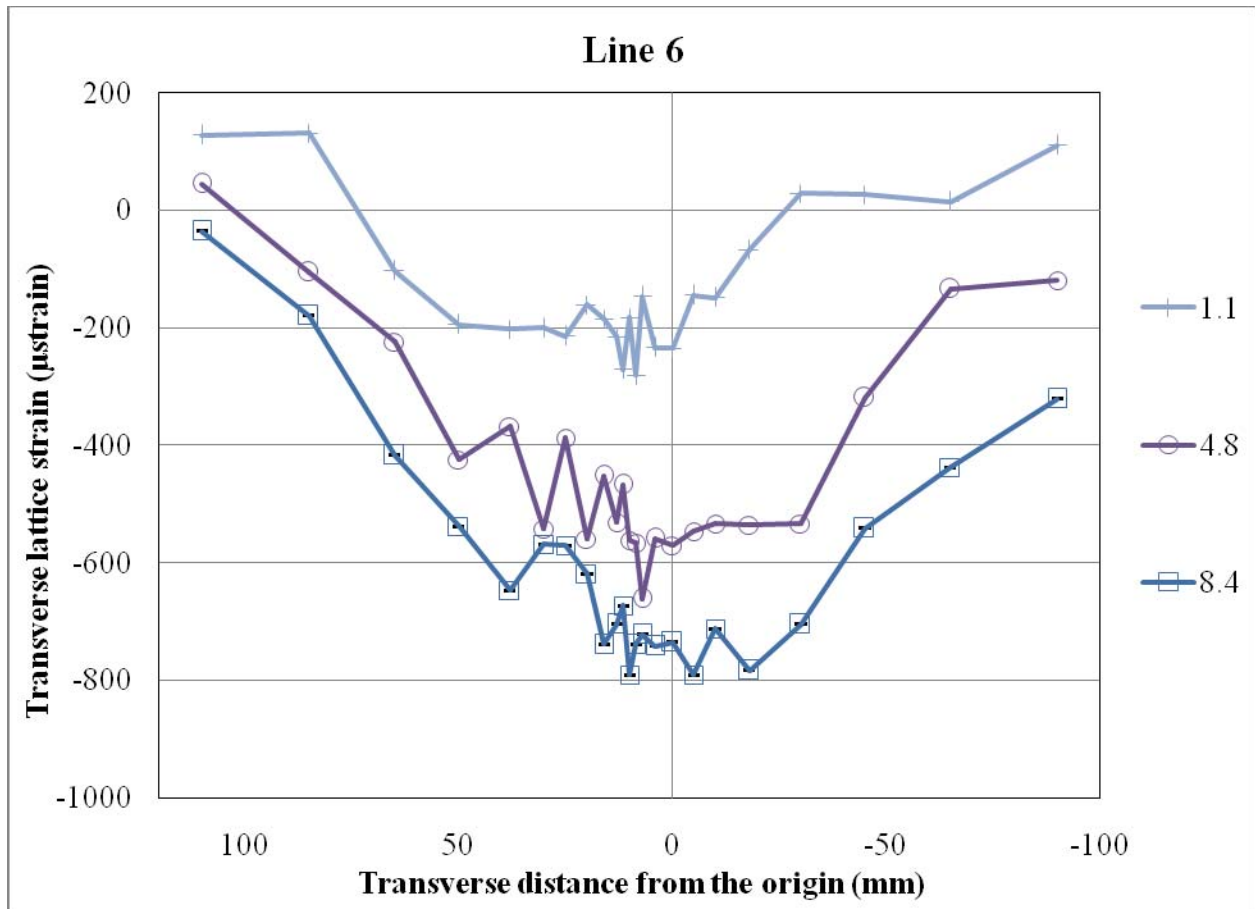


Figure 8.10: Transverse strain at various depths in the transverse (T) direction on line 6 (at L = -60 mm)

The transverse strain distributions in the transverse direction of the plate show a general pattern. It can be seen that the transverse strains shows maximum negative (compressive) value at the centre of the weld (that is, at T = 10 mm in Figure 8.3 and Figure 8.4) and the negative strain value gradually reduces as the transverse distance (T) from the weld increases. The strain value may finally become positive (tensile) depending upon the transverse distance of measurement. A comparison of all the transverse strain in the transverse direction on Lines 1, 3, 4, 5, and 6 at a depth of 8.4 mm (N = 8.4 mm in Figure 8.3 and Figure 8.4) are shown in Figure 8.11. This figure shows the transverse strain values and its distribution on line 4 which is located at the edge of the stiffener (at the termination line of the stiffener) are similar to those for line 1. Strain values on line 3 are more tensile (positive) than those on lines 1 and 4. On the other hand, lines 5 and 6 show higher negative strain values than those on lines 1 and 4.

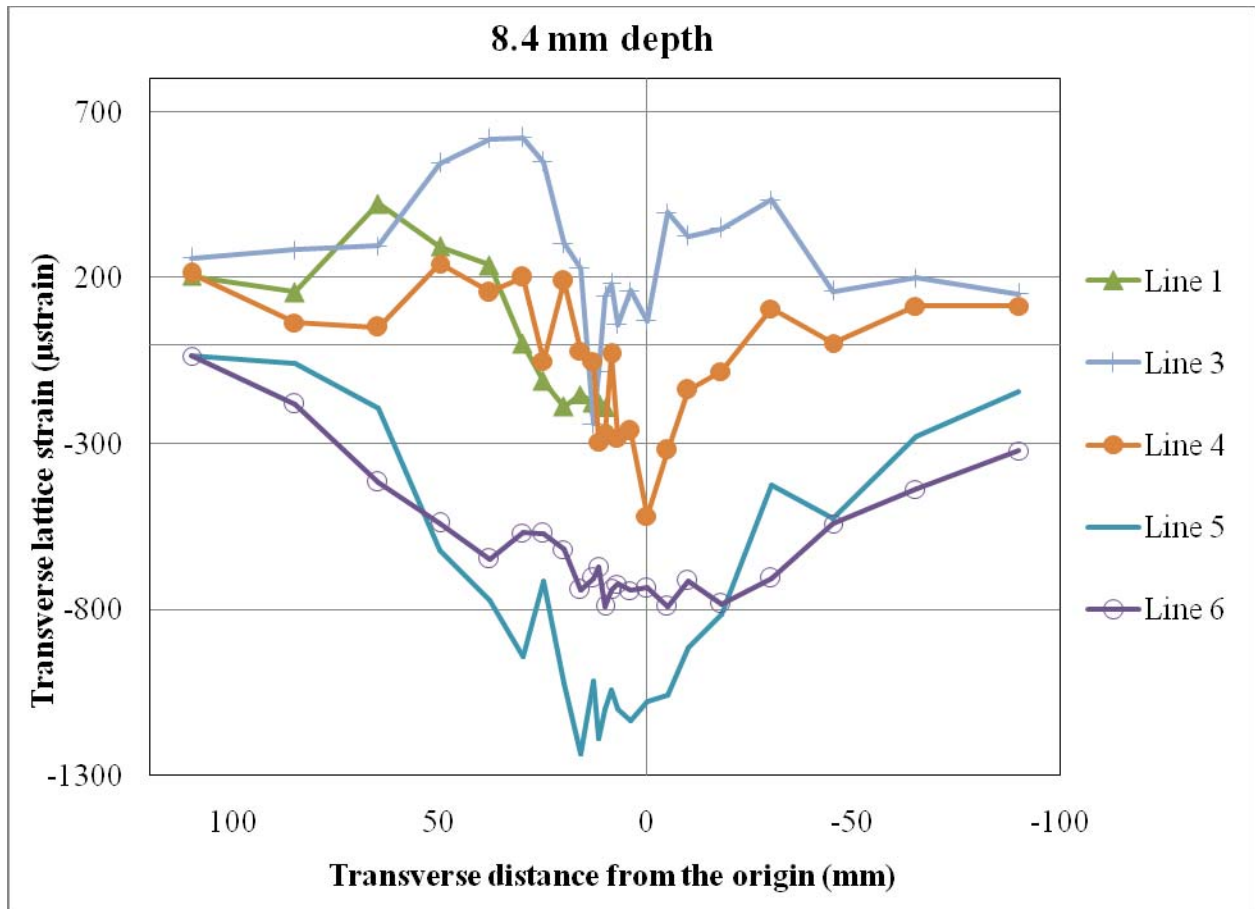


Figure 8.11: Transverse strain at a depth of 8.4 mm in the transverse (T) direction on lines 1, 3, 4, 5, and 6

Transverse strain measurements were taken in the longitudinal direction as well that is, on lines 7, 8, and 9. Line 7 was located at $T = 10$ mm that is, at the approximate weld centreline. Lines 8 and 9 were at $T = 30$ mm and $T = 50$ mm, respectively. The strain measurements in the longitudinal direction (direction L) of the weld were taken to study the pattern of residual strain parallel to the weld. The main focus was to understand the pattern of strains in the parent plate near the toe of the weld and the change in strain levels as the distance perpendicular to the weld (distance T) increases. The transverse strain distributions for lines 7, 8, and 9 are shown in Figure 8.12, Figure 8.13, and Figure 8.14, respectively. Value of strain on line 7 (that is, at the weld centreline) ranges from 1450 micro strains in compression to 400 micro strains in tension. The strain values on line 8 ranges from 1050 micro strains in compression to 700 micro strains in tension (Figure 8.13). The strain value on line 9 varies from 700 micro strains in compression to 800 micro strains in tension (Figure 8.14).

Figure 8.15 shows the comparison of strain distribution (at depth of 8.4 mm) obtained from three longitudinal lines (lines 7, 8, and 9). These three lines show same pattern of transverse strains. As the longitudinal distance increases in the positive L direction, the transverse residual strain values increases. On line 7, there is a sudden drop in the transverse strain values at and near $L = 0$ mm and this may be due to the physical end or toe of the weld. On lines 8 and 9, similar behaviour (at and near $L = 0$ mm) is not seen and this is because these lines are relatively away from the weld. Therefore, it can be concluded that as the transverse distance from the weld centreline (from line 7) increases the transverse tensile residual strain values increases and transverse compressive strain value decreases (see Figure 8.15).

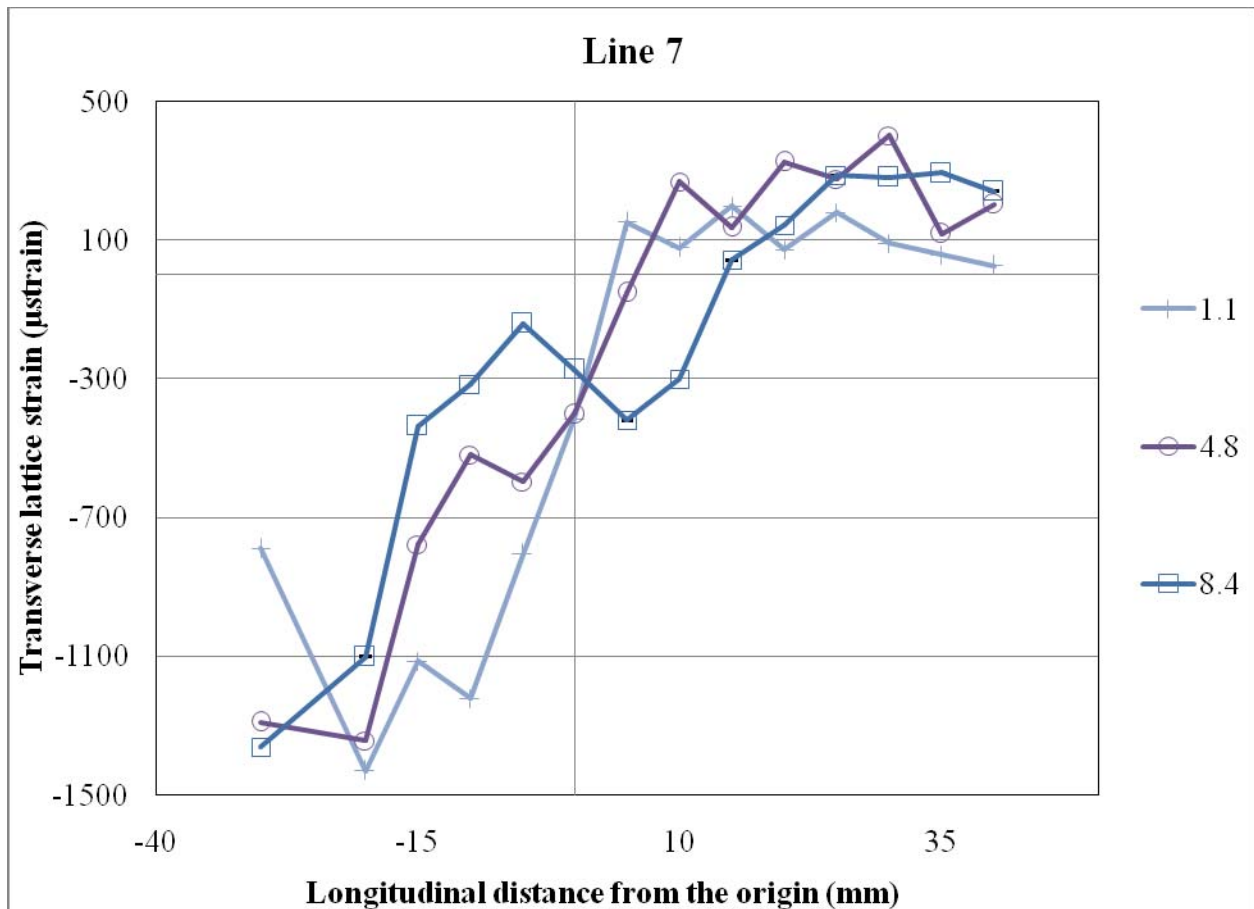


Figure 8.12: Transverse strain at various depths in the longitudinal (L) direction on line 7 (at $T = 10$ mm)

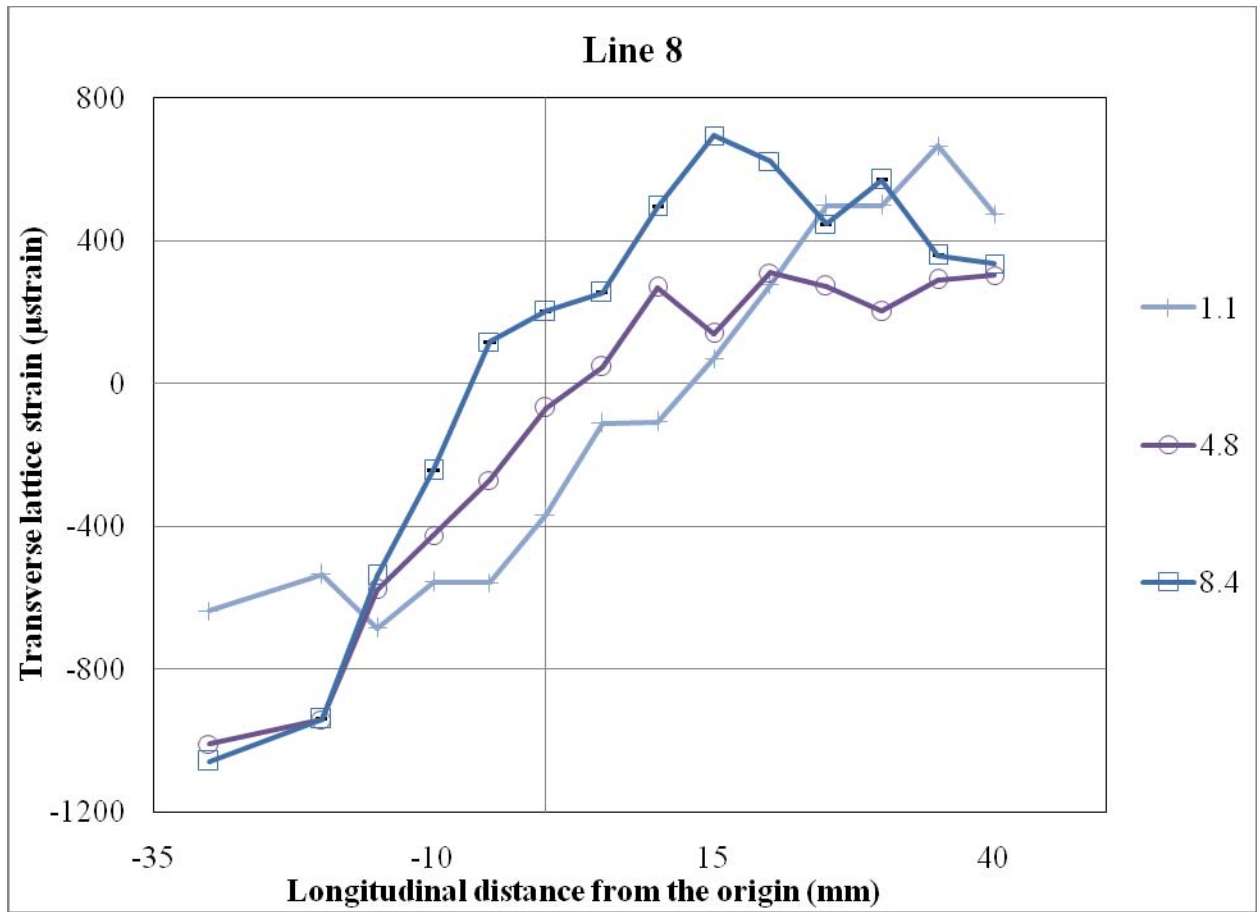


Figure 8.13: Transverse strain at various depths in the longitudinal (L) direction on line 8 (at T = 30 mm)

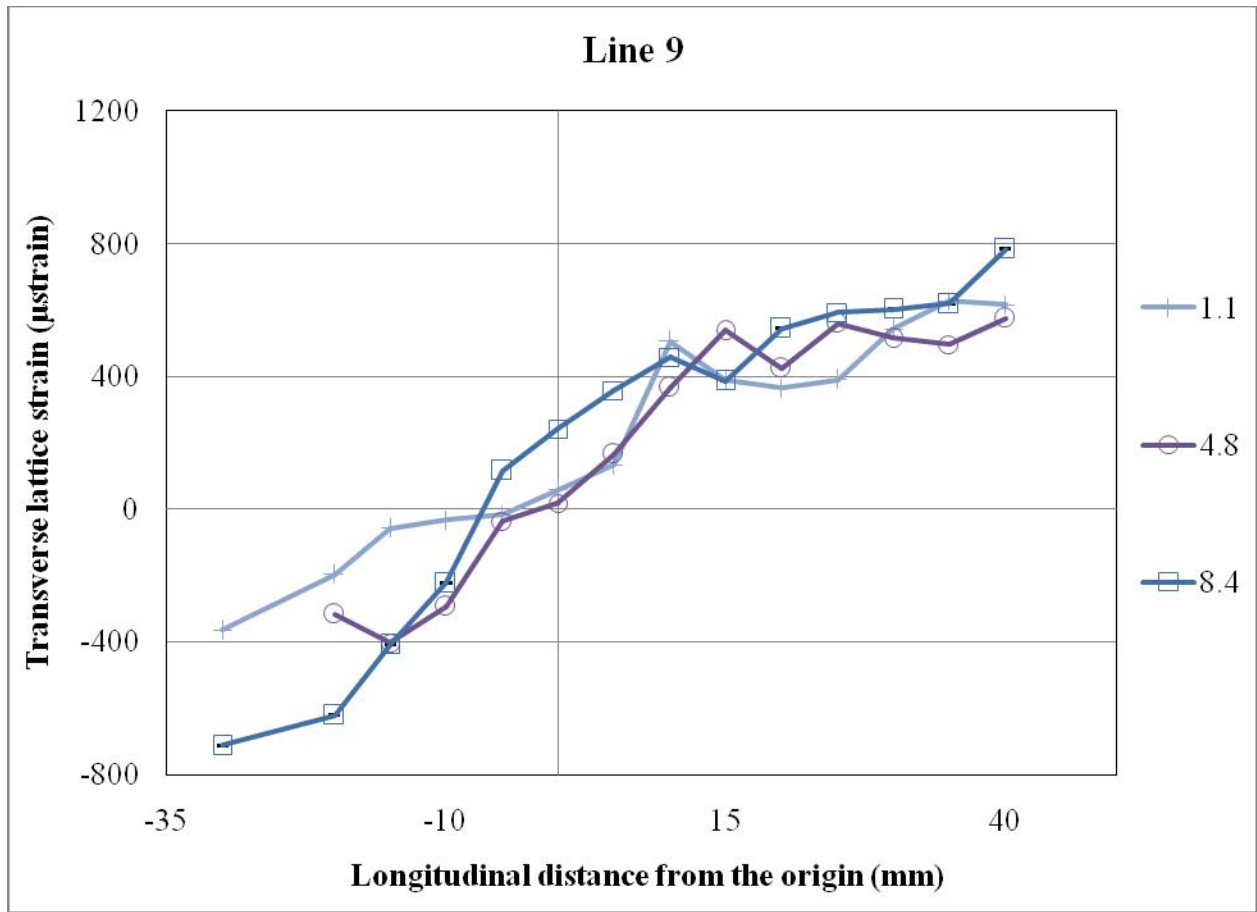


Figure 8.14: Transverse strain at various depths in the longitudinal (L) direction on line 9 (at T = 50 mm)

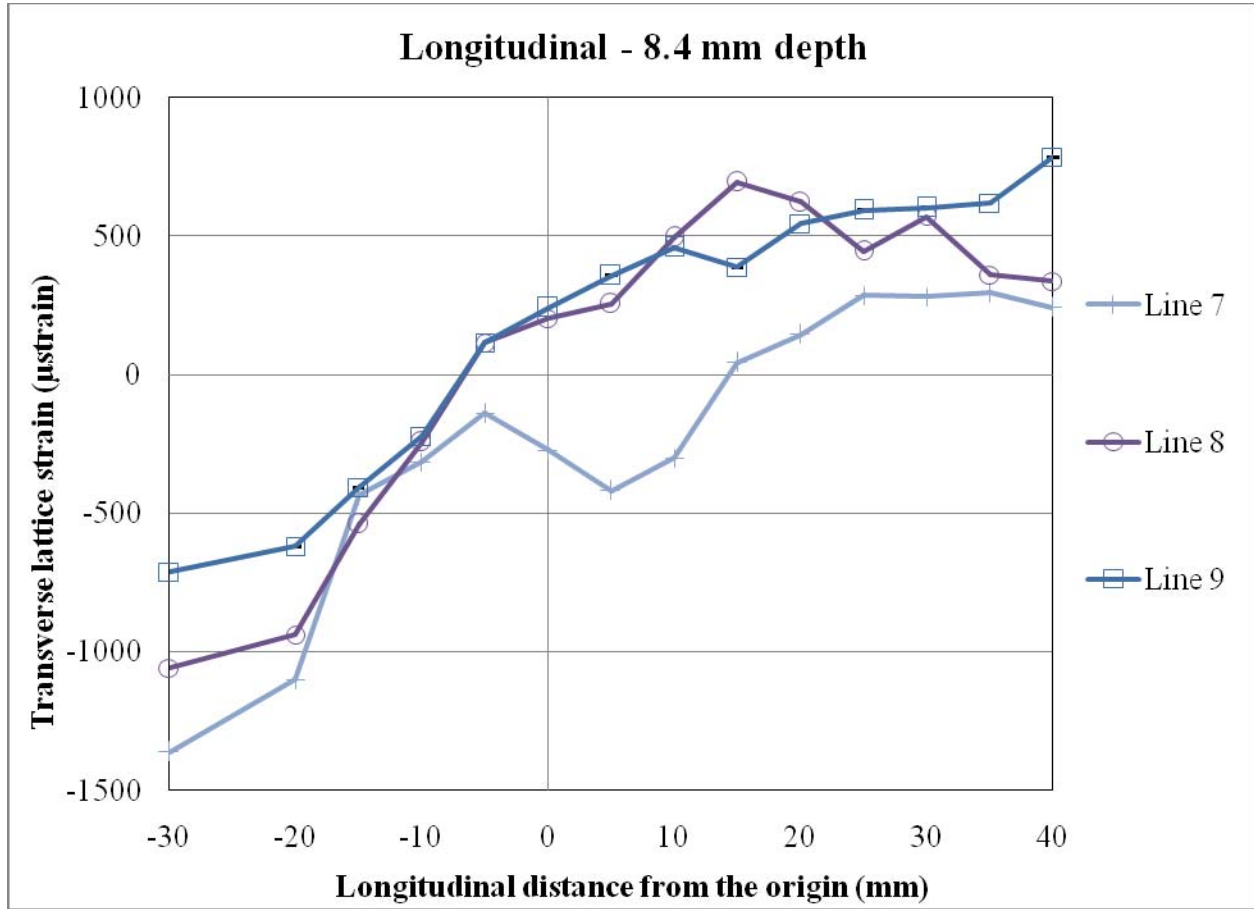


Figure 8.15: Transverse strain at a depth of 8.4 mm in the longitudinal (L) direction on lines 7, 8, and 9

8.2.1.2 Longitudinal Strain for Specimen 4

The longitudinal strain is the strain in the direction parallel to the stiffener (direction L in Figure 8.3). The longitudinal strain (strain in the direction of L) measurements in the transverse direction (direction T), that is, on lines 1, 3, 4, 5, and 6, were acquired at the same points where the transverse strain measurements were acquired (Figure 8.4). However, as mentioned before, longitudinal strain measurements were acquired only at one depth of 8.4 mm (at N = 8.4 mm in Figure 8.1), that is, closest to the welded surface of the plate. Measurements of longitudinal strain components in the longitudinal direction (that is, on lines 7, 8, and 9) were also taken at the points where the transverse strain component was measured, that is, at 5 mm intervals. Again, the measurements were only made at one depth of 8.4 mm (at N = 8.4 mm in Figure 8.1) along these lines.

Measurements of longitudinal strain component (strain component in L direction in Figure 8.3) in the transverse direction (direction T) are shown in Figure 8.16. The figure shows that the strain distribution of longitudinal strain component on five lines in the transverse direction (that is, on lines 1, 3, 4, 5, and 6) of the plate at depth of 8.4 mm (that is, at $N = 8.4$ mm in Figure 8.1, which means close to the welded surface of the plate). Longitudinal strain on line 1 was measured from the centreline of the weld (located at $T = 10$) to only positive transverse direction (positive T direction in Figure 8.3 on the plate. However, for other transverse lines (lines 3, 4, 5, and 6), measurements for both positive and negative transverse directions were acquired. The longitudinal strain distributions for lines 1, 3, and 4 are of similar magnitude and pattern, with the highest tensile strain of about 1850 micro strains and a plateau of compressive strain of approximately 500 micro strains. Both tensile and compressive strain values on line 4, which is located at the termination point of the stiffener, are slightly lower than those on lines 1 and 3. Therefore, it can be concluded that the longitudinal strain at the termination point of the stiffener is not greatly affected and in fact, at the stiffener termination point (on line 4) the longitudinal strain value is slightly lesser than on other line (line 1).

Lines 5 and 6 are away from the weld and the termination line (line 4) of the stiffener and it can be observed that the longitudinal strain values (both tension and compression) are significantly lower than those on lines 1, 3, and 4. Line 5, which is 20 mm away from the end of the stiffener, shows a maximum tensile strain value of approximately 1400 micro strains and a very small (in the range of 100 to 200 micro strains) compressive strain. Line 6, which is the furthest (60 mm away), from the stiffener termination line (line 4), has a maximum tensile longitudinal strain value of 400 micro strains only and almost no compressive strain. Longitudinal strain distribution on line 6 indicates that a small longitudinal (L) distance (60 mm) away from the stiffener termination line (line 4), the longitudinal strain values reduces to a negligible value. Thus, termination of stiffener may not be a matter of concern for the longitudinal strain component.

Distributions of the longitudinal strain component in the longitudinal direction (on lines 7, 8, and 9) are shown in Figure 8.17. Lines 7, 8, and 9 are drawn parallel to the length of the weld and at transverse distance of 0 mm, 20 mm, and 40 mm away from the centreline of the weld, respectively. Since the specimens were very large and the complex type of set-up was required

for measurement of the longitudinal strain component, the last five measurements on line 7 beyond line 3 (in the positive L direction) could not be collected properly. However, even with the absence of those five measurements, the pattern of longitudinal strain distribution is evident from the data collected. The three lines in Figure 8.17 show the pattern of longitudinal strain expected at these locations. The highest longitudinal tensile strain values were found along the centreline of the weld that is, on line 7 and the range of tensile strain values on this line varied between 925 and 1900 micro strains. The longitudinal strain values on line 8, which is 20 mm from the centreline of the weld, are also all tensile. However, the strain values drop significantly and range from only 650 to 950 micro strains. The strain values on line 9, which is 40 mm from the centreline of the weld, drop even further and become eventually compressive in the stiffener. The longitudinal strain values on line 9 range from +300 (tensile) to -650 (compressive) micro strains.

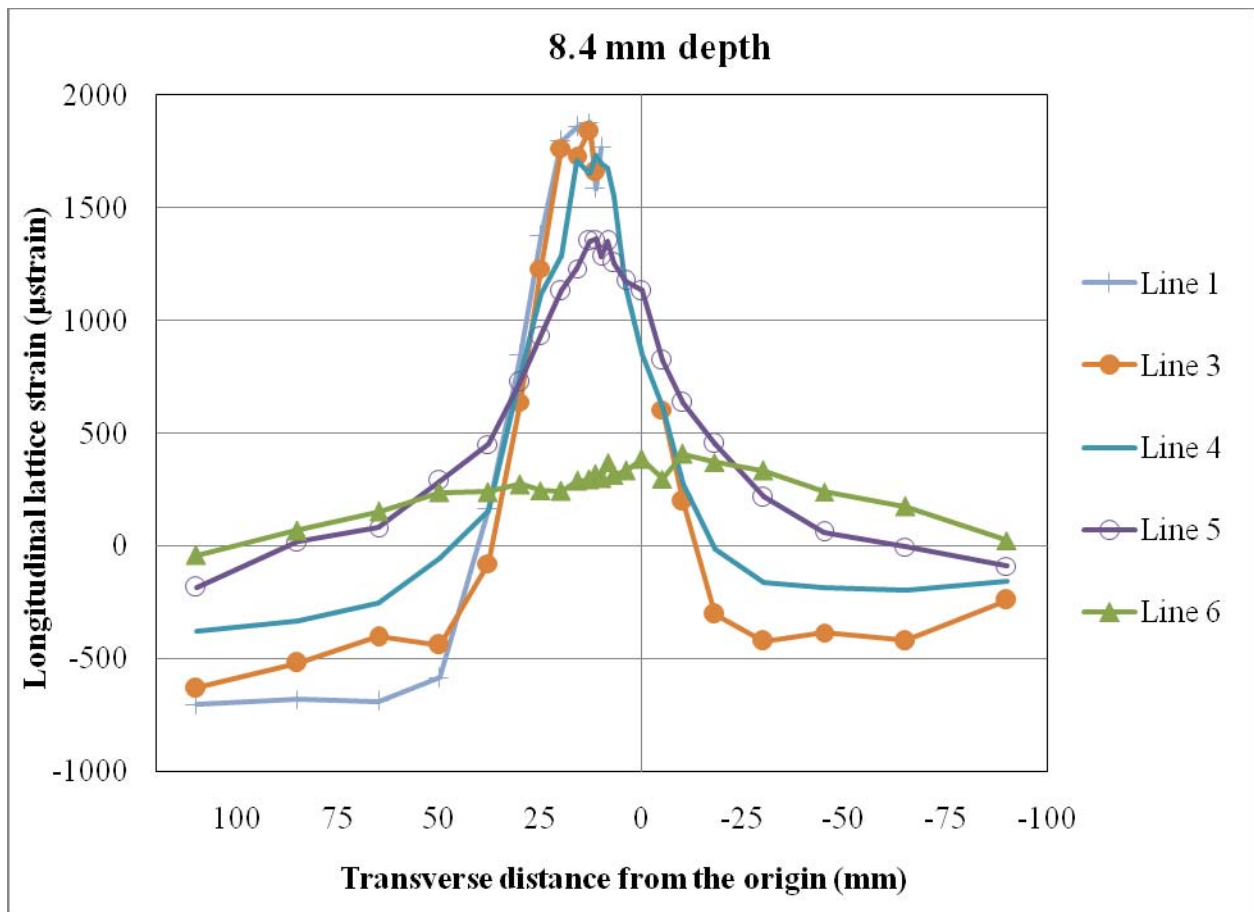


Figure 8.16: Longitudinal strain at a depth of 8.4 mm in the transverse (T) direction on lines 1, 3, 4, 5, and 6

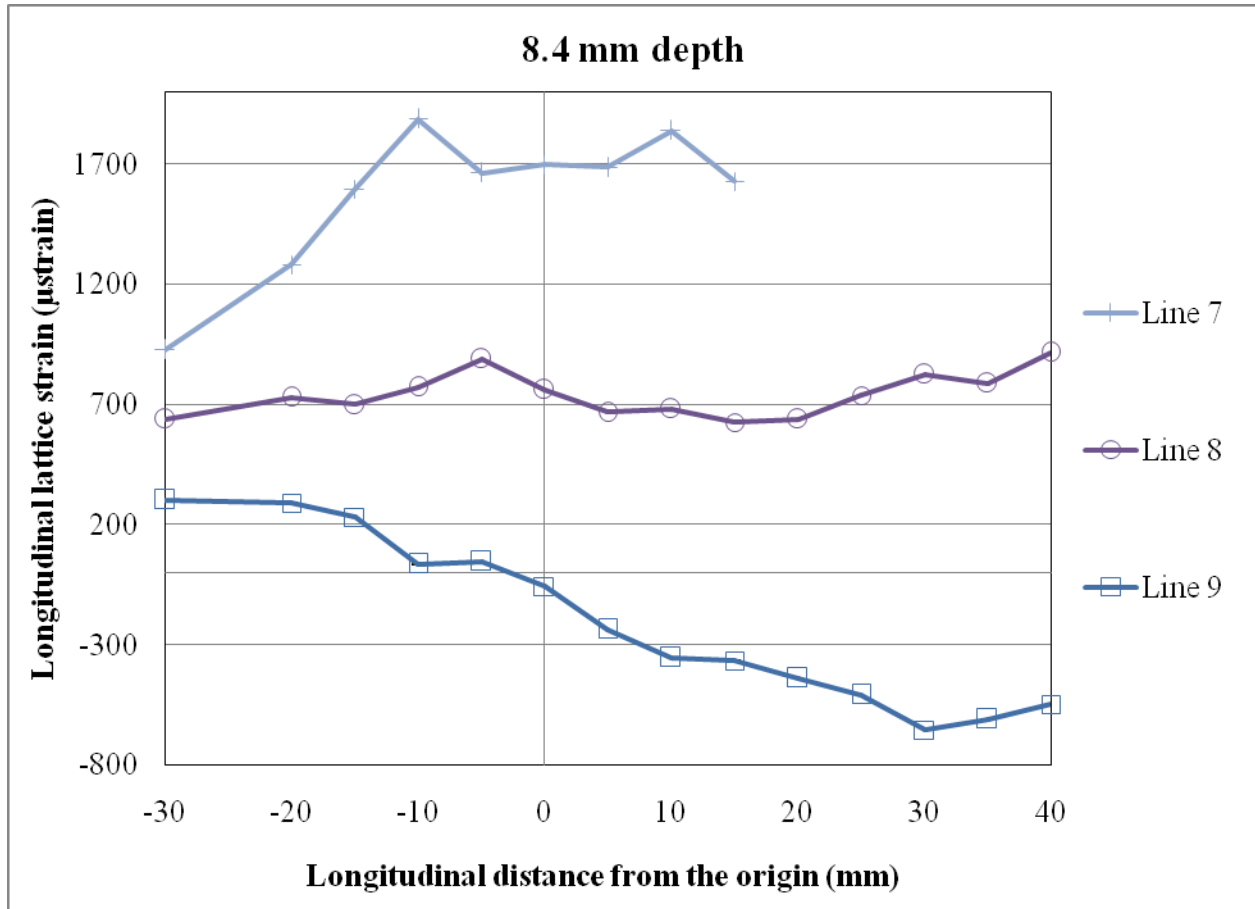


Figure 8.17: Longitudinal strain at a depth of 8.4 mm in the longitudinal (L) direction on lines 7, 8, and 9

8.2.2 Specimen 5

Specimen 5, as shown in Figure 8.2, was a plate with dimensions of 400 mm long (L) x 600 mm wide (T) x 9.53 mm thick (N). Two 400 mm long stiffeners were welded on this plate spaced at 400 mm on centre using high heat input (~2.5 kJ/mm). The objective was to determine the effect of stiffener spacing on residual stress distributions. Therefore, the stress distributions of this specimen are compared with those of Specimen 3 of Phase I. The specimen was measured for all the three residual strain components along both longitudinal (L) and transverse (T) directions at five depths (that is, in the normal (N) direction). Figure 8.18 shows the lines on which the strain measurements were taken and the location of the origin (0, 0, 0) shown by a small open circle, which was located at negative 10 mm away from point 2 in transverse direction (See Figure 8.19).

In the transverse direction, measurements were taken along the line 1-2-3-4, as shown in Figure 8.18. The spacing of measurements along the transverse line 1-2-3-4 is shown in Figure 8.19. Measurements were also taken at one depth (at $N = 8.4$ mm) along the weld centreline in the longitudinal direction (on lines 2-5 and 3-6 in Figure 8.18). These measurements were taken at both welds (on lines 2-5 and 3-6 in Figure 8.18) to study if there is any change in stress distribution between these two welds for two stiffeners. The measurements along the welds (on lines 2-5 and 3-6) started at $L = 0$ mm and $L = -15$ mm and then acquired at an interval of 20 mm up to -95 mm (until points 5 and 6, respectively).

A total of 285 points were considered for strain measurements, though not all points were measured for all the three strain components. Due to time constraints and the complex nature of the test set-up, some of the longitudinal strain values could not be collected directly under the weld-stiffener connection. However, from the previous results in Phase I, it was found that through the weld the strain values were almost uniform and it is assumed that the same is true for this specimen as well.

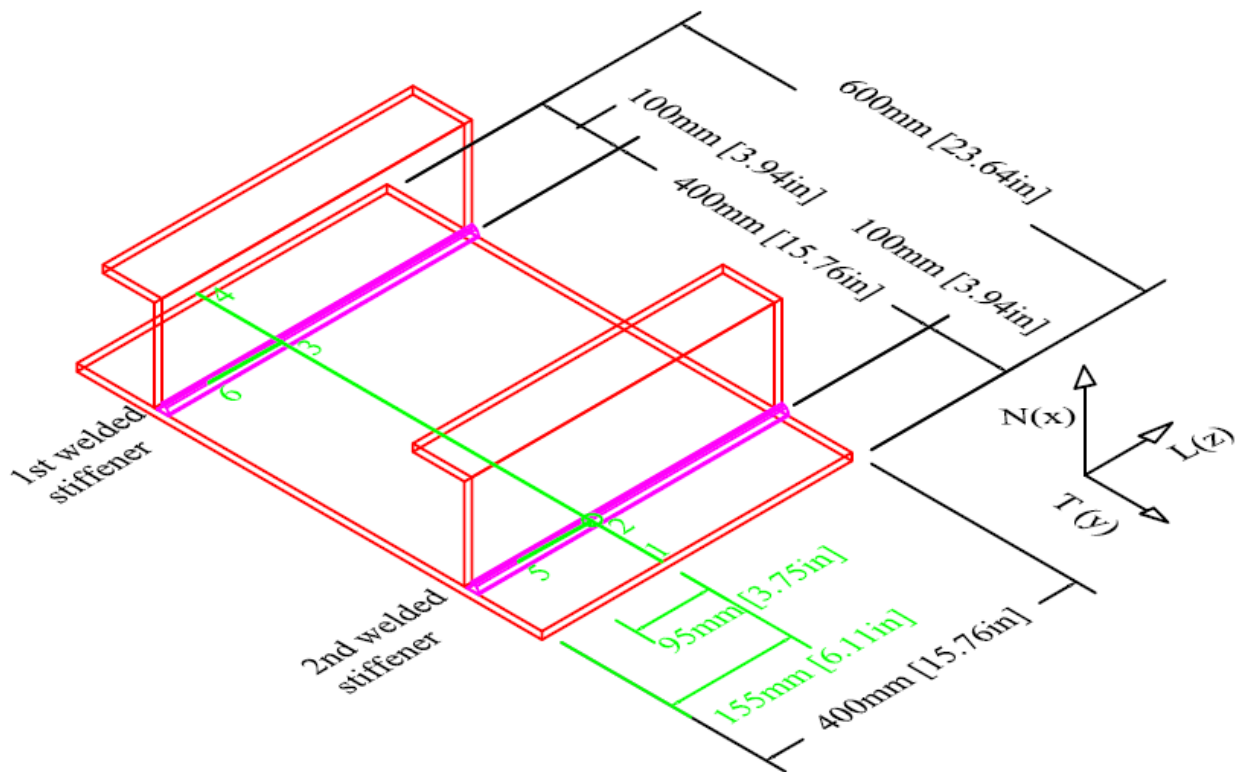


Figure 8.18: Detail for Measurement Points for Specimen 5

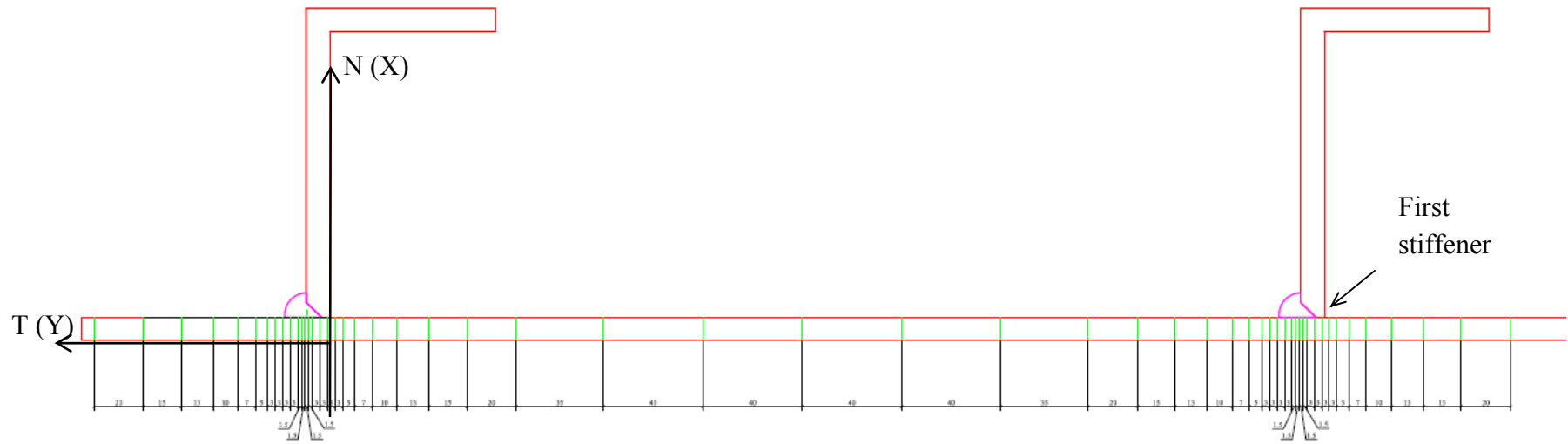


Figure 8.19: Spacing of the transverse direction measurements (in mm) on Specimen 5 (line 1-2-3-4)

8.2.2.1 Normal Stress for Specimen 5

The normal stresses (σ_x or σ_{normal}) are calculated using all three strain components as described for other specimens. The normal stress is the stress in the direction through the thickness of the plate (direction N in Figure 8.2 and Figure 8.18). The strain measurements for the normal component were acquired along line 1-2-3-4 in the transverse direction and on lines 2-5 and 3-6 in the longitudinal direction. The measurements were taken at five depths along line 1-2-3-4 and at one depth of 8.4 mm (at N = 8.4 mm) on lines 2-5 and 3-6. The spacing of the measurements in the transverse direction is shown in Figure 8.19. Six measurements on each of lines 2-5 and 3-6 were acquired at L = 0 mm, -15 mm, -35 mm, -55 mm, -75 mm, and -95 mm. The normal stress distribution is shown in Figure 8.20. The normal stress distributions are irregular and they do not have a very clear pattern. However, it seems that a plateau of normal stress exists between the two stiffeners and the stress values change suddenly at the stiffener. A total of 285 normal strain measurements were collected for this specimen.

The normal stress measurements that were taken on lines 2-5 and 3-6 along the longitudinal direction will be shown and discussed in a later section with all stress components.

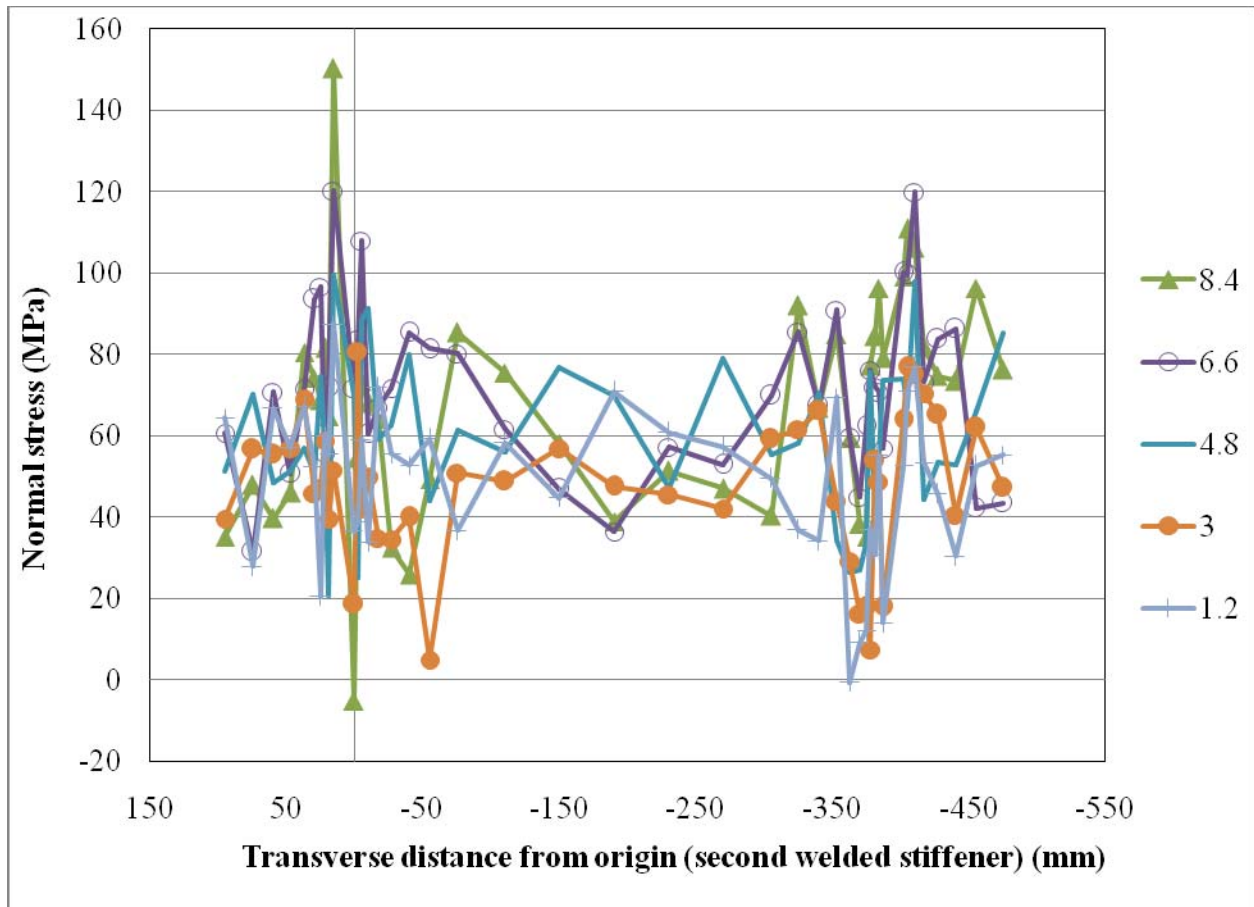


Figure 8.20: Normal stress through the depth in the transverse (T) direction on line 1-2-3-4 (at $L = 0$ mm)

8.2.2.2 Transverse Stress for Specimen 5

The transverse stresses (σ_y or $\sigma_{\text{transverse}}$) are calculated using all three strain components as described in a previous section. The transverse stress is the stress in the direction perpendicular to the stiffeners (direction T in Figure 8.2 and Figure 8.18). The strain measurements for transverse component were collected along line 1-2-3-4 in the transverse direction at five depths and at one depth of 8.4 mm (at $N = 8.4$ mm in Figure 8.18) on lines 2-5 and 3-6 in the longitudinal direction. Both lines 2-5 and 3-6 are located at the approximate centreline of the weld in longitudinal direction. The spacing of the strain measurements in the transverse direction (on line 1-2-3-4) was the same as was for normal strain measurements and as shown in Figure 8.19. The spacing of the measurements for transverse strain component along the weld centreline (on lines 2-5 and 3-6) were also same as for the measurements of normal strain

component. Therefore, a total of 285 transverse strain measurements were acquired for this specimen.

The transverse stress distribution for Specimen 5 on line 1-2-3-4 is shown in Figure 8.21. The pattern of residual stress is better than in the normal stress component distribution. The distribution shows a plateau (between the two stiffeners) of tensile stress with values between 25 MPa in tension and 75 MPa in tension. The tensile stress is highest at the stiffener-weld connections for both stiffeners. The maximum value of tensile stresses for the stiffener welded first is 165 MPa and for the stiffener welded second is 192 MPa. The maximum stress at the stiffener welded second is slightly higher than the maximum stress at the stiffener welded first and the difference is only 27 MPa.

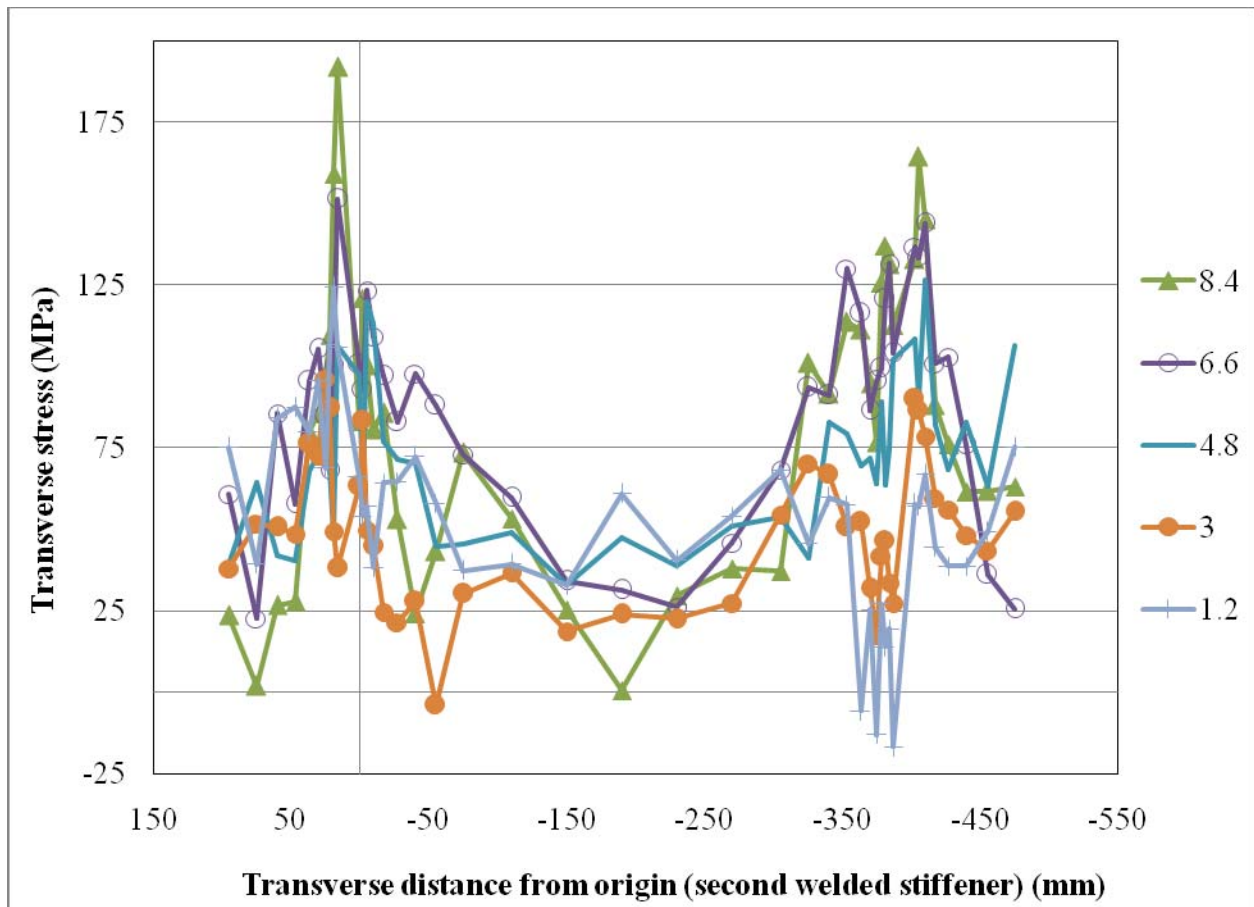


Figure 8.21: Transverse stress through the depth in the transverse (T) direction on line 1-2-3-4 (at $L = 0$ mm)

8.2.2.2 Longitudinal Stress for Specimen 5

The longitudinal stresses (σ_z or $\sigma_{\text{longitudinal}}$) are calculated using all three strain components as described earlier. The longitudinal stress is the stress in the direction parallel to the stiffeners (stress component in the direction of L in Figure 8.2 and Figure 8.18). Like the other two strain components, measurements for longitudinal strain component were collected on line 1-2-3-4 (in the transverse direction) at five depths and on lines 2-5 and 3-6 (in the longitudinal direction) at one depth of 8.4 mm (at $N = 8.4$ mm). The lines 2-5 and 3-6 are located at the centreline of the weld. The spacing of measurements of the longitudinal strain component on line 1-2-3-4 is shown in Figure 8.19. The spacing of the measurements of the longitudinal strain component on lines 2-5 and 3-6 are at the same locations as were for the normal and transverse strain components. Both normal and transverse strain components were collected at 285 points. However, the longitudinal measurements were not taken directly underneath the stiffener and at the peak of the weld as discussed before. Therefore, the total number of measurements for longitudinal strain component collected was (285 – 6 points at each stiffener x 5 depths x 2 stiffeners) 225 points.

The longitudinal stress distribution on line 1-2-3-4 for Specimen 5 is shown in Figure 8.22. It is observed that the pattern of residual stress distribution for the longitudinal stress component has the maximum tensile stress at the stiffener and a compressive stress plateau in between the two stiffeners. The pattern of stress distribution agrees with the one obtained from Specimen 3. It is also observed that the maximum tensile stress at the stiffener welded second (last) is higher than that at the first welded stiffener, with a difference of about 100 MPa. It should be noted that the yield stress of the parent plate material is 405 MPa.

Variation of longitudinal stress through the depth of the plate is not much. At the second welded stiffener, the maximum stresses were observed near the welded surface of the plate (at depths of 8.4 mm and 6.6 mm) and the value is about 525 MPa, which is well above the first yield stress of the plate. The maximum longitudinal stress at the stiffener welded first is 410 MPa which is close to the yield stress value (405 MPa) and similar to the value observed from Specimen 3 of Phase I (see Figure 7.32). The Specimen 3 has two stiffeners spaced at 250 mm on centres and the stiffeners were welded with similar heat input (high heat input). The maximum tensile stress (523 MPa) under the stiffener welded last (second) for Specimen 5 is much higher than that was

observed for the stiffener welded first for Specimen 3 (430 MPa). From these results, it shows that an increase in the spacing of the stiffeners can cause an increase in the tensile stress peak values, which are found under the weld-stiffener connection.

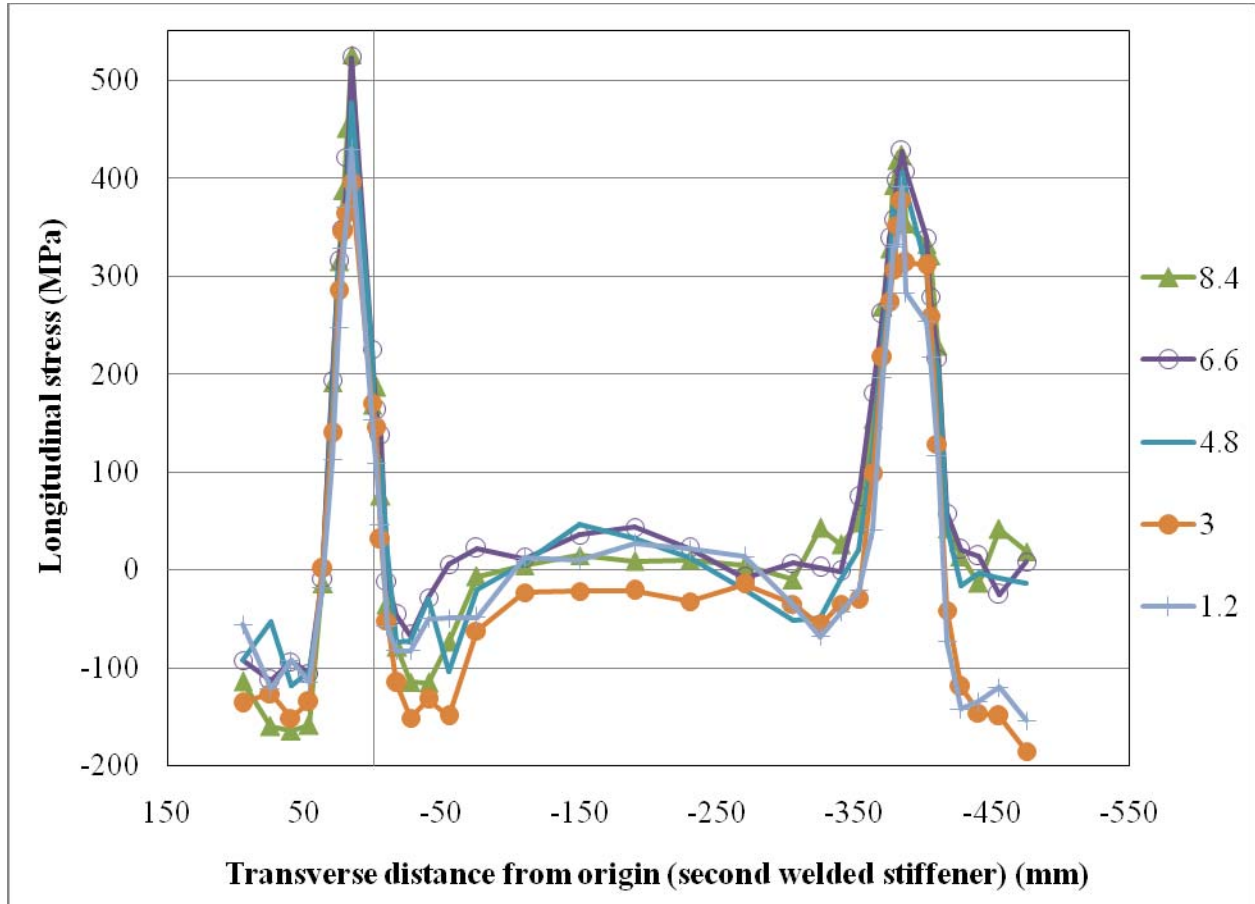


Figure 8.22: Longitudinal stress through the depth in the transverse (T) direction on line 1-2-3-4 (at $L = 0$ mm)

The plateau between the stiffeners ranges from 35 MPa in compression to 45 MPa in tension, which is not significant. However, for Specimen 3, with stiffeners spaced at 250 mm on centre, the values were much higher (see Figure 7.32). The plateau between the stiffeners on Specimen 3 ranged from 250 MPa in compression to 100 MPa in compression. For the Specimen 5, stress value drops from the maximum tensile peak down to a compressive value of about 150 MPa, immediately adjacent to the stiffeners. Similar behaviour was also observed in Specimen 3 where the stress value dropped to about 200 MPa in compression. Therefore, it can be concluded

that the compressive stress levels (between two stiffeners) increases as the spacing between two stiffeners reduces.

8.2.2.3 All Stresses at Weld Centerline for Specimen 5

All the three strain components were collected along the centreline of both welds at one depth of 8.4 mm, that is, near the welded side of the plate. Strains at six points were collected on both weld lines (on lines 2-5 and 3-6) as shown in Figure 8.18. The distribution for longitudinal stress for the stiffener welded first (on line 3-6 or at $T = -390$ mm) is shown in Figure 8.23. In this figure, distributions for other two stress components (normal and transverse) are also shown. The three stress distributions show the same pattern of stress with a lower value at $L = 0$ mm (point 3 in Figure 8.18). The stress values gradually increase to a relatively higher value at a distance of 80 mm (that is, at $L = -80$ mm). Beyond this distance, the stress values stabilize and drop slightly as the longitudinal distance (distance in the negative L direction) increases further. Figure 8.23 shows a higher value of longitudinal tensile stress (in the range of 500 MPa) away from the origin and this suggests that the highest (peak) tensile stress value in the first welded stiffener may actually be similar to the tensile stress level at the second welded stiffener even though it is not apparent in Figure 8.22. Once the welding was completed, it was observed that the weld for first stiffener of Specimen 5 had some irregularities in its finished shape. This is because the gas ran out when the welding gun was near the end of the stiffener and a slight catch in the track of the welding trolley created a bump in the weld bead. This may be the reason why the tensile stress value in the first stiffener is much lower than the value at the second stiffener for Specimen 5 (see Figure 8.22) which was not the case for Specimen 3 (see Figure 7.32).

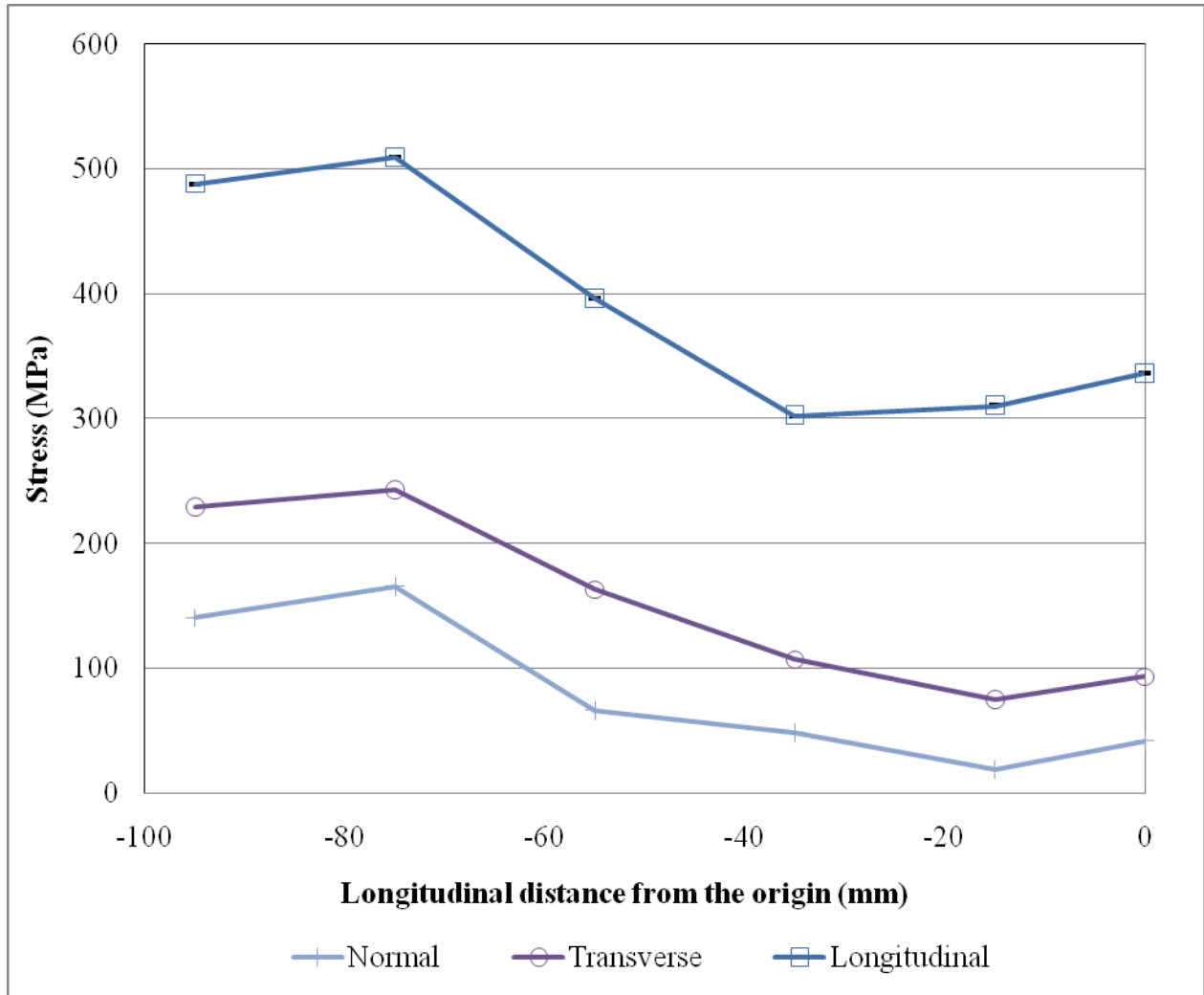


Figure 8.23: All stresses at first welded stiffener, at T = -390 mm, at N = 8.4 mm (on line 3-6)

The stress values for the second welded stiffener which was located at T = +10 mm (that is, on line 2-5) are shown in Figure 8.24. These stress distributions on second stiffener (on line 2-5) are more consistent if they are compared to the stress distributions found on the first welded stiffener (on line 3-6). This may be due to better finishing and no interruption in the weld for second stiffener. The stress values for second stiffener are fairly consistent with the exception of the small peak at about 55 mm (that is, at L = -55 mm) away from the origin, which could be a result of various minor things.

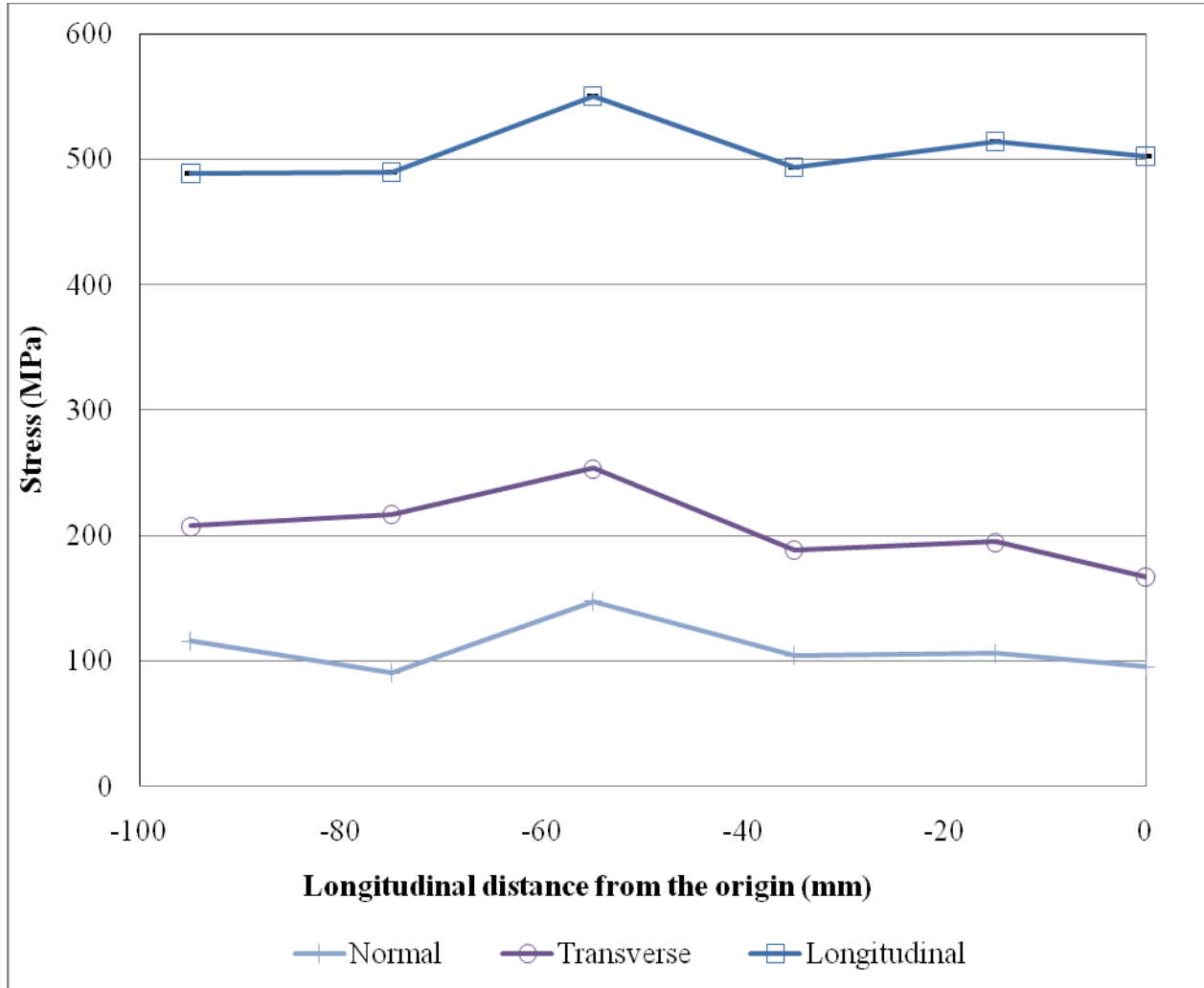


Figure 8.24: All stresses at second welded stiffener, at T = +10 mm, at N = 8.4 mm (on line 2-5)

8.2.3 Specimen 6

Specimen 6 as shown in Figure 8.2 was a plate with dimensions of 400 mm long (L) x 600 mm wide (T) x 9.53 mm thick (N). Two 400 mm long stiffeners were welded on this plate at 100 mm from the edge and spaced at 400 mm on centre. The specimen has exactly the same dimensions and specifications as Specimen 5. However, Specimen 6 was welded using a relatively lower heat input (~1.75 kJ/mm, which is considered as moderate heat input) to compare the results with the specimen (Specimen 5) welded with higher heat input (~2.5 kJ/mm). The specimen was measured for residual strain along the longitudinal (L) and

transverse (T) directions at five depths through the normal (N) direction. Figure 8.25 shows the locations where the measurements were taken.

In the transverse direction, measurements were taken across the line 1-2-3, as shown in Figure 8.25. The spacing of measurements along the transverse line 1-2-3 are shown in Figure 8.26 and are the same spacing as the measurements for Specimen 5 were used. Measurements were also taken along the weld centreline (on line 2-4) of second welded stiffener at one depth (at $N = 8.4$ mm) that is closest to the welded surface of the plate. The measurements along the weld started at the origin (point 2 in Figure 8.25) and at intervals of 20 mm up to 100 mm from the transverse measurement line (line 1-2-3). The origin of the measurements is at point 2, 10 mm away from the centreline of the weld on the second welded stiffener. Since the stiffener orientation and spacing were same for both Specimen 5 and Specimen 6, it was assumed that the residual stress distribution pattern would be the same on both specimens and therefore, to minimize beam time needed measurements were only performed around the second welded stiffener. A total number of 155 points were measured on this plate, though not all points were measured for all three strain components.

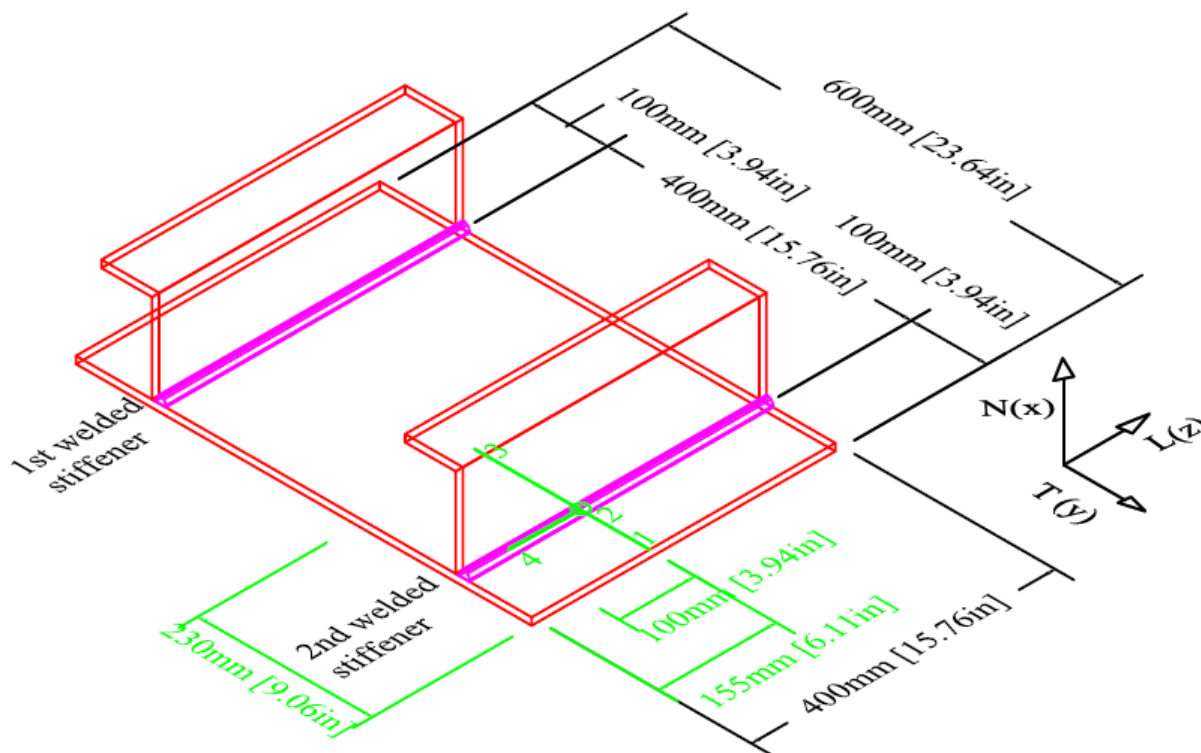


Figure 8.25: Details for Measurement Points for Specimen 6

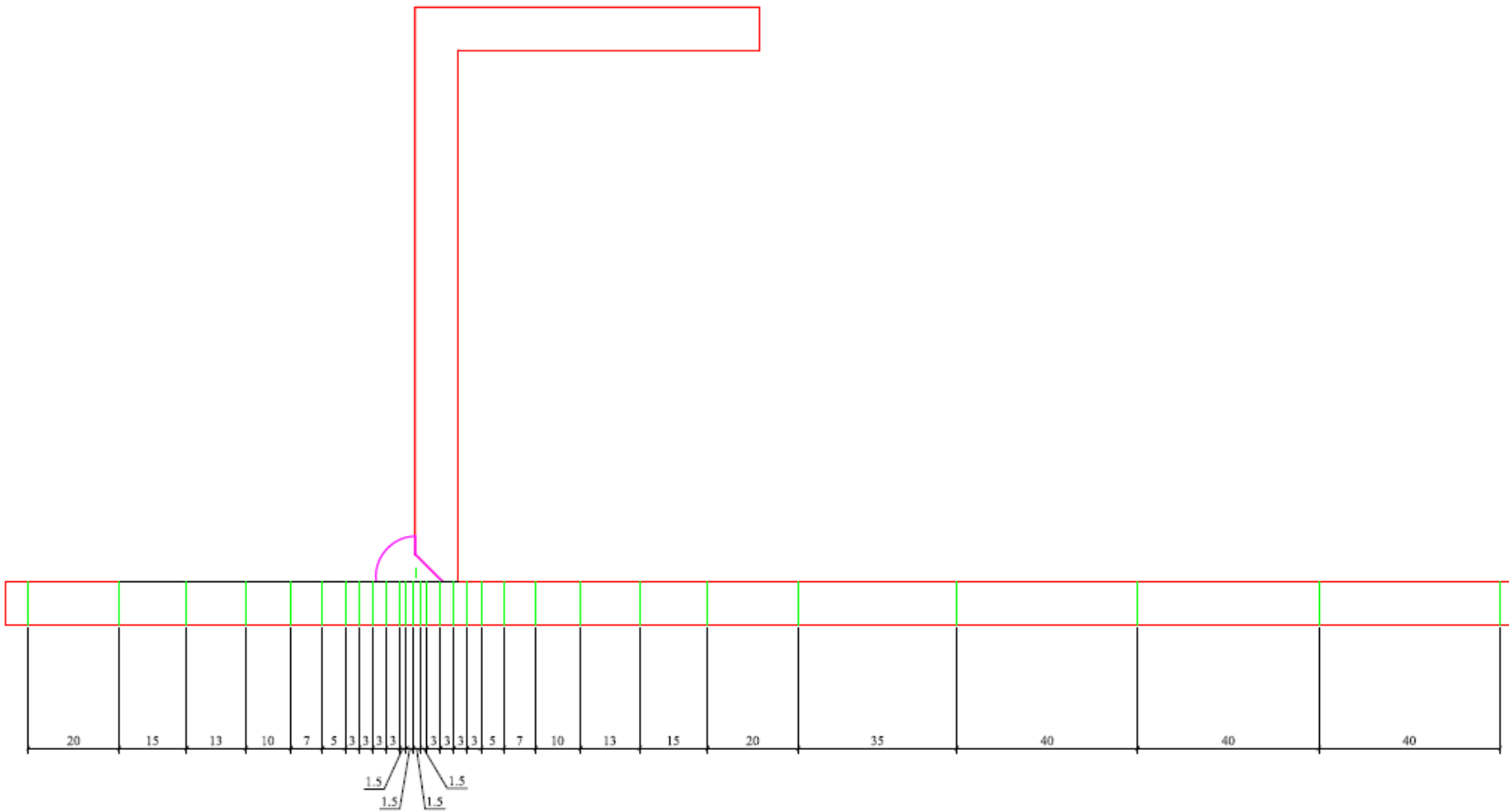


Figure 8.26: Spacing of measurements (in mm) in transverse direction for Specimen 6 (on line 1-2-3)

8.2.3.1 Normal Stress for Specimen 6

The normal stresses (σ_x or σ_{normal}) are calculated using all three strain components as described in earlier sections. The normal stress is the stress in the direction through the thickness of the plate (direction N in Figure 8.25). The measurements were taken at five depths along line 1-2-3 and at one depth (at N = 8.4 mm) along line 2-4. A total number of 155 normal strain measurement points were collected for this component. The measurements along line 2-4 which is at the centreline of the weld will be discussed in a later sub-section.

The normal stress distribution for Specimen 6 at the second welded stiffener is shown in Figure 8.27. The range of stress values for the normal distribution is from about 50 MPa in tension to about 180 MPa in tension. This range is similar to the normal stress distribution found in Specimen 5, though the range has been shifted slightly towards positive values (on tension side). The stress values in the plateau (zone in between two stiffeners) for Specimen 5 range from 40 MPa in tension to 80 MPa in tension, whereas, this range for Specimen 6 is from 70 MPa in tension to 120 MPa in tension. The normal stress distribution does not show a clear pattern as was for Specimen 5. However, it still shows a plateau of stress between the stiffeners and a sudden peak tensile stress at the stiffener-weld connection.

Figure 8.28 shows the average normal stress distributions from both Specimen 5 and Specimen 6, as well as the extrapolated data around the first welded stiffener of Specimen 6. The average value is obtained by taking average of all normal stresses at the same measurement point through the plate thickness. The solid line is drawn for the test data actually collected. The broken line for Specimen 6 is extrapolated data for the other half (around first welded stiffener) of the test data. The extrapolated data was calculated assuming the difference between the average stress levels between Specimen 5 and Specimen 6 remain same both for the plateau and for the stiffener-weld connection zones.

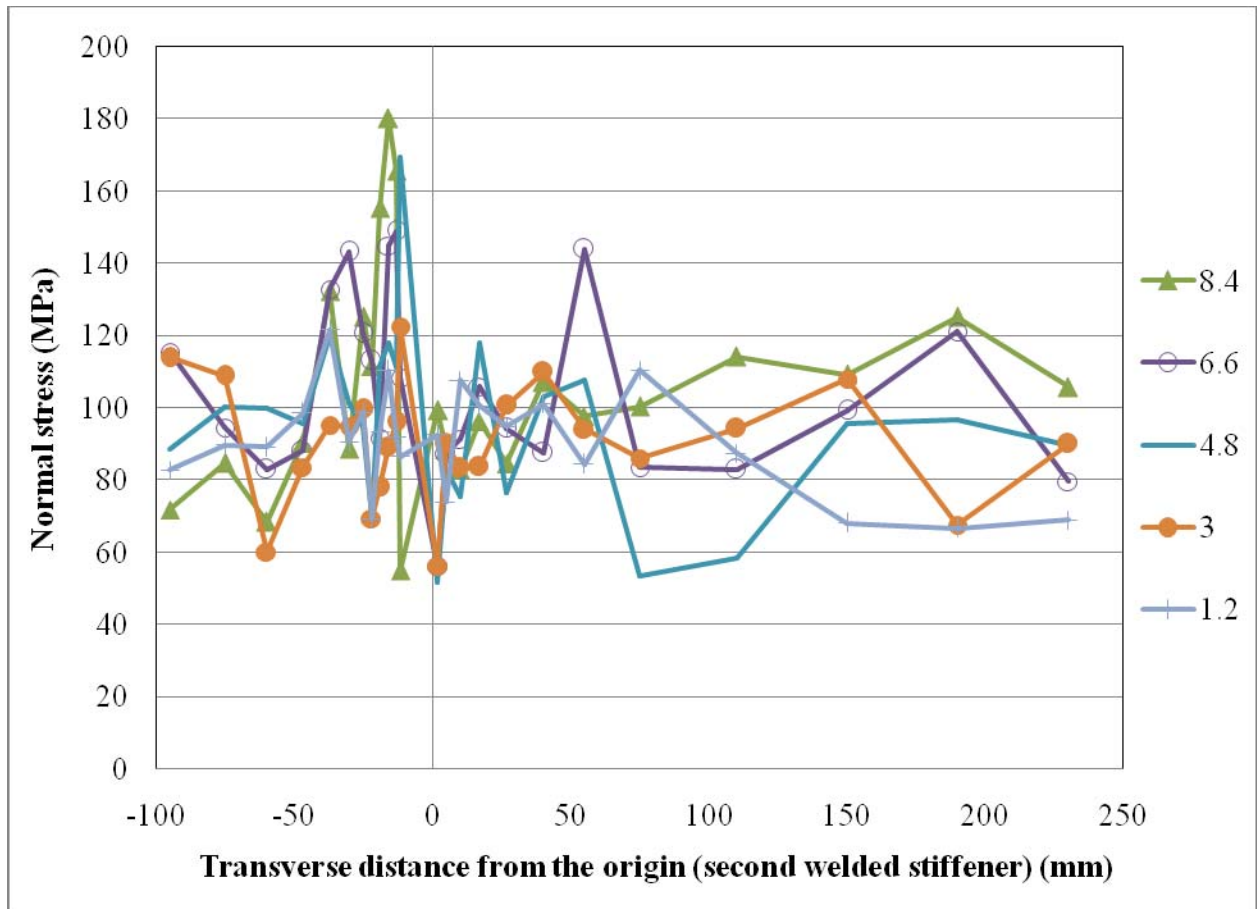


Figure 8.27: Normal stress at various depths in the transverse (T) direction on line 1-2-3 (at $L = 0$ mm)

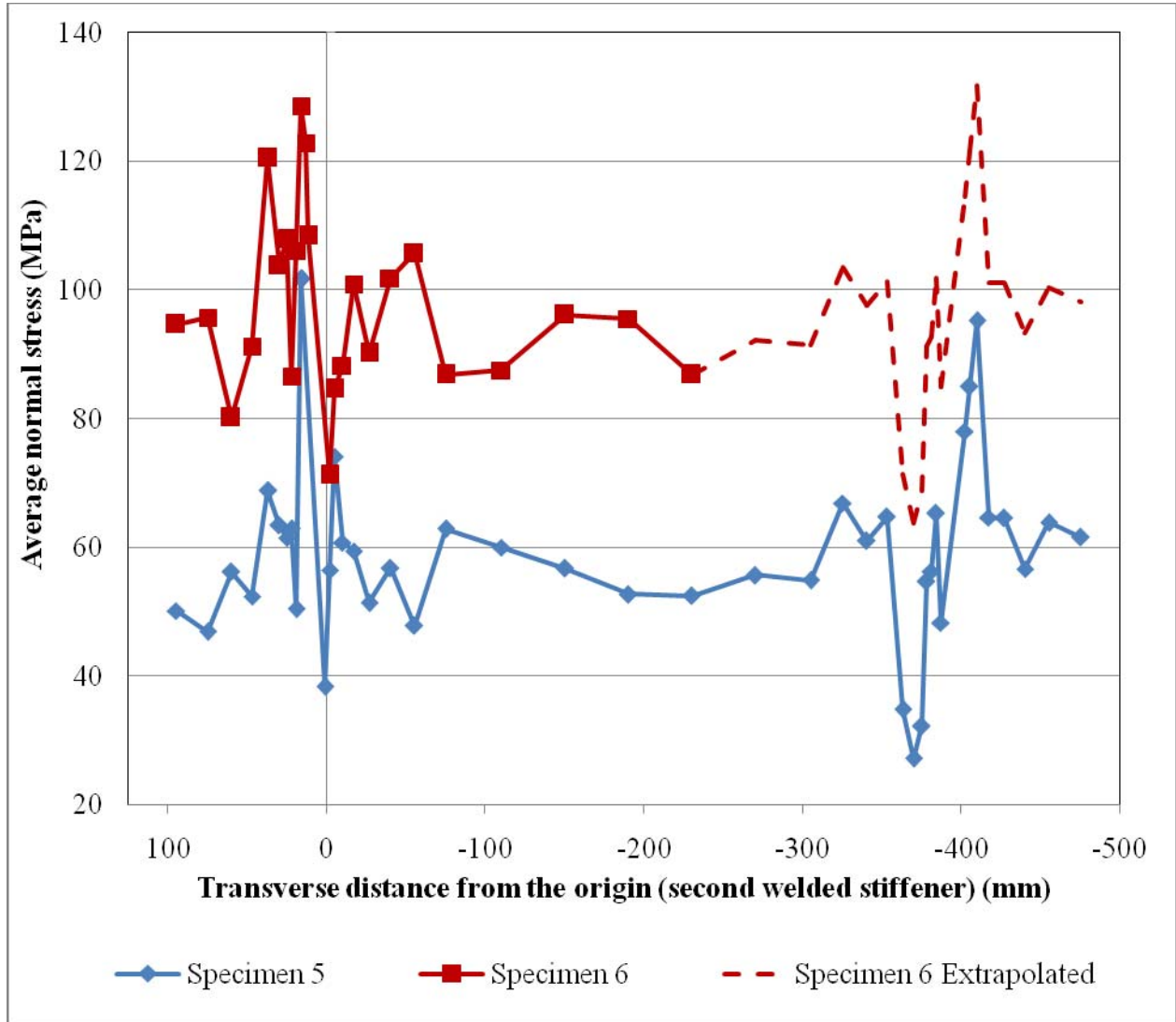


Figure 8.28: Average normal stress distributions along the transverse lines (line 1-2-3-4 for Specimen 5 and line 1-2-3 for Specimen 6)

8.2.3.2 Transverse Stress for Specimen 6

The transverse stress (σ_y or $\sigma_{\text{transverse}}$) is the stress in the direction perpendicular to the stiffener (direction T in Figure 8.25). The measurements were taken at five depths along line 1-2-3 and at one depth (at $N = 8.4$ mm) along line 2-4. A total number of 155 transverse strain measurement points were collected for this component. The measurements along line 2-4 which is located at centreline of the weld will be discussed in a later section.

The transverse stress distribution for Specimen 6 is shown in Figure 8.29. The transverse stress distribution shows the patterns that were observed from Specimens 5 and 3. For all these three specimens, the maximum tensile stress occurs at the stiffener and the compressive stress away from the weld, that is, the plateau zone (in between two stiffeners). The transverse stress values for Specimen 6 vary from 30 MPa in tension to 220 MPa in tension with a plateau (zone in between two stiffeners) in the range of 30 MPa in tension to 60 MPa in tension. The transverse stress values for Specimen 5 range from 25 MPa in compression to 160 MPa in tension at the first welded stiffener, and 0 MPa to 185 MPa in tension at the second welded stiffener, with a plateau between the stiffeners in the range of 25 in tension to 50 MPa in tension. Pattern of stress distributions for normal and transverse stress components are similar and a clearer pattern for transverse stress is noticed.

Figure 8.30 shows the distributions for average transverse stress for Specimen 5, Specimen 6, and the extrapolated data for Specimen 6. The extrapolated data for the stress around the first welded stiffener on the Specimen 6 was calculated in the same way as discussed for the normal stress component.

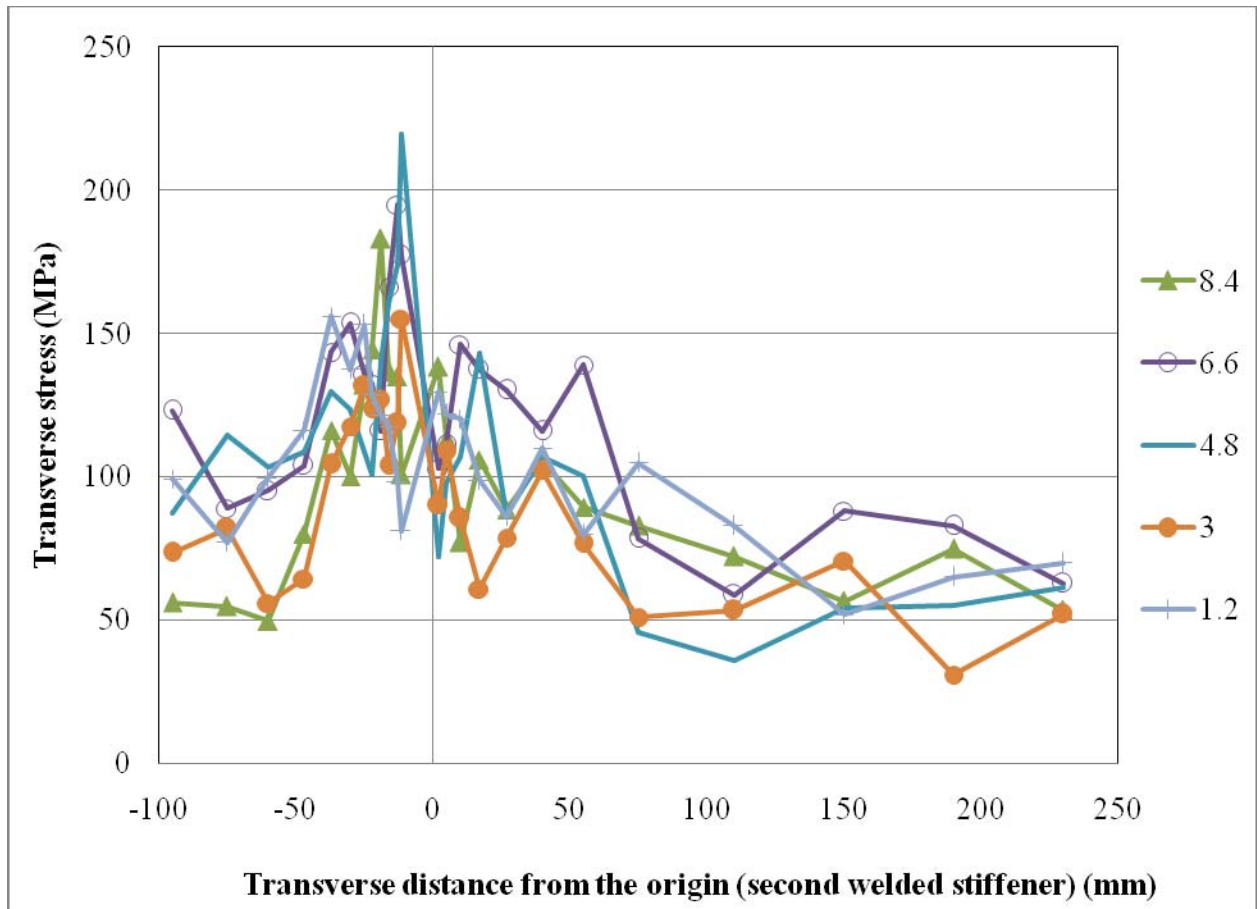


Figure 8.29: Transverse stress at various depths in the transverse (T) direction on line 1-2-3 (at L = 0 mm)

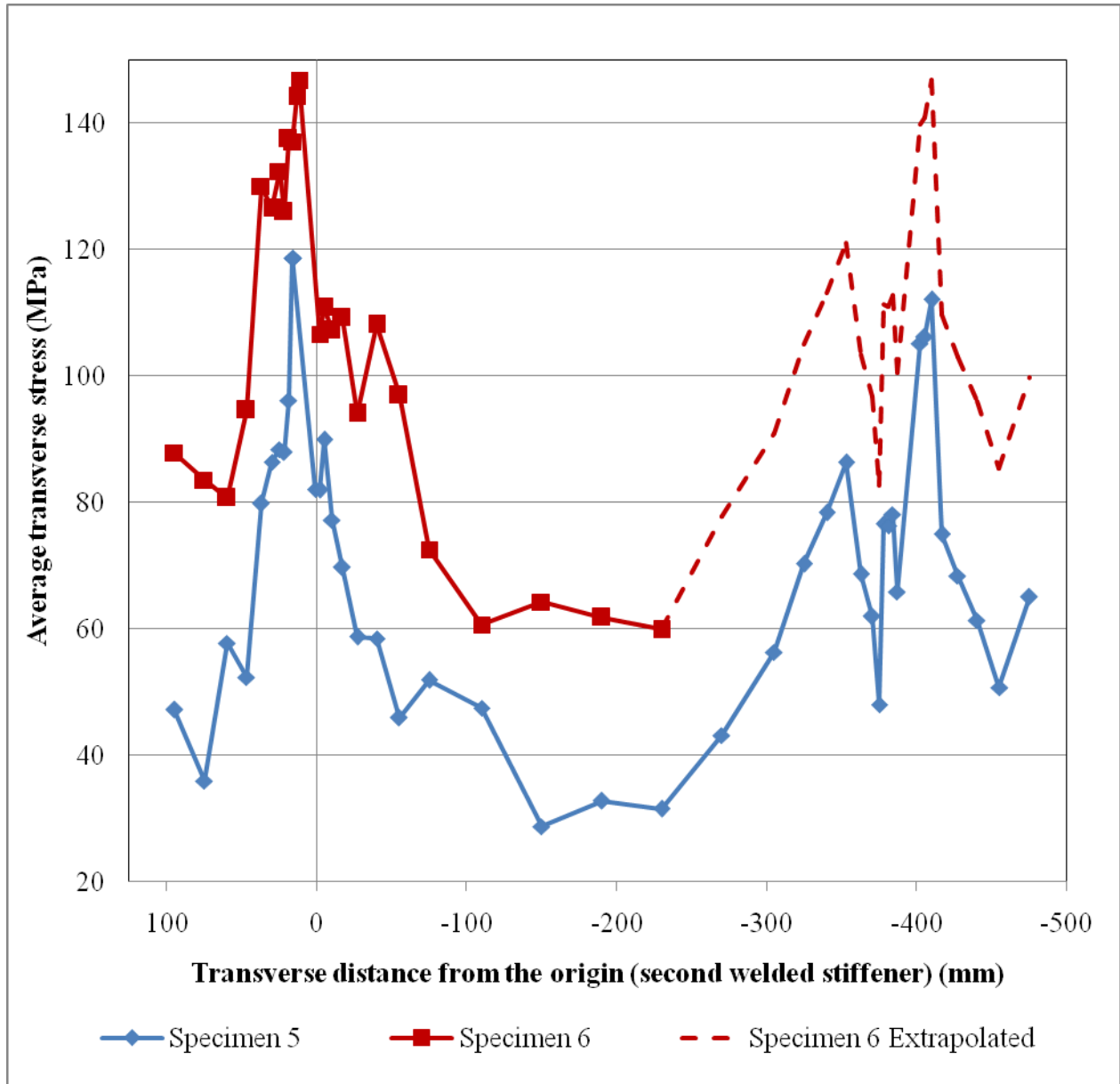


Figure 8.30: Average transverse stress distributions along the transverse lines (line 1-2-3-4 for Specimen 5 and line 1-2-3 for Specimen 6)

8.2.3.3 Longitudinal Stress for Specimen 6

The longitudinal stress (σ_z or $\sigma_{\text{longitudinal}}$) is the stress in the direction parallel to the weld (direction L in Figure 8.25). The measurements were taken at five depths along line 1-2-3 and at one depth (at $N = 8.4$ mm) along line 2-4. A total number of 130 longitudinal strain

measurement points were collected for this specimen. The measurements along line 2-4 which is at the centreline of the weld will be discussed in a later section.

The longitudinal stress distribution of Specimen 6 is shown in Figure 8.31. The longitudinal stress distribution shows the pattern which was obtained from Specimens 5 and 3 with a peak for tensile stress at the stiffener and the compressive stress away from the weld. The longitudinal stress values near the stiffener-plate connection range from 160 MPa in compression to 625 MPa in tension. The stress values in the plateau (in between two stiffeners) range from 75 MPa in compression to 70 MPa in tension. The longitudinal stress for Specimen 5 which was welded with a higher heat input (~2.5 kJ/mm) ranged from 200 MPa in compression to 425 MPa in tension at the first welded stiffener and 60 MPa in compression to 525 MPa in tension at the second welded stiffener, with a plateau (between the stiffeners) in the range of 30 MPa in compression to 30 MPa in tension.

The pattern of stress distributions for all the three stress components obtained from both specimens (Specimen 5 and Specimen 6) is similar. However, the stress values for Specimen 6 were shifted to more tension in general as compared to Specimen 5. Stress distributions for normal and transverse components were about 30 MPa higher (more positive) in Specimen 6 both for tension and compression (plateau) zones. For longitudinal stress component, the difference in maximum tensile stress (at the weld) between these two specimens was much higher (about 60 MPa) though the difference in the plateau (in between two stiffeners) was not that high. Therefore, in general, higher stress values found in all of three stress components for Specimen 6 and this observation agrees with other researches by Gao et. al. (1997) and James et. al. (2006) though their specimens were different. The residual stress values for Specimen 6 are higher due to the faster cooling rate associated with the lower heat input. The faster cooling rate allows for shrinkage and phase transformations in the specimen which leads to the higher residual stress readings.

Figure 8.32 shows the distribution for average longitudinal stress values for both Specimen 5 and Specimen 6, and the extrapolated data for Specimen 6 around the first welded stiffener. The extrapolated data for longitudinal stress component was calculated slightly different way than the method used for the normal and transverse stress components. For normal and transverse components, difference between the average values for Specimen 5 and Specimen 6 was

assumed the same for both the tension and compression stress zones since the difference was approximately uniform (about 30 MPa). However, for the longitudinal stress component, the tension and compression zones yielded varying differences. Therefore, for the longitudinal stress distribution two different calculations were made to produce the extrapolated data around the first welded stiffener, one calculation at the stiffener and the second for the values away from the stiffeners in the compression zone.

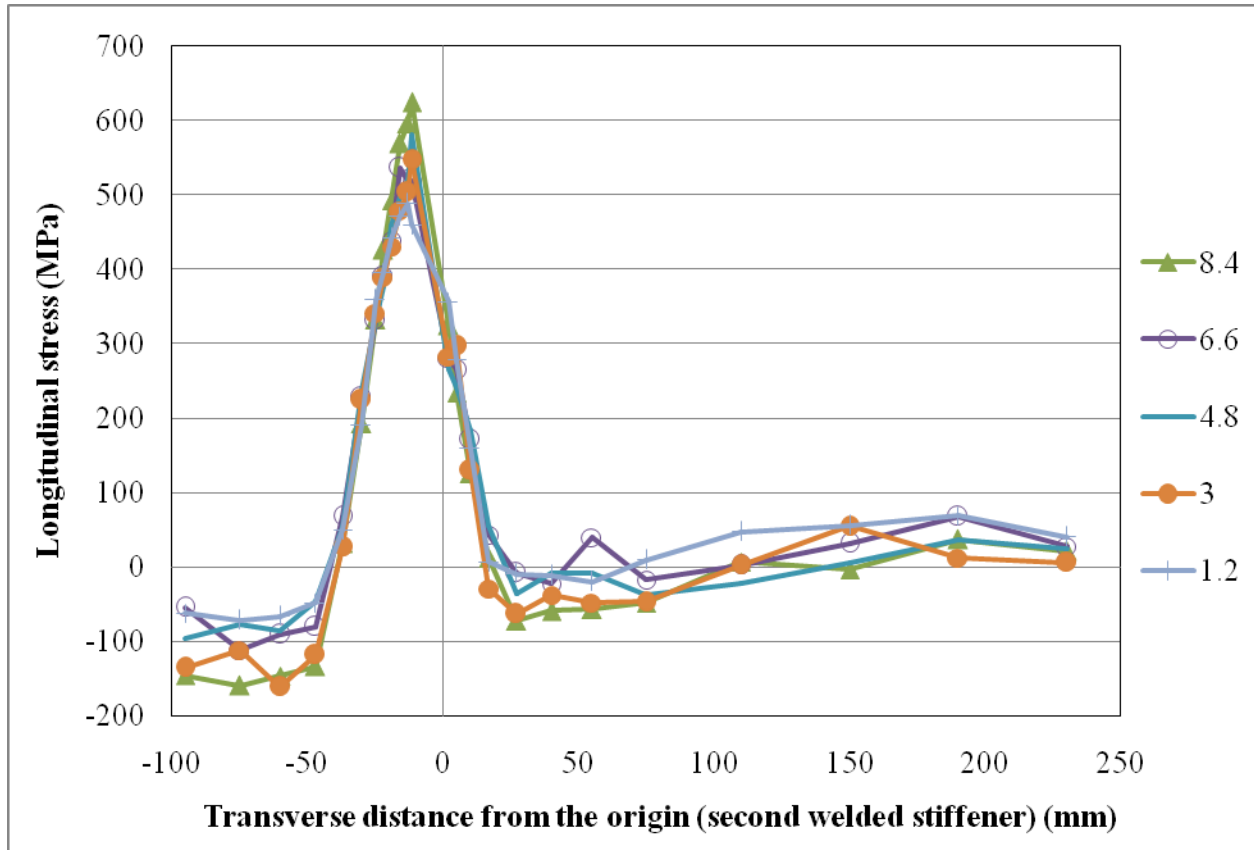


Figure 8.31: Longitudinal stress at various depths in the transverse (T) direction on line 1-2-3 (at L = 0 mm)

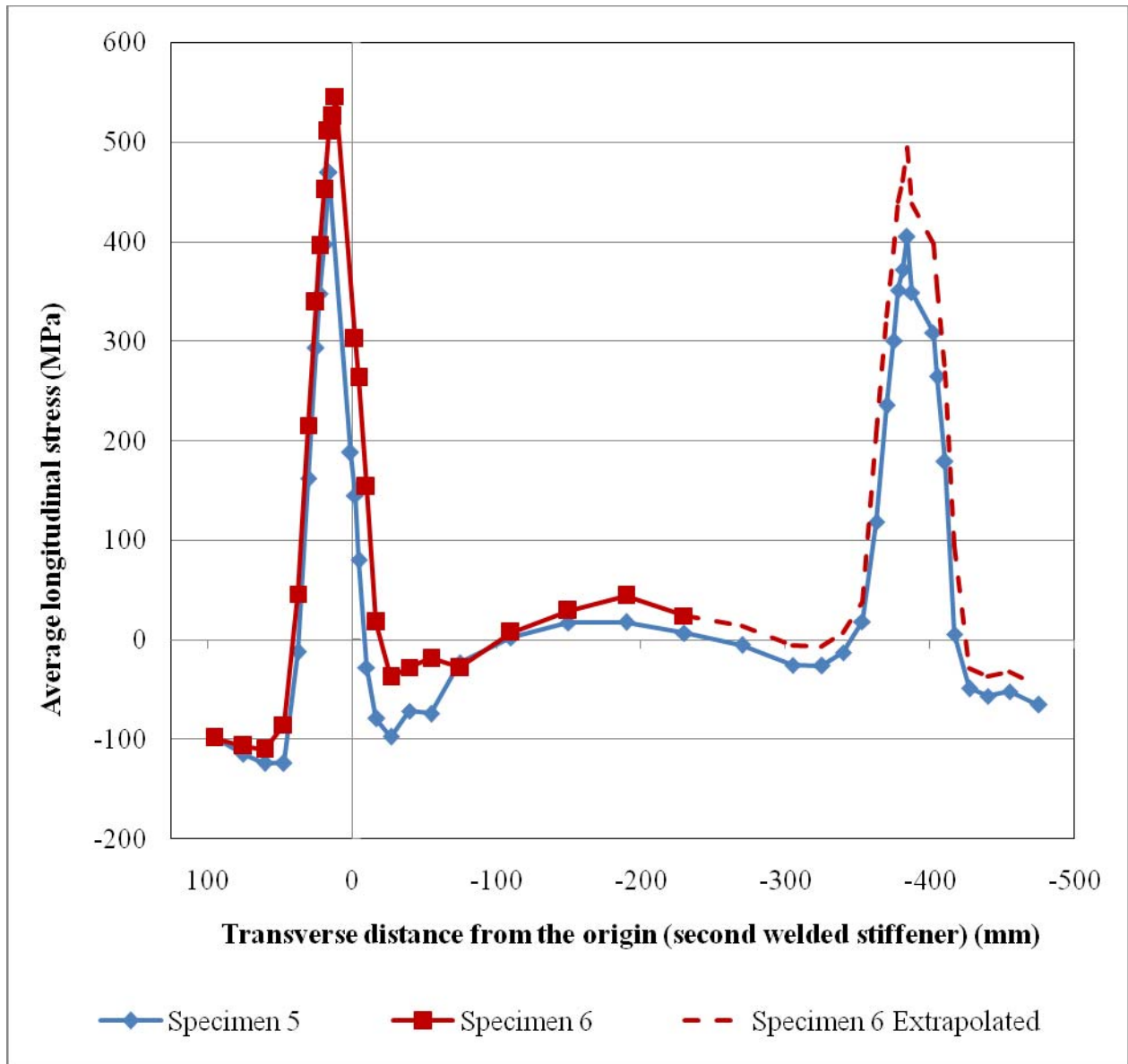


Figure 8.32: Average longitudinal stress distributions along the transverse lines (line 1-2-3-4 for Specimen 5 and line 1-2-3 for Specimen 6)

8.2.3.4 All Stresses at Weld Centerline for Specimen 6

The three stress values were collected on line 2-4, which was at the centreline of the second welded stiffener, at one depth (at $N = 8.4$ mm) closest to the welded face of the plate. Six points (at spacing of 20 mm) were collected at the weld along line 2-4, as shown in Figure 8.25. The stress values for the second welded stiffener are shown in Figure 8.33. The three stress distributions show the same pattern of stress and stress values remain almost uniform with a

maximum difference of ± 50 MPa only indicating that the weld was uniform and consistent nature.

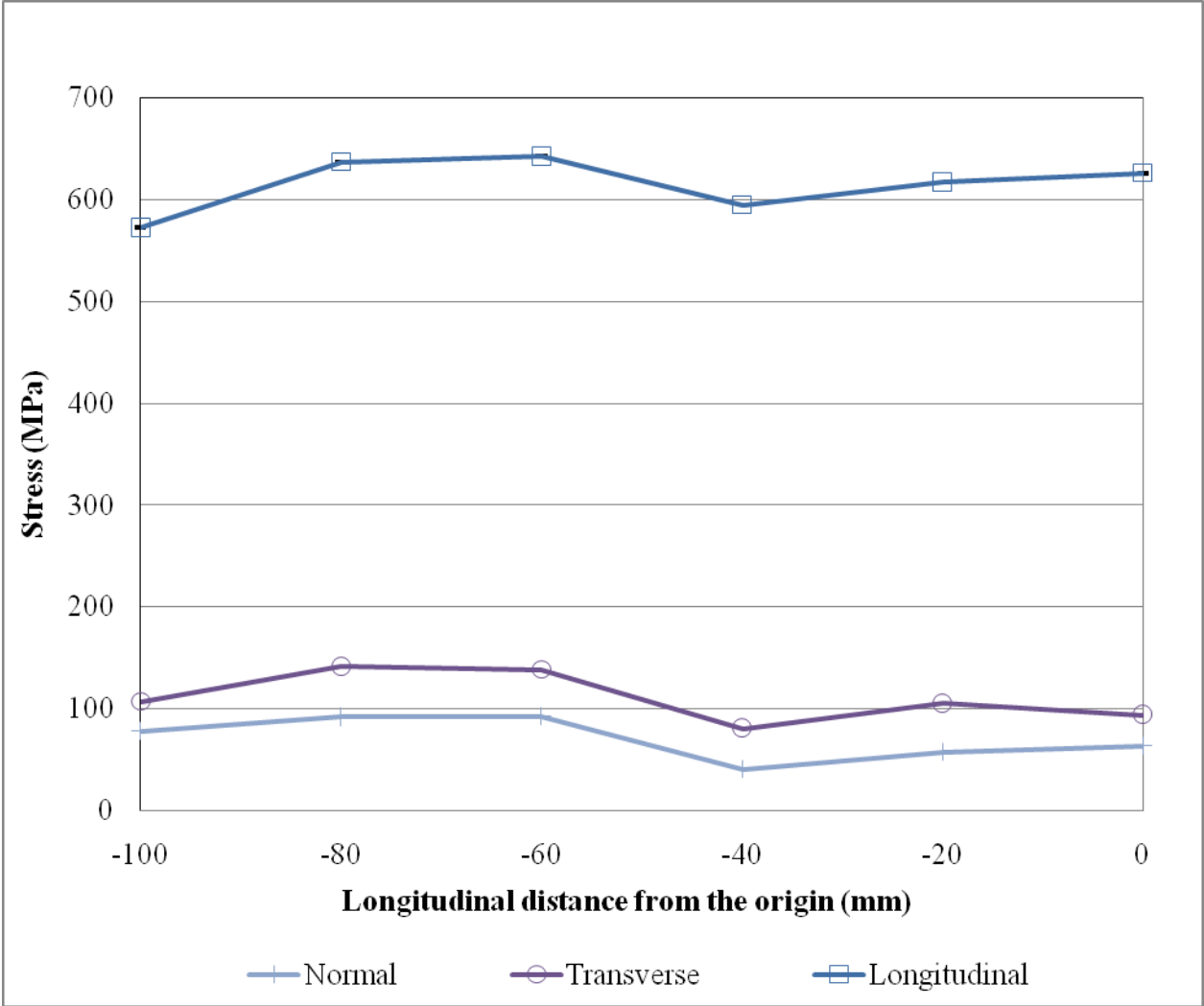


Figure 8.33: All stresses at second welded stiffener, Transverse = 10 mm, Normal = 8.4 mm (on line 2-4)

9 COMPARISON OF RESULTS

Dexter and Pilarski (2000) used the sectioning method to find the residual stress values in two specimens (Cases 2 and 3). Case 2 is a stiffened plate with a 51 mm diameter rathole at the centre of the stiffener and a 28 cm notch between the interior stiffeners. Case 3 is a stiffened plate with a drainhole introduced in the stiffener and a 30 cm notch between the interior stiffeners. Details of specimens for Case 2 and 3 are shown in Figure 9.1.

For each specimen a nominal gauge length of 254 mm was used and they were sectioned using 41 coupons. Four coupons 12 mm wide were cut from either side of the stiffener. Between the stiffeners, three 37 mm wide coupons were cut. The coupons cut from one of the specimens are shown in Figure 9.2. The residual stress values for both cases are shown in Figure 9.3 and compared to the Faulkner (Faulkner, 1975) distribution of residual stresses. It is noted that there is not a stress balance between the compressive and tensile stresses in the specimens. This is most likely due to the inaccurate nature of the testing method. Using the residual stress knowledge of these specimens, it is likely that to balance the residual stresses the x-axis could be moved negatively by 60 MPa.

Faulkner's model was used to compare the residual stress distribution obtained from their two specimens. Faulkner's model assumes a tensile stress peak which is near or at yield stress level regardless of stiffener spacing. It specifies that the width of the tensile zone is equal to about 4 to 5 times the thickness of the parent plate. The tensile peak is modelled as a triangular shape and the base width in proportion to the plate thickness, as shown in Figure 9.4. The tensile triangle is balanced with an area of constant compression between the stiffeners. For the data collected in their study, the triangle has a base width of 3.5 times the plate thickness on each side of the stiffener. As well, the maximum tensile stress is equal to the yield stress of the parent plate. Similar to the current study, the residual stress values within the stiffeners were ignored.

Comparing the work by Dexter and Pilarski and the Faulkner model with the results obtained in this study show similar concepts. Figure 9.5 shows the longitudinal stress data from Specimen 3 in Phase I and the superimposed Faulkner model. From this graph it can be observed the current

study (Specimen 3) agrees well with the Faulkner model with a triangle base width of 3.67 times the plate thickness on either side of the stiffener, which is within the limit of 3 to 4 for as-built ship structures. Figure 9.6 shows the longitudinal stress data from Specimen 5 in Phase II, as well as the Faulkner model. This data is also in agreement with the Faulkner model with a triangle base width of 3.36 times the plate thickness on either side of the stiffener. This value is slightly lower than the value found for Specimen 3 however; it is still within the range. Figure 9.7 shows the longitudinal stress data from the second welded stiffener on Specimen 6 in Phase II and the Faulkner model, assuming tensile peak at yield stress. The stress values at the stiffener do not agree with that of the Faulkner model because the tensile peak found on this specimen was significantly higher than the yield stress of the material, 405 MPa. However, the width of the base of the triangle for Specimen 5 is also 3.36 times the plate thickness on either side of the stiffener which agrees with the range (3 to 4 times the plate thickness) proposed by the Faulkner model.

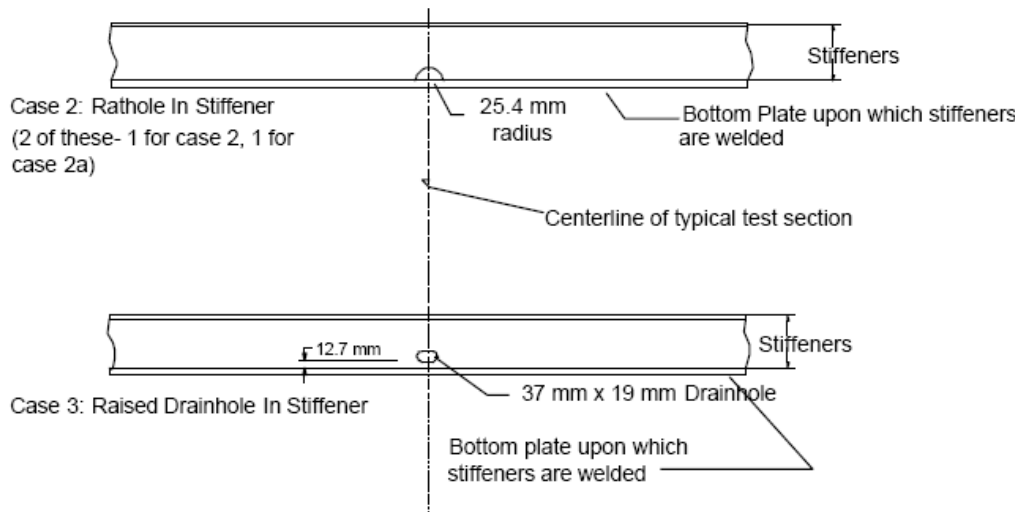


Figure 9.1: Specimen Details (Dexter & Pilarski, 2000)



Figure 9.2: Sectioning coupons used for measuring residual stress distributions (Dexter & Pilarski, 2000)

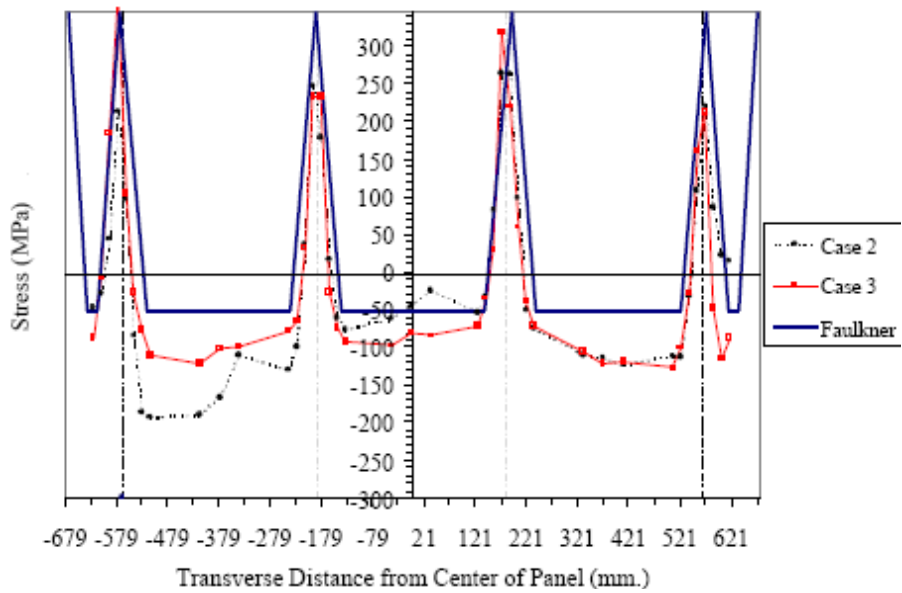


Figure 9.3: Faulkner residual stress model compared to measured values of two specimens (Dexter & Pilarski, 2000)

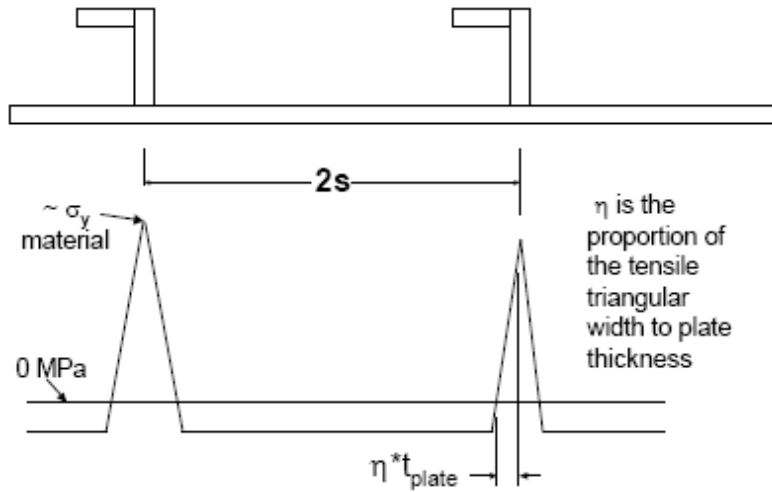


Figure 9.4: Faulkner model for residual stresses (Dexter & Pilarski, 2000)

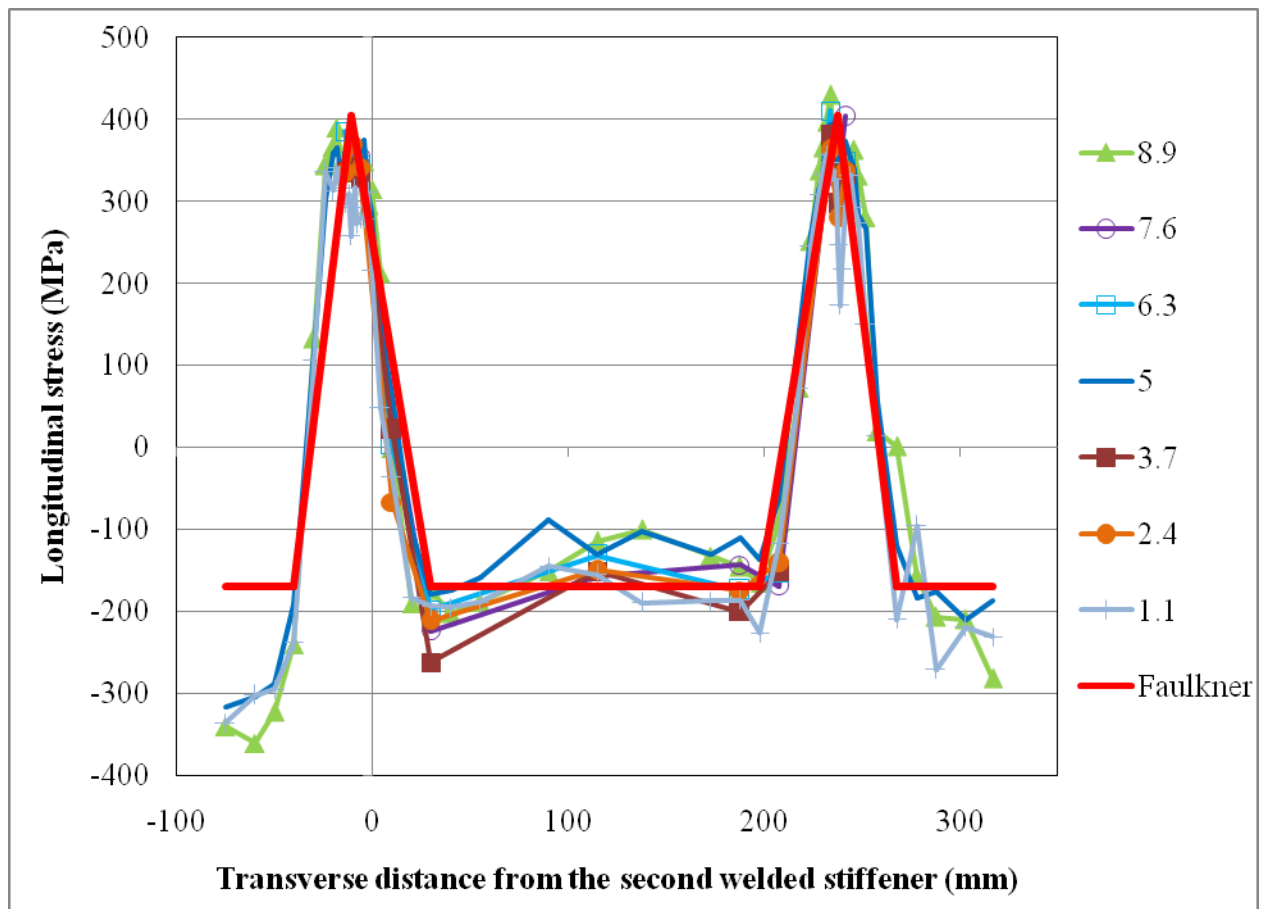


Figure 9.5: Specimen 3, two stiffeners spaced at 250 mm, high heat input

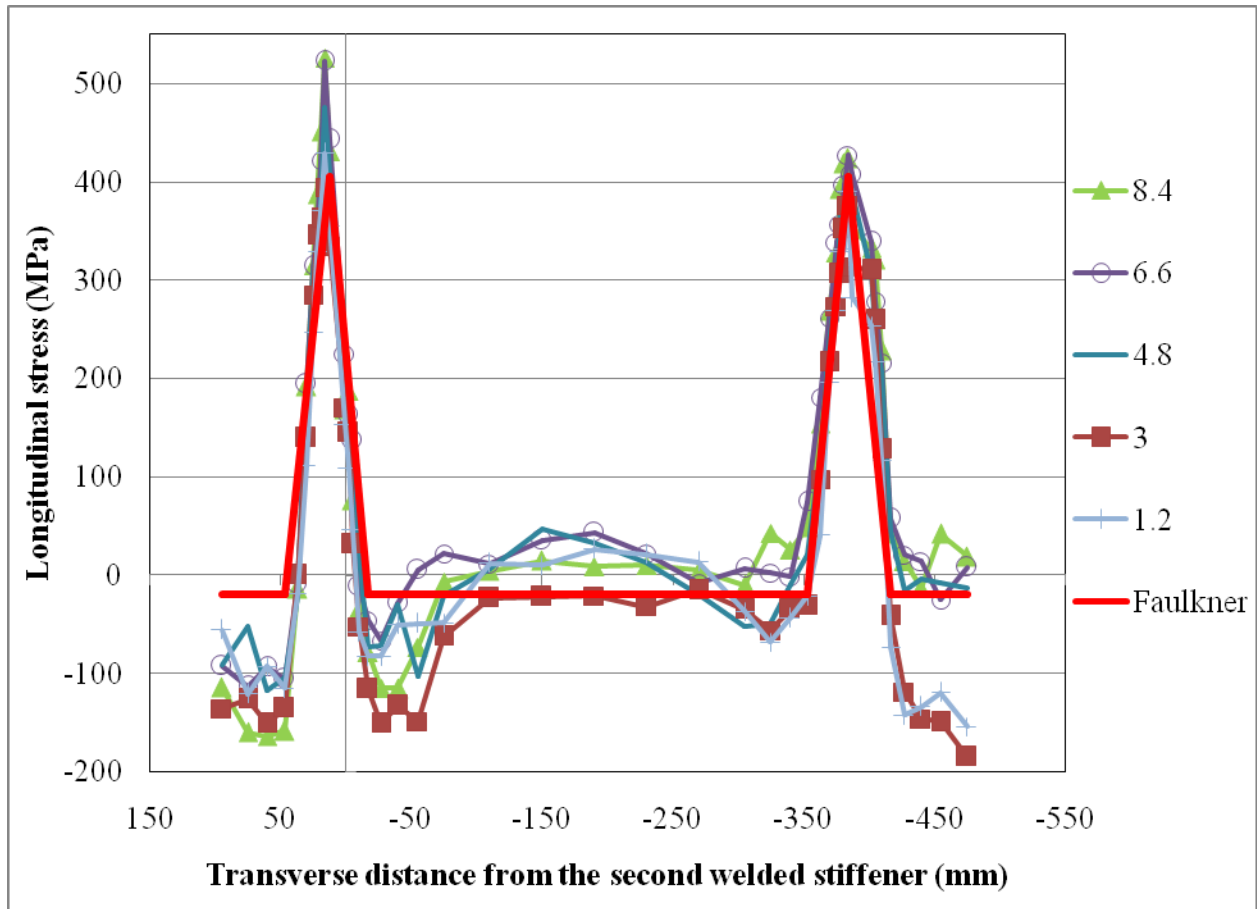


Figure 9.6: Specimen 5, two stiffeners spaced at 400 mm, high heat input

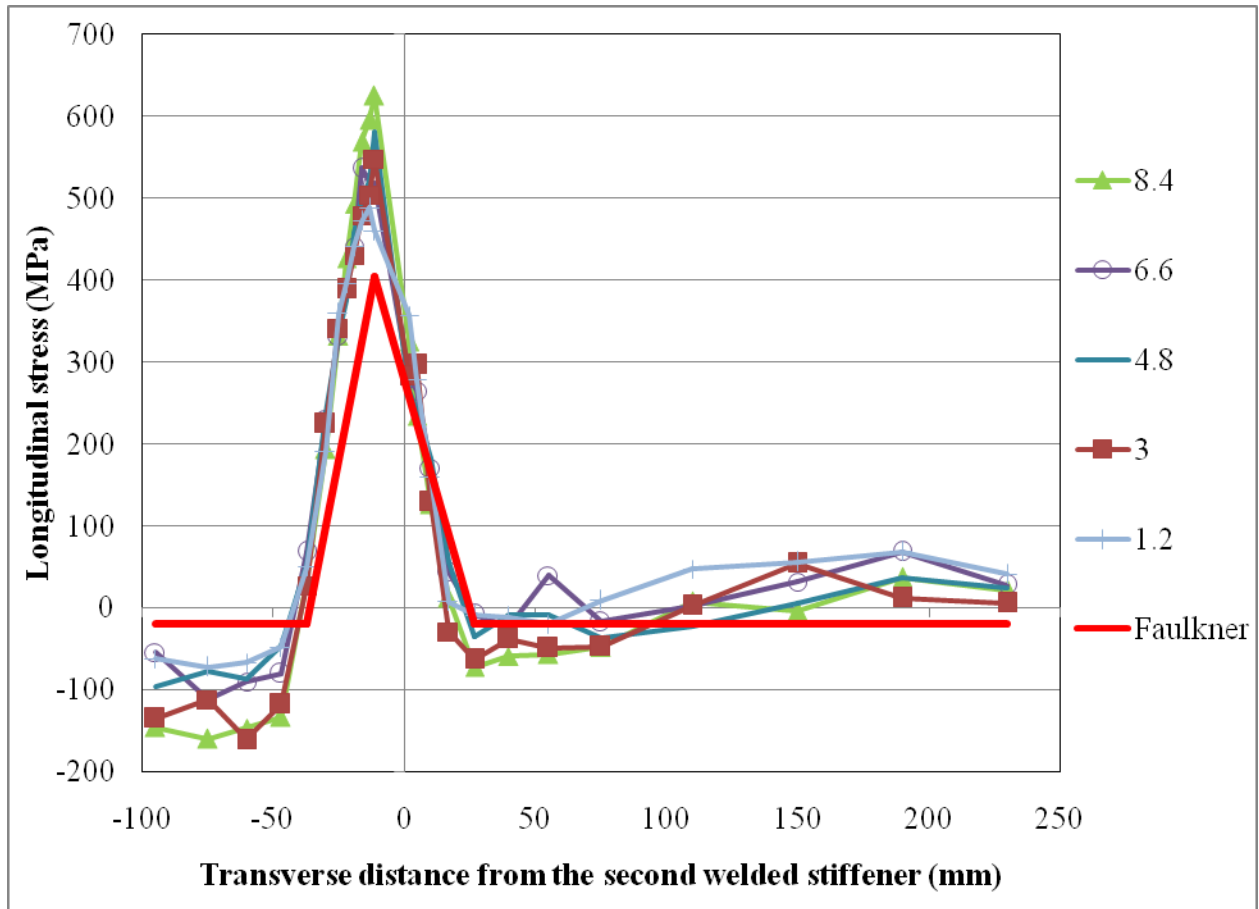


Figure 9.7: Specimen 6, two stiffeners spaced at 400 mm, moderate heat input

10 PORTABLE DEVICES

The high penetration of neutrons in engineering materials is due primarily to the fact that neutrons are electrically neutral. With the exception of magnetic scattering, this means that the neutron experiences a short-range interaction with the nuclei of the material. In other words, the neutron sees the material as mostly empty space. This translates into a low probability of interaction such that a high neutron flux on the sample is needed to obtain diffraction peaks of good statistical quality. Currently, there are only two sources of neutrons that can produce a high enough flux in the 0.1 to 1 nm wavelength range: nuclear reactors and spallation sources. These are both large-scale facilities.

There are portable neutron sources. Deuterium-Tritium (D-T) Neutron Generators that use a small accelerator remain the highest flux, portable neutron sources, but their time-averaged flux is at least four orders of magnitude below the core flux of the NRU reactor. There are many applications for which a D-T Neutron Generator is useful, but neutron diffraction requires the much higher flux of the large-scale facilities. Therefore, at this moment, with the available technology and knowhow, product development for a portable tool that uses ND method for the measurement of residual stresses of in-service ship structures is not possible.

11 SUMMARY, CONCLUSIONS, AND RECOMMENDATIONS

This study provided an accurate representation of the stress distributions of residual stresses that are created due to welding process in the ship hull. ND has successfully mapped the residual stresses in panels that represent ship structure to a degree of detail never seen previously. A total of six specimens were built and tested using ND method. The residual stress patterns found in this study agree well with results from previous investigations that used destructive sectioning and semi-destructive hole boring methods.

Specimen 1 provided the information necessary to have a basis to compare the stress results from the welded specimens. The bending stress found through the thickness of the plate in Specimen 1 was most prevalent in the transverse and longitudinal stresses.

Specimen 2 is the benchmark specimen for comparing stress distributions in other stiffened plate specimens. This specimen shows a triangular stress distribution with the maximum tensile stress at the weld centre and a stress plateau away from the weld in the transverse direction. It is found that the normal and transverse stress distributions do not show a clear pattern though a relatively better pattern is observed for the transverse stress distributions. The longitudinal stress distribution has a clear pattern with tensile stress in the stiffener-plate welded connection zone and a compressive stress plateau away from that zone. The maximum tensile stress value occurred under the weld (near the weld centreline) and it was 450 MPa which is higher than the yield stress (405 MPa) of parent plate. The stress values of the stress plateau that is present away from the plate-stiffener connection region ranged from about 200 MPa in compression to about 30 MPa in compression.

A stop and start occurred in the welding in Specimen 2. This study was not intended to study the effect of stop and start in the weld. However, this accidental stop and start was taken as an opportunity to study what happens if a stop and start do occur in real ship hull construction. This study shows that stop and start decreases the maximum tensile longitudinal stress and therefore, it creates no danger to the tensile stress levels and thus, a stop and start may be beneficial in ship design and construction. However, a further and detailed study needs to be undertaken for complete understanding of the effect of stop and start in the welding process on the residual stress distributions.

Specimen 3 presented a first look at the effect of welding a second stiffener on the residual stress distributions. Similar to Specimen 1, the stress distributions for normal and transverse stresses do not show clear patterns. Also, similar to Specimen 2, the longitudinal stress in plate-stiffener connection zone is tensile and the stress value reduces at a fast rate as the transverse distance from the weld increases. The maximum stress values of the first welded stiffener are slightly higher than those of the second welded stiffener. Since there were two stiffeners in this specimen, a stress plateau between the two stiffeners exists and the stress value ranges from 250 MPa in compression to 100 MPa in compression. The longitudinal maximum tensile stresses are slightly lower in Specimen 3 as compare to Specimen 2 (450 MPa in Specimen 2 vs. 430 MPa in Specimen 3) and therefore, it can be concluded that welding of second stiffener reduces the tensile stress level at the plate-stiffener connections.

Specimen 4 was used to determine the effect of discontinuity of a stiffener on the residual stresses. The normal strain components could not be collected because measurement of other two strain components for this specimen took unexpectedly very long time. Nevertheless, the distributions for transverse and longitudinal strain components show important understanding what happens when a stiffener needs to be discontinued for construction constraints or for other reasons. In general, it was found that the termination of a stiffener may not be a matter of concern. The longitudinal strain at the termination point of the stiffener is not much affected and in fact, at the stiffener termination point, the longitudinal strain value is slightly lower than that found away from the termination point. However, it is strongly recommended that a future study be undertaken for complete understanding of the effect of sudden termination of stiffener on the residual stress distributions.

Specimen 5 was built and tested to study the effect of changing the spacing between two stiffeners. It was found that an increase in the spacing of the stiffeners can cause an increase in the tensile stress peak values. However, the compressive stress levels (between two stiffeners) increases as the spacing between two stiffeners reduces.

Specimen 6 was used to study the effect of heat input level on the residual stress distributions. In general, higher stress values found in all of three stress components for Specimen 6 which was welded with moderate (relatively higher than other specimens) heat input.

This study was undertaken on a parent plate of 9.5 mm thickness. It was found that variation in stress distributions through the depth (thickness) of the plate is not much. However, this finding may not be applicable if the plate thickness is reduced or increased. Therefore, another study is recommended for determining the effect of changing plate thickness on the distributions of residual stresses through the depth of plate. In this study, it is also recommended that the weld metal strength be changed. The effect of very low heat input (in the range of 1 kJ/mm) should also be investigated.

The lack of suitable high-energy source of neutrons today precludes the use of ND for the measurement of residual stresses in the in-service structure of a ship. However, the results of this investigation could be used to help calibrate finite element analysis methods that could then be applied to large sections of ship structure to determine the level of residual stresses.

Therefore, it is recommended that finite element analysis of these specimens be conducted, and validated by the data collected here. A finite element model of a larger ship structure could then be analyzed for its residual stress distribution to assist in future ship construction methods.

12 ACKNOWLEDGEMENTS

The authors sincerely thank the Ship Structure Committee, located in Washington, D.C., USA, Dr. Dave Stredulinsky and Dr. James Huang of the Defence Research and Development Canada (Atlantic), for their financial and technical assistance. Also many thanks to Dr. Ronald Rogge, Dr. Michael Gharghouri, and Mr. Ronald Donaberger from the Canadian Neutron Beam Centre at Chalk River Laboratories located in Chalk River, ON, Canada, for the beam time and technical guidance for completion of the tests.

13 REFERENCES

- [1] ADINA R &D, I. (2008). *Automatic Dynamic Incremental Nonlinear Analysis*. Retrieved 2008, from The Finite Element System for Structures, Heat Transfer, and CFD: www.adina.com
- [2] Akhras, George, Stephen Gibson, Stephen Yang, and Richard Morchat. "Ultimate strength of a box girder simulating the hull of a ship." *Canadian Journal of Civil Engineering* (NRC Canada) 25 (1998): 829-843.
- [3] ANSYS. (2008). *ANSYS*. Retrieved 2008, from www.ansys.com
- [4] ASTM. (2007). American Society for Testing and Materials. *Standard Specification for Steel, Sheet, Carbon, Structural, and High-Strength, Low-Alloy, Hot-Rolled and Cold-Rolled, General Requirements for , ASTM A568 / A568M - 07a*. West Conshohocken, PA, USA: ASTM International.
- [5] ASTM. (2008a). ASTM E 837-08. Determining Residual Stresses by the Hole-Drilling Strain-Gage Method. American Society for Testing and Materials.
- [6] ASTM. (2008b). ASTM E8M-08. Standard Test Methods for Tension Testing of Metallic Materials. American Society for Testing and Materials.
- [7] Ayala-Uraga, Efren, and Torgeir Moan. "Time-Variant Reliability Assessment of FPSO Hull Girder With Long Cracks." *Journal of Offshore Mechanics and Arctic Engineering* 129 (May 2007): 81-89.
- [8] National Research Council (NRC). *The Canadian Neutron Beam Centre*. January 31, 2008. www.neutron.nrc-cnrc.gc.ca (accessed January 2008).
- [9] Cho, J R, B Y Lee, Y H Moon, and C J Van Tyne. "Investigation of residual stress and post weld heat treatment of multi-pass welds by finite element method and experiments." *Journal of Materials Processing Technology* 155-156 (2004): 1690-1695.

- [10] CSA. (2004, February). Canadian Standards Association: General Requirements for Rolled or Welded Structural Quality Steel/Structural Quality Steel. CSA G40.20-04 / CSA G40.21-04. Canadian Standards Association.
- [11] Dexter, R. J., & Pilarski, P. J. (2000). *Effect of Welded Stiffeners on Fatigue Crack Growth Rate*. Washington, D.C.: Ship Structure Committee.
- [12] Faulkner, D. (1975). A Review of Effective Plating for Use in the Analysis of Stiffened Plating in Bending and Compression. *Journal of Ship Research*, 19 (1), 1-17.
- [13] Ganguly, S, M E Fitzpatrick, and L Edwards. "Use of neutron and synchrotron X-ray diffraction for evaluation of residual stresses in a 2024-T351 Aluminum alloy variable-polarity plasma-arc weld." *Metallurgical and Materials Transactions A (Physical Metallurgy and Materials Science)* 37A (February 2006): 411-420.
- [14] Gao, H, H Guo, J M Blackburn, and R W Hendricks. "Determination of residual stress by X-ray diffraction in HSLA-100 steel weldments." *Fifth International Conference on Residual Stress*. Linkoping, Sweden: Linkopings Universitet, 1997. 320-325.
- [15] Gauthier, J, T W Krause, and D L Atherton. "Measurement of residual stress in steel using the magnetic Barkhausen noise technique." *NDT&E International* 31, no. 1 (1998): 23-31.
- [16] Holden, T M, B M Powell, and G Dolling. "Neutron scattering facilities at Chalk River." *Neutron Scattering in Materials Science II Symposium*. Pittsburgh, PA, USA: Materials Research Society, 1995. 7-12.
- [17] Holden, T M, H Suzuki, D G Carr, M I Ripley, and B Clausen. "Stress measurements in welds: Problem areas." *Materials Science and Engineering A* 437 (2006): 33-37.
- [18] Hu, S Z, and L Jiang. "A finite element simulation of the test procedure of stiffened panels." *Marine Structures*, no. 11 (1998): 75-99.
- [19] Hutchings, M T, P J Withers, T M Holden, and T Lorentzen. *Introduction to the characterization of residual stress by neutron diffraction*. Boca Raton, FL: Taylor & Francis Group, 2005.

- [20] International Organization for Standardization, Geneva, Switzerland. "Technology Trends Assessment." *Polycrystalline materials - Determination of residual stresses by neutron diffraction (ISO/TTA 3:2001, 1-48)*. Gaithersburg, Maryland, USA: Versailles Project on Advanced Materials and Standards, National Institute of Standards and Technology, 2001.
- [21] James, M. N., Webster, P. J., Hughes, D. J., Chen, Z., Ratel, N., Ting, S. -P., et al. (2006). Correlating weld process conditions, residual strain and stress, microstructure and mechanical properties for high strength steel - the role of neutron diffraction strain scanning. *Material Science and Engineering A*, 427, 16-26.
- [22] Krawitz, A D. *Introduction to diffraction in materials science and engineering*. Toronto, Ontario: John Wiley & Sons Inc., 2001.
- [23] Lorentzen, T, and J B Ibsø. "Neutron diffraction measurements of residual strains in offshore welds." *Materials Science and Engineering A* A197 (1995): 209-214.
- [24] Meriam, J L, E Paul DeGarmo, and Finn Jonassen. "A method for the measurement of residual welding stresses." *Welding Journal* 25 (1946): 340-s - 343-s.
- [25] National Research Council (NRC) Canada (2008, January 31). The Canadian Neutron Beam Centre. Retrieved January 2008, from www.neutron.nrc-cnrc.gc.ca
- [26] Okumoto, Y. "Residual stress on ship hull structure." *Journal of Ship Production* 14 (1998): 277-286.
- [27] Osgood, W R. *Residual stresses in metals and metal construction*. New York, New York: Reinhold Publishing Corporation, 1954.
- [28] Paradowska, Anna, John W.H. Price, R Ibrahim, T R Finlayson, M Ripley, and R Blevins. "Residual stress evaluation in multi-beads steel weldments using neutron diffraction." *Proceedings of the IIW International Conference on Benefits of New Methods and Trends in Welding to Economy, Productivity and Quality*. Prague, Czech Republic, 2005. 40-51.

- [29] Paradowska, Anna, T R Finlayson, J W.H. Price, R Ibrahim, A Steuwer, and M Ripley. "Investigation of reference samples for residual strain measurements in a welded specimen by neutron and synchrotron X-ray diffraction." *Physica B* 385-386 (2006): 904-907.
- [30] Pearce, S V, and V M Linton. "Neutron diffraction measurement of residual stress in high strength, highly restrained, thick section steel welds." *Physica B* 385-386 (2006): 590-593.
- [31] Price, John W.H., Anna Paradowska, Suraj Joshi, and Trevor Finlayson. "Residual stresses measurement by neutron diffraction and theoretical estimation in a single weld bead." *International Journal of Pressure Vessels and Piping* 83 (2006): 381-387.
- [32] Prime, M B, R J Sebring, J M Edwards, D J Hughes, and P J Webster. "Laser surface-contouring and spline data-smoothing for residual stress measurement." *Experimental Mechanics* 44, no. 2 (April 2004): 176-184.
- [33] Rörup, J. "Mean compressive stresses - Experimental and theoretical investigations into their influence on the fatigue strength of welded structures." *Journal of Strain Analysis for Engineering Design* 40, no. 7 (2005): 631-642.
- [34] Simulia. (2008). *Simulia*. Retrieved 2008, from www.simulia.com
- [35] Somerville, W L, J W Swan, and J D Clarke. "Measurement of residual stresses and distortions in stiffened panels." *Journal of Strain Analysis* 12, no. 2 (1977): 107-116.
- [36] Sumi, Y, M Mohri, and Y Kawamura. "Computational prediction of fatigue crack paths in ship structural details." *Fatigue and Fracture of Engineering Materials and Structures* 28 (2004): 107-115.
- [37] Totten, G, M Howes, and T Inoue. *Handbook of residual stress and deformation of steel*. Materials Park, OH: ASM International, 2002.
- [38] Webster, G A, and R C Wimpory. "Non-destructive measurement of residual stress by neutron diffraction." *Journal of Materials Processing Technology* 117 (2001): 395-399.

- [39] Weng, C C, and S C Lo. "Measurement of residual stresses in welded steel joints using hole drilling method." *Materials Science and Technology* 8 (March 1992): 213-218.
- [40] Wilken, K. "The measurement of residual stresses in welded ship structure and their effect on the strength of the structure." *International Conference of Structural Des and Fabr in Shipbuild*. London, England: Weld Institute, Abington, Cambridge, England, 1976. 169-177.
- [41] Wimpory, R C, P S May, N P O'Dowd, G A Webster, D J Smith, and E Kingston. "Measurement of residual stresses in T-plate weldments." *Journal of Strain Analysis* 38 (2003): 349-365.

SHIP STRUCTURE COMMITTEE LIAISON MEMBERS

LIAISON MEMBERS

American Society of Naval Engineers	Captain Dennis K. Kruse (USN Ret.)
Bath Iron Works	Mr. Steve Tarpay
Colorado School of Mines	Dr. Stephen Liu
Edison Welding Institute	Mr. Rich Green
International Maritime Organization	Mr. Igor Ponomarev
Int'l Ship and Offshore Structure Congress	Dr. Alaa Mansour
INTERTANKO	Mr. Dragos Rauta
Massachusetts Institute of Technology	
Memorial University of Newfoundland	Dr. M. R. Haddara
National Cargo Bureau	Captain Jim McNamara
National Transportation Safety Board - OMS	Dr. Jack Spencer
Office of Naval Research	Dr. Yapa Rajapaksie
Oil Companies International Maritime Forum	Mr. Phillip Murphy
Samsung Heavy Industries, Inc.	Dr. Satish Kumar
United States Coast Guard Academy	Commander Kurt Colella
United States Merchant Marine Academy	William Caliendo / Peter Web
United States Naval Academy	Dr. Ramswar Bhattacharyya
University of British Columbia	Dr. S. Calisal
University of California Berkeley	Dr. Robert Bea
Univ. of Houston - Composites Eng & Appl.	
University of Maryland	Dr. Bilal Ayyub
University of Michigan	Dr. Michael Bernitsas
Virginia Polytechnic and State Institute	Dr. Alan Brown
Webb Institute	Prof. Roger Compton

RECENT SHIP STRUCTURE COMMITTEE PUBLICATIONS

Ship Structure Committee Publications on the Web - All reports from SSC 1 to current are available to be downloaded from the Ship Structure Committee Web Site at URL:

<http://www.shipstructure.org>

SSC 445 – SSC 393 are available on the SSC CD-ROM Library. Visit the National Technical Information Service (NTIS) Web Site for ordering hard copies of all SSC research reports at

URL: <http://www.ntis.gov>

SSC Report Number	Report Bibliography
SSC 457	Investigation of Plastic Limit States for Design of Ship Hull Structures
SSC 456	Buckling Collapse Testing on Friction Stir Welded Aluminum Stiffened Plate Structures, Paik J.K. 2009
SSC 455	Feasibility, Conceptual Design and Optimization of a Large Composite Hybrid Hull, Braun D., Pejcic M. 2008
SSC 454	Ultimate Strength and Optimization of Aluminum Extrusions, Collette M., Wang C. 2008
SSC 453	Welding Distortion Analysis Of Hull Blocks Using Equivalent Load Method Based On Inherent Strain, Jang C.D. 2008
SSC 452	Aluminum Structure Design and Fabrication Guide, Sielski R.A. 2007
SSC 451	Mechanical Collapse Testing on Aluminum Stiffened Panels for Marine Applications, Paik J.K. 2007
SSC 450	Ship Structure Committee: Effectiveness Survey, Phillips M.L., Buck R., Jones L.M. 2007
SSC 449	Hydrodynamic Pressures and Impact Loads for High Speed Catamaran / SES, Vorus W. 2007
SSC 448	Fracture Mechanics Characterization of Aluminum Alloys for Marine Structural Applications, Donald J.K., Blair A. 2007
SSC 447	Fatigue and Fracture Behavior of Fusion and Friction Stir Welded Aluminum Components, Kramer R. 2007
SSC 446	Comparative Study of Naval and Commercial Ship Structure Design Standards, Kendrick A., Daley C. 2007
SSC 445	Structural Survivability of Modern Liners, Iversen R. 2005